AD NUMBER

AD822414

NEW LIMITATION CHANGE

TO

Approved for public release, distribution unlimited

FROM

Distribution authorized to U.S. Gov't. agencies and their contractors; Critical Technology; AUG 1967. Other requests shall be referred to Air Force Flight Dynamics Laboratory, Attn: FDDA, Wright-Patterson AFB, OH 45433.

AUTHORITY

AFFDL ltr, 29 Oct 1973

AFFDL-TR-67-43

NEAR FIELD NOISE ANALYSES OF AIRCRAFT PROPULSION SYSTEMS WITH EMPHASIS ON PREDICTION TECHNIQUES FOR JETS

H. E. PLUMBLEE
J. R. BALLENTINE
B. PASSINOS

LOCKHEED-GEORGIA COMPANY

TECHNICAL REPORT AFFDL-TR-67-43

AUGUST 1967

AIR FORCE FLIGHT DYNAMICS LABORATORY
RESEARCH AND TECHNOLOGY DIVISION
AIR FORCE SYSTEMS COMMAND
WRIGHT-PATTERSON AIR FORCE BASE, OHIO

NOTICE

When Government drawings, specifications, or other data are used for any purpose other than in connection with a definitely related Government procurement operation, the United States Government thereby incurs no responsibility nor any obligation whatsoever; and the fact that the Government may have formulated, furnished, or in any way supplied the said drawings, specifications, or other data, is not to be regarded by implication or otherwise as in any manner licensing the holder or any other person or corporation, or conveying any rights or permission to manufacture, use, or sell any patented invention that may in any way be related thereto.

Copies of this report should not be returned unless return is required by security considerations, contractual obligations, or notice on a specific document.

200 - September 1967 - CO455 - 9-207

AFFDL-TR-67-43

NEAR FIELD NOISE ANALYSES OF AIRCRAFT PROPULSION SYSTEMS WITH EMPHASIS ON PREDICTION TECHNIQUES FOR JETS

H. E. PLUMBLEE
J. R. BALLENTINE
B. PASSINOS

LOCKHEED-GEORGIA COMPANY

FOREWORD

This report was prepared by the Lockheed-Georgia Company, Marietta, Georgia, for the Aero-Acoustics Branch, Vehicle Dynamics Division, Air Force Flight Dynamics Laboratory, Wright-Patterson Air Force Base, Ohio, under Contract AF33(615)-2503. The work described herein is a part of the Air Force Systems Command exploratory development program to predict the noise environment of flight vehicles. The work was directed under Project 1471, "Aero-Acoustic Problems", Task 147102, "Prediction and Control of Noise". Mr. P. Hermes and later Mr. D. L. Smith of the Aero-Acoustics Branch were the task engineers.

The authors acknowledge the assistance of F. F. Rudder, Jr., R. L. Young, J. R. Bay, and L. V. Mazzarella in the data reduction and report preparation; D. K. Wood, R. Snider, and J. P. Dusenbury for the test set-up and data acquisition; G. Hart, T. D. R. Neil, and S. Austin for the preparation and check-out of computer programs; and R. Dziallias, R. Kendrick and L. A. Neal for preparation of the computer data.

The Lockheed-Georgia Company report identification number is ER 8983.

Manuscript was released by the authors on 28 February 1967 for publication as an AFFDL Technical Report.

This Technical Report has been reviewed and is approved.

Howard A. Magrath

HOWARD A. MAGRATH
Chief, Vehicle Dynamics Division

ABSTRACT

Semi-empirical methods are presented for calculating the sound pressure level in a jet near noise field, including temperature and Mach number effects. A digital computer program for calculating constant SPL contours for the overall and octave-band frequencies is incorporated. Machine-plotted contours from model jet tests for a basic jet, VTOL jet, deflected jet, and jet with ejector are included. Results of tip-turbine fan tests are given. Cruise fan, VTOL shroud fan, and wing-mounted configurations were tested.

TABLE OF CONTENTS

ILLUSTRATIONS

ILLUSTRATIONS (Continued)

ILLUSTRATIONS (Continued)

ILLUSTRATIONS (Continued)

ILLUSTRATIONS (Continued)

ILLUSTRATIONS (Continued)

TABLES

SYMBOLS

A_{exit}	area of jet exhaust
B	number of blades in fan engine rotor
BW	frequency bandwidth
c	speed of sound
c_j	speed of sound in jet exhaust gas
C_1 to C_7	functions used to define jet near field
D	engine exit diameter (in computer program, D is SPL increment for contour plots)
DF	directivity factor (The logarithm and actual ratio are both referred to as directivity factor in the text.)
G	number of blades in stator
k	ratio of specific heats
m	integer
M	Mach number (in jet exhaust)
M_c	eddy convection Mach number
n	integer
p	rms sound pressure
r	non-dimensional distance from acoustic source to point in sound field (non-dimensionalized to jet exit diameter)
r'	actual distance from sound source to point in jet noise field
SPL	sound pressure level, $[20 \text{ Log}_{10}(p/0.0002 \text{ Dynes/cm}^2)]$
T	exhaust plane gas temperature
TAP	total acoustic power
V	velocity of jet flow at exhaust plane
XO	sound source location along jet axis
YO	sound source location (perpendicular distance from jet centerline to jet boundary at position XO)
α	eddy length/decay distance (defined in Reference 8)

θ angle from jet exhaust centerline, with origin at the source location along the jet expansion boundary

φ angle from jet exhaust centerline, with the origin at the center of the jet exit plane

SECTION I

INTRODUCTION

There have been a number of experimental investigations of the near noise field of both full-scale and model jet engines (References 1-5, 7). Each investigation had its merits and usefulness in the development of near-field noise prediction techniques. From the viewpoint of the engineer who is frequently confronted with the task of detailed noise prediction for hypothetical engines, however, the state-of-the-art lacks a unified prediction technique which has proven accuracy.

Existing near-field noise prediction techniques use base point noise data taken from full-scale engines or scaled models with similar configuration and operational characteristics. Effects on sound pressures created by differences in engine operational parameters such as exhaust velocity, exhaust temperature, pressure ratio, nozzle configuration, and nozzle diameter are accounted for by applying similarity laws derived from existing data. To make an assessment of the effect of noise on flight vehicle structure, an accurate description of the near noise field in the presence of the structure is needed. Consequently, more than just a few isolated data points in the near field are required. In fact, enough data must be provided so that contour mapping of the near-field sound pressures can be accomplished.

This investigation used a highly automated method of obtaining a voluminous amount of noise data from models of a tip-turbine fan engine and jet engines which are projected for use in the next decade. A thorough parametric variation was made for each engine configuration, encompassing the entire expected operational range. This included independent variations of exhaust temperature, pressure ratio, and fan rpm (for the tip-turbine fan). Charts, contour plots, and 1/3-octave band analyses were devised from the parameter variations. Using the measured noise data, an accurate prediction technique was developed for the near noise field of subsonic, sonic, and supersonic jets.

Section II is a comprehensive survey of the propulsion systems anticipated within the next decade. This is considered a very important aspect of the overall program, since realism in model design is essential. Section III presents the results of the investigation of the near noise field of jets, highlighted by the prediction techniques. Section IV presents the results of the investigation of the near noise field of tip-turbine fans. Both VTOL and cruise conditions are described. Jet engine design details and sound pressure level contours are given in Appendix I and Appendix II.

SECTION II

SURVEY OF FUTURE PROPULSION SYSTEMS

During the early portion of this study, it became obvious that the trend to larger and more powerful, higher-velocity powerplants was being accelerated considerably, bringing an equal rise in the level of the acoustical environment. It was recognized at the initiation of the program that the present methods of predicting noise parameters were not adequate to analyze the type of propulsion systems being contemplated for the next 10 years. Since theoretical approaches to this problem were not complete, an experimental program was needed to obtain empirical data for predicting the noise fields. The problem then became one of establishing the range of operation of the parameters affecting noise level (such as pressure ratio, temperature, and Mach number).

The survey revealed that the following types of propulsion systems are being contemplated:

- Afterburning Turbojets
- Duct-burning Turbojets
- High-Bypass-Ratio Fanjets
- Lift/Cruise Fans
- Turbo-Ramjet Systems

Each of these is discussed in detail below.

Afterburning Turbojets

The afterburning turbojet idea is not new, but the futuristic system envisions much higher pressure ratios and very high temperatures. This type of powerplant is likely to be found on advanced fighter/interceptor aircraft systems as well as on commercial vehicles such as the supersonic transport. The survey indicated that exhaust nozzle pressure ratios in excess of 3.5 would be required with temperature levels exceeding 3000°F.

Duct-Burning Turbojets

The duct-burning turbojet system was primarily conceived for the supersonic transport. The feature that distinguishes this propulsion system from the others is that the jet efflux contains a relatively cool center core and a very hot outer core or annular jet. Efficiency is the reason for selecting it, as the combustion processes could be better controlled in the duct as compared to an afterburner. The resulting geometry, however, is very complex. The pressure ratios and temperature levels fall slightly below that of the afterburning turbojet.

High-Bypass-Ratio Fanjets

The high-bypass-ratio fanjet is an extension of an existing concept, with the principal purpose of increasing thrust levels as well as efficiency. This type of propulsion system is likely to be found in aircraft systems such as the C-5A and large commercial vehicles. Pressure ratios and temperature are low compared to the afterburning and duct-burning turbojets.

Lift/Cruise Fans

The lift/cruise fan configuration was chosen as the representative powerplant from the V/STOL field. Other V/STOL propulsion systems such as tilt wing props, helicopters, and lift jets were considered to be conventional systems. The lift/cruise fans present nothing unusual in terms of pressure ratio and temperature levels. However, the effect of the annulus of hot air in the exhaust is an unknown, and its effect on noise is thought to be significant.

Turbo-Ramjet Systems

The turbo-ramjet system is considered a possible powerplant for very futuristic suborbital vehicles. This system is much like the simple turbojet, but with slightly higher exhaust velocity (higher pressure ratio and temperature levels). Complete information on this system is not available since the propulsion system has not been completely defined. One consideration was the use of hydrogen as a fuel, which may introduce another parameter to those already established as controlling the noise generation.

The range of operation of the controlling parameters (pressure ratio, temperature, and Mach number) of all the systems mentioned above were defined. Then two model powerplants capable of representing all of the systems were conceived.

SECTION III

NEAR-FIELD NOISE FOR JET ENGINES

The intent of this section is to present the experimental and empirical analyses for near-field jet noise, such that the final result provides the capability of calculating free-field sound pressure level contours, within acceptable error limits.

A. Introduction

It is possible to define most phenomena to a given degree of accuracy by experimental methods if the following information is known:

1. What is to be defined (i.e., sound pressure level).
2. The physical boundaries.
3. The controlling parameters — this is the most important.
4. Is instrumentation available for measuring and recording the phenomenon — if so, is it accurate enough?
5. Can the controlling parameters be measured or accurately calculated from other measured data? This was almost the downfall in the present study. It was found that thermocouples to measure exhaust temperatures above 3000°F, in a highly oxidizing atmosphere, were very difficult to obtain.

In previous studies conducted to determine the near noise field, items 1, 2, and 4 were capably dealt with, but 3 and 5 have been slighted. In Reference 5 it was stated that the engine operational parameters were in the correct range. This is hardly adequate as one wishes to relate the sound pressure to the engine parameters.

After a thorough study of the controlling characteristics of turbojet engines, it was determined that the two major independent variables which most adequately describe the state of the jet exhaust are local exhaust Mach number (or exhaust pressure ratio) and exhaust tailplane temperature. In a more refined analysis, it will be necessary to include such parameters as velocity profile, temperature profile, and nozzle shape. These variables were excluded (or fixed) from the basic study in an effort to empirically relate the sound pressure to the two major independent variables.

An attempt has also been made to determine qualitatively the effects of such operational constraints as a reflecting ground plane for both a normal jet and a VTOL jet. An ejector configuration and two turning vane configurations were also tested.

The following sections give the engine design philosophy, the test description and data reduction, a discussion of the test results, the analysis, the computer program (which most facilities should be able to use, since the subprograms have been rewritten in non-machine-orientated language), and the comparison of predicted data with both the model engine measurements and with available full-scale turbojet data.

B. Engine Design Philosophy

As stated in Section II, many variables and many power plants had to be considered. In the initial planning stages of this research, it was thought that several different engine types would be modeled as accurately as possible. Then the noise characteristics of specific engines could be reported.

After studying the proposals for 50 or more advanced propulsion systems, it was decided that selection of the engines to be used would tend to be arbitrary and inexact. Therefore, a chart was made up which listed the basic parameters peculiar to each of these systems, where possible (many of the designs were classified). The parameters included exhaust gas temperature (tailplane temperature), exit velocity and nozzle pressure ratio, estimates of velocity and temperature profiles, and bypass ratios.

Figure 1 is an envelope plot of the exhaust tailplane temperature versus Mach number which encompasses the operational conditions of all the proposed systems surveyed. Near-field noise data had been reported for the J57 and J79 engines (References 2, 3, and 19). The operational conditions for these data are plotted on the chart. However, the knowledge of near-field noise characteristics of a basic jet which operates within this envelope was almost totally lacking except for the isolated points. The decision was then made to build a model engine which operates within and to the limits of the envelope of Figure 1. The proposed data points for acquiring near field noise data are shown as circles. It was also decided that such effects as velocity profiles and temperature profiles could not be studied until the basic jet was more thoroughly defined. From this concept a model jet engine was designed, and the process included some of the most advanced techniques. For instance, transpiration and film cooling techniques were used. Further, a multi-purpose screech liner was used to prevent combustion screech and implement the film cooling of the engine case and nozzle. Design details are included in Appendix I.

All free-field tests were run with the engine exhausting upward to prevent ground reflections. To include the effect of ground reflections in the experimental data, an 8' x 12' simulated ground plane was built.

Some of the future system proposals surveyed included jet engines with deflecting vanes for VTOL operation. The configuration of the vanes was rather nebulous; therefore, to determine qualitatively the effects of vanes on near-field noise, a simple plate was used to deflect the flow. Two angles of deflection were chosen, and the deflected jet flow was directed toward the simulated ground plane.

Other propulsion system configurations included a thrust-augmenting ejector, designed and constructed by the airframe manufacturer. One configuration of the ejector was built to give a qualitative effect on the noise field of a supersonic nozzle.

VTOL jets are presently being installed in several VTOL aircraft. For instance, a new configuration that was studied includes four JT-12 engines for vertical lift with two JT-12 engines operating in a deflected jet VTOL mode. To simulate this condition, the model engine was mounted in the VTOL position in a continuously adjustable test rig. (This configuration is shown in the Test Description of this Section.)

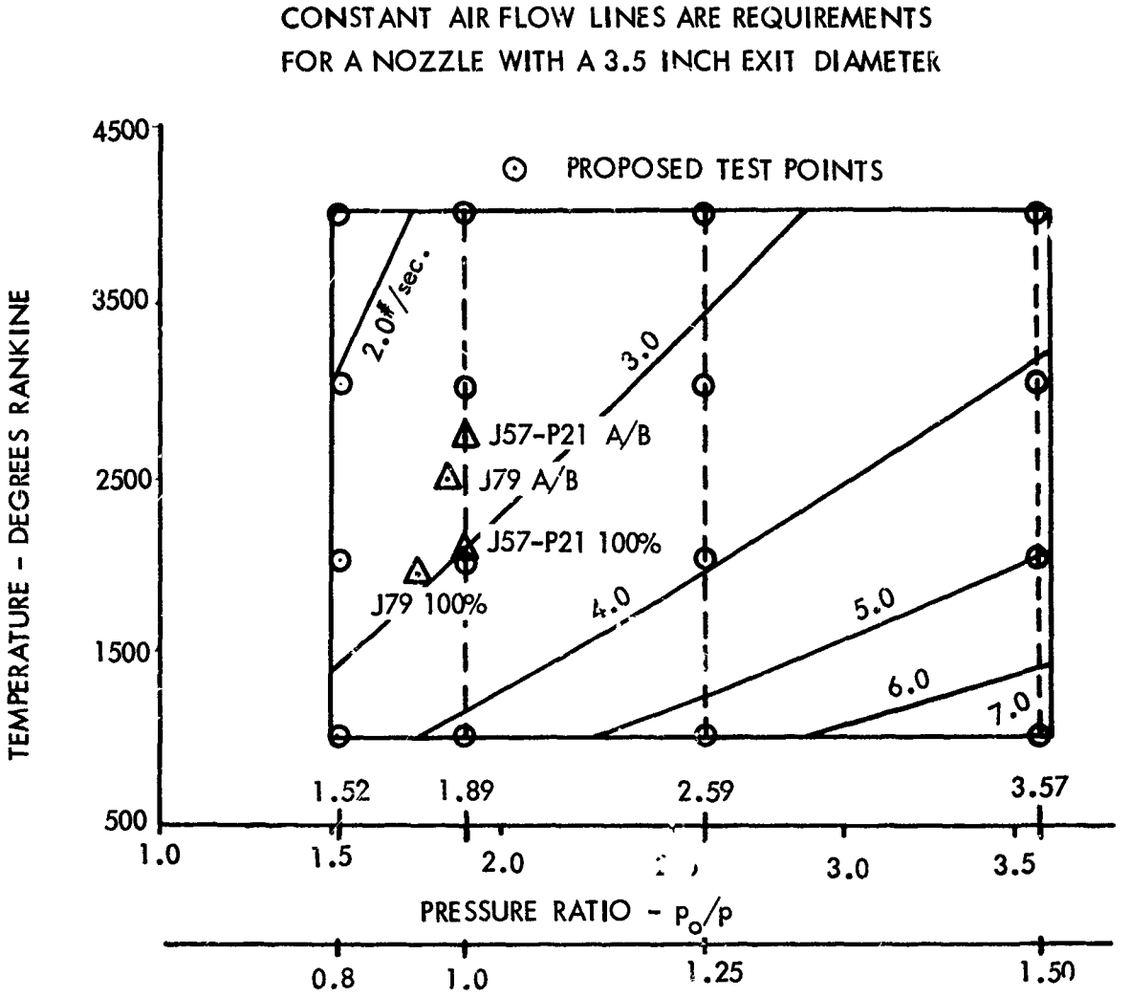

FIGURE 1. TEMPERATURE-MACH NUMBER ENVELOPE FOR PROPOSED ADVANCED PROPULSION SYSTEMS

C. Experimental Program - Near Field Jet Noise

1. Test Procedure

One requisite of the near-field jet noise test was a completely systematic, and where possible, automatic recording of all data, both sound pressure levels and engine operational parameters. The high quality of the results obtained justified the considerable amount of pretest planning needed to achieve the desired system.

In the model engine design stage, there was some indication that engine operation over five minutes long might exceed the life of the engine nozzles for the high-temperature runs. Therefore, a trolley to hold and move the microphones was designed and built. This trolley (shown in Figure 2) holds 12 microphones simultaneously. It rolls on three triangular rails and may be freely positioned in a lateral or radial direction. The vertical rod to which the microphones are attached is adjustable to an angle of 20 degrees with respect to the vertical. This allows the vertical array of microphones to assume a position parallel to the jet expansion boundary.

The angle of jet flow boundary was experimentally determined by measuring flow velocity at positions along the boom in the near-flow region. The jet expansion angle was defined when the velocity at the uppermost microphone position was 50 percent of the velocity halfway down the boom. The average value of this angle for all jet nozzle configurations tested was 7.5 degrees.

The microphones used in the test were very sensitive to environment. The temperature specification was below 200°C for continuous operation. Since the exhaust gas temperature was expected to reach nearly 4000°R, a radiated temperature profile was measured along the 7.5-degree boundary. Figure 3 is a plot of the temperature indicated on dummy microphones placed along the boundary.

The high temperatures recorded resulted in a decision to bring the microphones no closer than 1.5 exit diameters from the exhaust boundary. Although this resulted in a loss of the highest sound pressure levels generated at the source, the loss of these data is not considered serious, since most aircraft structures will be over one diameter from the boundary.

The microphones were attached with rubber-sleeved Adel clamps to the mounting angles welded to the boom as shown in Figure 4. The grid of microphone positions covered an area from 3 diameters upstream of the exit plane to 24 diameters downstream. The radial distance covered was 1.5 diameters from the 7.5° boundary out to 19.5 diameters from the boundary. The microphones were spaced on an isotropic grid of 3 exhaust diameters. The result was the 70-point grid shown in Figure 5.

2. Acoustic Instrumentation

The premise of acoustic modeling is that frequency increases as size is decreased. To measure the scaled frequency spectrum that would normally be associated with a full-scale jet engine requires extremely high-frequency instrumentation, especially when the model is 3.50 inches in diameter and full-scale engines may be as large as 96 inches in diameter.

The microphones selected were Bruel and Kjaer 1/4-inch, high-intensity, high-frequency-response, Model 4131, microphones. The high-frequency response is above 100 KHz.

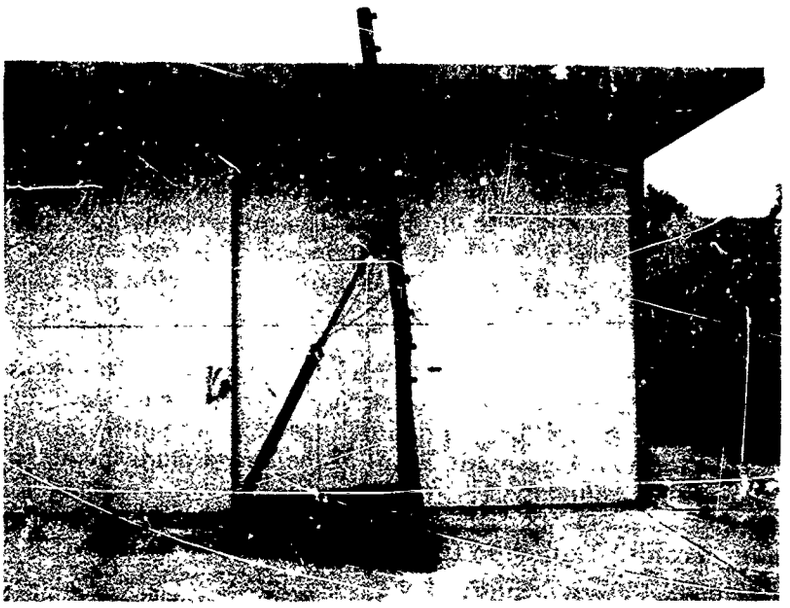

FIGURE 2. MICROPHONE STAND

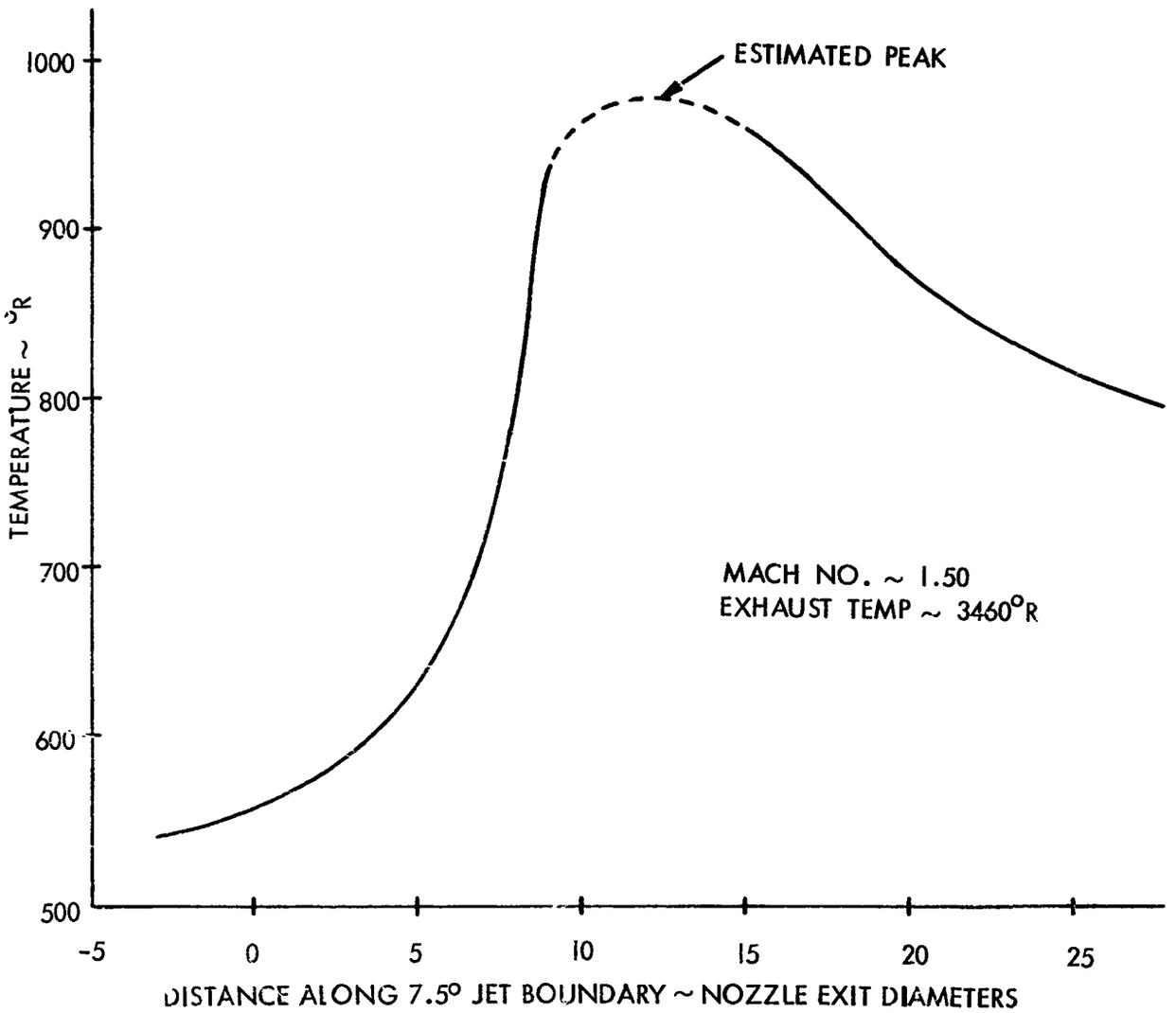

FIGURE 3. RADIATED TEMPERATURE PROFILE ALONG JET BOUNDARY

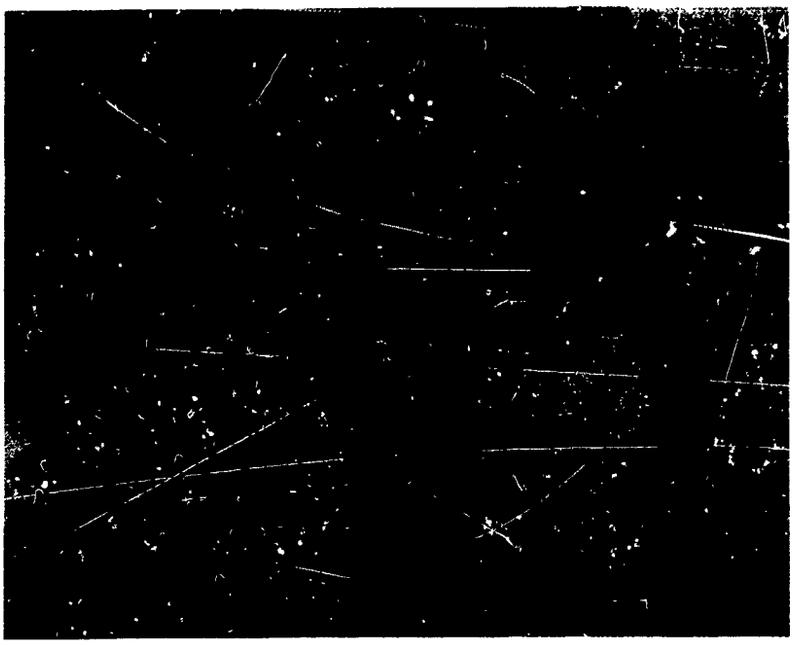

FIGURE 4. MICROPHONE ATTACHMENT ARRANGEMENT

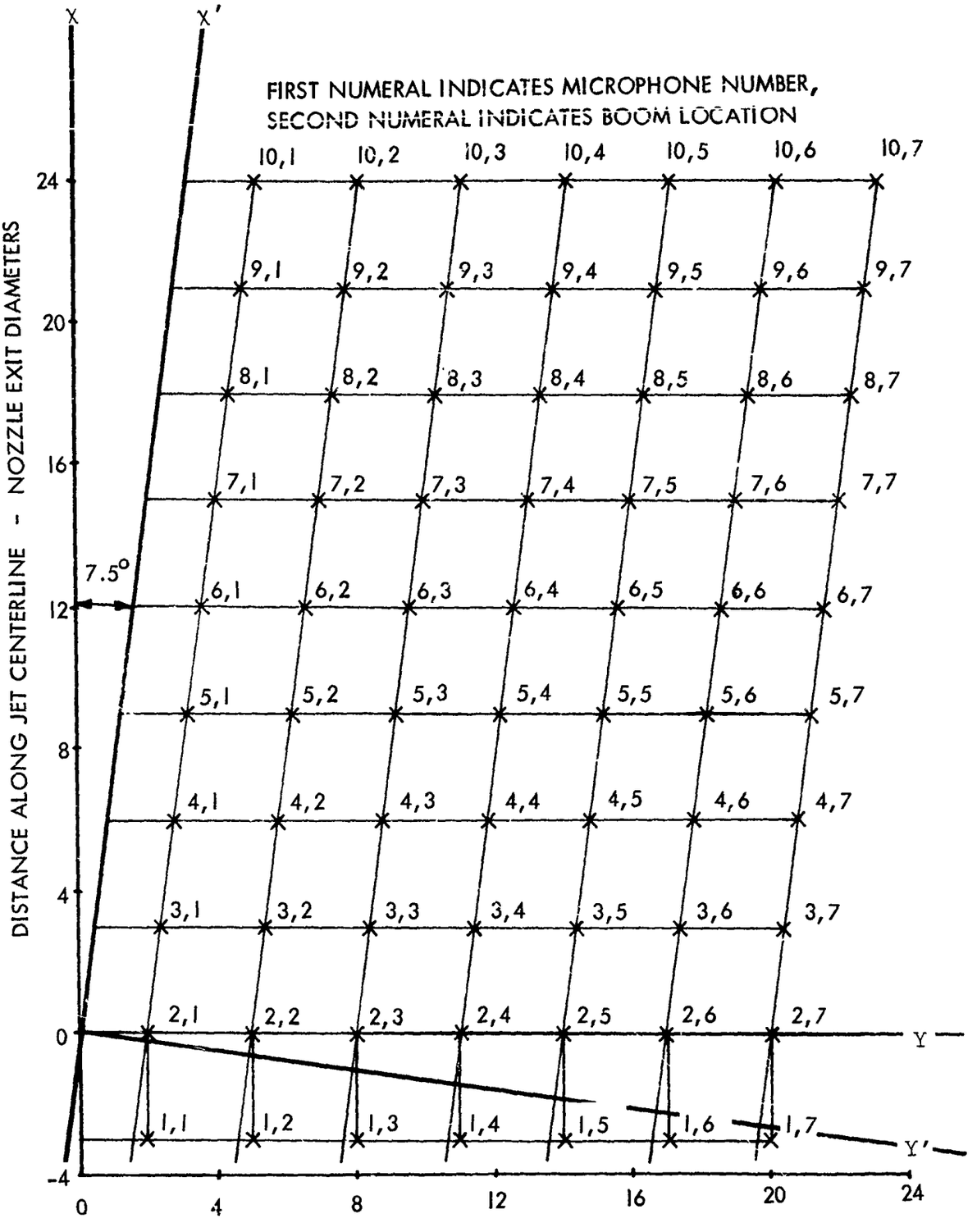

FIGURE 5 MICROPHONE GRID

To amplify and record these high-frequency signals also required some special equipment. Hewlett-Packard Model 3872-A D.C. to 80 KHz differential amplifiers were used to condition the microphone signals before recording on tape. Figure 6 is a block diagram of the instrumentation set-up.

Before each day's run, a 140-decibel calibration signal was inserted into each microphone. The microphone output was recorded on the CEC tape recorder at 60 ips. The calibrator used was a Photocon Model PC 125.

Before each data run, the output of each microphone amplifier was visually monitored on a true rms voltmeter, and the amplifier gain was changed when necessary. The amplifier gains, in conjunction with the pre-recorded calibrated signals, were used to determine absolute sound pressure levels.

A time-code signal was recorded on one track of the tape recorder. This reduced the time required to search out a data run in later analysis. A 100-KHz reference signal was recorded on another channel as a precaution in case tape speed should change.

3. Engine Instrumentation

The required instrumentation for the gas generator was established by determining the functions it had to perform. It was necessary to monitor skin temperature in the gas generator so that malfunctions, such as hot spots, could be detected quickly. Also, the nozzle performance had to be assessed.

The following instrumentation existed for the data acquisition phase of the test:

Total Inlet Pressure - This consisted of a total pressure probe installed at the inlet of the gas generator. This pressure was used to set the exhaust nozzle total pressure. A calibration was necessary to obtain a relationship between engine inlet and nozzle inlet pressures. The use of engine inlet pressure to set nozzle inlet pressure avoided placing pressure probes in the hot gas stream.

Combustion Liner Skin Temperature - Four "skin" thermocouples were installed on the combustion liner to monitor its operating temperature, which was limited to 1800°F, and to locate any hot spots produced from improper combustion processes.

Gas Temperature - A traversing, water-cooled thermocouple was used to obtain the gas temperature and the temperature profile of the combustion products. This thermocouple was located at the inlet of the exhaust nozzle, although the data were to be correlated to nozzle exit conditions. It seemed inadvisable to place the thermocouple at the nozzle exit plane due to supersonic flow conditions (trailing shocks would have affected the noise data). The assumption was made that the nozzle would perform in a nearly isentropic manner and that temperature and temperature profiles would not be affected throughout the nozzle.

Prior to the installation of the water-cooled thermocouple, other schemes using ceramic insulation were attempted without success.

Nozzle Exit Static Pressure - This pressure was used to assess the over/under expansion of the nozzle. It was also used to define the total pressure at the nozzle inlet plane by varying the inlet pressure of the gas generator until the nozzle exit pressure approached ambient conditions.

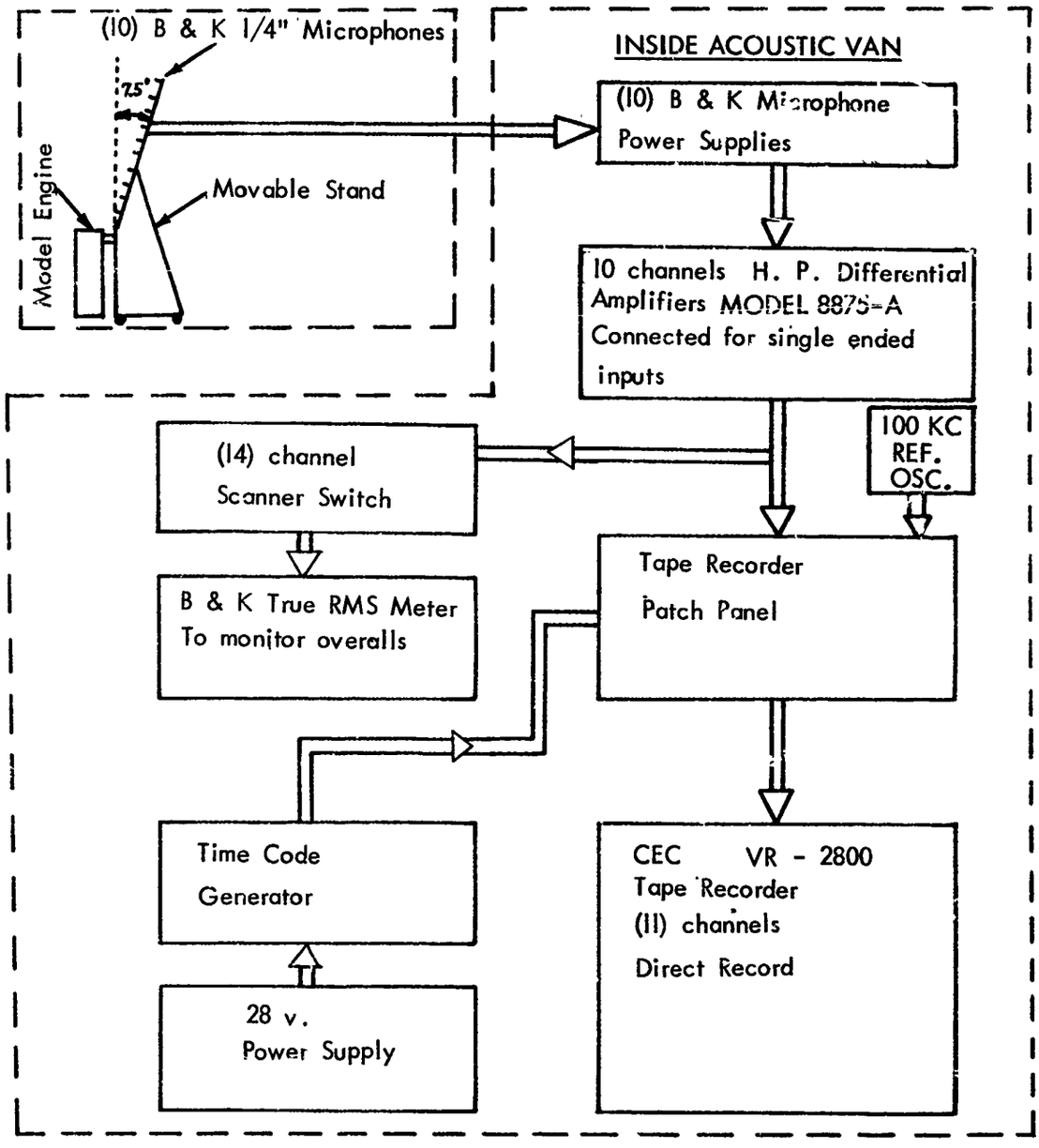

FIGURE 6. BLOCK DIAGRAM OF ACOUSTIC DATA RECORDING SYSTEM

4. Description of Tests

Thirty-four test runs were made with the jet engine models. Seventy microphone positions were recorded for each test. Table I is a tabulation of the basic engine run conditions. Sixteen runs were made to give qualitative effects of ejectors, ground planes, deflecting vanes, and ground proximity for VTOL jets. These run conditions are listed in Table II.

As stated in Section II, the two major operational parameters which characterize the energy state of a jet engine are the nozzle pressure ratio (Mach number) and exhaust gas temperature. Figure 7 shows the engine operational envelope. The Mach 0.80 and Mach 1.00 data points were taken with the sonic nozzle configuration. The Mach 1.25 and Mach 1.50 data points were obtained with the respective nozzle configurations. The Mach 1.59 data points were taken with the Mach 1.50 nozzle configuration operating in an overexpanded condition.

Figure 8 is a photo of the Mach 1.50 nozzle in operation. The temperature of this run was approximately 3000°R. The visible hot exhaust gases extend about 12 diameters downstream of the exit plane. The background shown in this photo is over 50 feet from the engine model. The closest reflecting surface during any of the tests was over 100 nozzle exit diameters away.

Figure 9 shows the nozzle-ejector configuration. Here again, the background was far enough away to provide no reflections for the acoustic near-field.

A schematic drawing of the jet deflector vane is given in Figure 10. The distance from the nozzle exit plane to the center of the deflecting vane was held constant when the vane angle was changed.

The VTOL jet test rig is shown in Figure 11. The height of the jet exit plane above the ground plane is continuously variable from 2 to 20 diameters.

D. Data Reduction and Presentation

One of the primary reasons for the lack of information on characteristics of the near noise field of jet engines is the failure to provide an accurate, consistent presentation of the data.

Near-field noise is extremely complicated. This makes reduction of the noise characteristics to a single number value, such as total acoustic power, very uninformative and almost unrelated to sound pressure level at a given field point. This is why Howe's (Reference 3) method of constant level contours for each frequency band is an extremely useful presentation.

The contours provide a very clear picture of levels to be expected, as well as trends and characteristics of the field.

The contour plots have some serious disadvantages, if they must be done manually. It is difficult and time-consuming to obtain accuracy and consistency. For these reasons, an automatic data processing system was developed to produce a contour map of the near-field sound pressure levels. Basically, the system consists of four major steps:

1. The tape-recorded data are fed through a frequency analyzer which provides simultaneous output for all bands. The analyzer used in this system had eight

TABLE I

BASIC ENGINE RUN CONDITIONS

Test No.	Mach No.	Temp. °R	Thrust (calculated) lbs.	Nozzle pressure ratio	Speed of sound FPS	Exhaust velocity
17	0.80	570	116	1.53	1170	936
22	0.80	1260	119	1.54	1715	1372
19	0.80	2817	113	1.53	2516	2013
20	0.80	2943	112	1.53	2570	2056
16	1.00	575	171	1.89	1175	1175
23	1.00	1290	184	1.89	1734	1734
18	1.00	2823	172	1.89	2518	2518
21	1.00	2915	172	1.88	2557	2557
12	1.25	580	277	2.61	1156	1445
11	1.25	1360	282	2.58	1777	2221
10	1.25	3069	258	2.60	2621	3276
9	1.25	3671	253	2.59	2860	3575
8	1.49	560	377	3.61	1160	1740
2	1.51	1360	393	3.73	1785	2677
6	1.49	1985	382	3.61	2126	3188
5	1.51	2460	380	3.74	2356	3534
3	1.50	2960	381	3.66	2528	3873
7	1.50	2960	381	3.69	2528	3873
4	1.52	3460	376	3.77	2784	4176
34	1.59	3735	399	4.20*	2885	4590
35	1.59	3865	401	4.18*	2930	4660

*Nozzle was designed for pressure ratio of 3.67.

TABLE II

RUN CONDITIONS FOR VARIOUS CONFIGURATIONS OF THE BASIC ENGINE

Test Configuration	Test No.	Mach No.	Temp. °R	Thrust (calculated) lbs.	Nozzle pressure ratio	Speed of sound FPS	Exhaust velocity
Mach 1.25 nozzle w/ejector	13	1.25	555			1155	1443
Mach 1.25 nozzle w/ejector	15	1.25	1280			1737	2172
Mach 1.25 nozzle w/ejector	14	1.25	2993			2589	3236
Ground plane 5 diameters from engine centerline	24	1.00	1300	185	1.89	1740	1740
Ground plane 5 diameters from engine centerline	25	0.80	1315	118	1.53	1749	1399
Ground plane 5 diameters from engine centerline	26	1.00	2816	171	1.89	2517	2517
Ground plane 5 diameters from engine centerline	27	0.80	2824	108	1.53	2519	2015
Ground plane 10 diameters from engine centerline	28	1.00	2847	171	1.89	2528	2528
Ground plane 10 diameters from engine centerline	29	0.80	2821	112	1.53	2518	2014
45° jet deflecting vane with ground plane @ 5 diameters	30	1.00	1275	183	1.89	1724	1724
45° jet deflecting vane with ground plane @ 10 diameters	31	1.00	1295	183	1.89	1737	1737
30° jet deflecting vane with ground plane @ 10 diameters	32	1.00	1270	183	1.89	1722	1722
VTOL engine with nozzle 3 diameters above ground plane	36	1.00	530	171	1.89	1135	1135
VTOL engine with nozzle 6 diameters above ground plane	37	1.00	530	171	1.89	1135	1135
VTOL engine with nozzle 9 diameters above ground plane	38	1.00	530	171	1.89	1135	1135

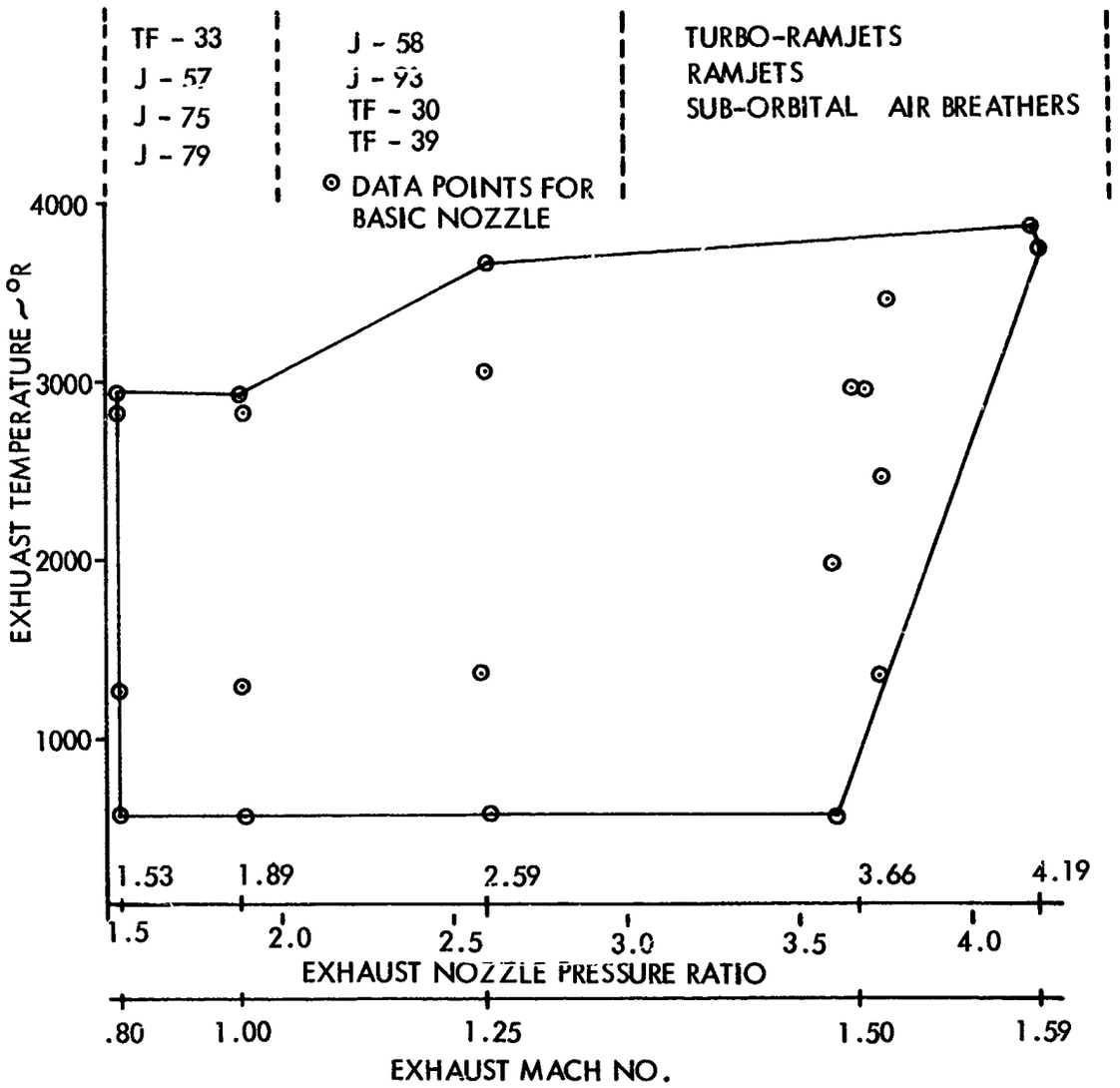

FIGURE 7. ACTUAL OPERATIONAL ENVELOPE FOR MODEL ENGINE

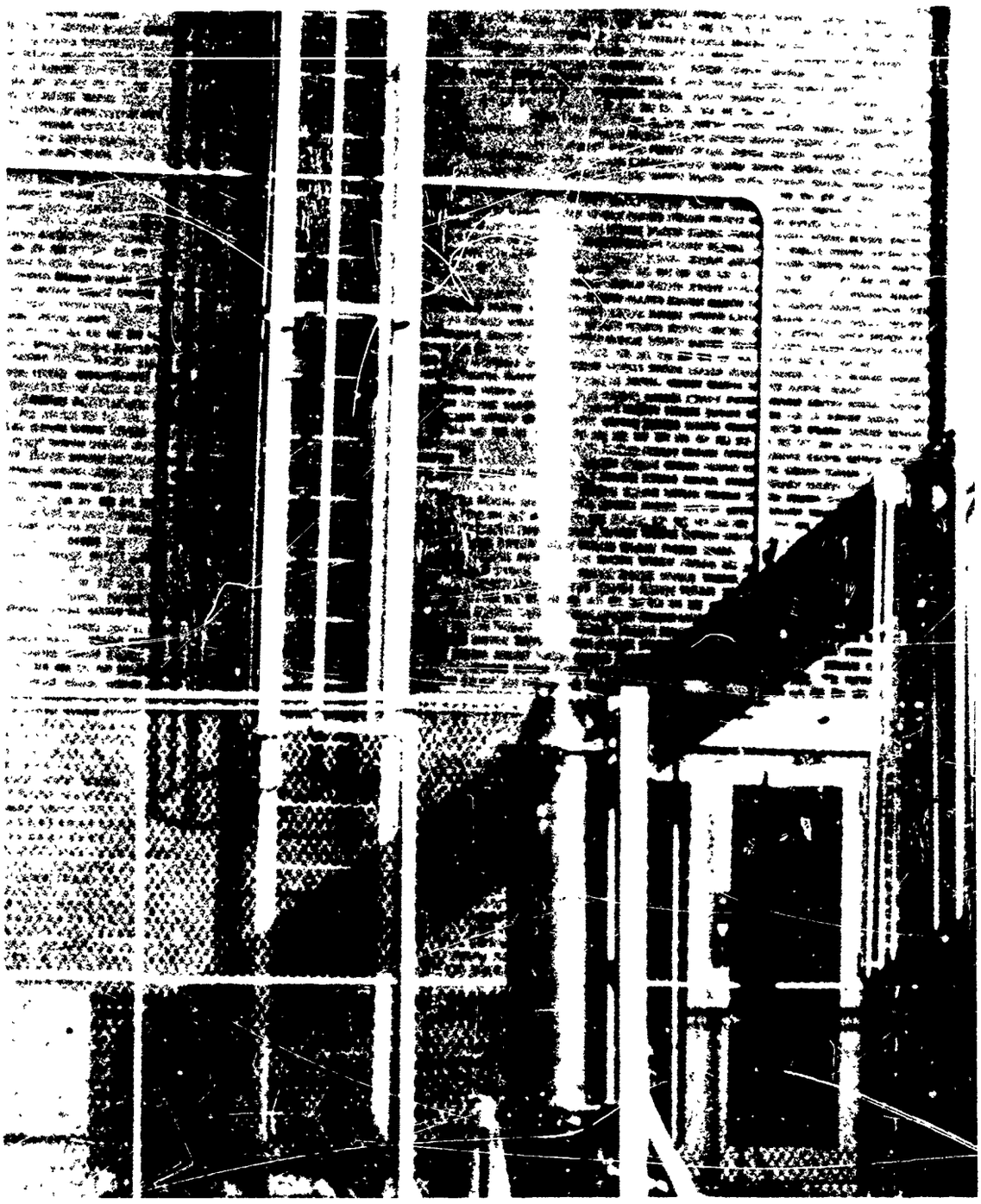

FIGURE 8. MODEL ENGINE, WITH MACH 1.5 NOZZLE, IN OPERATION

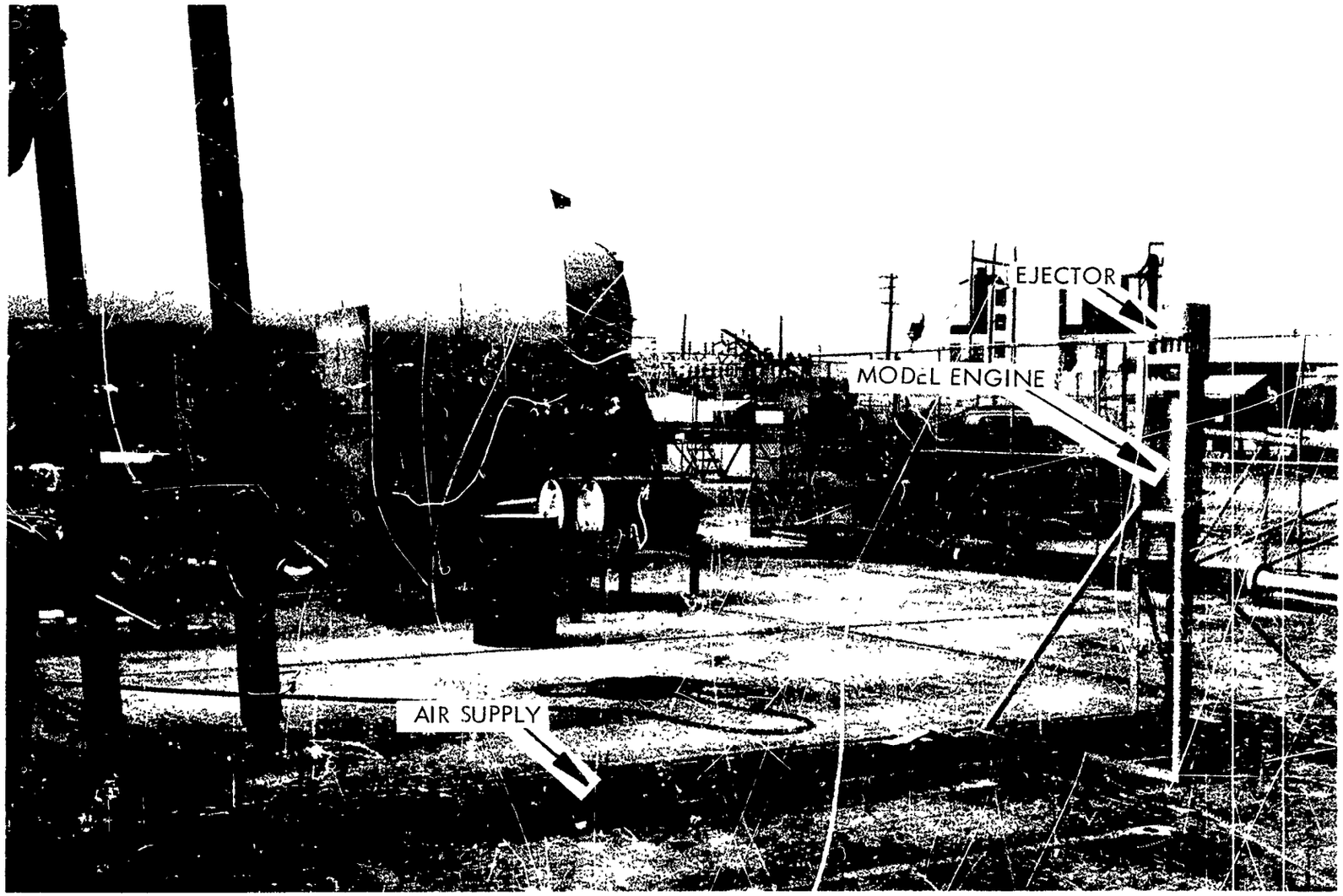

FIGURE 9. SET-UP FOR EJECTOR/NOZZLE CONFIGURATION

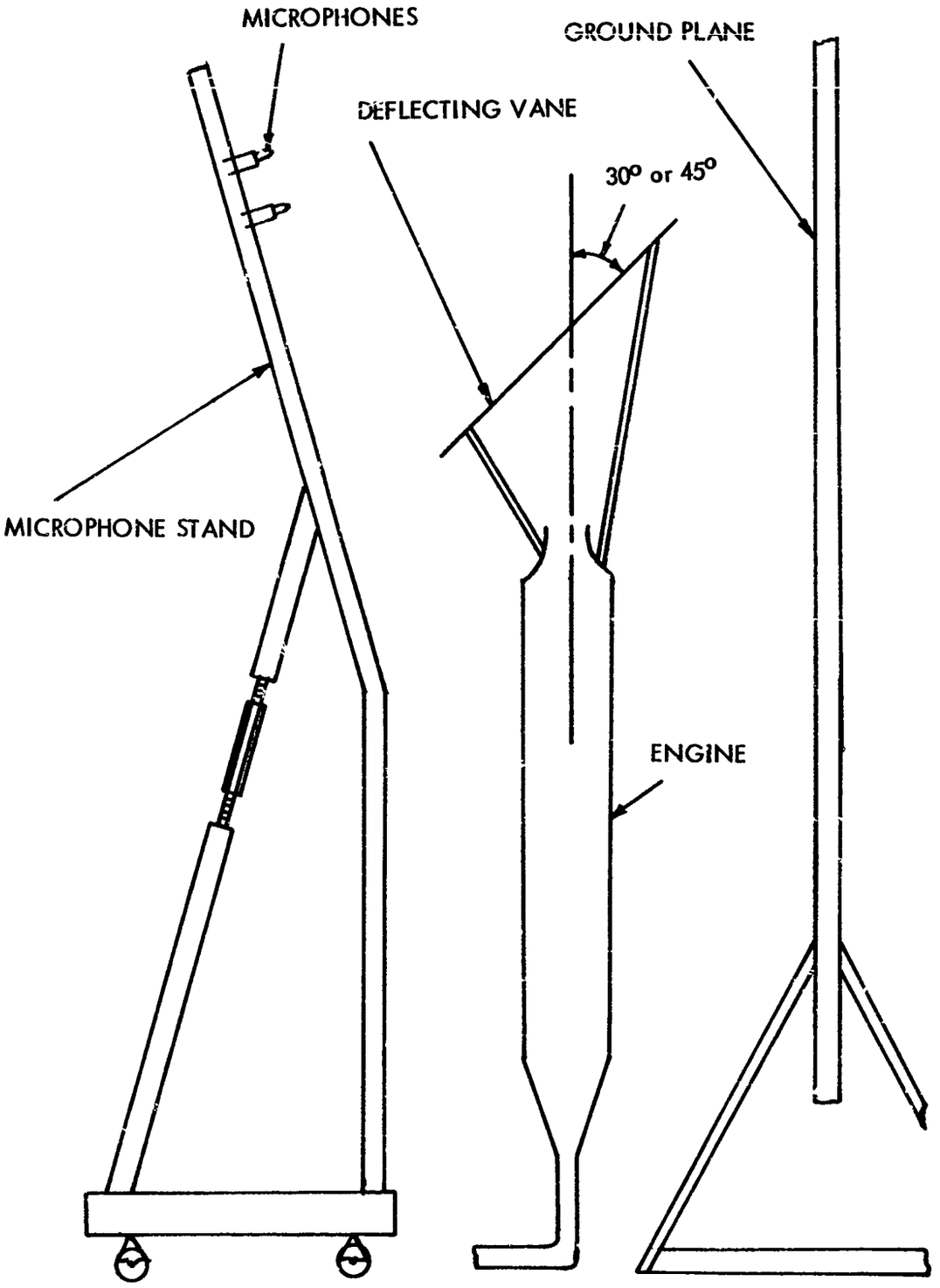

FIGURE 10. JET DEFLECTOR VANE CONFIGURATION

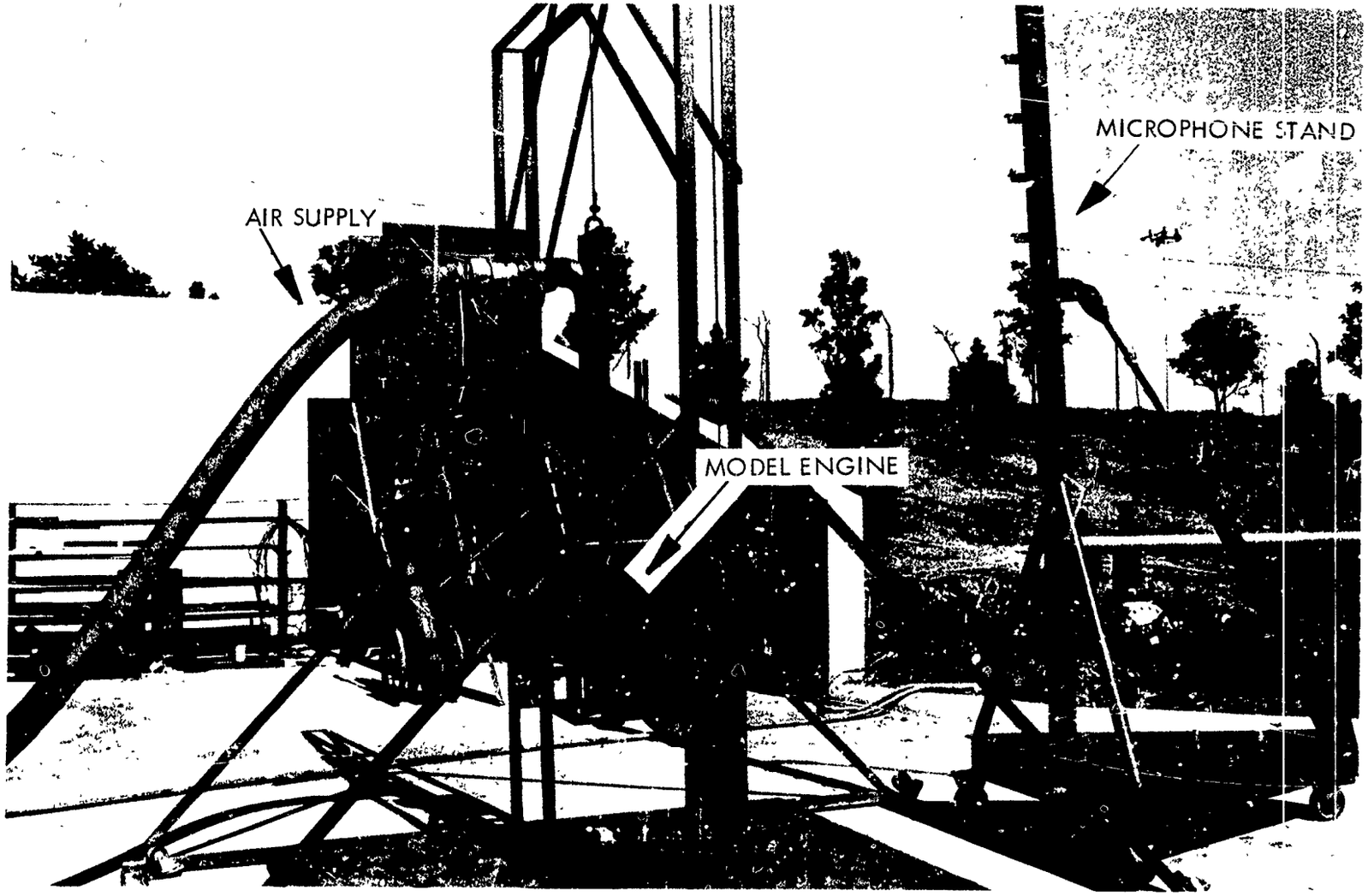

FIGURE 11. VTOL JET ARRANGEMENT

simultaneous octave bands and an overall band. The data had been recorded at 60 inches per second and contained data up to about 80 KHz. The upper cutoff frequency of the highest octave band was 10 KHz. To resolve this difference, the tape speeds were slowed by a factor of eight before analysis.

2. The frequency bands are converted into DC with a short time constant and fed into a 10-channel digitizing unit. Fifty-four samples were recorded for each data point in each frequency band.

3. The digital data samples are converted into rms sound pressure levels and a polynominal surface (cubic) is fitted through the data.

4. After the surface fit, many thousands of data points are calculated, and then the coordinates of constant-level contours are determined and plotted with a Cal. Comp. Model 765 incremental X-Y plotter. Figure 12 shows a typical output from the plotter. The contours, headings, contour identification, axes, and axis scaling are all accomplished in one operation by the plotter.

The advantage of this type of computerized display is obvious. The chance of introducing errors is greatly reduced, accuracy is increased, and consistency is introduced and maintained.

All the jet noise data obtained during this series of tests are presented in this manner. A complete set of contours for the overall and seven octave bands is given in Appendix II. The eighth octave band is not presented because of inconsistencies in the plots. It appears that the microphones did not have uniform high-frequency response (above 40 KHz).

E. Semi-Empirical Analysis

Over 1,000 technical papers, reports, and books have been published on the subject of jet noise. This collection of research originated with M. J. Lighthill in 1952 (Reference 10). His solution has been discussed, modified, or extended in many of the subsequent works.

Papers on near-field noise are only a small portion of the total collection on jet noise. References 1 through 6 provide some fairly useful information for predicting near-field noise based on measured data.

The only papers concerned with analytical methods are References 5 and 6. In Reference 5, Dahlen presents measured noise data and compares with results calculated from the theory of Franz (which is an extension of Lighthill's Theory), Reference 6.

Franz utilized the Lighthill solution (Equations 11 and 15, Reference 10) and obtained an expression for the sound pressure in the near field. The Lighthill solution used was:

$$p = -\frac{1}{4\pi}\int\left[\frac{\partial}{\partial x_i}\left(\frac{F_i}{r}\right) - \frac{\partial^2}{\partial x_i\,\partial x_j}\left(\frac{T_{ij}}{r}\right)\right] d\bar{y} \qquad (1)$$

where $F_i(\bar{y},t)$ is the i^{th} component of the instantaneous applied force or acoustic dipole strength per unit volume at time t and at point $\bar{y}$ in the turbulent region,

$T_{ij}(\bar{y},t)$ is the ij component of the instantaneous applied stress or acoustic quadrupole strength per unit volume at time t and at point $\bar{y}$ in the turbulent region,

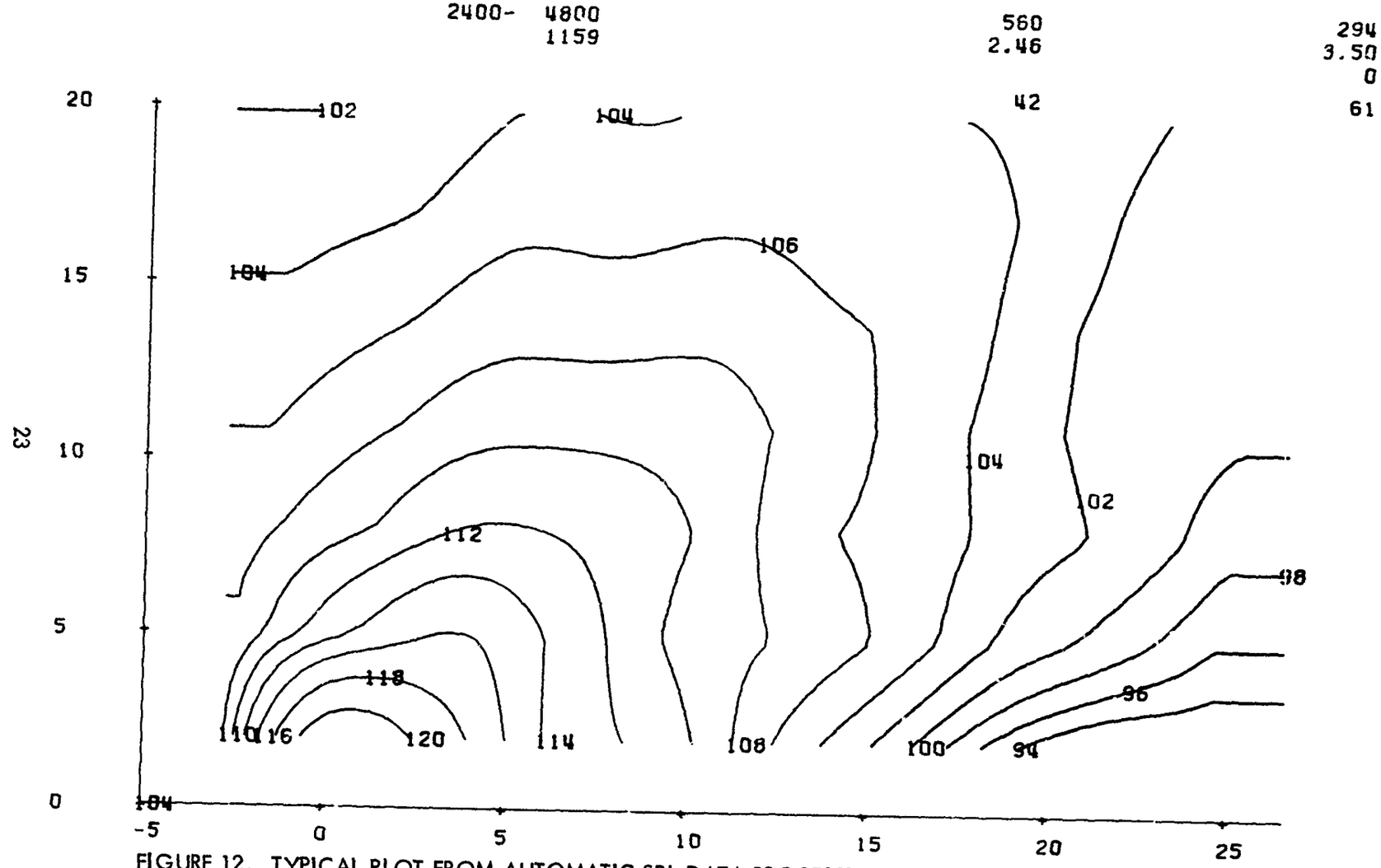

FIGURE 12. TYPICAL PLOT FROM AUTOMATIC SPL DATA PROCESSING SYSTEM

$$r = |\bar{x} - \bar{y}|.$$

The expanded solution contains $(1 - M \cos \theta)^{-1}$ terms and are, therefore, not realistic when M cos θ is near 1. The solution is also given in terms of quadrupole strength (which can be related to turbulence velocity). Although it is a logical approach, these shortcomings make practical applications impossible at high Mach numbers.

In Reference 2, Hermes and Smith present the most correlated set of jet noise data available. The data were measured in the near field of a J57-P21 for five different operating conditions: 50%, 70%, 96%, and 100% military thrust and afterburner. After removal of the effects of the reflecting ground plane by using Howes method (Reference 7), the directional characteristics of the data were removed in the annular region from 30° to 90° to the jet axis. The method used to take out directional effects is described by Ribner (Reference 8, pp 126-131). After normalization of the data for directionality, a velocity exponent was calculated for all the data points in the near field. The exponents ranged from 2.7 to 7.2; however, the median was 5.5 and the 80 percentile limits were 5.0 and 6.0.

Of all the references available, Reference 2 presents the most valid method for estimating near-field noise levels; however, if the 80 percentile extremes in velocity coefficients are considered, a difference of approximately 30 decibels will be observed in the total acoustic power (TAP) calculated from the relationship

$$TAP \propto V^n. \tag{2}$$

Differences of the magnitudes mentioned would not occur if ratios of jet velocity were used to modify existing data, since a change of 2 in velocity would give only a 3-decibel difference in TAP, using the 80 percentile limits.

1. Prediction Technique

Basically, all the previous methods are modified Lighthill solutions, trying to account for changes in the near field. It was decided that a different approach would be taken in this investigation.

A typical contour, Figure 13, reveals several characteristics. The source location is defined as the focus of the highest-intensity SPL contour on the jet boundary. A polar coordinate system is introduced with origin at the source location and with angle, θ, referenced to the jet centerline. Now, let the jet directivity factor be the SPL(r, θ) referenced to the SPL(r, 90°).

$$DF = SPL(r, \theta) - SPL(r, 90°) \tag{3}$$

Figure 14 is a plot of the measured directivity factor from the contours of Figure 13, plotted at a radius of 20 diameters. This directivity shape is about the same as the measured shapes shown in Figure 15 (from Reference 8) for the far field of three different jet engines. By checking the decay of SPL with distance, it has been experimentally determined that 20 diameters is, for all practical purposes, in the far field, except for angles less than 30° to 40°.

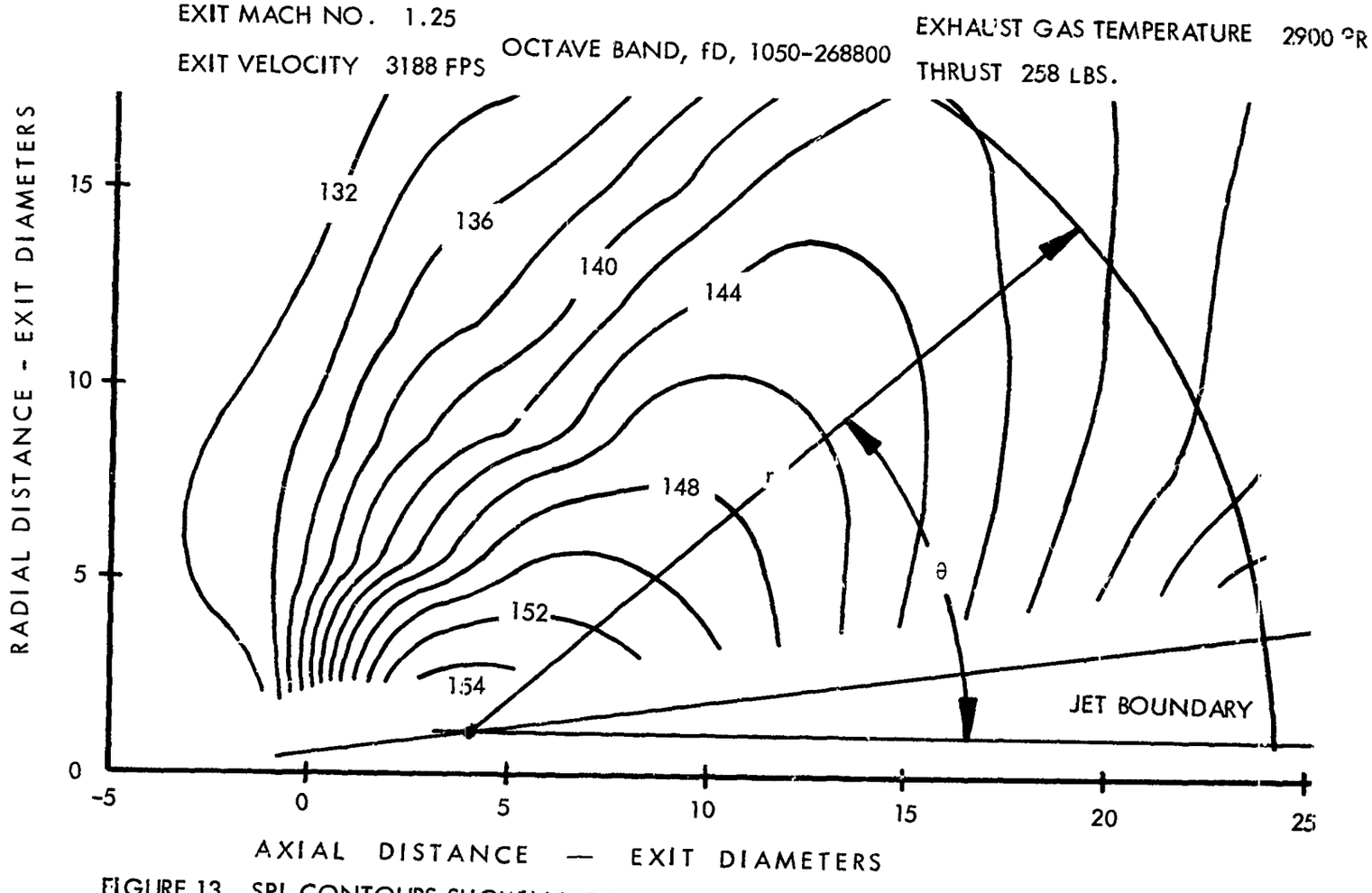

FIGURE 13. SPL CONTOURS SHOWING COORDINATE SYSTEM

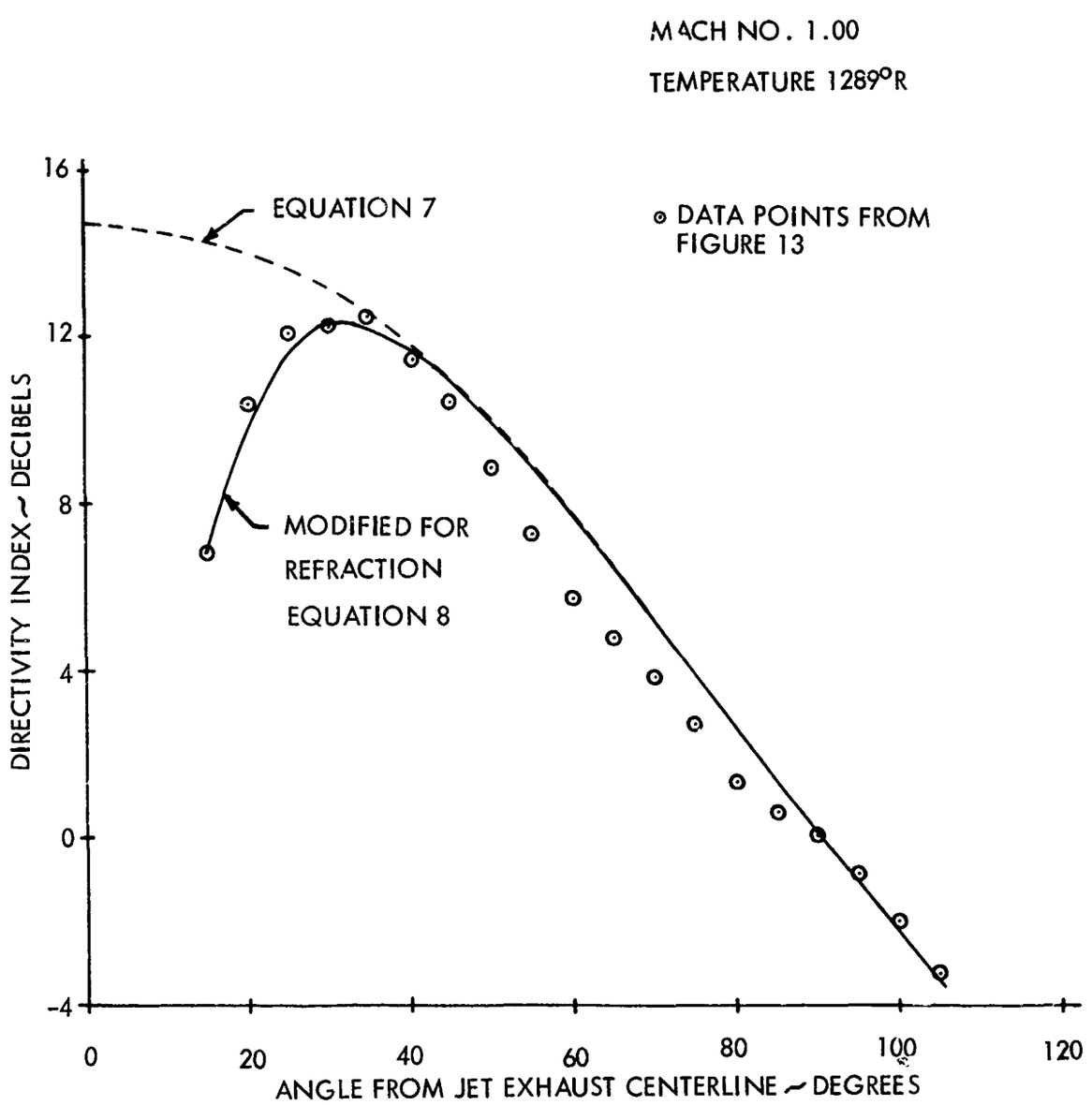

FIGURE 14. COMPARISON OF THEORETICAL DIRECTIVITY FACTOR, DIRECTIVITY FACTOR MODIFIED FOR REFRACTION, AND EXPERIMENTAL DATA

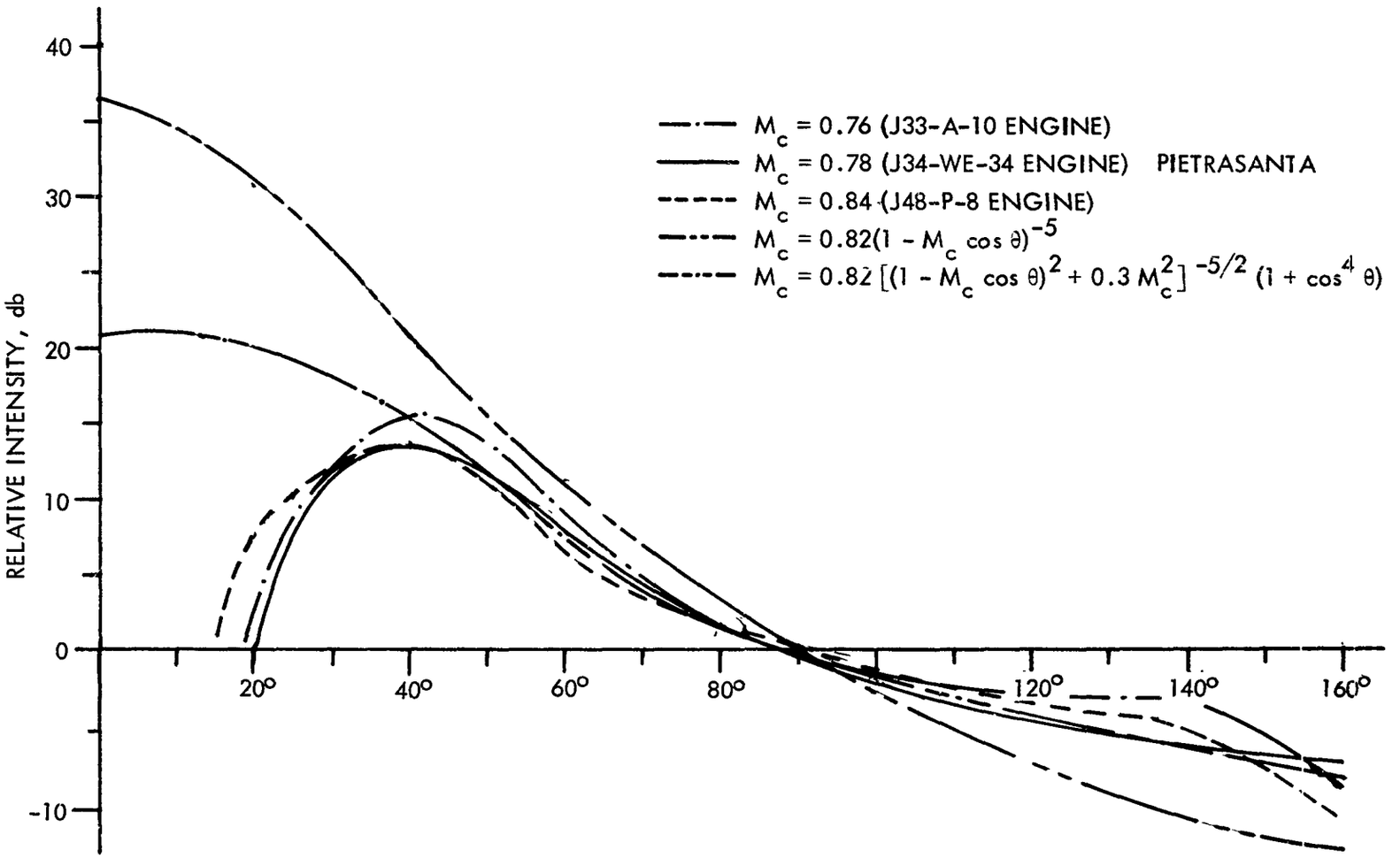

FIGURE 15. RELATIVE INTENSITY OF TURBOJET NOISE VERSUS ANGLE θ FROM FLOW DIRECTION (REFERRED TO ZERO db AT 90°). EXPERIMENTAL DATA FROM PIETRASANTA (9) IS COMPARED WITH THE THEORETICAL FACTORS. (ALLOWANCE IS NOT MADE FOR THE CUTOFF BELOW 40°, PRESUMABLY DUE TO REFRACTION.)

The directivity is governed by three distinct phenomena: convection, shear-noise emission, and refraction. In the far field, these effects are independent of distance from the source and can be separated from any decay terms due to distance. The initial convection term is attributed to Lighthill (Reference 10), who obtained a directivity approximation of the following form

$$(1 - M_c \cos\varphi)^{-6} \tag{4}$$

where M_c is defined as the eddy convection Mach number and

φ is the angle from the jet exhaust centerline, with the radius vector originating at the center of the exit plane.

As Ribner (Reference 8) points out, Williams (Reference 12) modified the -6 exponent to -5. The convection factor was further modified by Ribner and Williams (References 13-16) so that

$$C^{-5} = [(1 - M_c \cos\varphi)^2 + \alpha^2 M_c^2]^{-5/2}$$

where the term $\alpha^2 M_c^2$ tends to account for a finite eddy decay term.

The effect of shear-noise emission was derived by Lilley (Reference 11) and is approximately

$$(1 + \cos^4\varphi) \ . \tag{5}$$

Combining these two effects yields a directivity factor of the following form:

$$\frac{(1 + \cos^4\varphi)}{[(1 - M_c \cos\varphi)^2 + \alpha^2 M_c^2]^{5/2}} \tag{6}$$

Noting that since the directivity factor is usually normalized to 1 at 90°, this form is modified as shown below:

$$D.F. = \frac{(1 + \alpha^2 M_c^2)^{5/2} (1 + \cos^4\varphi)}{[(1 - M_c \cos\varphi)^2 + \alpha^2 M_c^2]^{5/2}} \tag{7}$$

If this form is to serve the near field as well as the far field, the angle φ must be changed to θ (i.e., the source location coordinates). Also, since the term M_c is somewhat nebulous in character, M will be substituted for M_c (since $\bar{\alpha}^2$ will be determined empirically over a complete range of temperature and Mach number).

This leaves the subject of refraction to be dealt with. Ribner (Reference 8) presents a somewhat rational analysis for refractive and diffractive effects through the jet flow; however, no practical results are obtained. But again examining Figures 13 and 14, it is observed that the directivity curve has an almost exponential roll-off below the peak angle. After examining all the data taken during the test phase of this program, it was determined that the final Ribner directivity factor should be modified to the following form for far-field noise contours:

$$D.F. = \frac{(1 + \alpha^2 M^2)^{5/2} (1 + \cos^4 \theta)}{[(1 - M \cos \theta)^2 + \alpha^2 M^2]^{5/2} (1 + C_4 e^{-C_5 \theta})} \tag{8}$$

There are three undetermined constants in Equation (8).

It is known that the curve of Equation (7) fits the data excellently for angles less than the angle of maximum directivity, provided the relationship for α is known. If the hypothesis is correct that α^2 is independent of Mach number, M, only a variation with temperature and frequency will occur. A typical curve calculated with the α^2 determined in this manner is shown in Figure 14. The coordinate system is that of Figure 13.

The term $\left(1 + C_4 e^{-C_5 \theta}\right)^{-1}$ will be calculated such that it reduces the curve of Equation (7) to the measured value at 15°, while decaying to a negligible effect at the measured peak. The effect of the approximate refraction correction is shown in Figure 14. Although no attempt has been made to give a physical explanation for the terms C_4 and C_5, Figure 14 reveals that this form of representation is adequate for an empirical approach.

It has been assumed so far that directivity is independent of distance from the source. However, observation of the experimental data indicates that significant changes in directivity occur as the source is approached. Examining a set of directivity curves in Figure 16 measured at 5, 10, and 20 exit diameters from the source, it can be seen that the angle of peak radiation traverses toward the axis of the jet for smaller values of r, and that the value of maximum directivity index is reduced for decreasing r. In fact, as r approaches the source, the contours are almost that of a simple source, modified by shear noise emission in some cases. In Figure 17, the contour at r = 1.75 diameters is almost that of a simple source, while in Figure 18, for a cold jet, the shape of the contour close to the source is almost exactly the $1 + \cos^4 \theta$ shape attributed to shear noise emission.

Two factors will be introduced to explain this change in contour shape. In an effort to avoid coupling effects in evaluating the constants, the factors will be included individually. The approximation chosen to produce the change in the directivity factor peak is given in the following equation.

$$DF' = \frac{(1 + \alpha^2 M^2)^{5/2} (1 + \cos^4 \theta)}{\left[\left(1 - \frac{M \cos \theta}{1 + C_6 e^{-C_7 r}}\right)^2 + \alpha^2 M^2\right]^{5/2} (1 + C_4 e^{-C_5 \theta})} \tag{9}$$

As the source is approached, the term $M \cos \theta / (1 + C_6 e^{-C_7 r})$ diminishes. The effect of this is to reduce the magnitude of the directivity factor. Another byproduct is that the term $1 + \cos^4 \theta$ becomes more important in controlling the angle of peak radiation.

The final modification in directivity factor shape arises from the nature of the contours at small angles in the very near field. Notice that the 134-decibel contour in Figure 19 exhibits the characteristic refractive effect at small angles. However, the 144-decibel curve has reversed this effect. The result is that the $C_4 e^{-C_5 \theta}$ term requires modification at small angles. It was found that a good approximation to this effect is obtained if the factor is modified as shown:

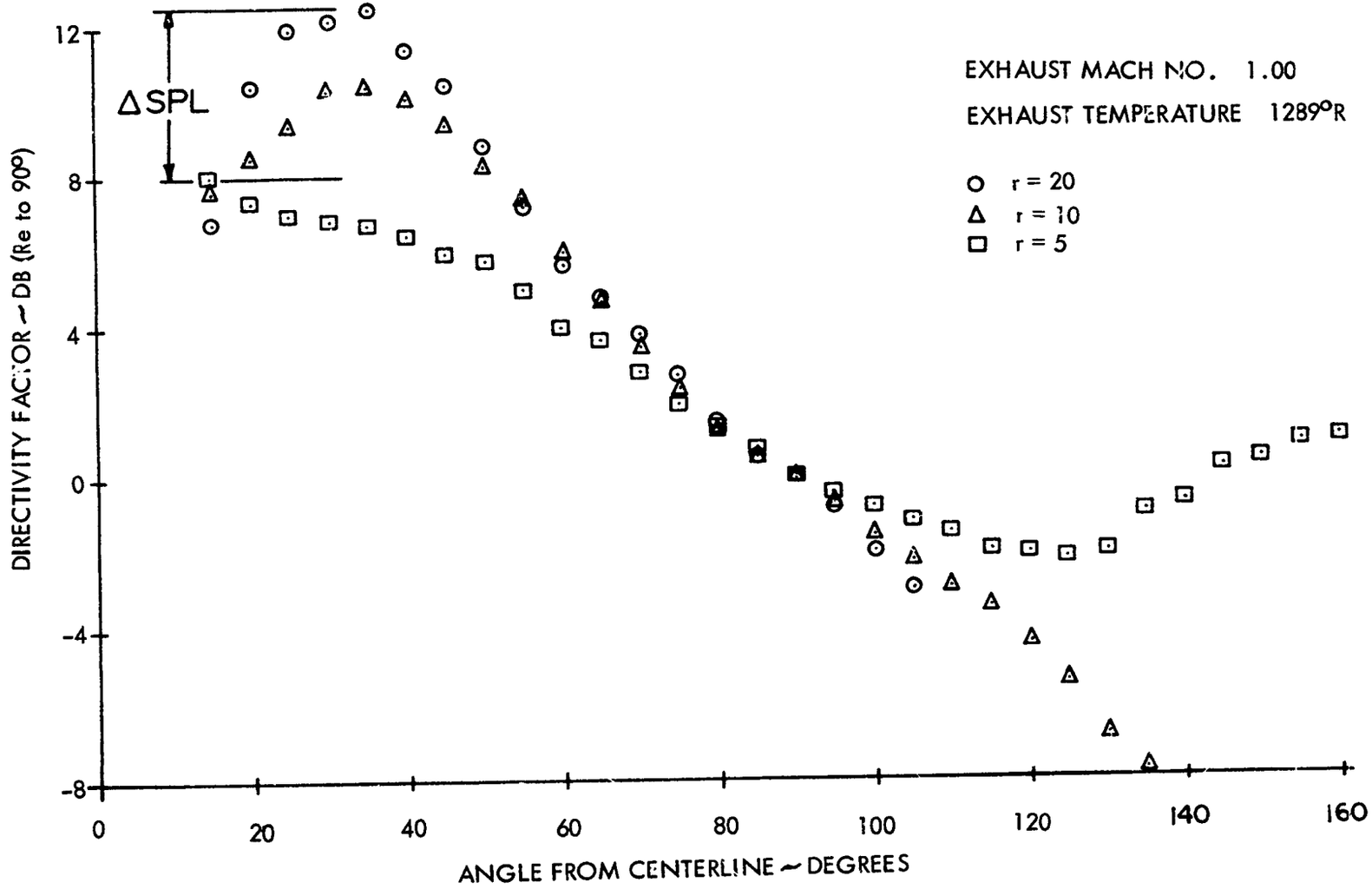

FIGURE 16. EFFECT OF DISTANCE FROM SOURCE ON DIRECTIVITY FACTOR

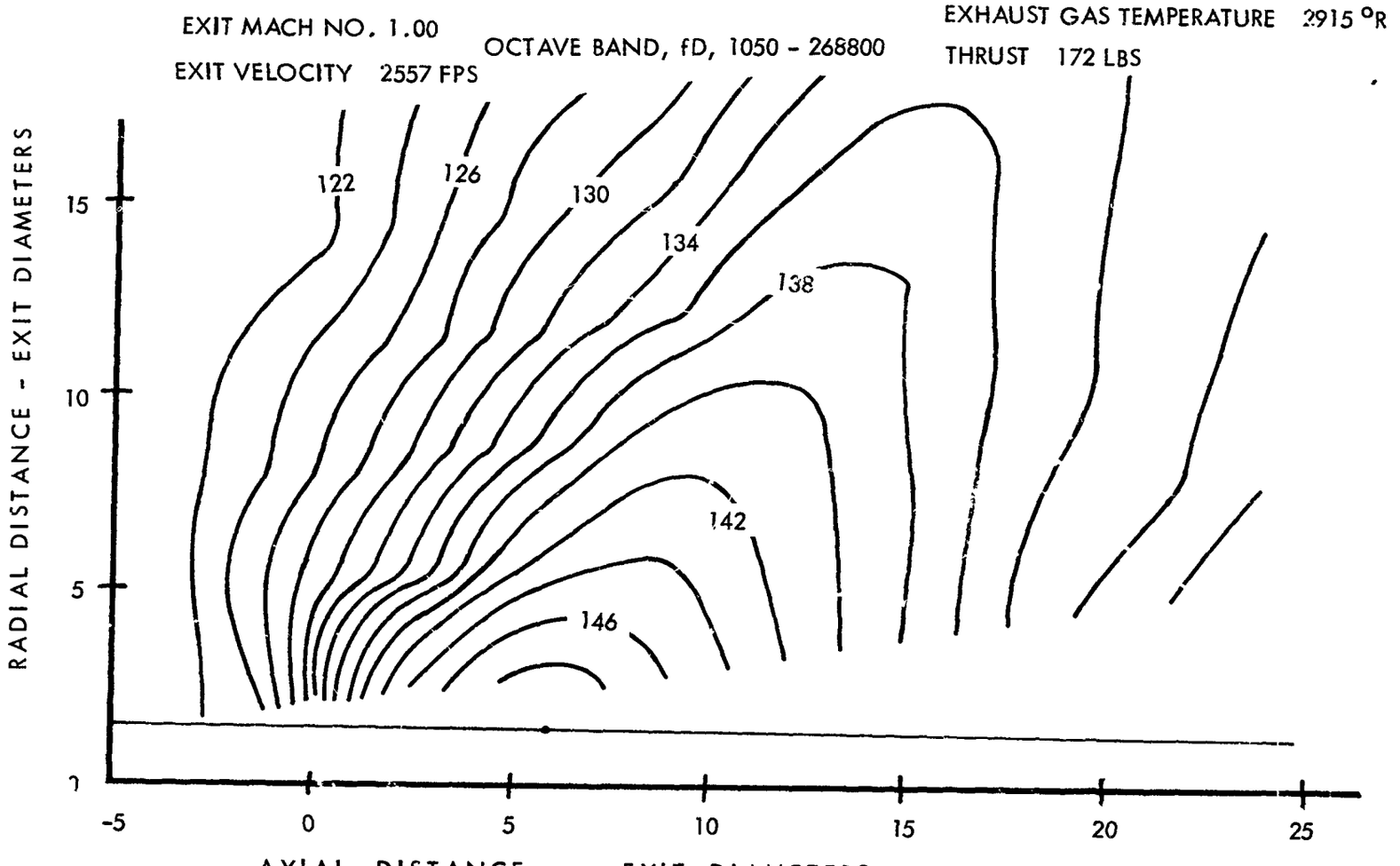

FIGURE 17. SHOWING MONOPOLE CHARACTER OF SOURCE

EXIT MACH NO. .80

EXHAUST GAS TEMPERATURE 1259 °R

OCTAVE BAND, fD, 1050 - 268800

EXIT VELOCITY 1714 FPS

THRUST 119 LBS.

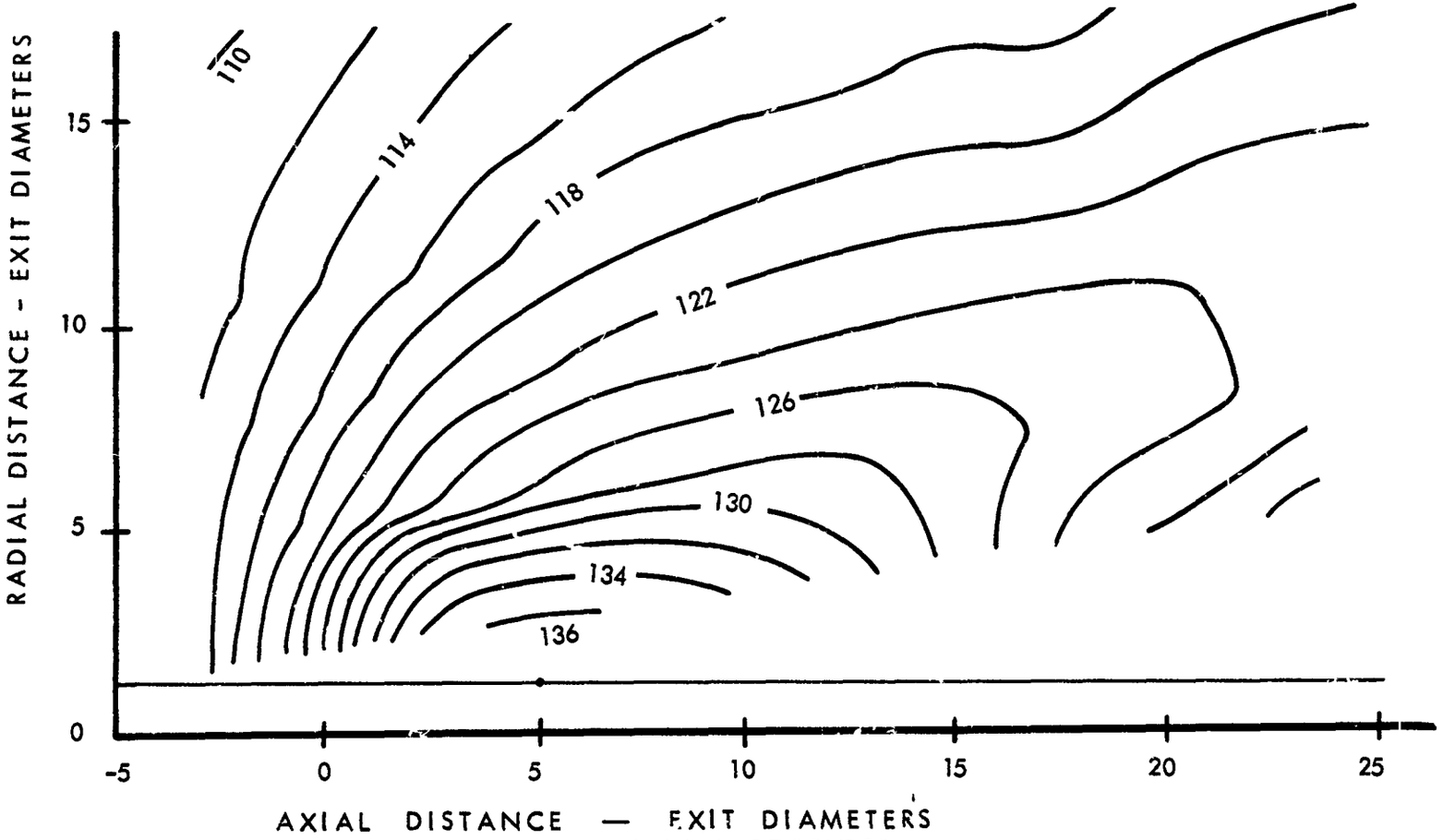

FIGURE 18. SHOWING SHEAR NOISE CHARACTER OF SOURCE

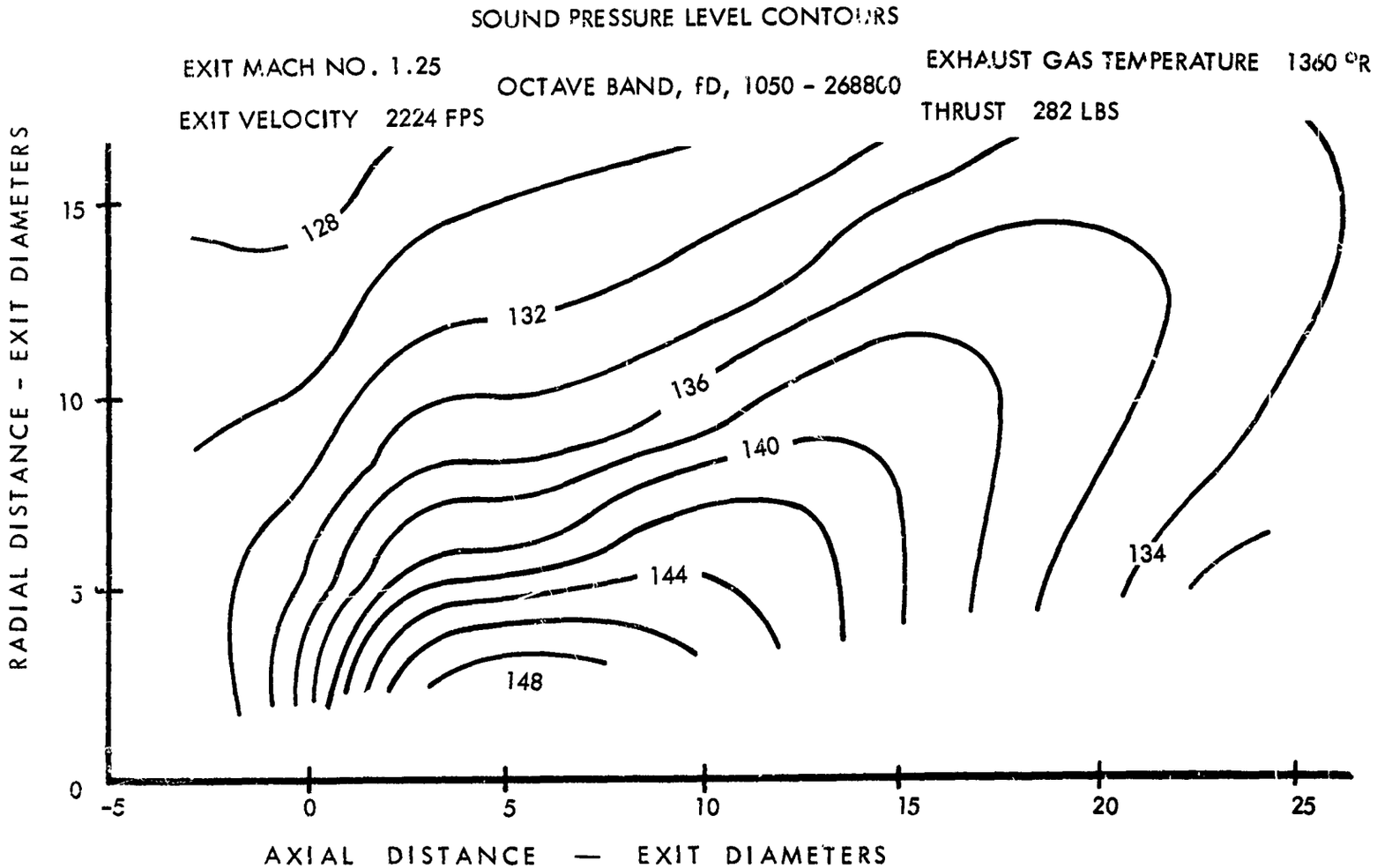

FIGURE 19. SHOWING EFFECT OF DISTANCE FROM SOURCE ON REFRACTION

$$\frac{C_4 e^{-C_5\theta}}{1 + C_6 e^{-C_7 r/4}} \tag{10}$$

Substitution into Equation (9) yields the final form of the Directivity Factor:

$$D.F. = \frac{(1 + \alpha^2 M^2)^{5/2} (1 + \cos^4\theta)}{\left[\left(1 - \frac{M \cos\theta}{1 + C_6 e^{-C_7 r}}\right)^2 + \alpha^2 M^2\right]^{5/2} \left(1 + \frac{C_4 e^{-C_5\theta}}{1 + C_6 e^{-C_7 r/4}}\right)} \tag{11}$$

(Evaluation of the functions α^2 and $C_1 - C_7$ will be discussed at the end of this subsection.)

The directivity factor has been of prime concern in this discussion. The effect of distance from the source, r, on sound pressure level has not been evaluated except where r modifies the directivity factor. Since the directivity factor is normalized to zero at 90°, it is convenient to evaluate the effect of distance on SPL at 90° to the jet centerline with origin at the source.

In all previous prediction methods it has been assumed that SPL varies as $1/r^n$, where n is a function of position in the near field. It seems more reasonable to assume that the SPL or mean square pressure, $\overline{p}^2$, is proportional to an inverse series in r^2 which has coefficients that are functions of velocity (or, more conveniently, Mach number and temperature).

The form assumed was

$$\overline{p}^2(r, \theta{=}90°) = \frac{C_1(T,M)}{r^2} + \frac{C_2(T,M)}{r^4} + \frac{C_3(T,M)}{r^6} \tag{12}$$

This approximation can be analytically verified to some extent by the work of Franz (Reference 6). In Franz's extension of Lighthill's theory, it is shown that the mean-square sound pressure for a single quadrupole is of the following form:

$$\overline{p}^2 \alpha \left(\tfrac{1}{2} \rho_o V^2\right)^2 \left(\frac{L^2}{r^2} M^4 + \frac{L^4}{r^4} M^2 + \frac{L^6}{r^6}\right). \tag{13}$$

The expression for a jet would not be expected to be identical to Franz's equation, but this derivation lends credence to the expression selected to represent the change in sound pressure level in the near field.

The functions, C_1, C_2, and C_3, are determined easily by using values of SPL at the point of maximum SPL, an intermediate point ($r \approx 5$), and the outer boundary of measurements ($r \approx 20$).

Three curves are compared in Figure 20. The inverse-square-law curve is first drawn using the value of SPL measured at 20 diameters, 90° to the jet axis. Next, a curve from measured data is shown. As the inverse-square-law curve approaches the source ($r = 0$),

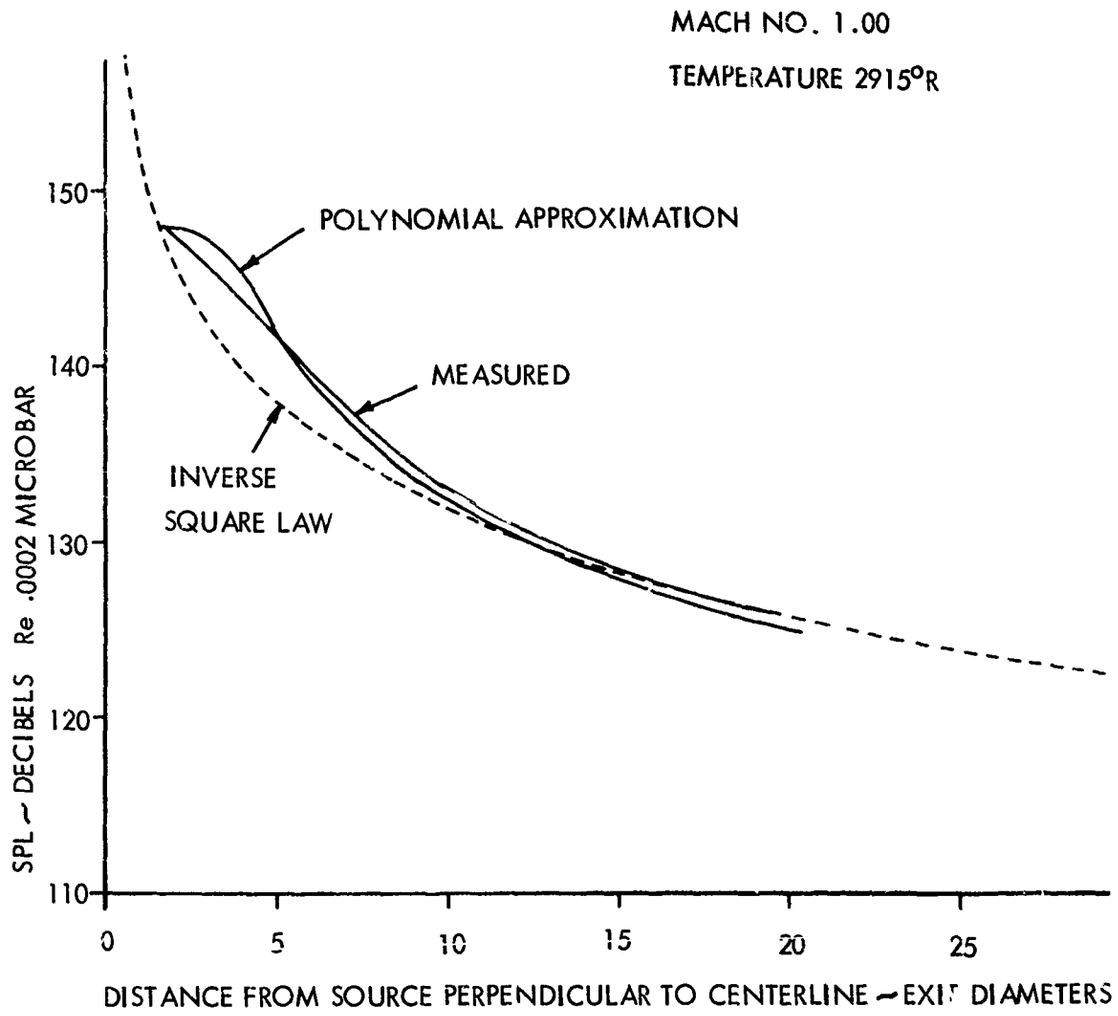

FIGURE 20. EFFECT OF DISTANCE FROM SOURCE ON SOUND PRESSURE LEVEL

the value of SPL increases without bound. But, examining the experimental curve, it is seen that as the source is approached, the slope of the curve decreases.

Also presented in Figure 20 is the polynomial approximation obtained by fitting to the measured values at r = 1.75, r = 5.0, and r = 20. The most prominent feature of the polynomial is the roll-off at small r. In evaluating the functions C_1, C_2, and C_3, it is found that C_1 and C_2 are always positive and that C_3 is always negative. Of course, the function reduces to the inverse-square law, C_1/r^2, at large r and in the intermediate range (from r = 5 to 15), C_2/r^4, contributes most significantly to the near-field characteristics. A convenient nomenclature for these terms is far-field $\sim C_1/r^2$, near-field $\sim C_2/r^4$, and near-near-field or induction near-field (after Franz) $\sim C_3/r^6$.

A calibration term is needed in calculating actual sound pressure levels, after the combination of Equations (11) and (12) which provide the sound field shape. It is, of course, expected that this calibration term will be a function of temperature and Mach number. If the Lighthill form of solution is accepted for the far field, this function will have the form:

$$\overline{p}^2(T,M) \underset{\substack{r=\text{const.}\\ \theta=\text{const.}}}{=} K T^s M^n \tag{14}$$

Combining Equations (11), (12), and (14) yields the final form of the expression which describes the near noise field of a jet engine, as presented in Equation (15).

$$\overline{p}^2(T,M,r,\theta) = \frac{KT^s M^n (1+\alpha^2 M^2)^{5/2} (1+\cos^4\theta)}{\left[\left(1 - \frac{M\cos\theta}{1+C_6 e^{-C_7 r}}\right)^2 + \alpha^2 M^2\right]^{5/2} \left(1 + \frac{C_4 e^{-C_5\theta}}{1+C_6 e^{-C_7 r/4}}\right)} \left(\frac{C_1}{r^2} + \frac{C_2}{r^4} + \frac{C_3}{r^6}\right) \tag{15}$$

The relationship of mean-square pressure with frequency has purposely been ignored in the development of Equation (15) because of the similarities of the contour plots for all frequency bands. The frequency relationship is introduced by calculating the functions $C_1 - C_7$, α^2, and KT^sM^n for each octave band and the overall band. Experimental evidence confirms that the sound pressure level in a scaled octave band for a scale model is equal to the sound pressure level in the unscaled octave band for the full-scale engine. Therefore, if spectrum level is required, the frequency limits on the full-scale band are first determined by dividing the scaled octave band limits, fD, by engine diameter, D. Then 10 Log_{10}(BW) is subtracted from the calculated sound pressure level, where BW is the full-scale bandwidth.

2. Evaluation of Empirical Functions

If the evaluation of the functions α^2, C_1 to C_7, and KT^sM^n were conducted under strict mathematical rules, they might never be determined. In certain ranges of the parameters r and θ, a high degree of coupling exists between all the above-mentioned functions. Therefore, it is advantageous to evaluate each of the functions in a range where it alone controls the SPL contours. This may not be possible in all instances, but the breakdown was made such that no more than three of the functions would have to be determined simultaneously. The functional grouping and evaluation was accomplished in the following manner:

(1) α^2 was evaluated separately in the approximate far field ($r \geq 15$ diameters). The conditions used to determine α^2 were the SPL at 90° and the SPL at the angle of peak directivity, at constant radius. These values, which in reality amount to the directivity factor at the angle of peak directivity, were used in Equation (7) to determine α^2.

(2) C_4 and C_5 were evaluated simultaneously at the radius used in the evaluation of α^2. The directivity factor at $\theta = 15°$ and at $\theta = \theta_{max} - 5°$ were used for determining C_4 and C_5. The criterion was that the modified directivity factor in Equation (9) be constrained to the measured directivity factor at these two values of θ. The value used for α^2 is that determined in step 1.

(3) C_6 and C_7 were determined from the difference in directivity factor peak at $r = 5$ diameters and $r = 20$ diameters. This value is the ΔSPL shown in Figure 16. The values of α^2, C_4, C_5, θ_{max} @ $r = 5$, θ_{max} @ $r = 20$, $r = 5$, $r = 20$, and ΔSPL were used in Equation (9) in the evaluation of C_6 and C_7.

(4) In the term, $1 + \dfrac{C_4 e^{-C_5\theta}}{1 + C_6 e^{-C_7 r/4}}$, the value of $C_6 e^{-C_7 R/4}$ was determined on a trial-and-error basis. Several values were used before selecting this particular combination.

(5) The decay terms C_1, C_2, and C_3 were evaluated at $\theta = 90°$. Examination of Equation (11) at $\theta = 90°$ reveals that the equation reduces to:

$$D.F. = \frac{1}{1 + \dfrac{C_4 e^{-C_5(\pi/2)}}{1 + C_6 e^{-C_7 r/4}}} \qquad (16)$$

The purpose of the decay term, $1 + C_4 e^{-C_5(\pi/2)}$, is to reduce the value of D.F. at small angles, while having minor effect at angles greater than θ_{max}. Therefore, at 90°,

$$D.F. \approx 1.$$

This allows the evaluation of C_1, C_2, and C_3 from the normalized values of SPL at three points along a radial vector projecting from the source, normal to the jet axis. As mentioned earlier, the radii chosen were $r \approx 2.0$, $r = 5.0$, and $r = 20.0$.

(6) After evaluation of all other functions, a magnitude was determined for each engine operational condition. This function comprises the KT^sM^n term.

These functions were evaluated at each basic engine operational condition as given in Table I. There were quite drastic changes in some of the functions for small changes in the parameters. In others, changes were more gradual. There was quite a bit of scatter in the calculated values. Therefore, to determine the functional relationship with Mach number and temperature, a first-order, least-square curve was fitted to the variation of the log f(T,M) versus log T. These least-square fits were determined for constant Mach number. The coefficients of the least-square fits were then plotted against Mach number,

and a least-square fit was made to these data. The final form of the functions is given in the following equations:

$$\alpha^2 = C_{i,1} M^{C_{i,2}} (T/1000)^{C_{i,3}+C_{i,4}M}$$

$$C_4 = C_{i,5} M^{C_{i,6}} (T/1000)^{C_{i,7}+C_{i,8}M}$$

$$C_5 = C_{i,9} M^{C_{i,10}} (T/1000)^{C_{i,11}+C_{i,12}M}$$

$$XO = C_{i,13} M^{C_{i,14}} (T/1000)^{C_{i,15}+C_{i,16}M}$$

where i denotes the octave band or overall band. The form determined for C_6 and C_7 is (they were not significantly affected by frequency):

$$C_6 = 17.5 \left(\frac{T}{3000}\right)^{.890(M^2-1)}$$

$$C_7 = 0.41 \left(\frac{T}{3600}\right)^{.566(M^2-1)}$$

The field functions were found to be (also not a function of frequency):

$$C_1 = M^{2.34}$$

$$C_2 = 10.65 \left(\frac{T}{T_o}\right)^{.93}$$

$$C_3 = -15.18 \left(\frac{T}{T_o}\right)^{1.11} M^{.89}$$

and finally the value for KT^sM^n was determined to be

$$KT^sM^n = C_{i,17} T^{1.54} M^4$$

The values of the constants $C_{i,j}$ are given in Table III. It is realized that some of the terms would be more pleasing if, for instance, instead of $T^{1.54}$, $T^{3/2}$ were substituted. However, this would and will wait until a suitable theoretical description is developed which allows rationalization of some of the powers.

Figure 21 shows the calculated values of α^2 plotted against temperature. Also given in the figure are the curves derived from the least-square fit. At 570°R extreme differences appear between the fitted values and the calculated values (empirically derived values). In spite of these differences, this method is justified because of the systemization which is effected. As shown below under sub-section G., the calculated contours are valid approximations.

TABLE III

COEFFICIENT MATRIX, C(MM, J)

	J/MM	1	2	3	4
α^2	1	0.8239	0.4176	0.32555	0.74038
	2	-1.24	-1.7269	0.2482	-3.4538
	3	-2.3019	-1.3226	-4.0206	-4.7181
	4	1.4745	1.3507	2.6807	3.2662
C_4	5	45.759	18.932	202.88	331.55
	6	-2.1086	-3.2199	3.8424	0.53294
	7	3.3692	1.3276	10.520	9.5983
	8	-2.3864	-0.1765	-8.0248	-6.829
C_5	9	12.808	8.4045	10.491	10.429
	10	-1.8167	-1.5494	-0.019983	0.36732
	11	-1.7894	-0.16571	0.73551	0.89132
	12	1.1641	0.22007	-0.76495	-0.87600
XO	13	4.512	5.2846	4.5428	2.6963
	14	-0.028729	1.3015	0.20763	1.8687
	15	0.789	0.85116	0.27691	3.0174
	16	-0.51772	-0.60053	0.036298	-2.1329
C_1	17	5.50×10^9	4.78×10^8	1.46×10^9	1.15×10^9

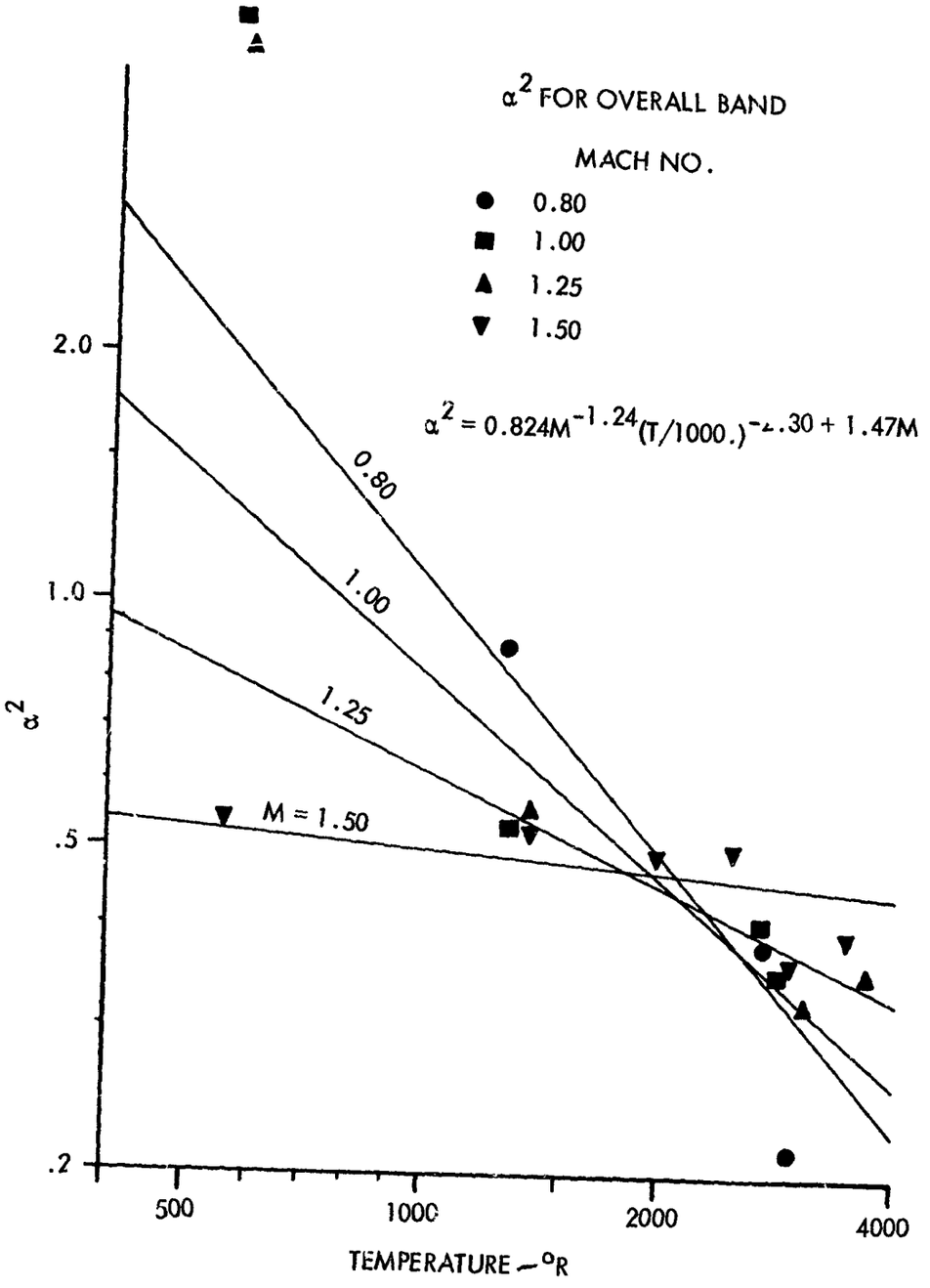

FIGURE 21. LEAST SQUARE CURVE FIT TO α^2

F. Computer Program for Calculating Jet Noise Contours

There were several ways that the semi-empirical relationship of Equation (15) could be used in calculating sound pressure levels. The most obvious would be to use the cartesian coordinates of a field point x,y and the calculated source location XO,YO to determine r and θ. The value of r and θ with a specified value of Mach number and temperature would then be substituted into Equation (15) to determine sound pressure.

However, since contours had been machine-plotted for all the experimental data, calculated constant-level contours for the predicted sound pressure levels would present a more desirable format for comparison. The program included in this section was formulated from that criterion.

The program is composed of a main or executive program and five subprograms. The function of the main program is to provide input data, change from polar to cartesian coordinates, call up the various subprograms, and write the calculated data. The heart of the program is subroutine SOND. This subroutine performs the calculation indicated by Equation (15). The constants, α^2 and $C_4 - C_7$, are calculated in subprogram SOND 1.

Subprogram BICT determines the value of radius, for an angle theta, where a particular sound pressure level occurs. In detail, the input to BICT is R1, R2, theta, and the increment in SPL contours, D. R1 is the smallest value of r, and R2 is the largest value. R1 should not be less than 1.5. First, BICT determines the SPL at R1 and then from this value calculates the maximum multiple of the increment D. Then, using the maximum level and the level at R2, the levels for each contour are determined. Once this is set up, an interative process between BICT and SOND is performed until the values of r for each contour are determined. This is repeated for each value of theta. Theta is determined as the initial value, TH(1), plus the increment, DTH, times the number of passes through the loop.

A typical output is shown in Figure 22. Listed at the top are the values of theta, the value of r for the maximum-level contour on a particular radius vector, the SPL for the maximum-level contour, the value of r for the minimum-level contour for the same radius vector, and the SPL for the minimum-level contour. The number of contour points found on a given radius vector is also listed. This number includes the two end points, which probably will not coincide with a contour.

Below this table are listed the input temperature, Mach number, and band number, MM, along with the calculated constants. The band number is described fully in the program comments. A typical plot is shown below the table. The resolution on points is ± 0.083" in the vertical direction and ± 0.050" horizontally. The size of a plot is 10" x 10". (Options on scaling are explained in the subroutine comments.)

The input constants C(I,J) are listed at the end of the program. These values, comprising the first nine lines of input data, are necessary for the calculation of contours and should not be changed. (The constants have been calculated for the overall and 3 octave bands.) The other data are variable and may be changed as desired. (A full description of the input data is included in the program comments.)

This program has been compiled on both the IBM 360-50 remote access system and the Univac 418 computer. The Fortran IV language is not machine-oriented.

NO PTS	THETA	R(2,J)	SPL(2)	R(L,J)	SPL(L)
4	10.000	3.641	130.000	27.199	120.000
4	15.000	17.704	130.000	34.478	120.000
4	20.000	21.675	130.000	44.219	120.000
3	25.000	25.555	130.000	25.555	130.000
4	30.000	3.203	140.000	28.832	130.000
3	35.000	25.378	130.000	30.378	130.000
4	40.000	3.167	140.000	29.007	130.000
3	45.000	25.020	130.000	25.020	130.000
4	50.000	2.938	140.000	20.167	130.000
4	55.000	15.574	130.000	47.243	120.000
4	60.000	10.677	130.000	36.991	120.000
4	65.000	7.115	130.000	29.123	120.000
5	70.000	2.606	140.000	23.232	120.000
4	75.000	5.753	130.000	18.821	120.000
5	80.000	5.427	130.000	46.074	110.000
5	85.000	5.178	130.000	37.876	110.000
6	90.000	2.425	140.000	31.571	110.000
4	95.000	10.062	120.000	26.677	110.000
5	100.000	4.665	130.000	22.877	110.000
4	105.000	8.610	120.000	19.923	110.000
6	110.000	2.294	140.000	17.662	110.000
5	115.000	7.824	120.000	46.668	100.000
6	120.000	4.314	130.000	42.127	100.000
5	125.000	7.396	120.000	38.686	100.000
7	130.000	2.288	140.000	36.125	100.000
5	135.000	7.194	120.000	34.248	100.000
6	140.000	4.293	130.000	32.896	100.000
5	145.000	7.127	120.000	31.946	100.000
7	150.000	2.414	140.000	31.290	100.000
5	155.000	7.125	120.000	30.848	100.000
6	160.000	4.412	130.000	30.557	100.000
5	165.000	7.145	120.000	30.369	100.000
7	170.000	2.524	140.000	30.257	100.000
5	175.000	7.160	120.000	30.197	100.000
6	180.000	4.472	130.000	30.177	100.000

MACH NO	TEMPERATURE	ALPHA**2	C4	C5	C6	C7	IT1
0.92000E 00	0.18900E 04	0.11855E 00	0.10849E 04	0.10723E 02	0.18641E 02	0.18641E 02	3

XO = 5.4399Y0 = 1.2105

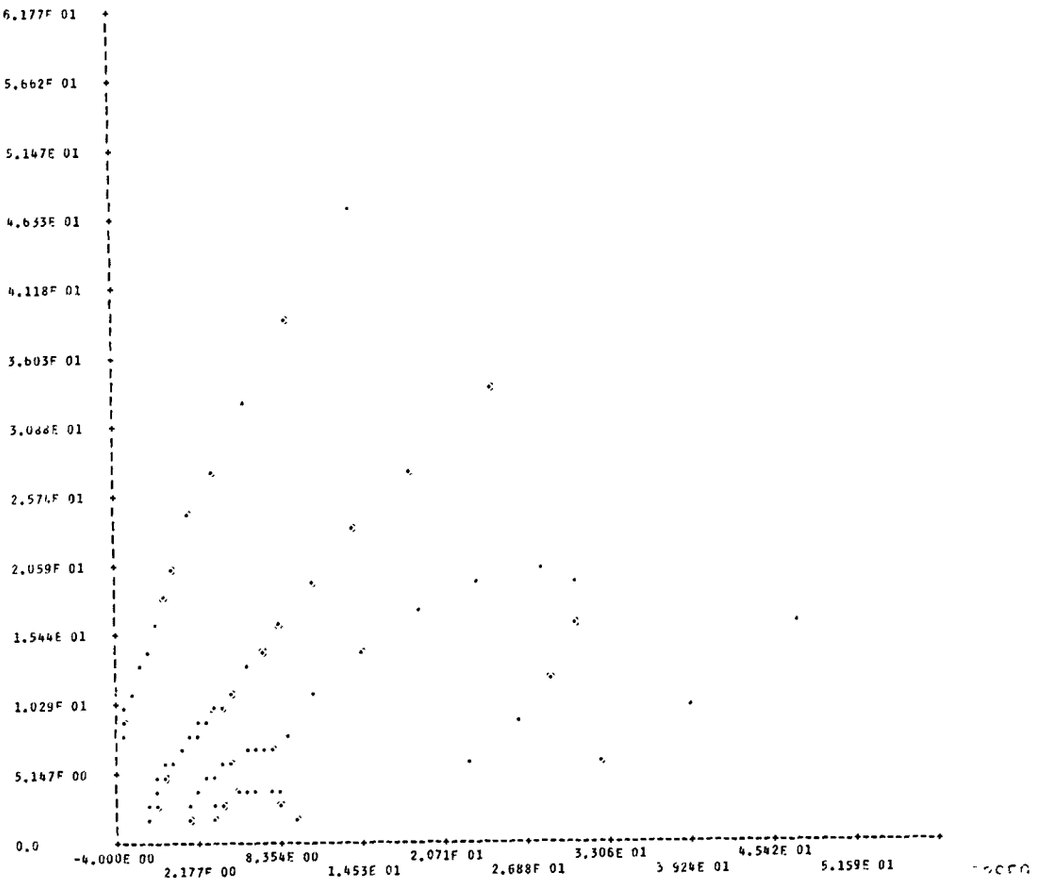

FIGURE 22. OUTPUT FROM SPL CONTOUR PROGRAM (SHEET 1 OF 10)

```
*EXECUTE SOUND
*COMPILE SOUND INPUT CARDS OUTPUT TAPE LIST SOURCE
      DIMENSION F(16,37),R(16,37),C(17,4),TH(37),IR(37),X(600),Y(600)
      COMMON IRD,IPR,C,ALP,DM,T,C4,C5,C6,C7,MM,F,R
C
C ////////////////////////////
      IRD=1
      IPR=2
C    IRD = SYSTEM INPUT  UNIT DATA SET NUMBER.
C    IPR = SYSTEM OUTPUT UNIT DATA SET NUMBER.
C ////////////////////////////////
C
      WRITE(IPR,9)
      READ(IRD,1)((C(I,J),J=1,4),I=1,17)
      WRITE(IPR,10)((C(I,J),J=1,4),I,I=1,17)
C
C THESE ARE THE COEFFICIENTS FOR THE NEAR-FIELD FUNCTIONS.
C
   99 READ(IRD,2)R1,R2,TH(1),DTH,N,D
      WRITE(IPR,10)R1,R2,TH(1),DTH,N,D
C
C R1 IS THE SMALLEST VALUE OR RADIUS FOR CALCULATING SPL, AND R2 IS THE
C LARGEST VALUE.  $$$  R1 IS ALWAYS GREATER THAN 1.50 $$$.
C TH(1) IS THE SMALLEST VALUE OF THETA FOR CALCULATING SPL.
C    $$$  TH(1) IS ALWAYS GREATER THAN 7.50 DEGREES.  $$$
C DTH IS THE INCREMENTAL VALUE OF THETA.  IT WILL BE ADDED N TIMES.
C D IS THE INCREMENT FOR SOUND PRESSURE LEVEL CONTOURS.
C
  100 READ(IRD,2)XL,XH,YL,YH,IPL
      WRITE(IPR,10)XL,XH,YL,YH,IPL
C
C SEE PLOTX ROUTINE FOR DEFINITION OF THESE VARIABLES.
C SET IPL TO -1 IF NEW VALUES FOR R1,R2,TH(1),DTH,N,D, ARE NEEDED.
C
      IF(IPL)99,180,180
  180 READ(IRD,3)DM,T,MM
C
C DM IS THE ENGINE MACH NUMBER.
C T  IS THE EXHAUST PLANE TEMPERATURE.
C /////// OCTAVE BAND NUMBER.  /////
C      MM = 1, OVERALL BAND, FD = 1050.0 TO 268800.0.
C      MM = 2, FD = 2100.0 TO 4200.0.
C      MM = 3, FD = 4200.0 TO 8400.0.
C      MM = 4, FD = 8400.0 TO 16800.0.
C SET DM = MACH NO. = 0.0 WHEN A NEW PLOT LIMIT FRAME OR CHANGE IN PLOT
C CODE IS REQUIRED.
C
      IF(DM)101,100,101
  101 CALL SOND1
      WRITE(IPR,9)
      NN=1
      CALL BICT(R1,R2,NN,TH(1),D,IR(1))
      DO 200 I=2,N
      IJ=I-(I/4)*4+1
```

FIGURE 22. (SHEET 2 OF 10)

```
      GOTO(203,201,203,202),IJ
  203 R3=2.5*R1
      GOTO 204
  202 R3=1.5*R1
      GOTO 204
  201 R3=R1
  204 TH(I)=TH(I-1)+DTH
      NN=I
      CALL BICT(R3,R2,NN,TH(I),D,IR(I),
  200 CONTINUE
      WRITE(IPR,9)
      WRITE(IPR,7)
      NM=0
      K=0
      I=MM
C
C CARTESIAN COORDINATES OF SOUND SOURCE LOCATION.
C
      XO=C(13,I)*DM**C(14,I)*(T*.001)**(C(15,I)+C(16,I)*DM)
      YO=.1316525*XO+.50
      DO 300 J=1,N
      L=IR(J)-1
      WRITE(IPR,4)IR(J),TH(J),R(2,J),F(2,J),R(L,J),F(L,J)
      NM=NM+L
      CT=COS(TH(J)*.01745329)
      ST=SIN(TH(J)*.01745329)
C
C CONVERT FROM POLAR TO CARTESIAN COORDINATES.
C
      DO 300 I=2,L
      K=K+1
      X(K)=CT*R(I,J)+XO
      IF(IPL)301,301,303
C
C IF IPL = 0 DO NOT SUPPRESS POINTS.
C IF IPL IS GREATER THAN ZERO ELIMINATE ALL POINTS OUTSIDE OF
C PICTURE FRAME SPECIFIED BY INPUT DATA XL AND XH.
C
  303 CALL REGION(XL,XH,X(K),IJ)
      GOTO(301,302),IJ
  301 Y(K)=ST*R(I,J)+YO
      YBL=X(K)*.1316525+.50
      CALL REGION(YBL,YH,Y(K),IJ)
      GOTO(300,302),IJ
  302 K=K-1
  300 CONTINUE
      WRITE(IPR,6)
      WRITE(IPR,5)DM,T,ALP,C4,C5,C6,C7,MM
      WRITE(IPR,8)XO,YO
      CALL PLOTX(X,Y,K,XL,XH,YL,YH,IPL)
      GOTO 180
    1 FORMAT(8E10.5)
    2 FORMAT(4F10.9,I2,8X,F10.9)
```

FIGURE 22. (SHEET 3 OF 10)

```
    3 FORMAT(2F10.9,I2)
    4 FORMAT(I4,5F8.3)
    5 FORMAT(7E13.5,I4)
    6 FORMAT(37H0    MACH NO.    TEMPERATURE    ALPHA**2,8X,2HC4,11X,
     12HC5,11X,2HC6,11X,2HC7,7X,2HMM)
    7 FORMAT(43H NO.  THETA   R(2,J) SPL(2)  R(L,J)  SPL(L),/,4H PTS)
    8 FORMAT(6H0X0 = ,F8.4,7H  Y0 = ,F8.4)
    9 FORMAT(1H1)
   10 FORMAT(4E20.8,I4)
      END
```

FIGURE 22. (SHEET 4 OF 10)

```
*COMPILE PLOTX INPUT CARDS OUTPUT TAPE LIST SOURCE
      SUBROUTINE PLOTX(X,Y,N,XL,XH,YL,YH,II)
      DIMENSION A(101),X(1),Y(1),AXIS(5)
      COMMON IRD,IPR
C
C NOTE    POINTS GIVEN NEED NOT BE IN ORDER - THIS ROUTINE RE-ORDERS THE
C     DATA AS NECESSARY.  THUS, AFTER PLOTTING, THE GIVEN POINTS ARE NOT
C     NECCESARILY IN THE SAME ORDER AS THEY WERE BEFORE THIS ROUTINE WAS
C     CALLED.
C     X   IS THE ARRAY OF X CO-ORDINATES.
C     Y   IS THE ARRAY OF Y CO-ORDINATES.
C     N   IS THE NO. OF (X,Y) POINTS.
C         IF II = 1 THEN -----
C     XL  IS THE BEGINNING VALUE OF X PRINTED ON THE X AXIS.
C     XH  IS THE LAST VALUE OF X PRINTED ON THE X AXIS.
C     YL  IS THE  BEGINNING VALUE OF Y PRINTED ON THE Y AXIS.
C     YH  IS THE LAST VALUE OF Y PRINTED ON THE Y AXIS.
C     II  =0 WILL CAUSE THE LOWEST AND HIGHEST VALUES IN THE X AND
C         Y ARRAY TO BE USED FOR THE LIMITS OF THE X AND Y AXES OF
C         THE PRINTED GRAPH.
C         =1 WILL CAUSE THE VALUES GIVEN TO XL,XH,YL, AND YH, IN THE
C         CALLING SEQUENCE, TO BE USED AS THE LIMITS FOR THE
C         X AND Y AXES.
C
      DATA HOLI,BLNK,BIT,CRO,FMS/1HI,1H ,1H.,1H+,1H-/
      WRITE(IPR,100)
  100 FORMAT(1H1)
      XSM=X(1)
      XLA=X(1)
      L1=N-1
      DO 2 I=1,L1
      L2=I+1
C
C     ***** THIS SECTION REARRANGES THE GIVEN DATA
C     IN ORDER OF DECREASING Y VALUES,I.E.,
C     YMAX=Y(1) AND YMIN=Y(N).
C
      DO 2 J=L2,N
      IF(Y(I)-Y(J))1,2,2
    1 DUM=Y(I)
      Y(I)=Y(J)
      Y(J)=DUM
      DUM=X(I)
      X(I)=X(J)
      X(J)=DUM
    2 CONTINUE
C     *****
      IF(II)10,10,11
   11 XSM=XL
      XLA=XH
      YSM=YL
      YLA=YH
      GOTO 12
```

FIGURE 22. (SHEET 5 OF 10)

```
   10 DO 6 L2=1,N
      IF(XSM-X(L2))4,4,3
    3 XSM=X(L2)
    4 IF(XLA-X(L2))5,6,6
    5 XLA=X(L2)
    6 CONTINUE
      YSM=Y(N)
      YLA=Y(1)
   12 DX=(XLA-XSM)/100.
      DY=(YLA-YSM)/60.
      IP=0
      LIN=0
      A(1)=HOLI
   13 LIN=LIN+1
      DO 14 I=2,101
   14 A(I)=BLNK
      IF(LIN-60)15,15,23
   15 IP=IP+1
      IF(IP-N)16,16,20
   16 RAT=60-LIN
      IF(Y(IP)-YSM-DY*RAT)20,17,17
   17 DO 19 I=2,101
      RAT=I-1
      IF(X(IP)-XSM-DX*RAT)18,18,19
   18 A(I)=BIT
      GOTO 15
   19 CONTINUE
      GOTO 15
   20 IP=IP-1
      IF(MOD(LIN,6)-1)22,21,22
   21 RAT=61-LIN
      DUM=YSM+DY*RAT
      WRITE(IPR,101)DUM,CRO,(A(I),I=2,101)
      GOTO 13
   22 WRITE(IPR,102)(A(I),I=1,101)
      GOTO 13
   23 DO 25 I=1,101
      A(I)=FMS
      IF(MOD(I,10)-1)25,24,25
   24 A(I)=CRO
   25 CONTINUE
      WRITE(IPR,101)YSM,(A(I),I=1,101)
      DO 26 I=1,5
      A(I)=HOLI
      RAT=(I-1)*20
   26 AXIS(I)=XSM+DX*RAT
      WRITE(IPR,103)(AXIS(I),A(I),I=1,5)
      DO 27 I=1,5
      RAT=I*20-10
   27 AXIS(I)=XSM+DX*RAT
      WRITE(IPR,104)(AXIS(I),I=1,5)
  101 FORMAT(1X,1PE15.3,3X,101A1)
  102 FORMAT(19X,101A1)
  103 FORMAT(10X,5(1PE14.3,5X,A1))
```

FIGURE 22. (SHEET 6 OF 10)

```
  104 FORMAT(14X,5(5X,1PE15.3))
      RETURN
      END



*COMPILE BICT INPUT CARDS OUTPUT TAPE LIST SOURCE
      SUBROUTINE BICT(R1,R2,N,TH,D,IR)
C
C THIS ROUTINE USES A RECURSIVE INTERPOLATION SCHEME KNOWN AS REGULA
C FALSI ( FALSE POSITION).  ALTHOUGH CONVERGENCE IS THEORETICALLY
C GUARANTEED, CERTAIN SPECIAL CASES MAY CONVERGE VERY SLOWLY WHEN DY/DX
C IS RELATIVELY LARGE.
C
      DIMENSION F(16,37),R(16,37),X(3),Y(3),CC(17,4)
      COMMON IRD,IPR,CC,ALP,DM,T,C4,C5,C6,C7,MM,F,R
      TH=TH
      N=N
      E=.01
      IR=0
      XL=AMIN1(R1,R2)
      YH=AMAX1(R1,R2)
   10 CALL SOND(TH,XL,YL)
      CALL SOND(TH,XH,YH)
      C=ABS(D)
      F(1,N)=YL-AMOD(YL,C)
C
C F(1,N) NOW EQUALS THE LARGEST MULTIPLE OF D WHICH IS
C LESS THAN YL.
C
      X(3)=1.0
      IF(YH-YL)11,12,12
   11 C=-C
      F(1,N)=F(1,N)-C
      X(3)=-1.0
C
C COMPUTE ALL INTEGRAL MULTIPLES OF D WHICH LIE BETWEEN YL AND YH.
C
   12 DO 20 I=2,30
      IR=I-1
      F(I,N)=F(IR,N)+C
      IF((F(I,N)-YH)*X(3))20,20,21
   20 CONTINUE
   21 C=X(3)
      IF(IR-15)26,32,27
   27 IR=15
      GO TO 32
   26 IF(IR-1)31,31,32
   32 DO 100 J=2,IR
      X(1)=XL
      X(2)=XH
      Y(1)=YL
      Y(2)=YH
```

FIGURE 22. (SHEET 7 OF 10)

```
C
C THE NEXT STATEMENT DETERMINES THE MAXIMUM NO. OF ITERATIONS.
C
      DO 99 KK=1,50
C
C THE NEXT STATEMENT IS THE RECURSION FORMULA.
C
      X(3)=((X(2)-X(1))/(Y(2)-Y(1)))*(F(J,N) -Y(1))+X(1)
      CALL SOND(TH,X(3),Y(3))
      RR=(F(J,N)-Y(3))*C
      IF(ABS(RR)-E)29,29,23
   23 IF(RR)25,29,24
   24 X(1)=X(3)
      Y(1)=Y(3)
      GOTO 99
   25 X(2)=X(3)
      Y(2)=Y(3)
   99 CONTINUE
C
C IF THE ITERATION DOES NOT CONVERGE TWO ALTERNATIVES ARE AVAILABLE ----
C          1. INCREASE THE MAXIMUM NO. OF ITERATIONS.
C          2. REPLACE THE RECURSION FORMULA WITH   X(3) = (X(2)+X(1))*.50
C
      WRITE(IPR,1)TH,F(J,N),RR
    1 FORMAT(30H DOES NOT CONVERGE AT THETA = ,F6.2,
     112H AND F(J) = ,F10.4,17H WITH RESIDUAL = ,F6.3)
      GOTO 100
   29 R(J,N)=X(3)
  100 CONTINUE
   31 IR=IR+1
      F(IR,N)=YH
      R(IR,N)=XH
      F(1,N)=YL
      R(1,N)=XL
      RETURN
      END
*COMPILE SOND INPUT CARDS OUTPUT TAPE LIST SOURCE
      SUBROUTINE SOND(TH,R,SPL)
      DIMENSION C(17,4)
      COMMON IRD,IPR,C,ALP,DM,T,C4,C5,C6,C7,K
C
C THIS SUBROUTINE CALCULATES THE SOUND PRESSURE LEVEL.
C INPUT REQUIRED IS THE ANGLE THETA, AND THE RADIUS R.
C SOND1 CALCULATES ALP,C4,C5,C6, AND C7.
C
      G1=ALP*DM**2
      G2=COS(.01745329*TH)
      RAT=1.0+C6*EXP(-C7*R/4.0)
      G3=1.0+C6*EXP(-C7*R)
      G4=DM*G2
      G5=1.0+C4*EXP(-C5*TH*.01745329)/RAT
      G6=((1.0+G1)/((1.0-G4/G3)**2+G1))**2.5
      G7=(1.0+G2**4)/G5
      SP=10.0*ALOG10(G6*G7)
```

FIGURE 22. (SHEET 8 OF 10)

```
      G1=DM**2.340/R**2
      G2=10.650*(T/530.0)**.930/R**4
      G3=15.160*DM**.890*(T/530.0)**1.110/R**6
      PL=10.0*ALOG10(G1+G2-G3)
      STM=10.0*ALOG10(C(17,K)*T**1.540*DM**4)
      SPL=SP+PL+STM
      RETURN
      END
```

```
*COMPILE SOND1 INPUT CARDS OUTPUT TAPE LIST SOURCE
      SUBROUTINE SOND1
      DIMENSION C(17,4)
      COMMON IRD,IPR,C,ALP,DM,T,C4,C5,C6,C7,K
C
C THIS SUBROUTINE COMPUTES VALUES FOR ALP,C4,C5,C6, AND C7 FOR USE IN
C SOND, THE SOUND PRESSURE LEVEL ROUTINE.
C MUST BE GIVEN THE C(I,K) MATRIX, I = 1,17 K = 1,4 , AND A VALUE FOR K.
C THE VALUES COMPUTED ARE FOR SPECIFIED VALUES OF DM AND T.
C
      W=T*.001
      ALP=C(1,K)*DM**C(2,K)*W**(C(3,K)+C(4,K)*DM)
      C4=C(5,K)*DM**C(6,K)*W**(C(7,K)+C(8,K)*DM)
      C5=C(9,K)*DM**C(10,K)*W**(C(11,K)+C(12,K)*DM)
      C6=17.5*(W/3.0)**(.890*(DM**2-1.0))
      C7=.410*(W/3.60)**(.566*(DM**2-1.0))
      RETURN
      END
```

```
*COMPILE REGION INPUT CARDS OUTPUT TAPE LIST SOURCE
      SUBROUTINE REGION(A,B,X,I)
C THIS ROUTINE DETERMINES WHETHER X IS IN THE CLOSED INTERVAL (A,B).
C IF X IS IN THE INTERVAL, I = 1 IS RETURNED.
C IF X IS NOT IN THE INTERVAL, I = 2 IS RETURNED.
C
      I=1
      IF(A-X)1,2,3
    1 IF(X-B)2,2,3
    3 I=2
      X=A
    2 RETURN
      END
```

FIGURE 22. (SHEET 9 OF 10)

```
*DATA
.82393E0   .4176E0    .32555E0   .74038E0   -1.24E0    -1.7269E0  .2482E0    -3.4538E0
-2.3019E0  -1.3226E0  -4.0206E0  -4.7181E0  1.4745E0   1.3507E0   2.6807E0   3.2662E0
45.759E0   18.932E0   202.88E0   331.56E0   -2.1086E0  -3.2199E0  3.8424E0   .53294E0
3.3692E0   1.3276E0   10.52E0    9.5983E0   -2.3864E0  -.1765E0   -8.0248E0  -6.8295E0
12.808E0   8.4045E0   10.491E0   10.429E0   -1.8167E0  -1.5494E0  -.019983E0 .36732E0
-1.7894E0  -.16871E0  .73551E0   .89132E0   1.1641E0   .22007E0   -.76495E0  -.87600E0
4.512E0    5.2846E0   4.5428E0   2.6963E0   -.028729E0 1.3015E0   .20763E0   1.8687E0
.789E0     .85116E0   .27691E0   3.0174E0   -.51772E0  -.60053E0  .036298E0  -22.1329E0
5.5     E094.78    E081.46    E091.15    E09
00002.0    000025.0   000010.0   00005.0    35         00005.0
-0010.0    000078.0   0.0        0008P.0    01
      .95     2410.0   01
      .95     2410.0   02
      .95     2410.0   03
      .95     2410.0   04
      .92     1890.0   01
      .92     1890.0   02
      .92     1890.0   03
      .92     1890.0   04
*END
```

FIGURE 22. (SHEET 10 OF 10)

G. Comparison of Empirical Analysis with Measured Model and Full-Scale Jet Engine Noise Contours

The empirical analysis must pass two tests to validate the results.

The first test is comparison of the calculated contours, for the overall band and the octave bands, with the measured-model data. This test should be relatively simple, since the empirical coefficients have been derived solely from the data taken during this study and reported here.

The second test, comparison with full-scale engine data, is more difficult. It is quite normal to list engine operational conditions from manufacturers' data, instead of actually monitoring the data during tests. However, none of the tests which reported near-field noise contours for afterburning listed (or measured) the exhaust plane temperature. Only the exhaust gas temperature (E G.T.) was given. The E.G.T. is always derived from a thermocouple reading directly aft of the turbine stage and definitely in front of the afterburner. Other parameters, such as pressure ratio, are difficult to ascertain from the reported data, so manufacturers' data have to be used again.

1. Comparison with Model Jet Tests

Using only the exhaust plane temperatures and engine local exhaust plane Mach numbers listed in Table I, the contours shown with solid lines were calculated. (The program used is described in the preceding subsection.) The dashed lines represent the experimental contours for the basic jet tests. The comparisons are shown in Figures 23 to 39 and are given exactly as they were calculated. As may be expected, the quality varies, since there was scatter in some of the data. Furthermore, the type of source radiation was not accounted for in the empirical analysis. It has been pointed out (References 6 and 8) that there are at least six types of sound sources present in a supersonic, turbulent, heated jet:

- Lateral quadrupoles (shear layer noise)
- Longitudinal quadrupoles (Combinations of these constitute isotropic turbulence.)
- Dipoles (from shed vortices)
- Simple sources (from edge-tone radiation)
- Mach waves radiated from the mixing region
- Shock structure in the core

To account for the different types of sources which might be present in an an empirical correlation would be exceedingly difficult without an experimental program an order of magnitude more difficult and expensive than the one reported here.

In examining the curves, it is evident that the comparisons which are poorest are generally at low temperatures. The experimental data showed the greatest variations during unheated tests, perhaps because of extreme pressure variations which the automatic valves could not smooth out.

Figure 23, the lowest-velocity experimental test, shows that the directional characteristics are predicted quite well for the overall and first frequency band, with the other two frequency bands showing considerable deviation. The source location is also predicted accurately except for the second frequency band. The other two figures (24 and 25) for

this series of Mach numbers compare quite reasonably, with variations not exceeding 5 decibels, in most instances.

In the Mach 1 series (Figures 26, 27, and 28) the directivity, source locations and levels agree quite well.

For Mach 1.25 (Figures 29, 30, 31, and 32), the levels are good at 580°R, but the source location prediction is not comparable with the experiment. This source location deviation could not be resolved without further experimentation. The other three temperatures in the series offer the best comparisons in the tests.

At 580°R, Mach 1.50 (Figure 33), there is no reasonable correlation between the prediction and theory. It is quite difficult to discount data when so many precautions are taken to ensure accuracy and uniformity. Perhaps another type of sound source is predominant in this case, or it is possible that the data may be bad. Whatever the cause, the trends are not the same for the predicted and the measured data.

The higher velocity-higher temperature comparison at Mach 1.50 (Figures 34 to 39) is generally good. It is noted that the third octave band experimental data show a peak in the contours at the exit plane which the prediction method does not provide.

2. Comparison of Prediction Method with Full-Scale Engine Data

The overall band has been calculated to compare with near-field noise contours reported in Reference 19. The engine is a J-79 in afterburning configuration. The comparison is shown in Figure 40. The levels compare quite well close to the turbulent boundary. However, in the far field, a 10-decibel difference is noted. Although Reference 19 reported octave-band levels, a comparison was not attempted since the reported levels seemed too low. All eight octaves were added logarithmically, and the result was more than 10 decibels below the reported octave-band levels.

A comparison is also made with the data from Reference 2 for the overall band. Here again, the comparison is fair (Figure 41). Although the data from Reference 2 shows levels considerably higher than predicted, the microphones used to measure these levels were in the edge or just outside the edge of the turbulent boundary. The experimental data taken in this study were 1.5 diameters from the edge of the mixing boundary.

It is emphasized that the full-scale jet noise data include ground reflective effects while the model jets were exhausting into a free field. Experimental data given in Reference 2 verifies that reflective effects create variations of more than 10 decibels in the far field. Variations of this order of magnitude explain the extreme differences evidenced between the predicted and measured data. The variations also amplify the requirement for including reflective effects in the prediction technique.

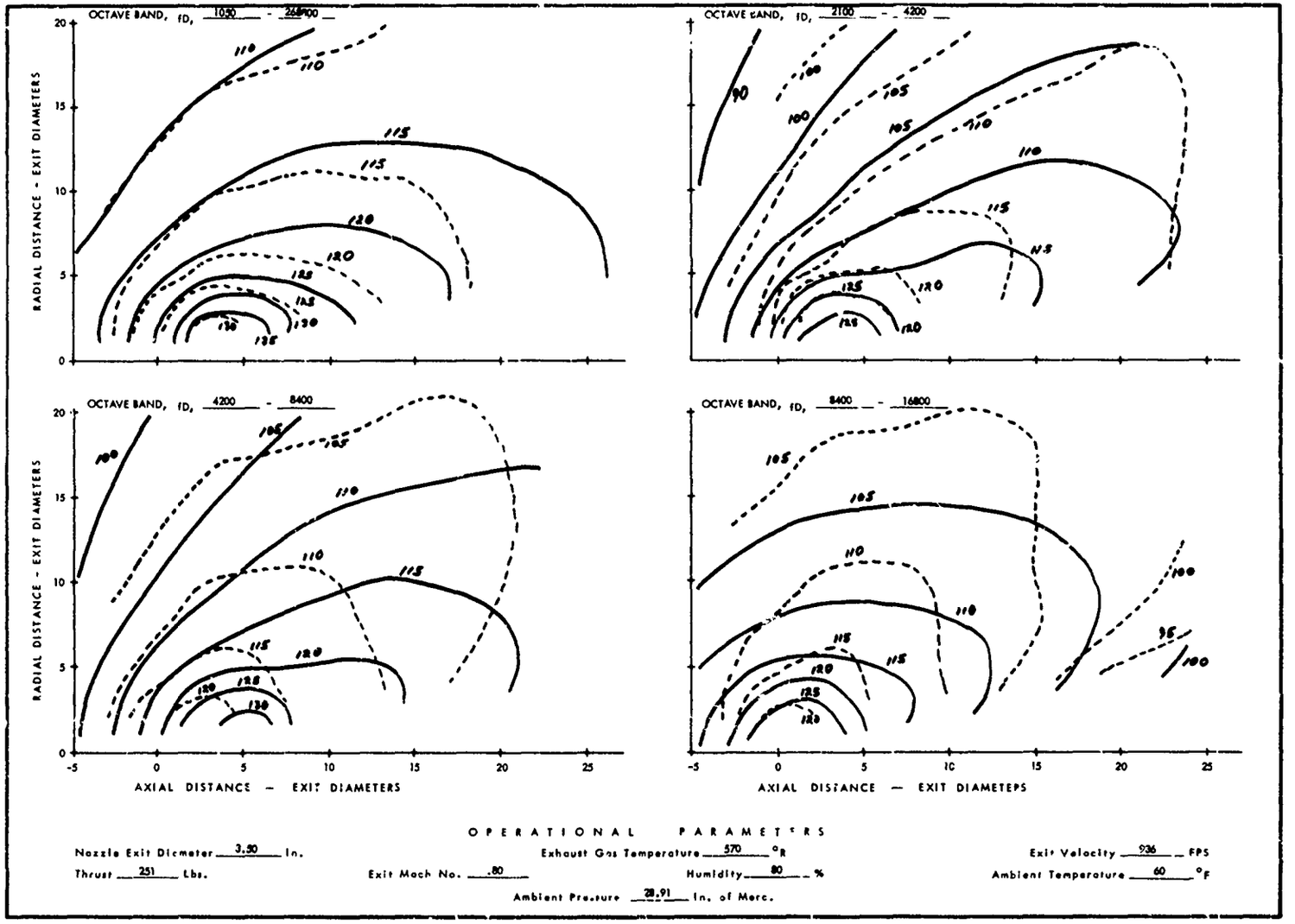

FIGURE 23 COMPARISON OF MODEL JET EXPERIMENTAL AND CALCULATED CONTOURS MACH NO. = .80, TEMP = 570°R

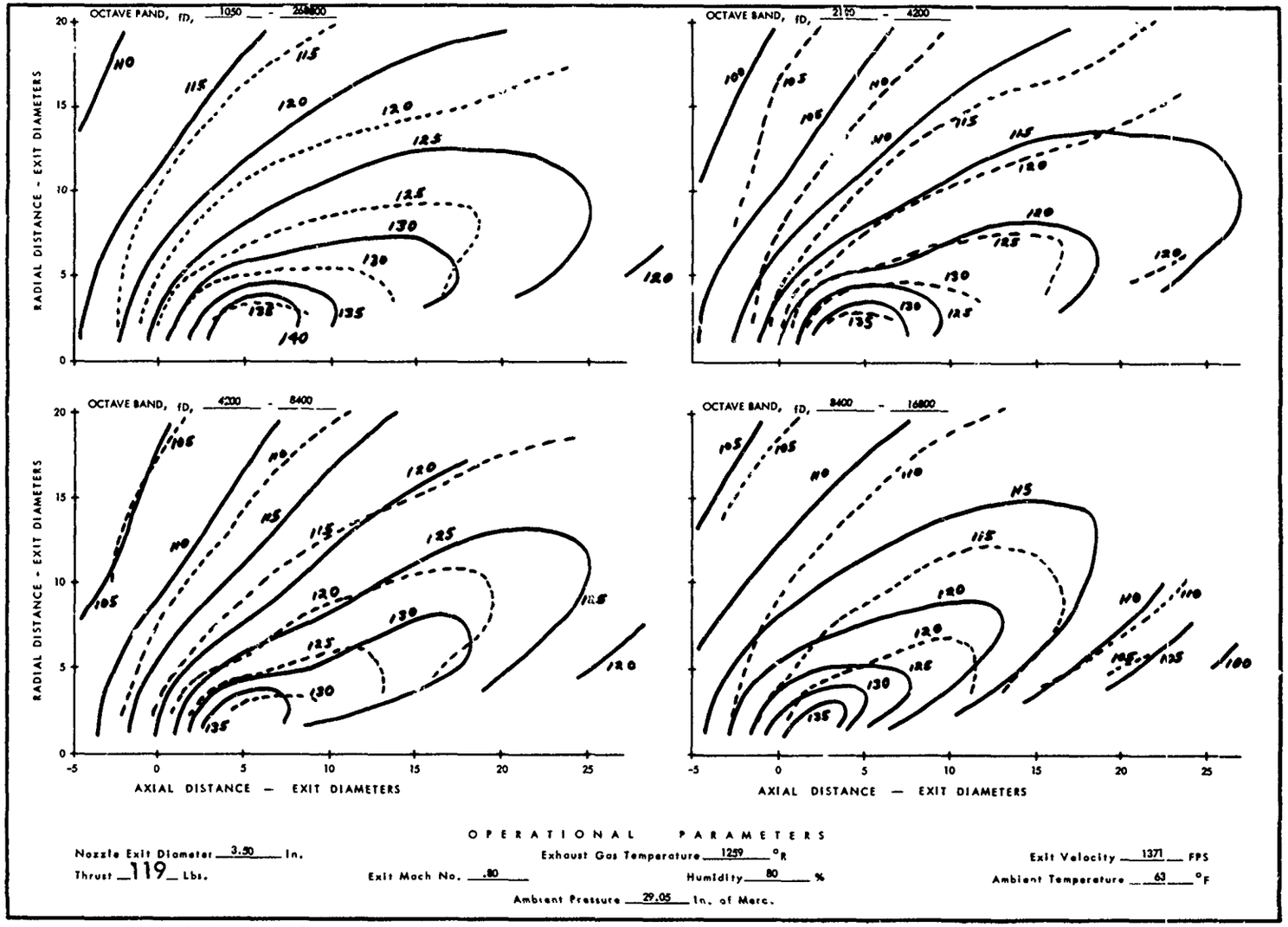

FIGURE 24 COMPARISON OF MODEL JET EXPERIMENTAL AND CALCULATED CONTOURS MACH NO. = .80, TEMP = 1259°R

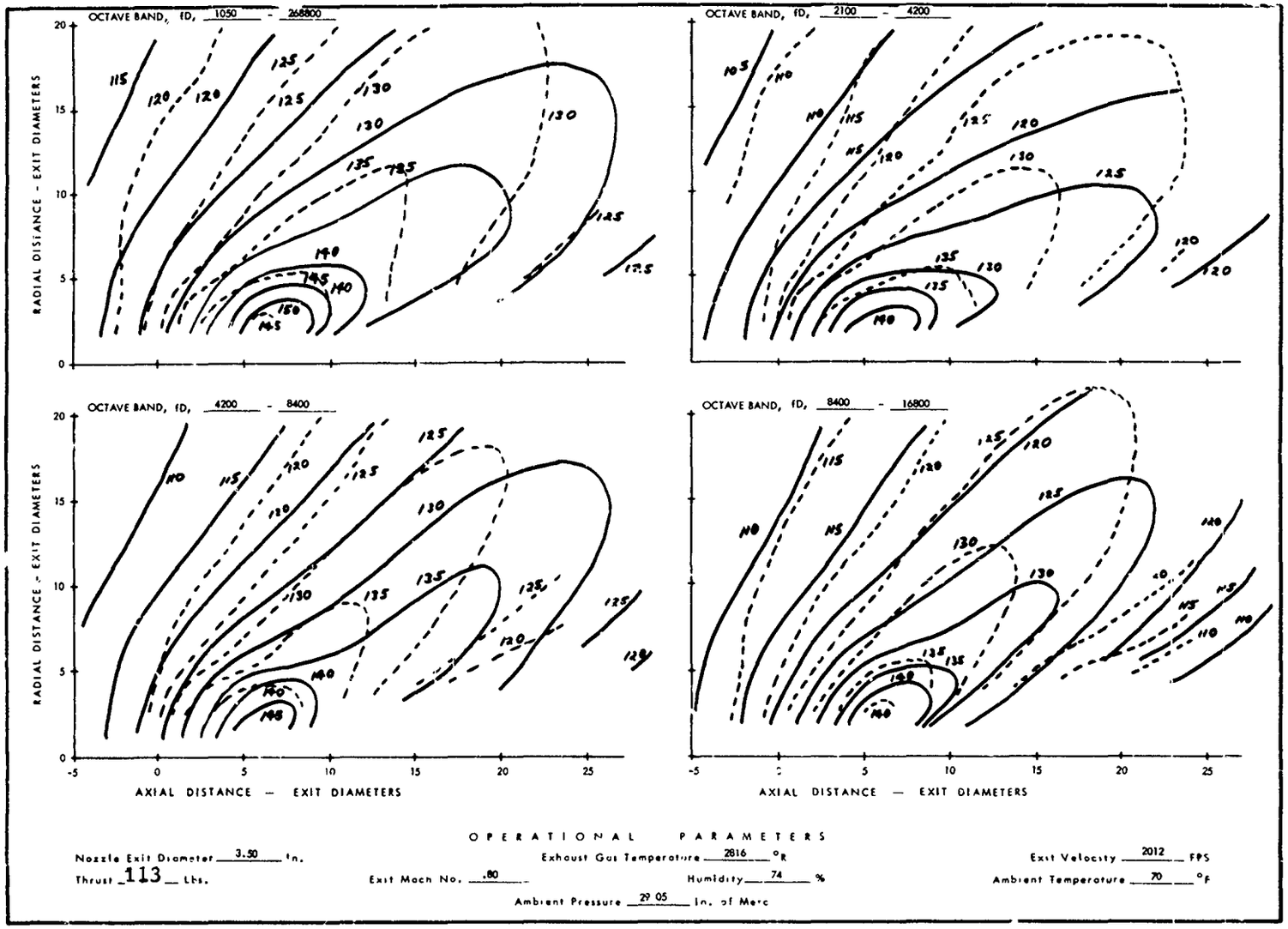

FIGURE 25 COMPARISON OF MODEL JET EXPERIMENTAL AND CALCULATED CONTOURS MACH NO. = .80, TEMP = 2816°R

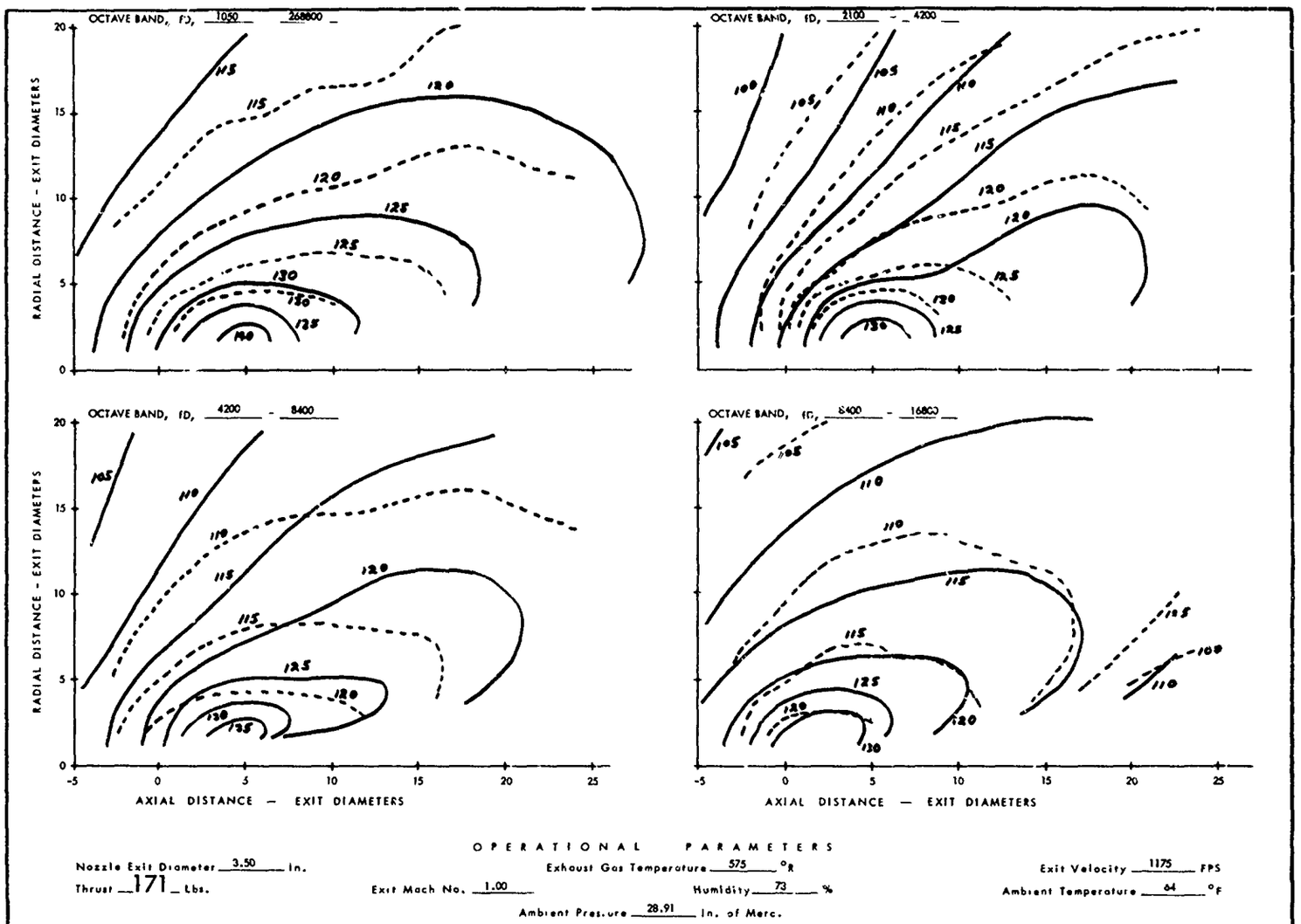

FIGURE 26 COMPARISON OF MODEL JET EXPERIMENTAL AND CALCULATED CONTOURS MACH NO. = 1.00, TEMP = 575°R

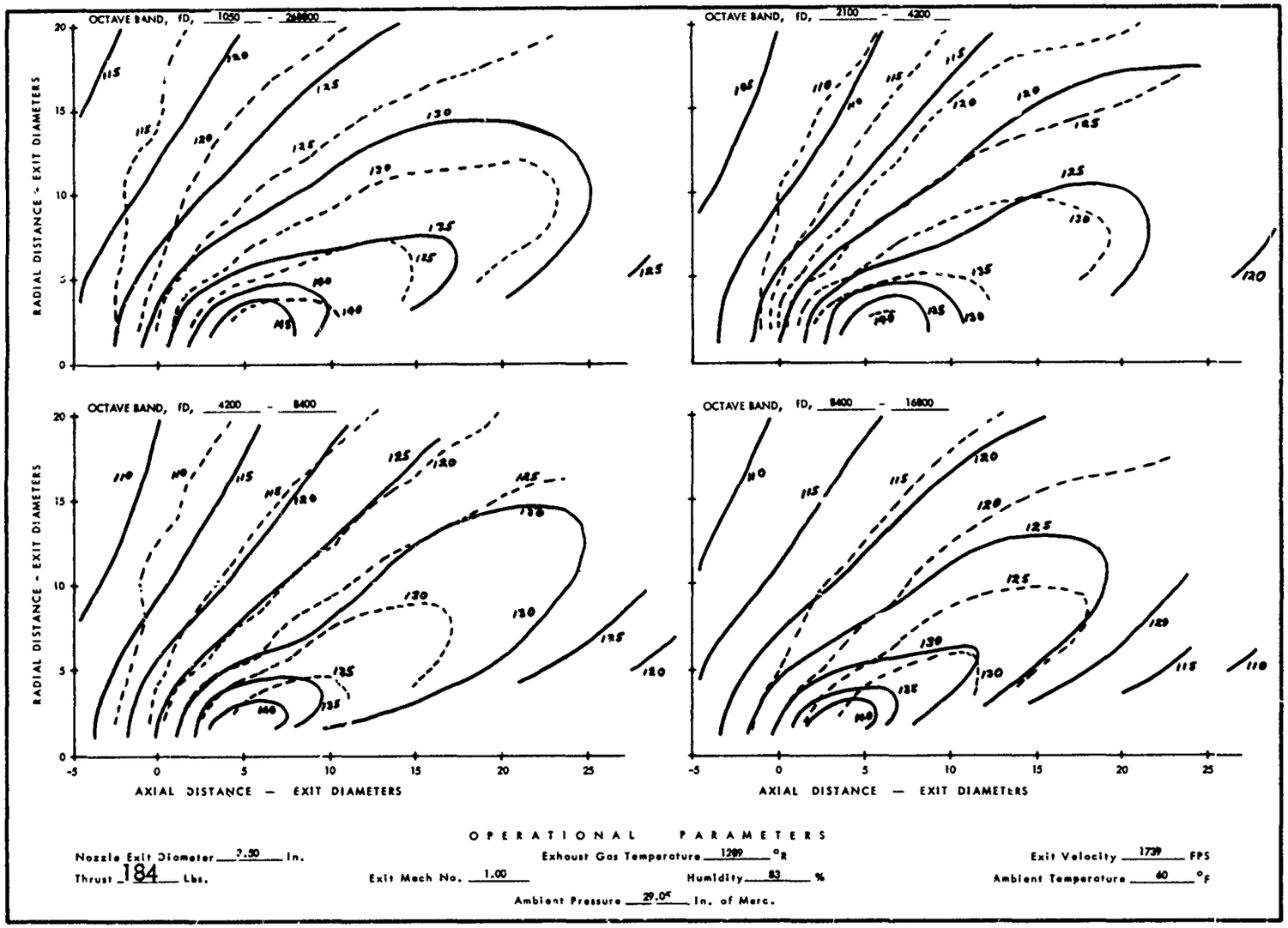

FIGURE 27 COMPARISON OF MODEL JET EXPERIMENTAL AND CALCULATED CONTOURS MACH NO. = 1.00, TEMP = 1289°R

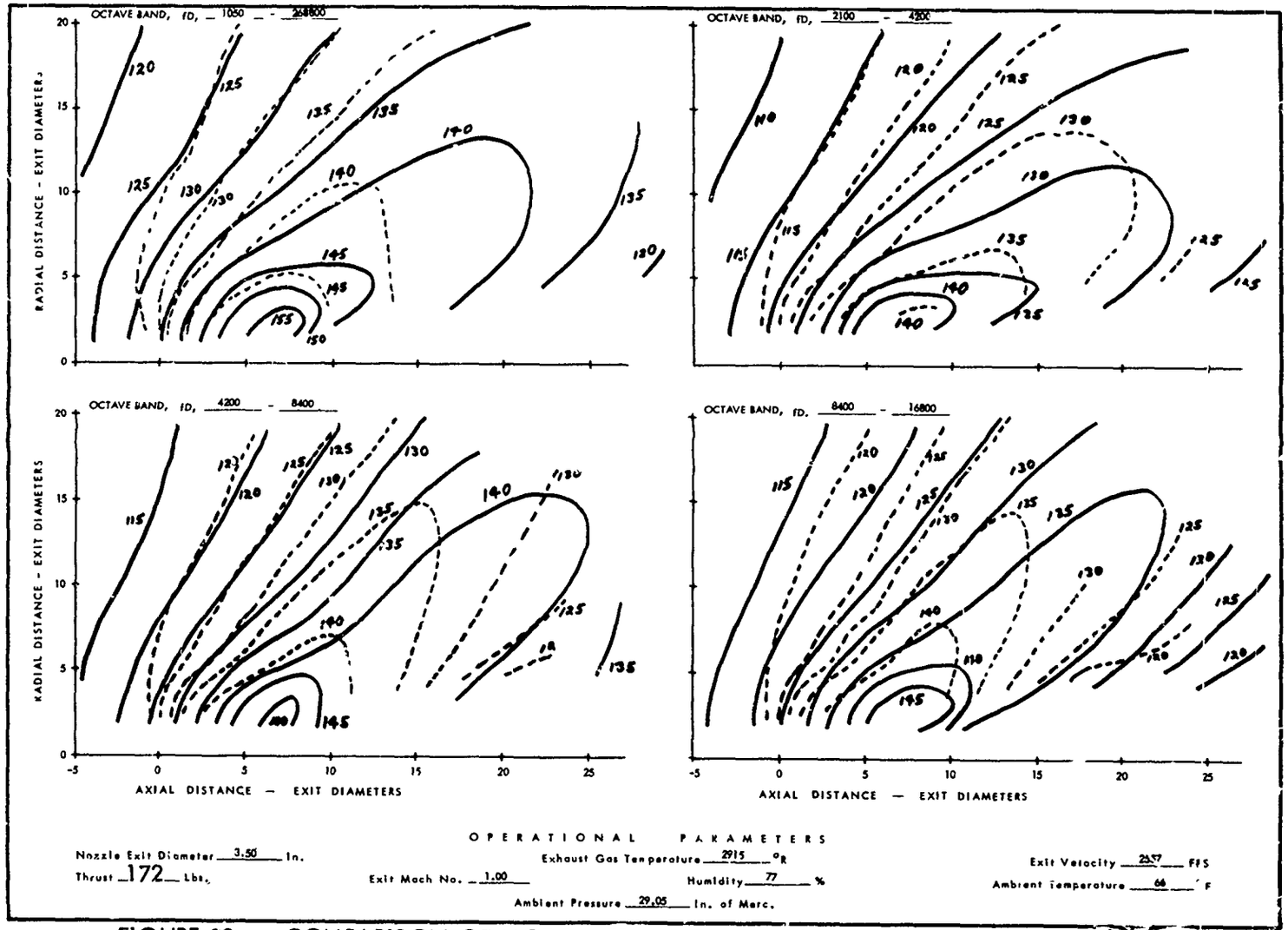

FIGURE 28 COMPARISON OF MODEL JET EXPERIMENTAL AND CALCULATED CONTOURS MACH NO. = 1.00, TEMP = 2915°R

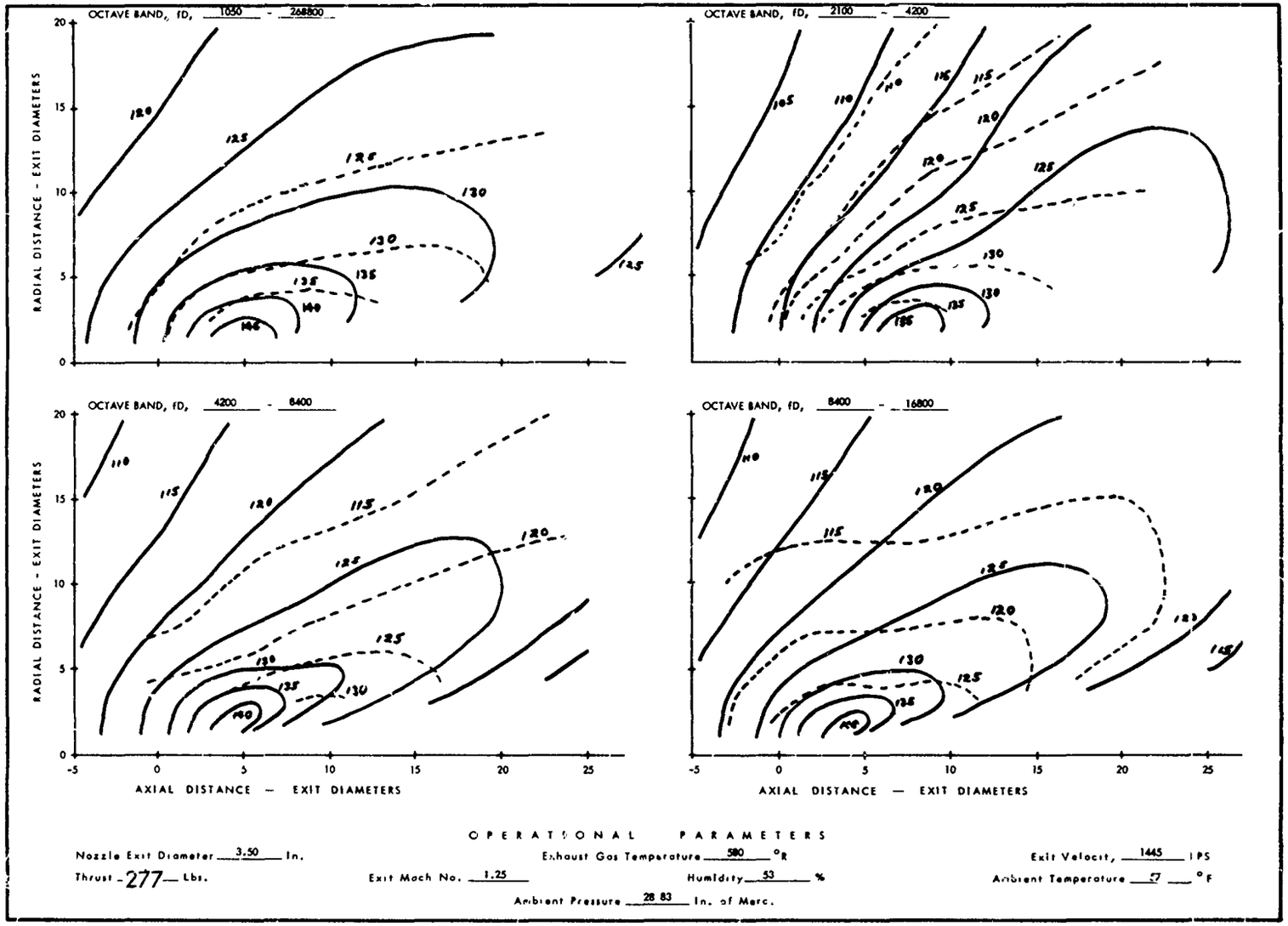

FIGURE 29 COMPARISON OF MODEL JET EXPERIMENTAL AND CALCULATED CONTOURS MACH NO. = 1.25, TEMP = 580°R

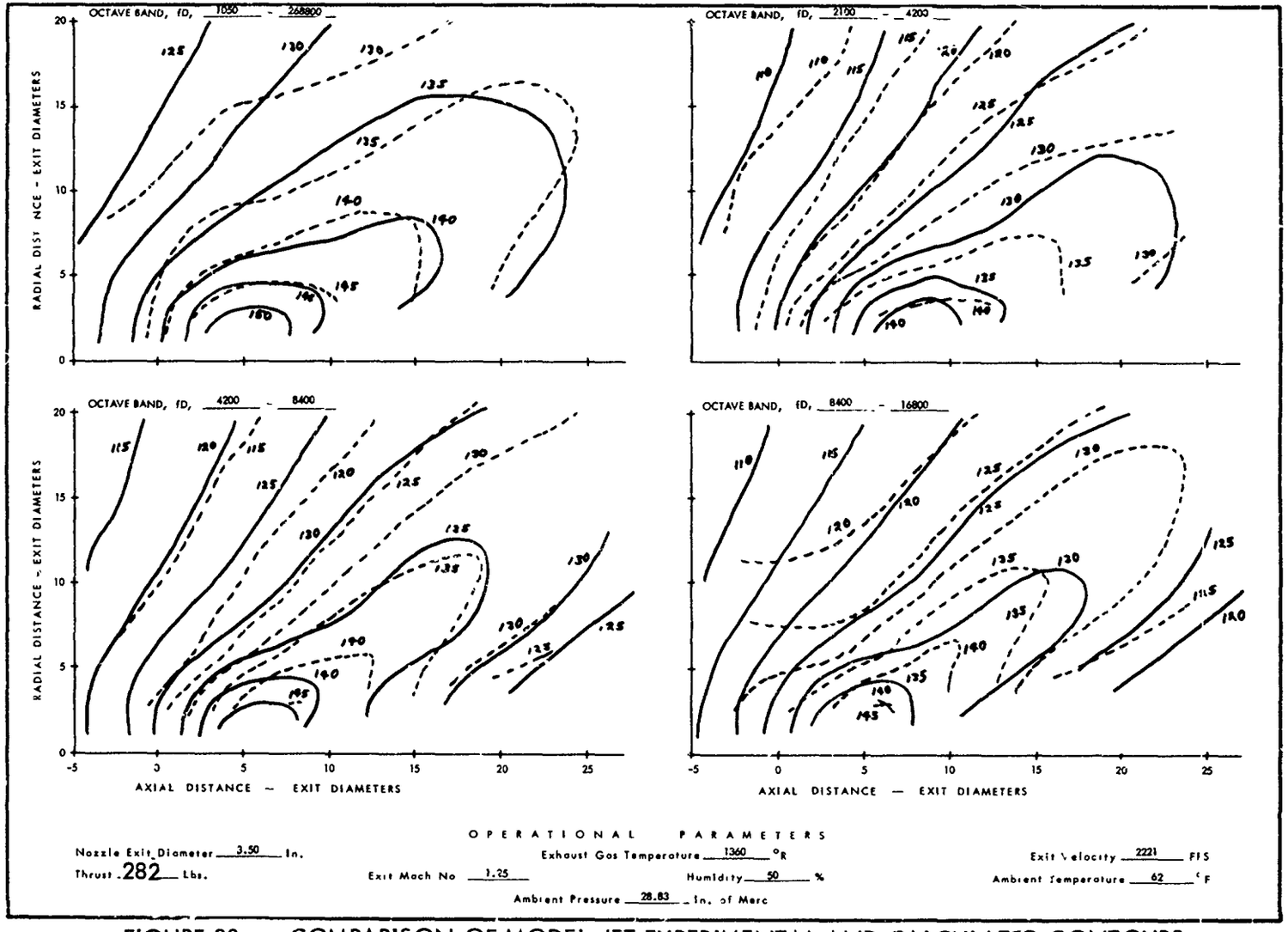

FIGURE 30 COMPARISON OF MODEL JET EXPERIMENTAL AND CALCULATED CONTOURS MACH NO. = 1.25, TEMP = 1360°R

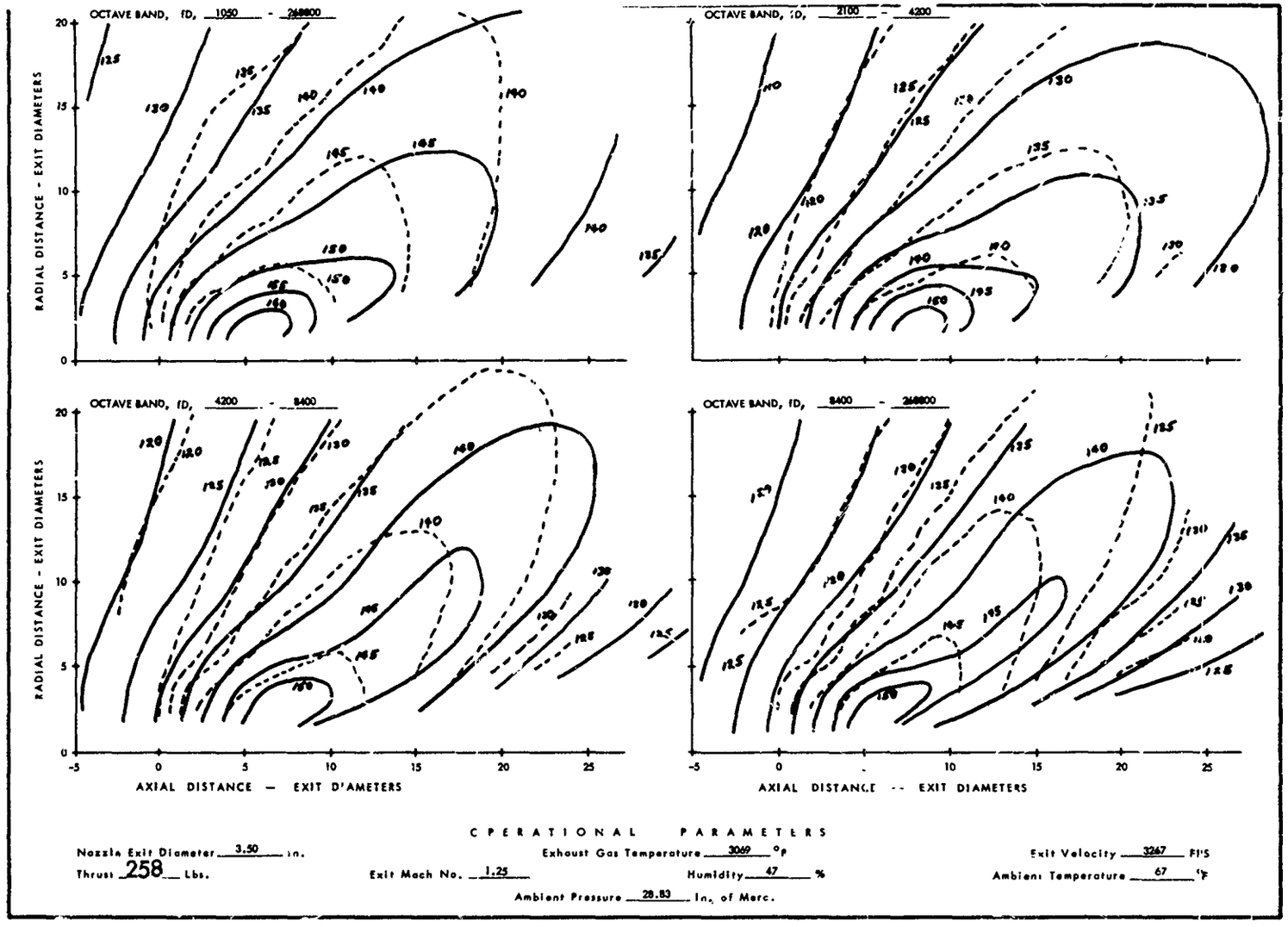

FIGURE 31 COMPARISON OF MODEL JET EXPERIMENTAL AND CALCULATED CONTOURS MACH NO. = 1.25, TEMP = 3069°R

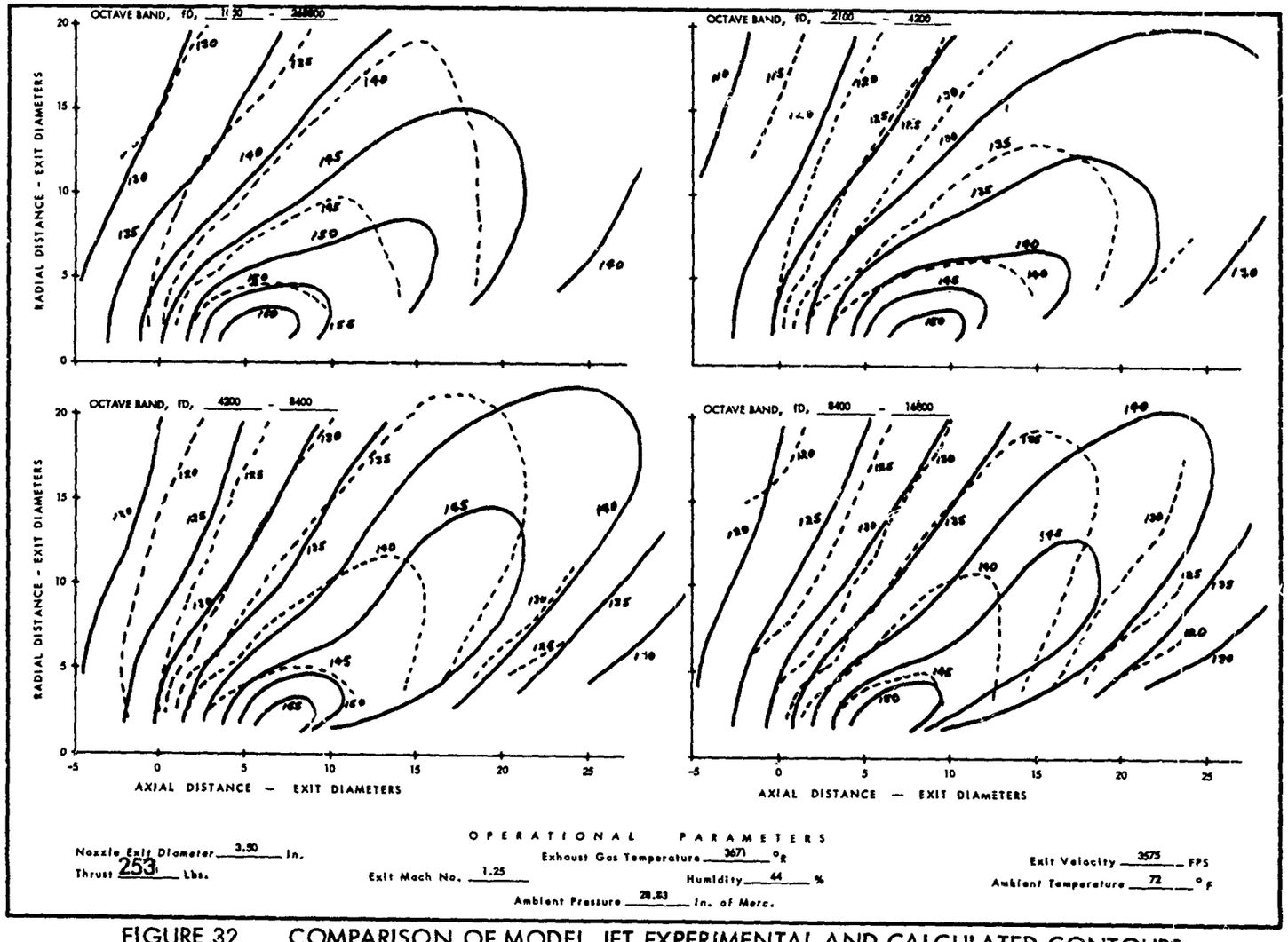

FIGURE 32 COMPARISON OF MODEL JET EXPERIMENTAL AND CALCULATED CONTOURS MACH NO. = 1.25, TEMP = 3671°R

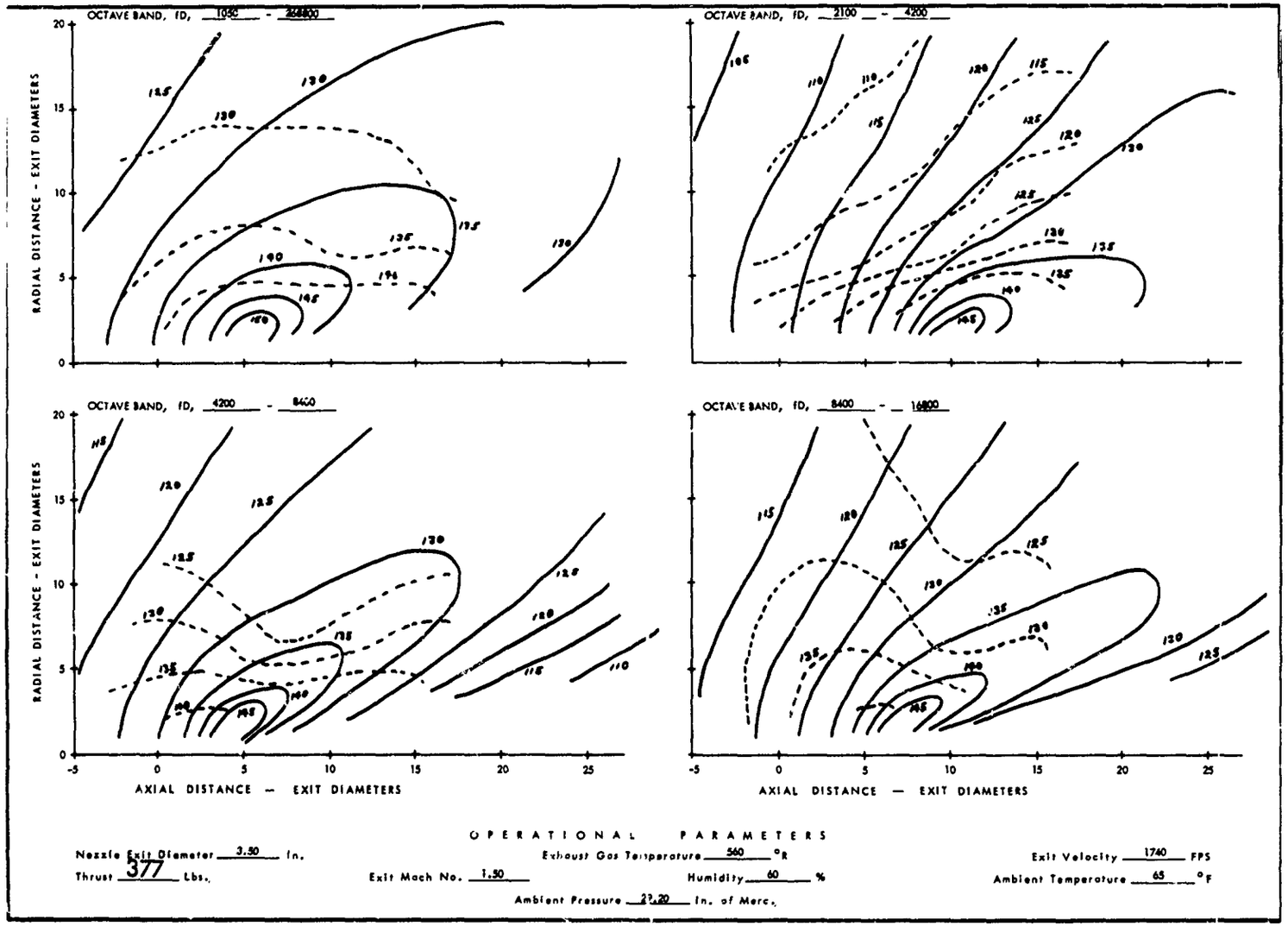

FIGURE 33 COMPARISON OF MODEL JET EXPERIMENTAL AND CALCULATED CONTOURS MACH NO. = 1.50, TEMP = 560°R

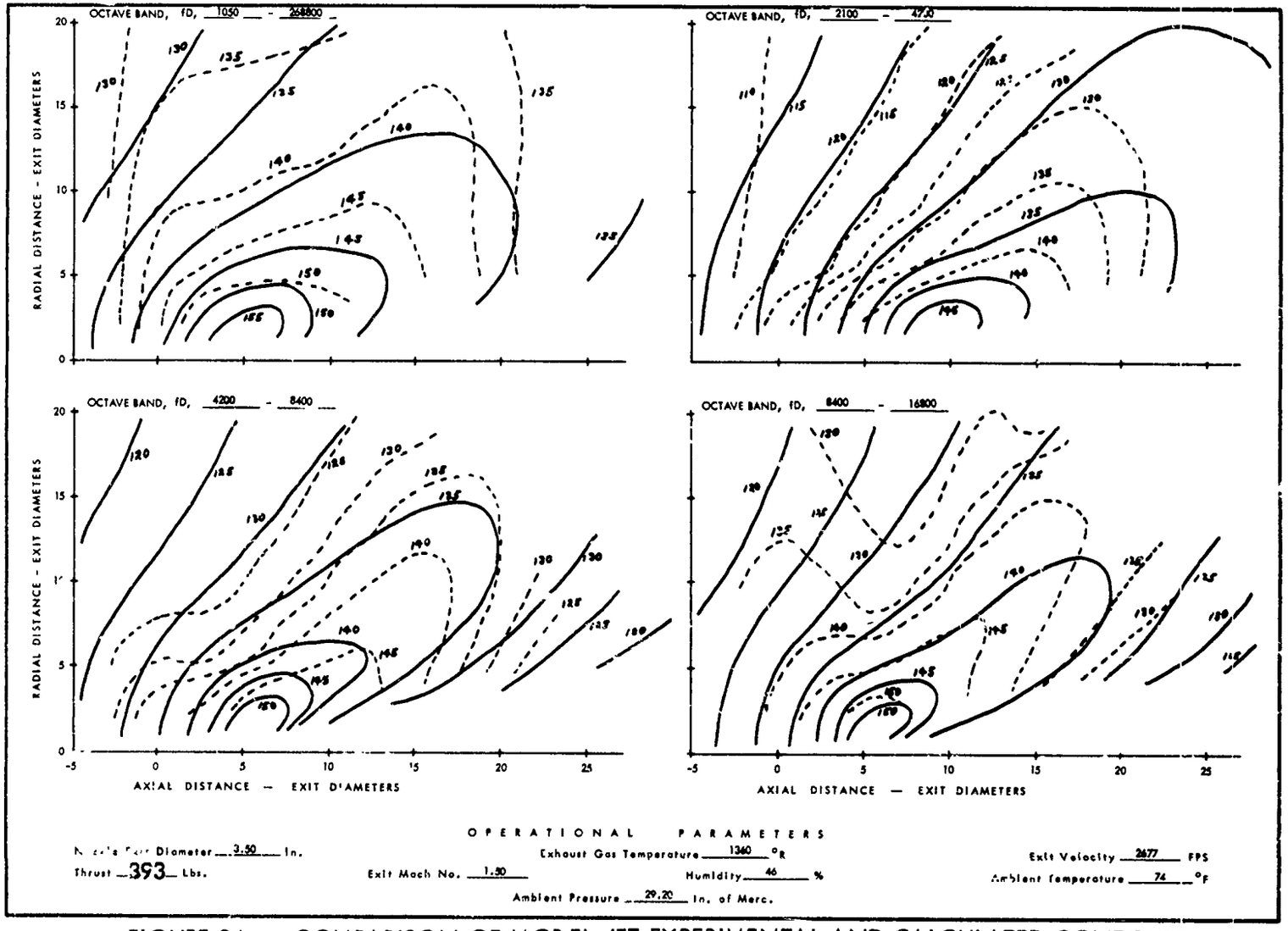

FIGURE 34 COMPARISON OF MODEL JET EXPERIMENTAL AND CALCULATED CONTOURS MACH NO. = 1.50, TEMP = 1360°R

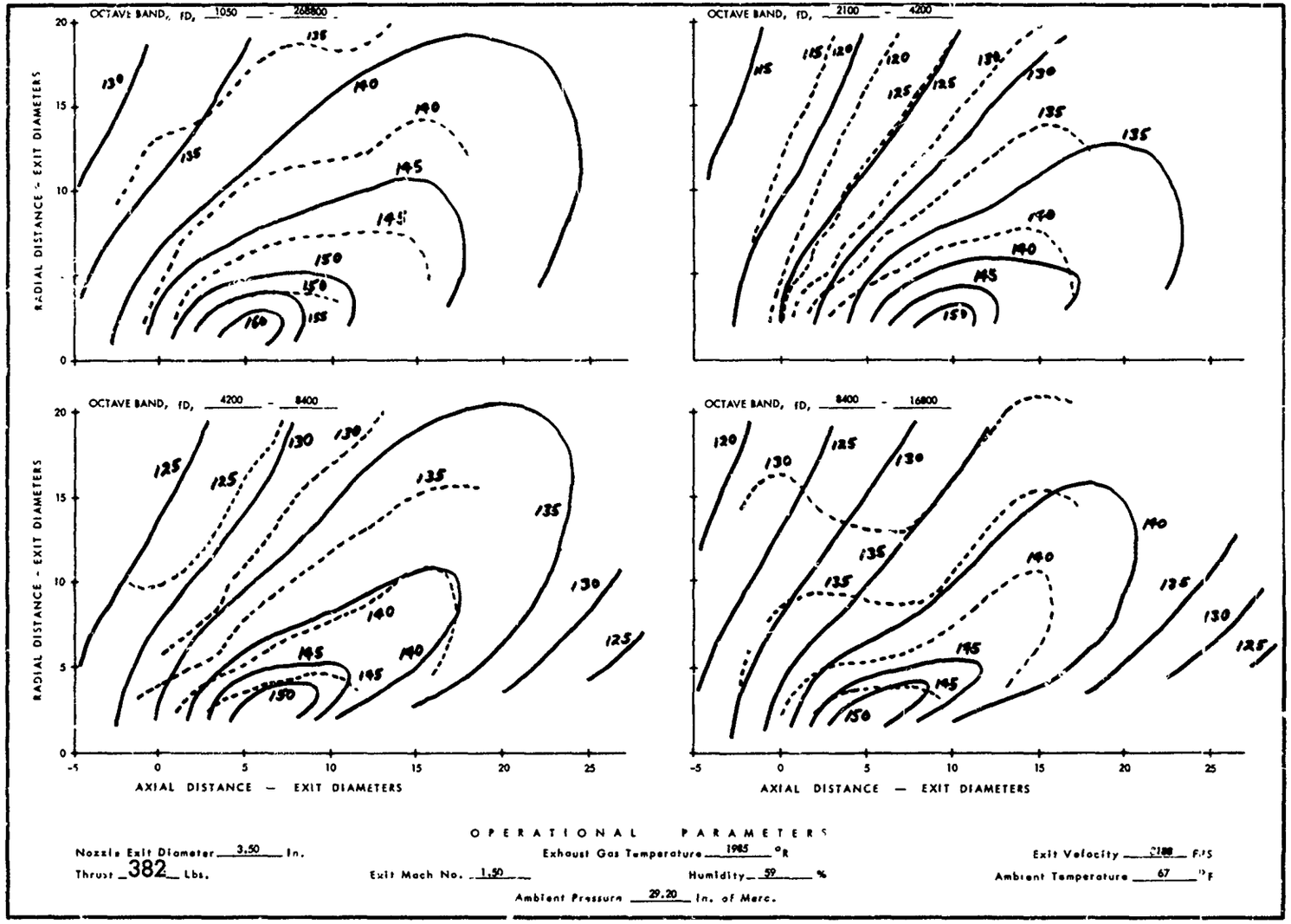

FIGURE 35 COMPARISON OF MODEL JET EXPERIMENTAL AND CALCULATED CONTOURS MACH NO. = 1.50, TEMP = 1985°R

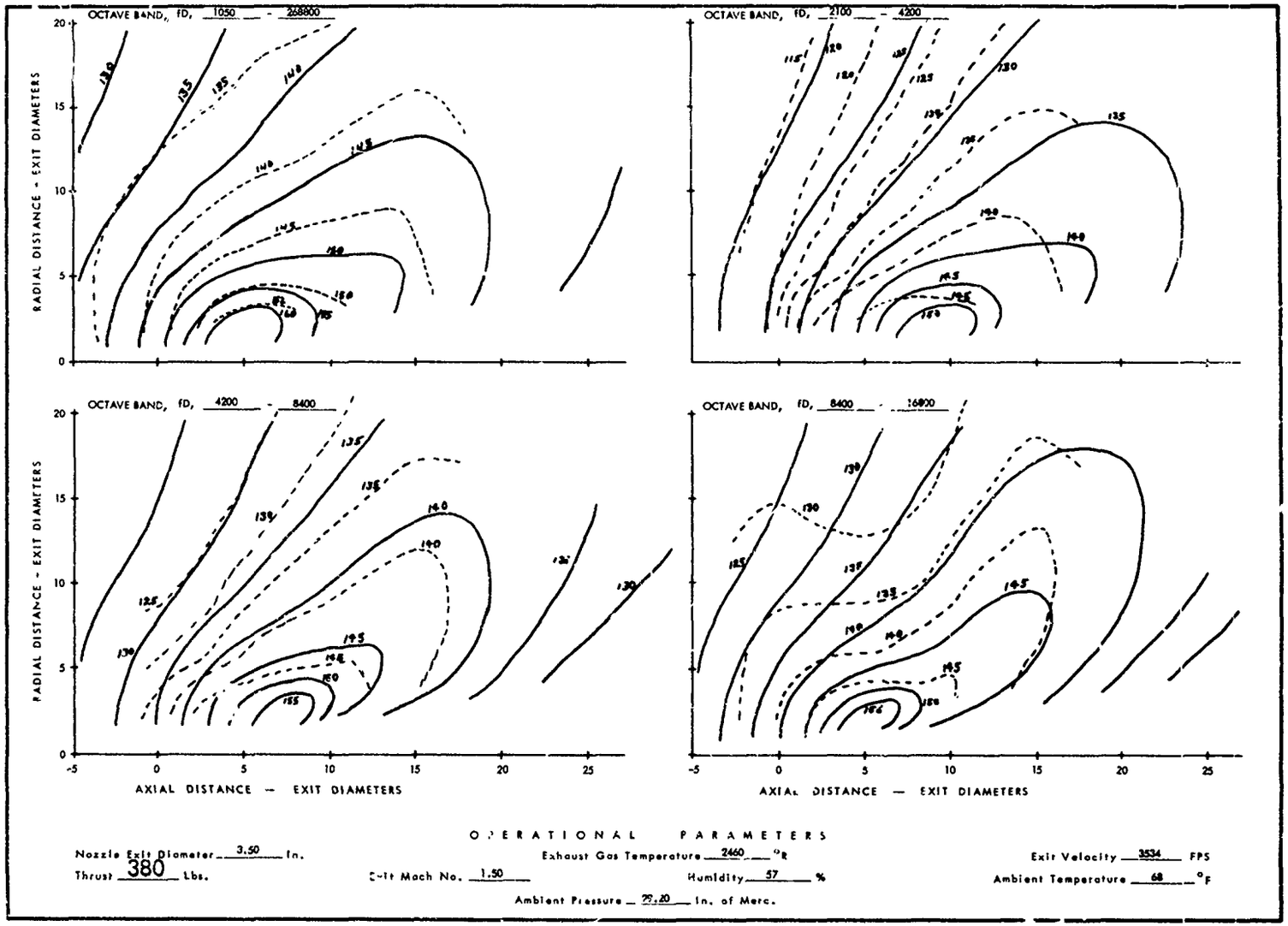

FIGURE 36 COMPARISON OF MODEL JET EXPERIMENTAL AND CALCULATED CONTOURS MACH NO. = 1.50, TEMP = 2460°R

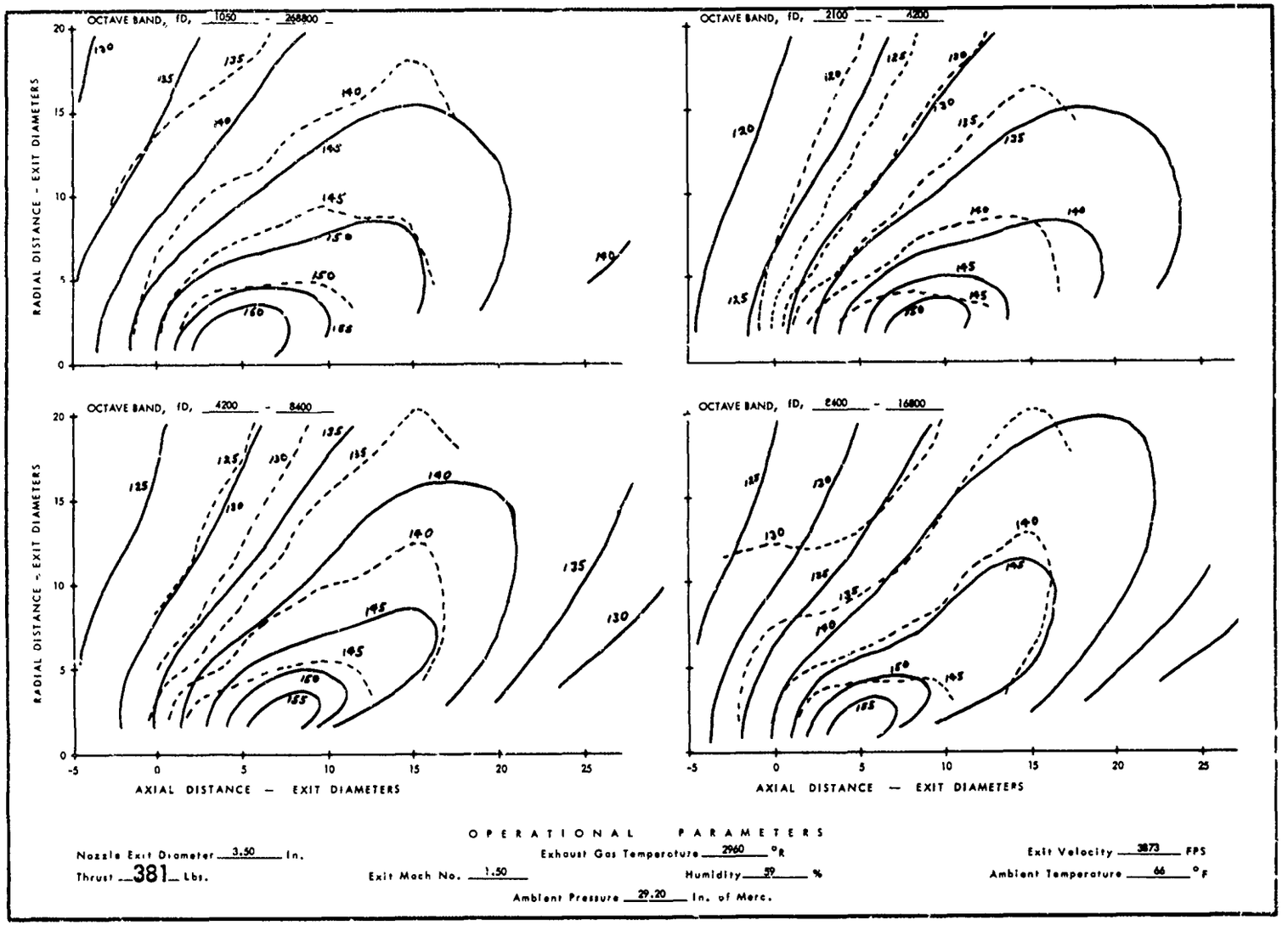

FIGURE 37 COMPARISON OF MODEL JET EXPERIMENTAL AND CALCULATED CONTOURS MACH NO. = 1.50, TEMP = 2960°R

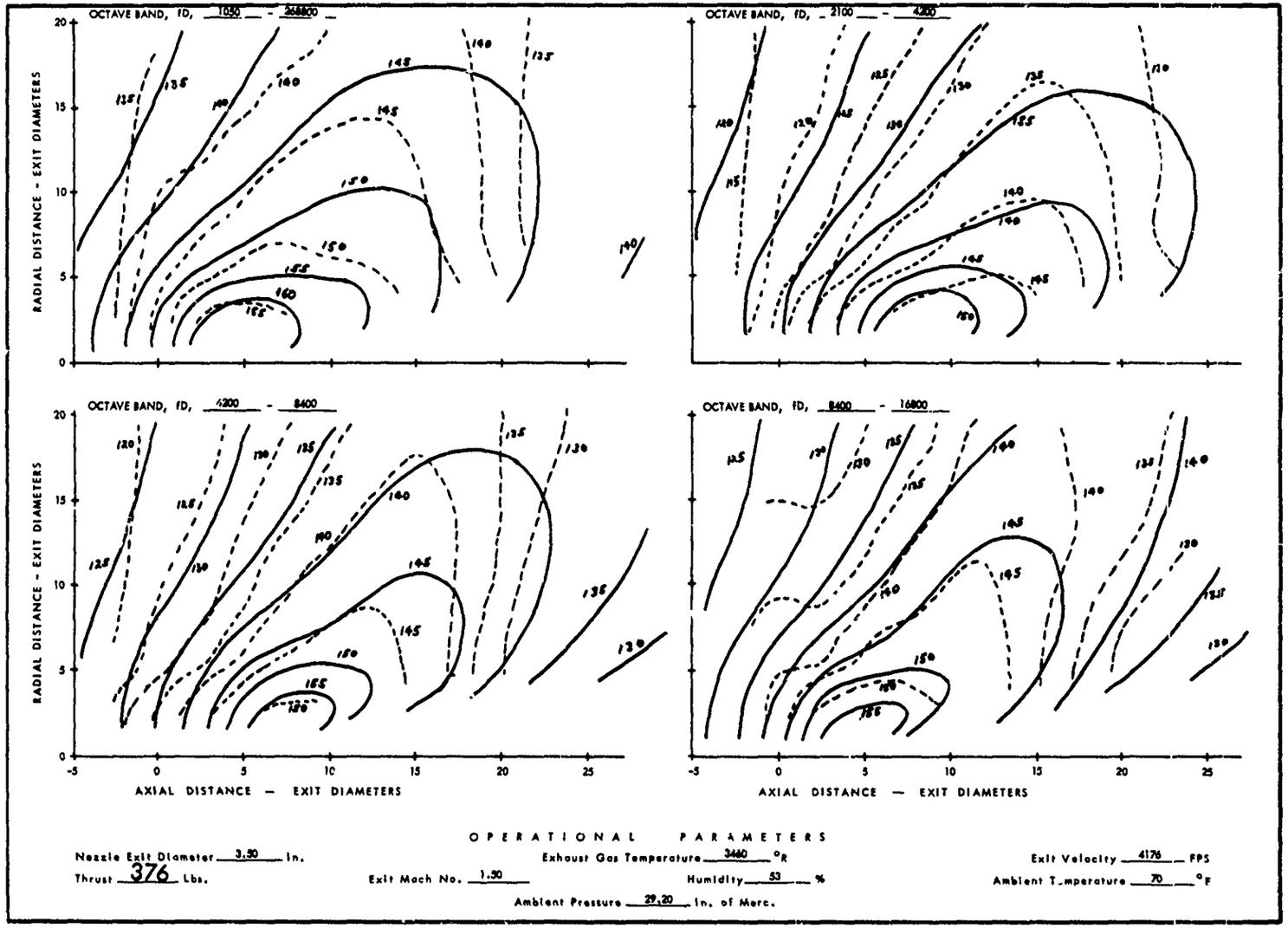

FIGURE 38 COMPARISON OF MODEL JET EXPERIMENTAL AND CALCULATED CONTOURS MACH NO. = 1.50, TEMP = 3460°R

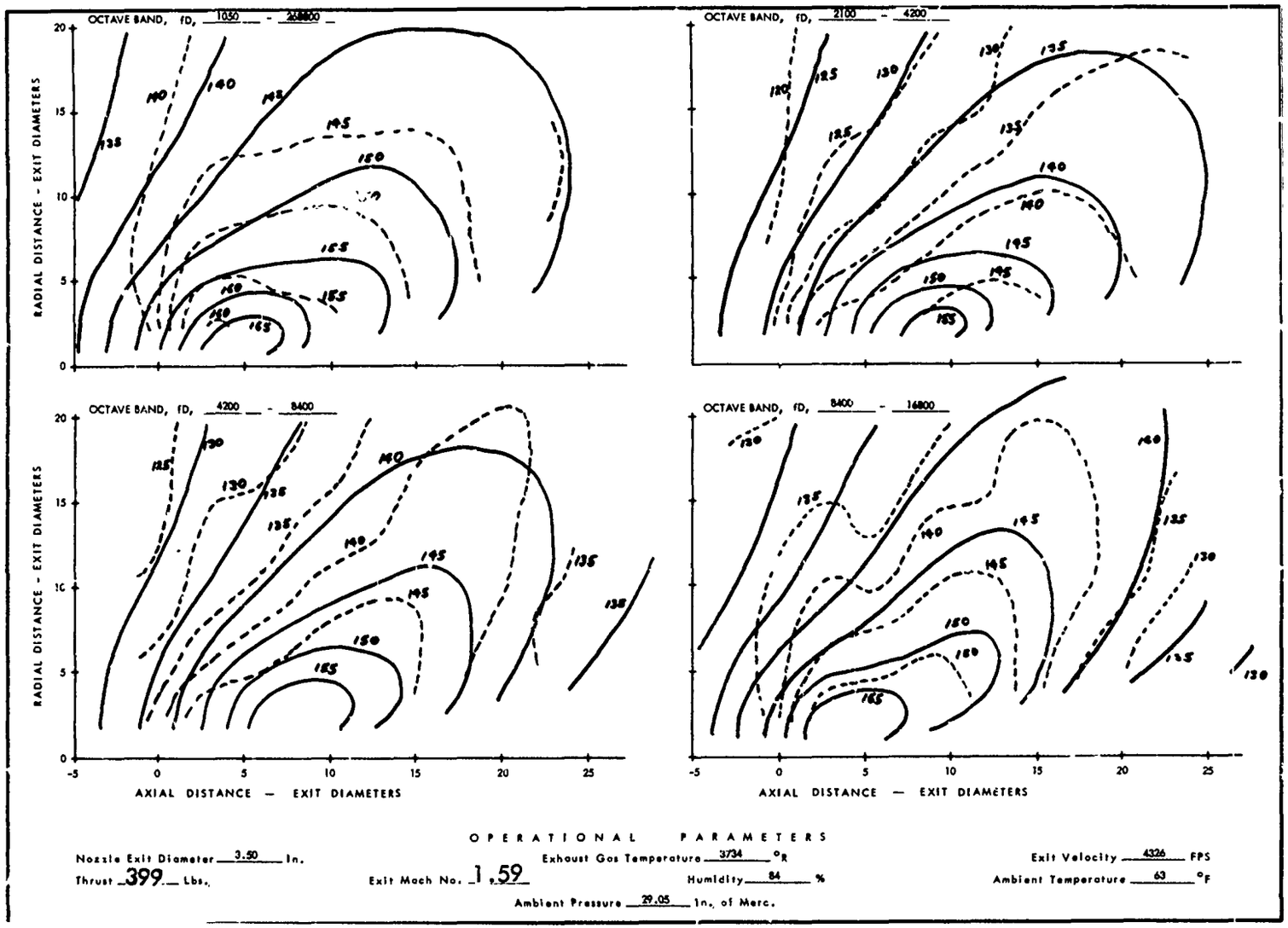

FIGURE 39 COMPARISON OF MODEL JET EXPERIMENTAL AND CALCULATED CONTOURS
MACH NO. = 1.59, TEMP = 3734°R

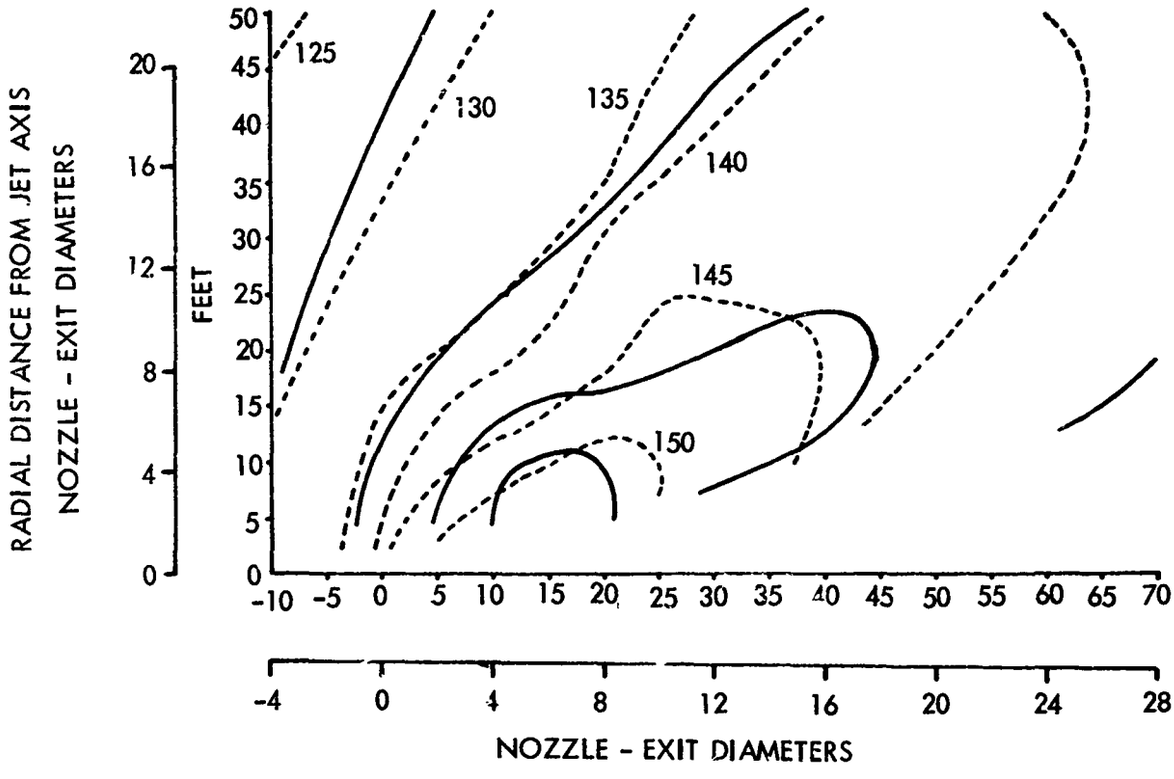

FIGURE 40 FOR J-79 AFTERBURNING CONFIGURATION (OVERALL BAND). CALCULATED CONTOURS COMPARED WITH SPL CONTOURS FROM REFERENCE 19.

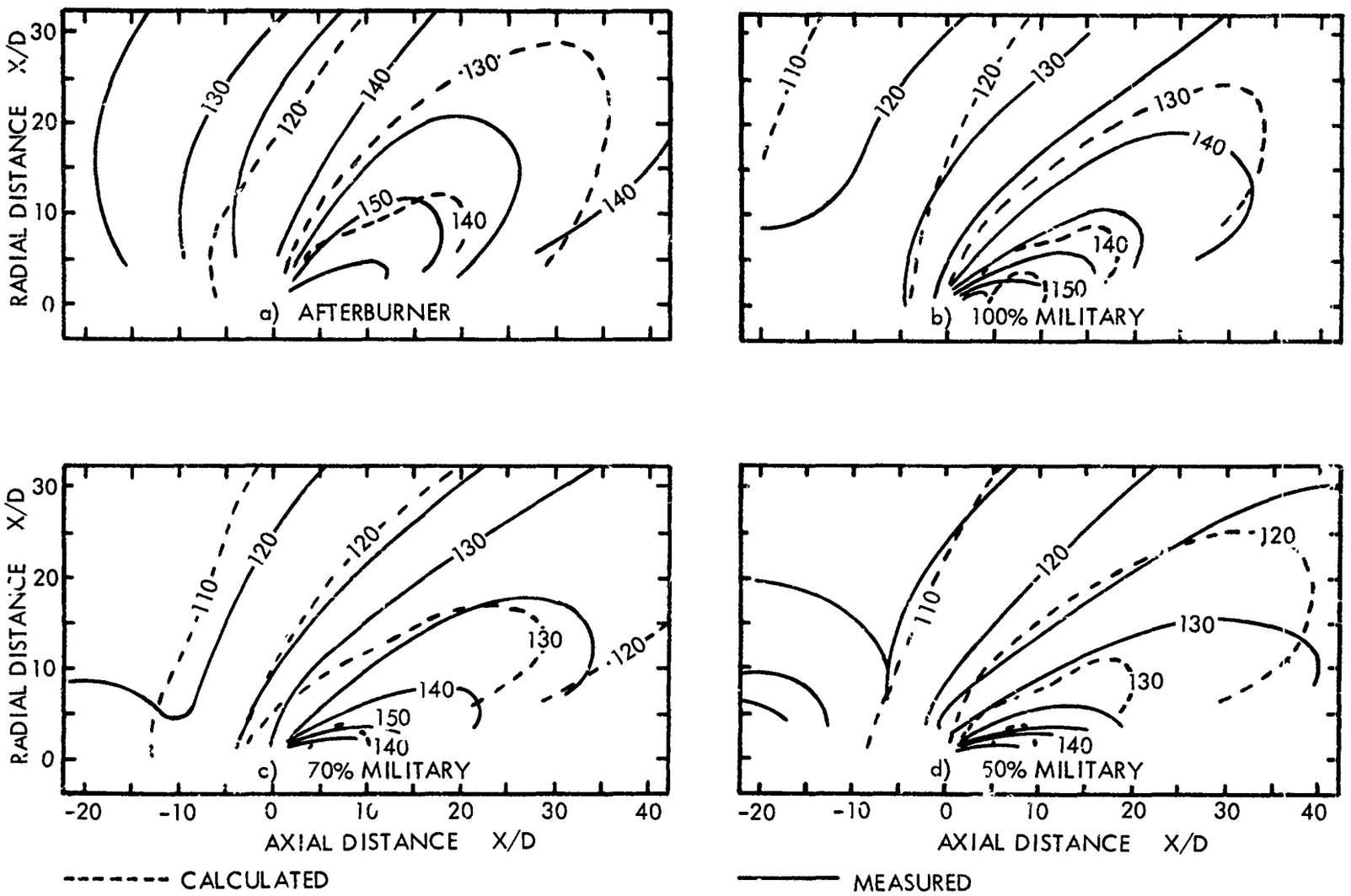

FIGURE 41. COMPARISON OF CALCULATED AND MEASURED NEAR FIELD NOISE FOR J57-P21 (FROM REF. 2)

H. Results

This subsection includes discussion of the analytical analysis and all jet noise tests.

1. Basic Engine Configuration

The tests conducted with the basic engine configuration are unique from the standpoint of parameter variations made. The data have been semi-empirically correlated to exhaust local Mach number and exhaust temperature. All previous data have been correlated to exhaust velocity and have implicitly left out a temperature effect, except for its effect on exhaust velocity.

The exhaust velocity is expressed as

$$V = cM \propto T^{1/2} M \tag{17}$$

and, therefore, exhaust velocity is proportional to the square root of temperature.

Evaluation of Equation (15) at $\theta = 90^{\circ}$ and substitution of the values of the functions C_1, C_2, C_3, and $K_1 T^s M^n$ gives

$$\bar{p}^2 = \frac{5.5 \times 10^9}{r^2}\left[T^{1.54} M^{6.34} + 0.0312 \frac{T^{2.47} M^4}{r^2} - 0.0146 \frac{T^{2.65} M^{4.89}}{r^4}\right] \tag{18}$$

One very important result in the far field ($r \gg 1$) is given by

$$\bar{p}^2 = 5.5 \times 10^9 \frac{T^{1.54} M^{6.34}}{r^2} \quad . \tag{19}$$

If variations in the ratio of specific heat at constant pressure to specific heat at constant temperature, k, are neglected, the speed of sound in the jet is

$$c_j = 49.4 \sqrt{T} \quad . \tag{20}$$

Substitution of Equation (20) into Equation (19) gives

$$\bar{p}^2 = 3.37 \times 10^4 \frac{c_j^{3.08} M^{6.34}}{r^2}$$

or (21)

$$p^2 = 3.37 \times 10^4 \frac{V^{6.34}}{c_j^{3.26} r^2}$$

This shows but slight disagreement with the final expression of Hermes and Smith (Reference 2) who find

$$\overline{p}^2 \propto \frac{V^{6.5}}{c_i^4 r^2} \tag{22}$$

It can be shown from relationships in Reference 17 that, for an isentropic, maximum-efficiency nozzle, whether subsonic or supersonic, the thrust is given by the following equation

$$T = P_{atm} A_{exit} k M^2 \tag{23}$$

Equation (23) in conjunction with Equation (19) provides a method for the engine designer to reduce sound pressure level. For example, given a hypothetical airplane with fixed engine exhaust velocity and thrust characteristics, the following relationship can be derived by substitution of Equations (17) and (23) into Equation (19):

$$\overline{p}^2 \propto \frac{V^{4.34} T}{(r')^2 T^{.63}} \tag{24}$$

It also contains thrust, which is, by Equation (23), proportional to exhaust area and nozzle Mach number squared. It should also be noted that, in Equation (24), the non-dimensional distance r was replaced by r'/D to bring the problem back into linear distance. In this case, the SPL should be evaluated at a fixed distance from the engine instead of a non-dimensional distance.

Now, note the significance of Equation (24). In an engine or airplane design analysis, thrust and engine tailpipe velocity are fixed. But exhaust gas temperature can vary from the very low temperature of a bypass fan engine to the almost 4000°R of a duct-burning turbofan. The significance of temperature variation is reflected in Mach number and engine size. More important, a higher temperature engine yields a lower sound pressure. This is a significant result, since lower community noise will be a specification criterion for all future engine/airframe designs. The result is offered to engine designers as a first step in the reduction of jet noise by control of operational parameters.

Generalizations about temperature and Mach number effects in the near field are not as apparent as the observations for the far field. The near-field terms in Equation (18) have somewhat different trends. If the same substitutions that were used in the far field are applied to Equation (18) (for fixed exhaust velocity and thrust), the mean-square sound pressure is expressed as

$$\overline{p}^2 = K_1 \frac{V^{4.34} T}{(r')^2 T^{.63}} + K_2 \frac{T^2 T^{2.47}}{(r')^4} - K_3 \frac{T^3 T^{3.20}}{(r')^6 V^{1.11}} \ . \tag{25}$$

The effect of temperature is more difficult to evaluate in this expression. The near-field and near-near-field terms are increased with temperature. However, since these two terms are not additive, the net effect could either increase or decrease in the near near field. There is a strong possibility that near-field SPL's will increase in some regions, if temperature is increased. If temperature is increased for the purpose of reducing community noise, the serious structural fatigue problem might be increased. These considerations require more investigation, however.

The prediction technique developed for near-field noise is unusual in that the temperature and Mach number powers do not change with field position. All other prediction techniques rely on this change in power for prediction.

2. Basic Nozzle with Ejector

Only one ejector configuration was tested. This configuration, shown in Figure I-6, Appendix I, was designed to be representative of what airframe manufacturers might install. For optimum noise characteristics, Middleton (Reference 18) shows that long ejectors are required. However, since weight is always at a premium, the configuration studied was chosen as typical.

For shorter ejectors, a predominant ejector whistle is possible at low velocities or low pressure ratios. The ejector/Mach 1.25 nozzle combination was tested at three temperatures: 555°R, 1279°R, and 2993°R. Examination of the SPL contours at 555°R (velocity = 1443 FPS) in Figure 42 reveals evidence of a discrete frequency radiation from the ejector in the 4200 to 8400 and 8400 to 16800 non-dimensional frequency bands. A distinct resonance was detected in the sound pressure spectra. The frequency of this whistle was approximately 2000 Hz.

The overall effect on the SPL contours for the cold jet is to increase noise levels in the far field. Near-field levels are approximately the same as for the bare nozzle (Figure 43).

The contours for the ejector at 1279°R as well as contours for the basic Mach 1.25 nozzle at 1360°R are given in Figures 44 and 45. The contours are very similar, with variations of ± 2 decibels noted in comparing the various bands. No shift in spectrum shape is detected.

The ejector/nozzle combination at 3000°R shows the same effects as at 1300°R (Figures 46 and 47). No significant change in noise level can be attributed to the ejector.

Therefore, the general conclusion is that the effect on SPL is negligible for a short ejector which is operating out of its flow-resonance operational regime. If the velocity-pressure ratio combination is such that a flow resonance can occur, distinct periodic resonant tones will be emitted. This problem can be resolved by proper design (see Reference 18). If the ejector is made longer (5 to 10 tailpipe diameters), SPL reductions of up to 7 db can be achieved (Reference 18).

3. Effect of Ground Plane on Basic Jet

The purpose of this test was to determine the effect of ground reflections on the free-field noise levels. The ground plane was placed on the side of the jet opposite the side where noise measurements were taken. In this configuration, the noise measurements were made in the field where a wing would be located relative to an underwing jet while on the ground.

Four basic studies were made, including variation of ground plane distance from the jet centerline, engine Mach number, and exhaust gas temperature. The parameters for the 10 test runs are listed in Table II.

The significant conclusion is that at the minimum ground-plane distance, there was no effect on the noise field on the side of the jet opposite the ground plane. This does not indicate that an increase in noise level would not occur when the engine exhaust was

located between a wing and the ground. In this case, standing wave modes would certainly be possible and highly probable.

Figures 48 to 57 support the conclusion that there is no effect in the area where the data were taken. Another significant conclusion is the repeatability of the data. There was no variation greater than 4 decibels where the Mach number and temperature were the same. This excellent repeatability creates a higher confidence level in the data.

4. Effect of Deflecting Vanes on Near-Field Noise Level

Some basic ideas about the sound field radiated from a deflected jet may be formed from examination of the configuration sketch in Figure 10. The configuration, of course, is not an actual operational configuration as was explained in Section III. From the sketch, a clear view of the exhaust stream can be seen from the field to the left of the jet. This exhaust noise radiates through an opening approximately 1.0 diameter high for the 45° vane and 1.7 diameters high for the 30° vane. This acted as a primary source of sound which radiated to the left of the jet as shown in Figure 10. While this may not be an exact representation of an operational deflected jet, it still requires explanation in the results.

The vane acted as a shield from 1.0 to 5.9 diameters downstream for the 45° jet and 1.7 to 5.1 diameters downstream for the 30° jet. Then another radiation source existed farther downstream.

The machine-plotted, experimental contours in Figures 58, 59, and 60 show the effects described. In Figure 60, for the 30° deflecting vane, a very strong source of noise originated from the exit plane to 3 diameters downstream, depending on the frequency. Another apparent source existed about 12 diameters downstream. The upstream source peaked in the second frequency band, while the downstream source peaked in the third band. Comparison of the sound pressure levels with the basic jet data (Figure 57) at the same operational conditions reveals that maximum overall noise levels were about 6 decibels lower for the deflected jet.

Noise levels between the jet centerline and the ground plane will probably be more intense than would be observed for the undeflected jet. However, judicious design should minimize placing sonic fatigue critical structures in this area; i.e., the engine should be placed as low on the structure as possible.

5. VTOL Jet

The VTOL jet was operated at ambient temperature, using the Mach 1.00 nozzle. The tests were run with the nozzle exhausting at 3, 6, and 9 exit diameters above the ground plane.

Contours were plotted for the overall band and octave bands with normalized band limits of fD = 1250 to 2500, fD = 2500 to 5000, and fD = 5000 to 10,000. The band limits are different for these tests because a different octave band analyzer was used which had filters in accordance with ISO standards.

The contours are shown in Figures 61, 62, and 63. At first inspection the effects seem contrary to expectations. It would be normal to expect that sound pressure levels in the radiated near field would increase as the VTOL jet approaches the ground. However, examination of a given point in the free field shows that the sound pressure level increases

slightly as the engine is moved from 9 to 6 diameters above the ground plane. Then, as the engine is moved from 6 diameters to 3 diameters, the sound level in the near field is dramatically reduced.

Examination of the basic free-field jet at the same exhaust conditions is revealing (Figure 64). The source location for the overall band is between 4 and 5 diameters downstream of the nozzle exit plane. For the various octave bands, the source location varies from 2 to 6 diameters downstream of the exit plane. If the ground plane distance is greater than the maximum source distance, then the noise field would not be affected significantly, except for radiation from the turbulence created by the impinging jet. Looking at Figure 65, if the source distance from the ground, d, is great, then the radiation from the low-frequency turbulence generated by the deflected jet would not significantly affect the general contour shapes of the basic jet, except very close to the ground plane. In terms of radiation efficiency, the primary sources of noise generation in the jet are lateral and longitudinal quadrupoles (Reference 6). However, from Reference 20, it is concluded that the radiation from a turbulent boundary layer above an infinite rigid plane is of omni-directional, quadrupole character. This is a very inefficient type of radiation compared with jet noise.

Now, if the distance H is decreased to such an extent that the jet noise sources are buried in the turbulence generated by impingement on the ground plane, the sound pressure levels will decrease markedly. This is exactly what occurs when the jet is 3 diameters above the ground plane. Maximum SPL decreases 10 decibels. This will obviously affect some frequency bands to a greater extent than others.

An analysis in Reference 4 shows the effect on source output created by distance of the jet exhaust and source location from the ground plane. A plot is also presented in Reference 4 which shows the effect of distance above the ground on radiated sound pressure levels. (The decrease in level explained here was noted in Reference 4.)

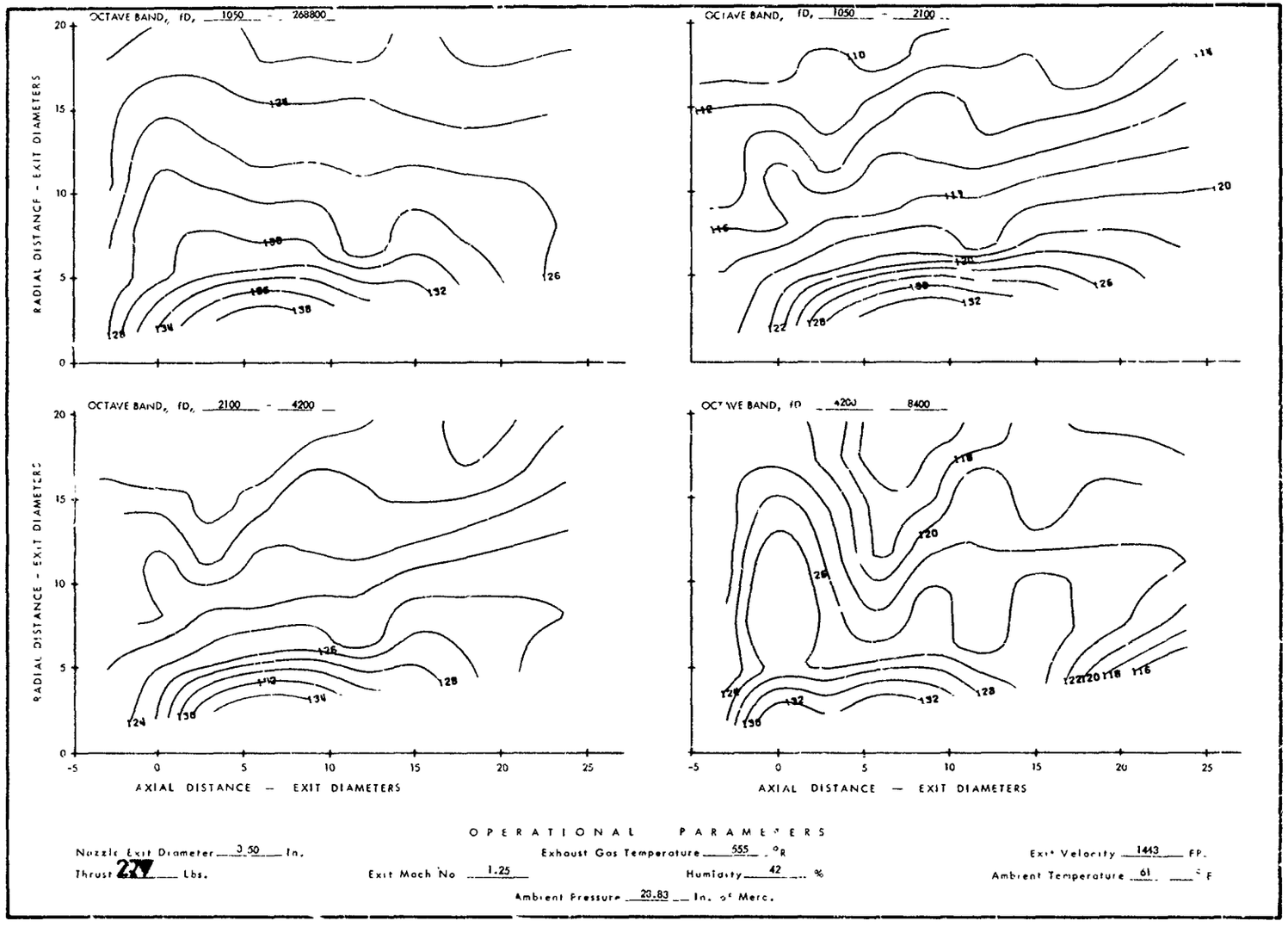

FIGURE 42 SPL CONTOURS FOR MACH 1.25 NOZZLE WITH EJECTOR, 555°R

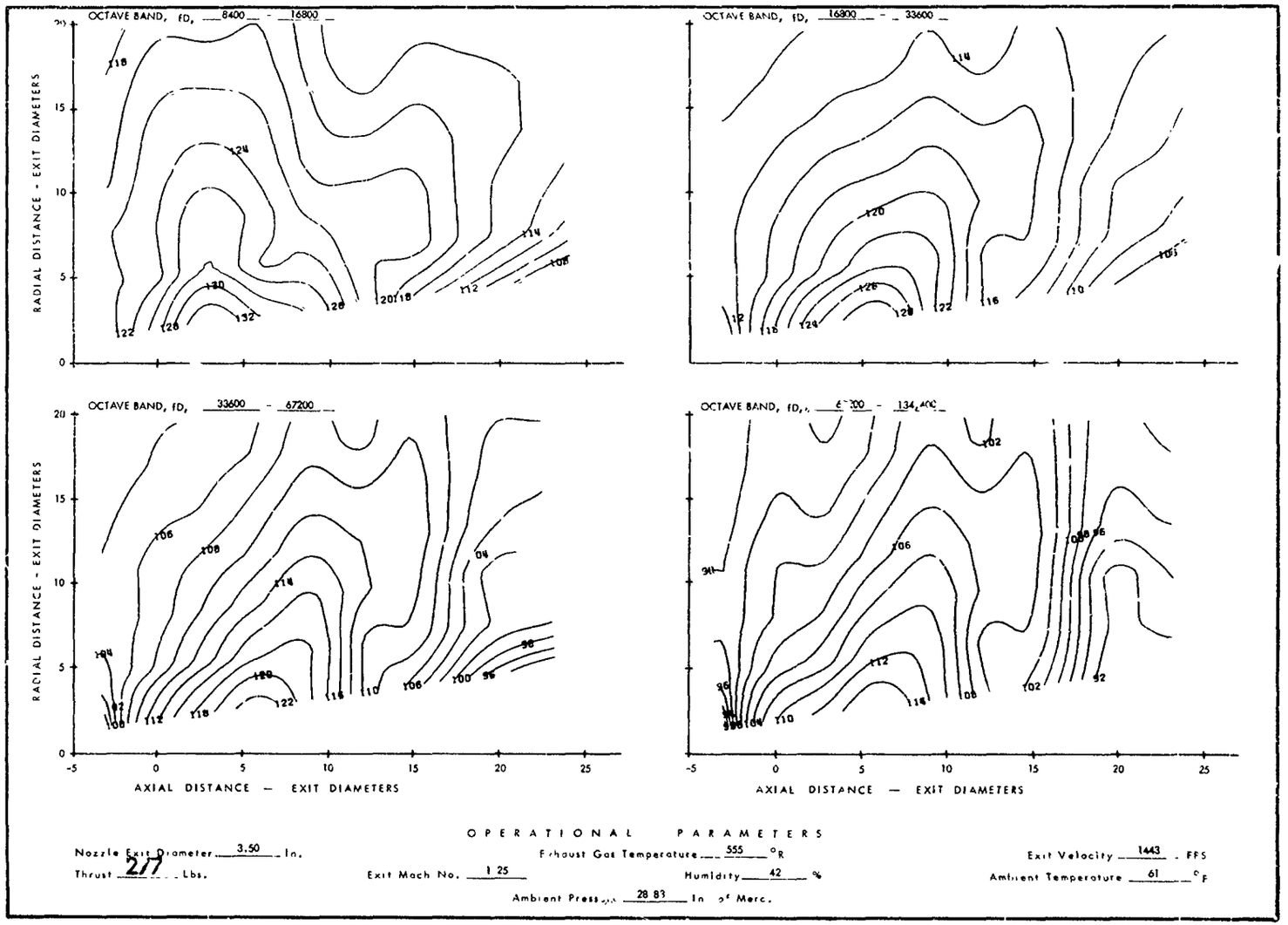

FIGURE 42 SPL CONTOURS FOR MACH 1.25 NOZZLE WITH EJECTOR, 555°R (Cont'd)

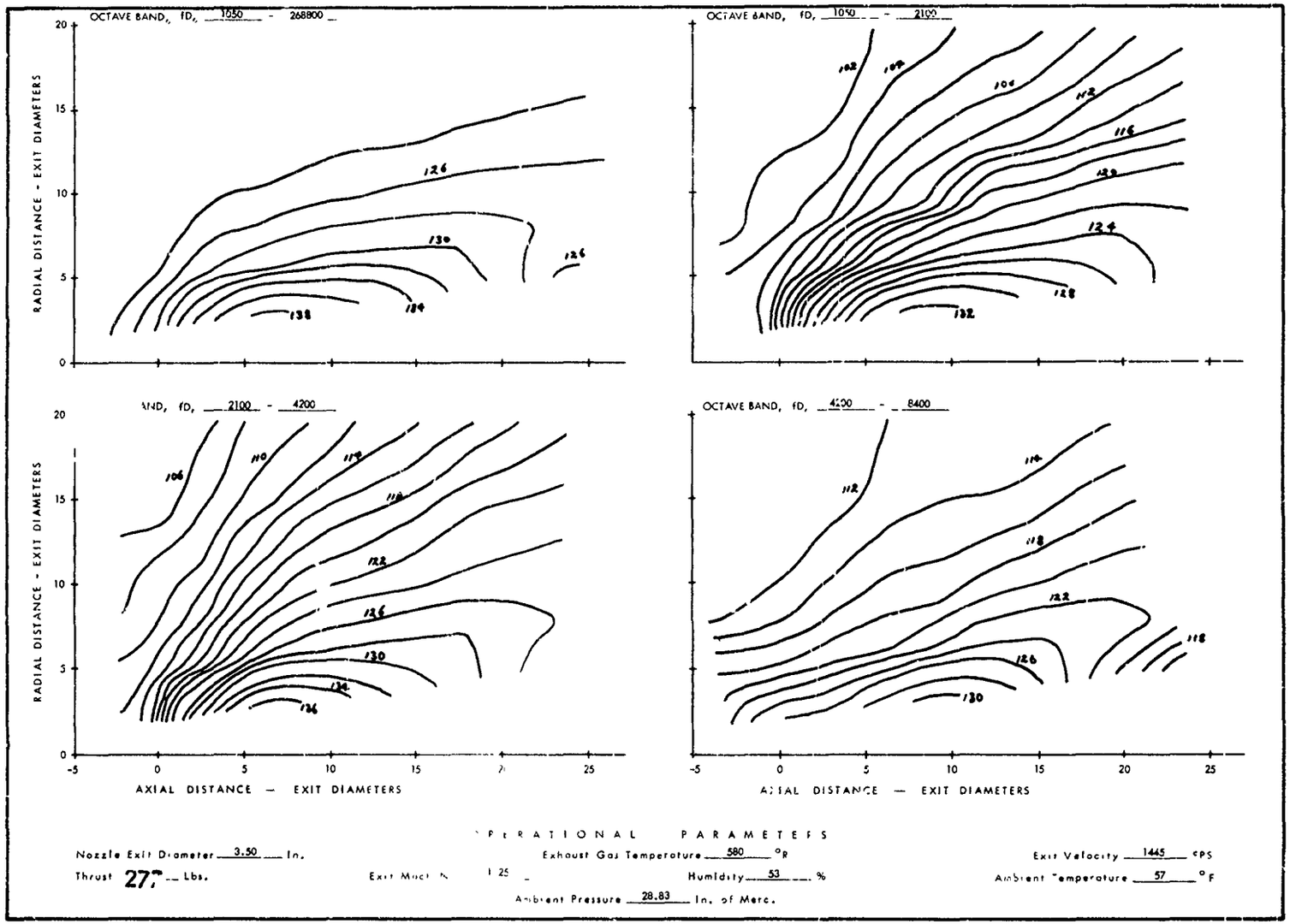

FIGURE 43 SPL CONTOURS FOR MACH 1.25 NOZZLE, 580°R

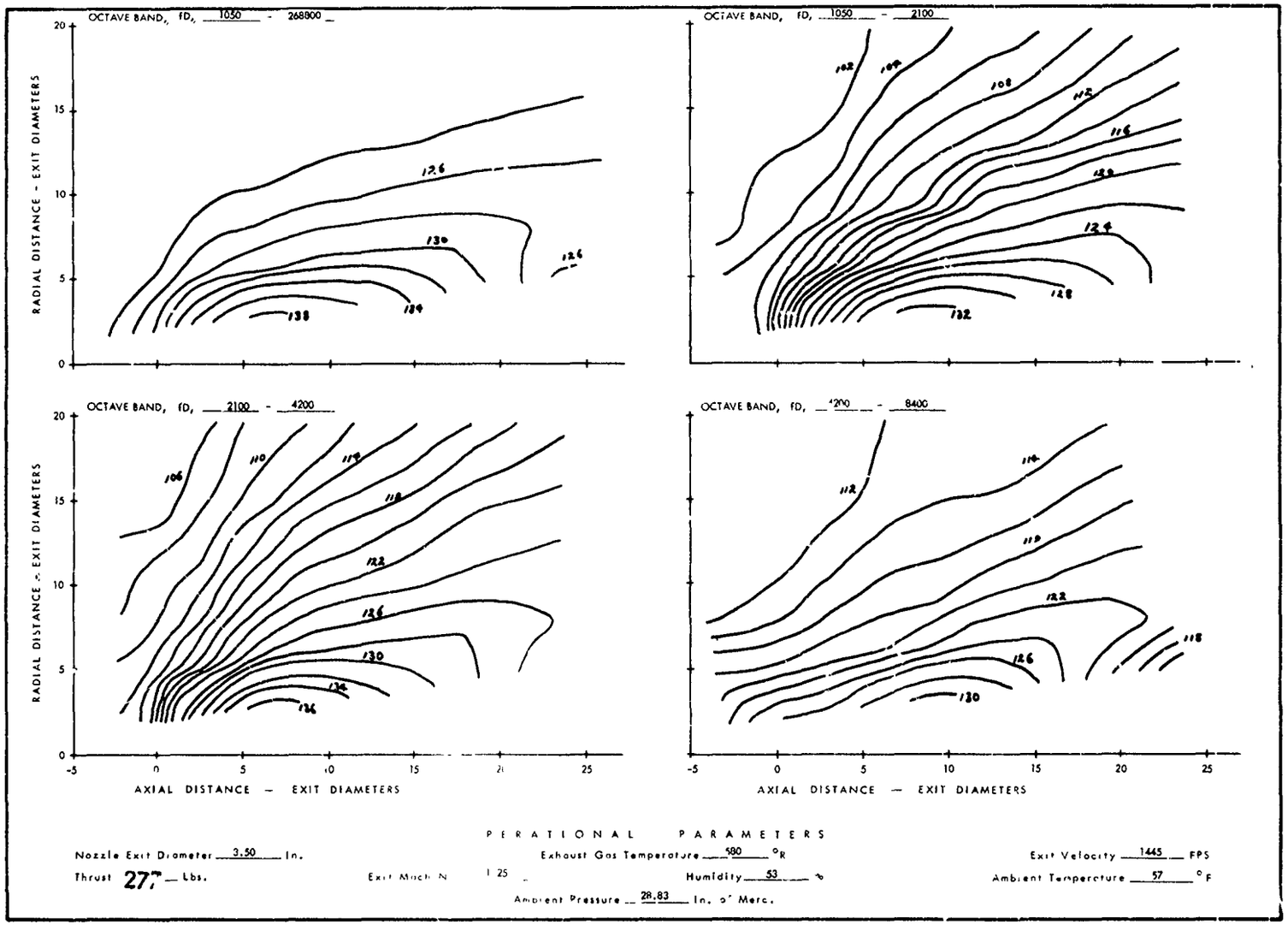

FIGURE 43 SPL CONTOURS FOR MACH 1.25 NOZZLE, 580°R

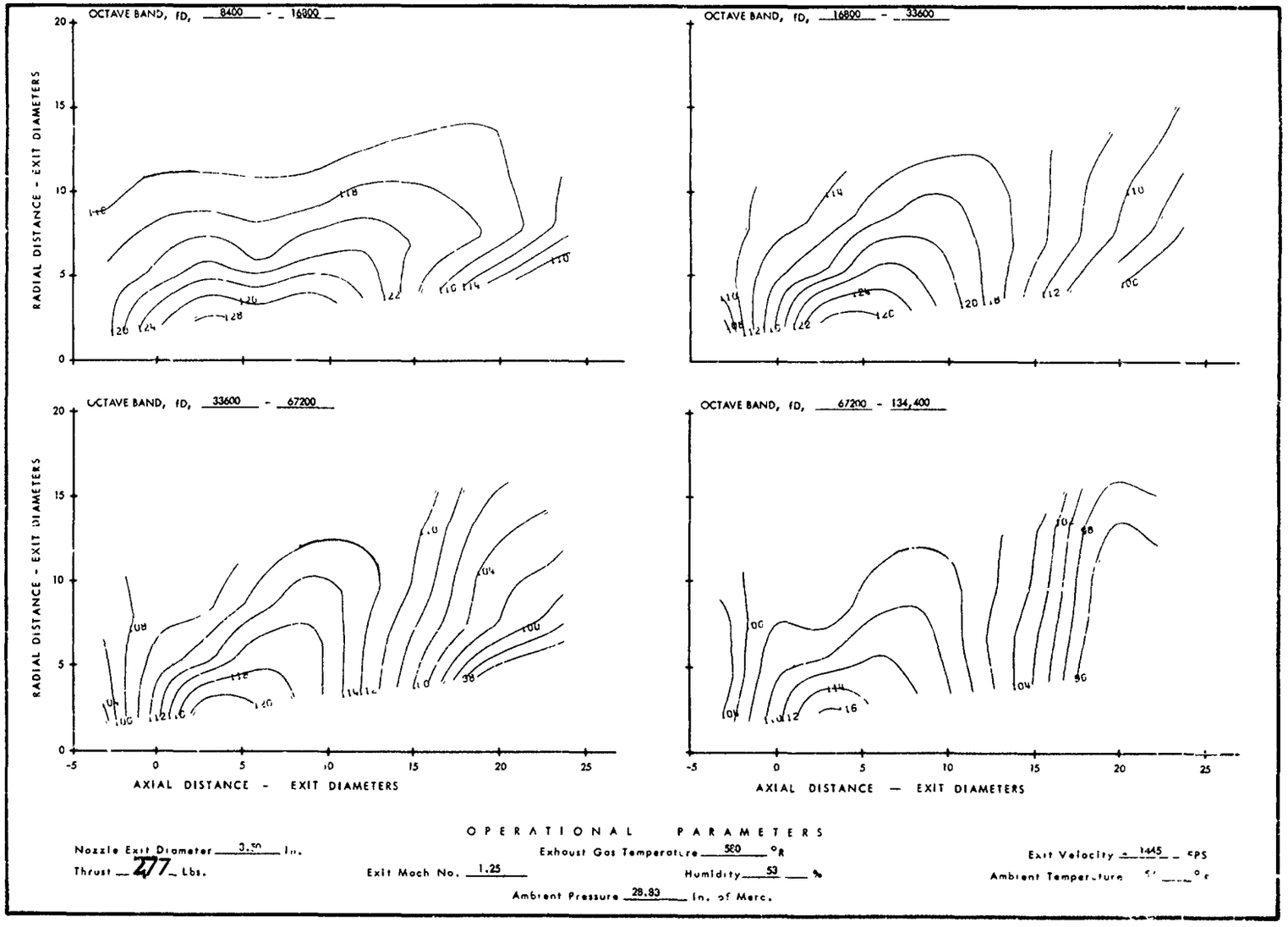

FIGURE 43 SPL CONTOURS FOR MACH 1.25 NOZZLE, 580°R (Cont'd)

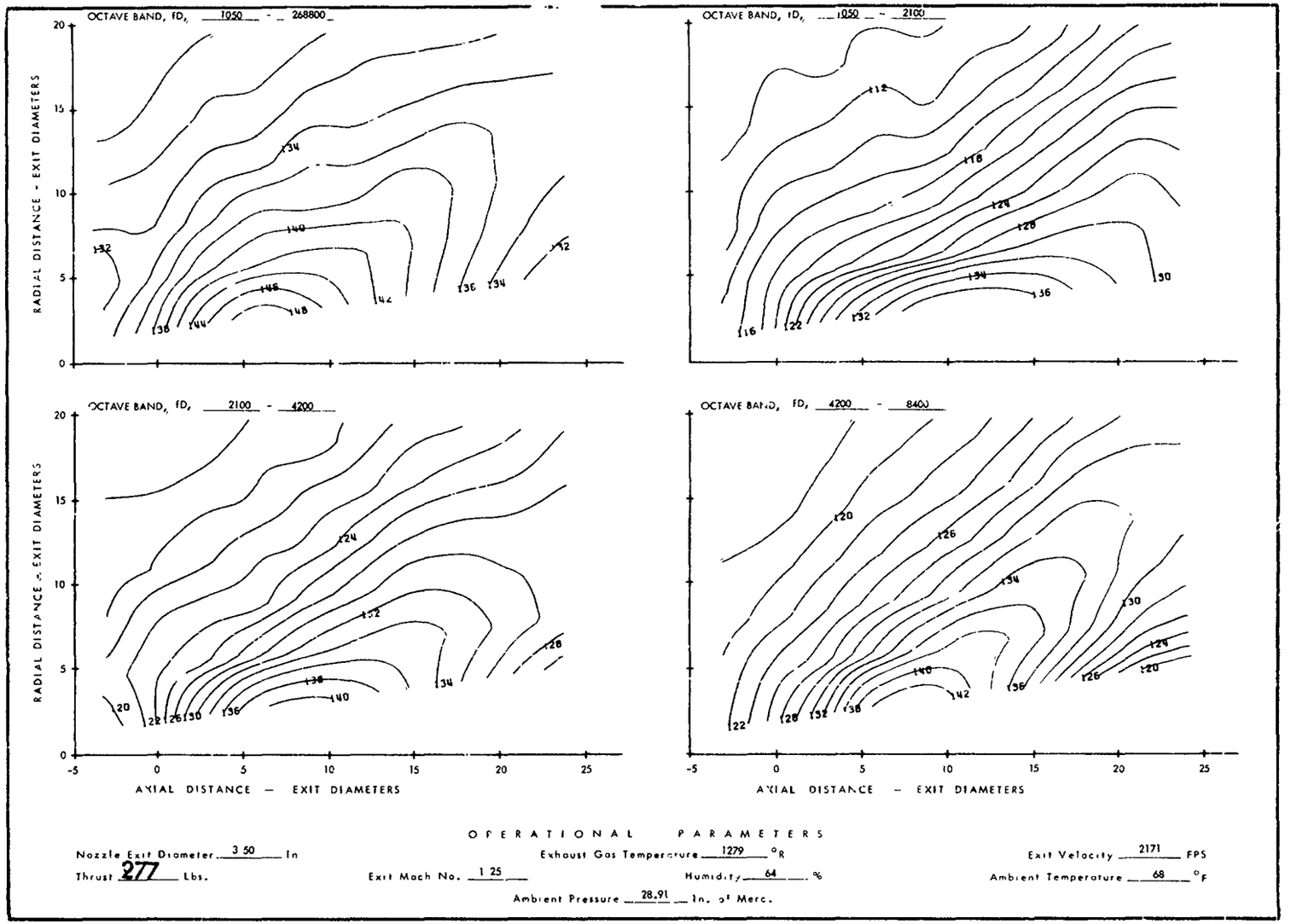

FIGURE 44 SPL CONTOURS FOR MACH 1.25 NOZZLE WITH EJECTOR, 1279°R

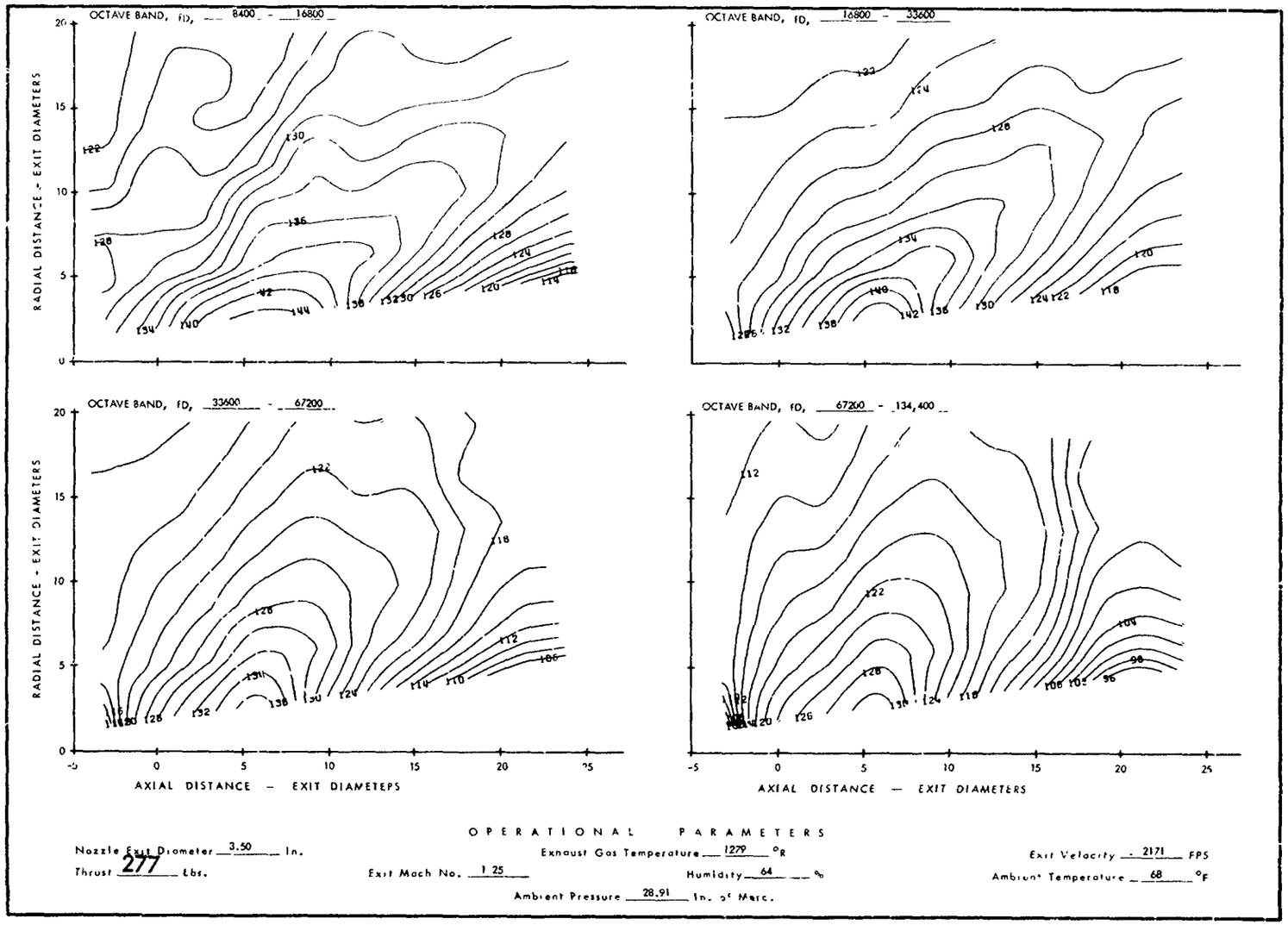

FIGURE 44 SPL CONTOURS FOR MACH 1.25 NOZZLE WITH EJECTOR, 1279°R (Cont'd)

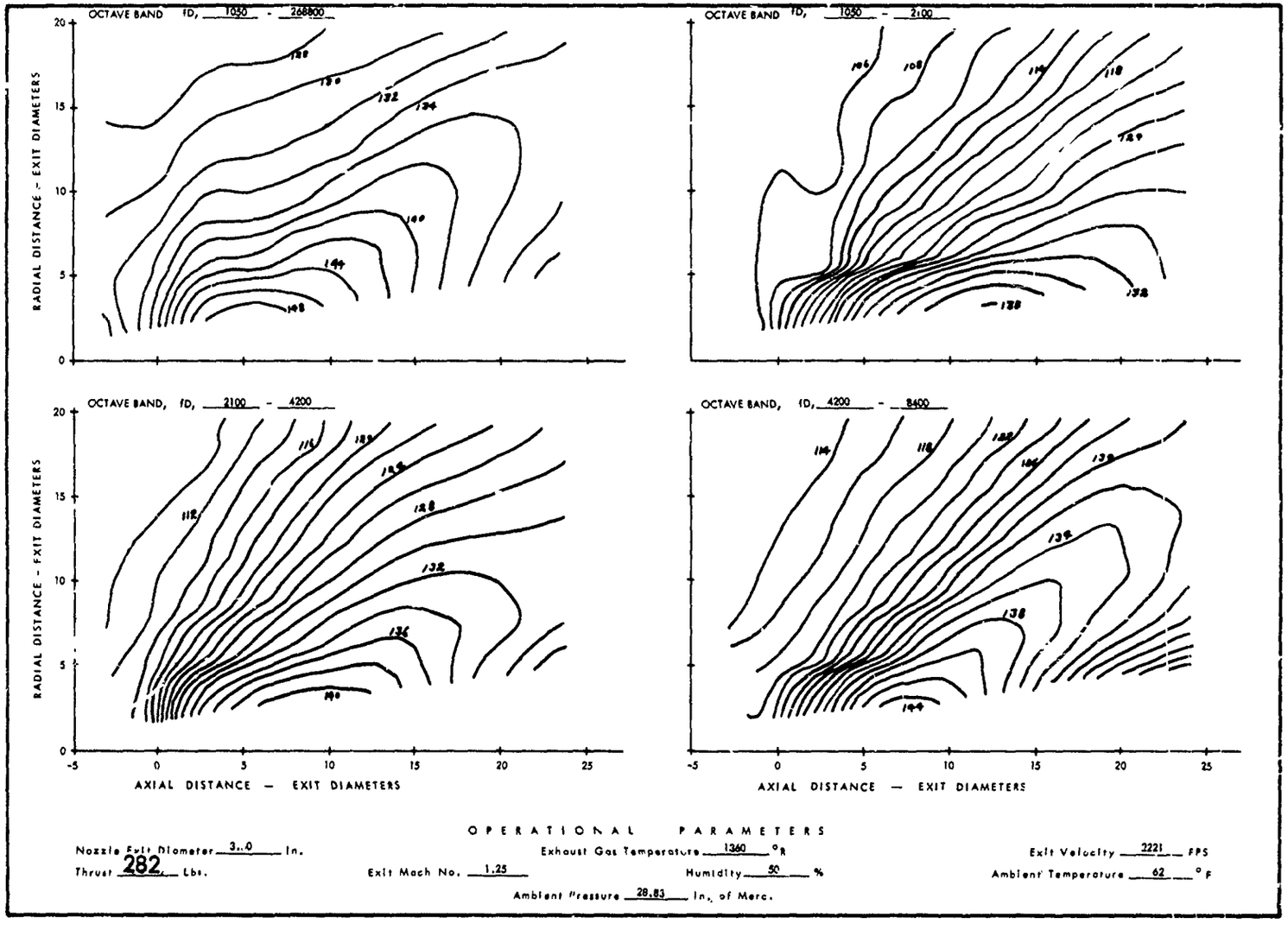

FIGURE 45 SPL CONTOURS FOR MACH 1.25 NOZZLE, 1360°R

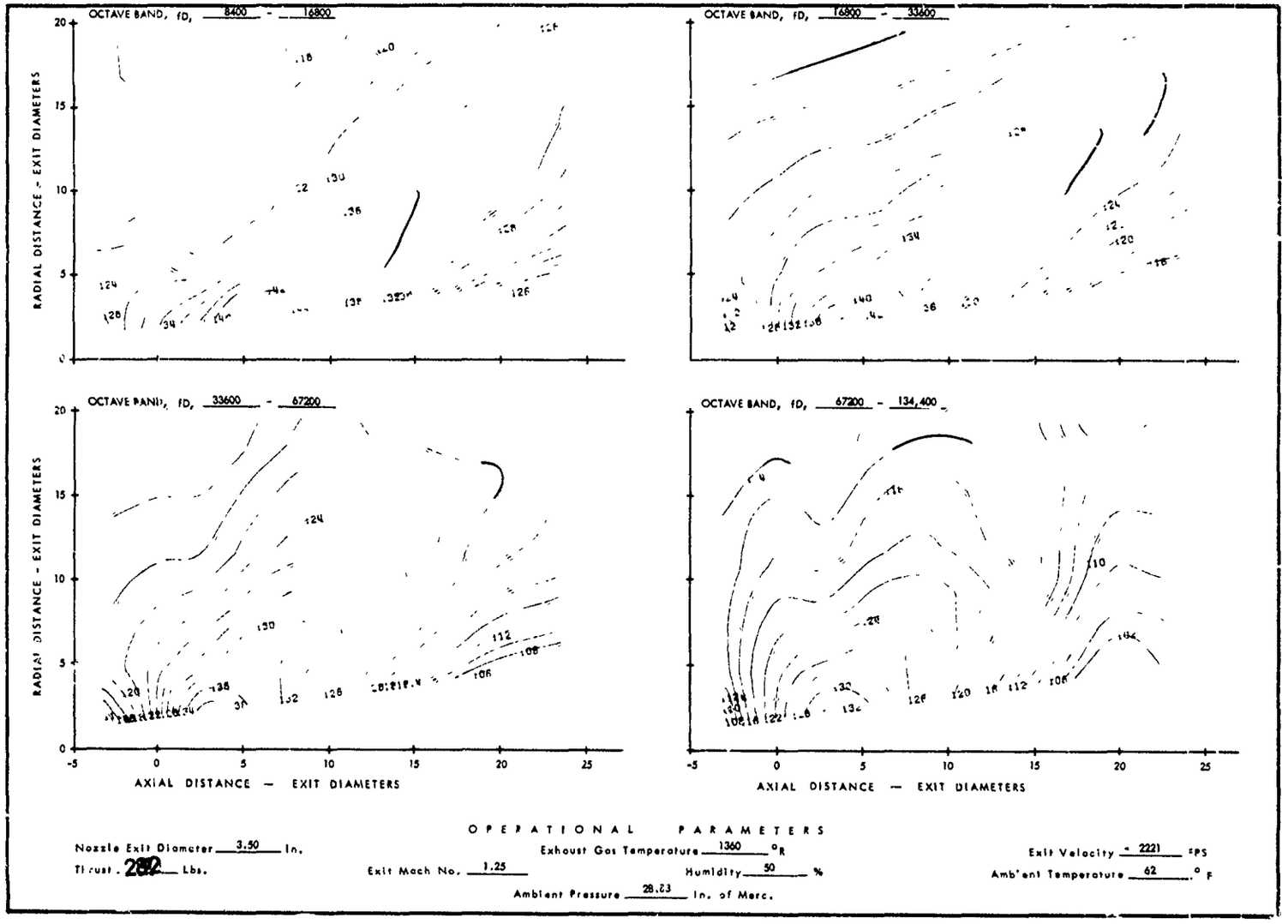

FIGURE 45 SPL CONTOURS FOR MACH 1.25 NOZZLE, 1360°R (Cont'd)

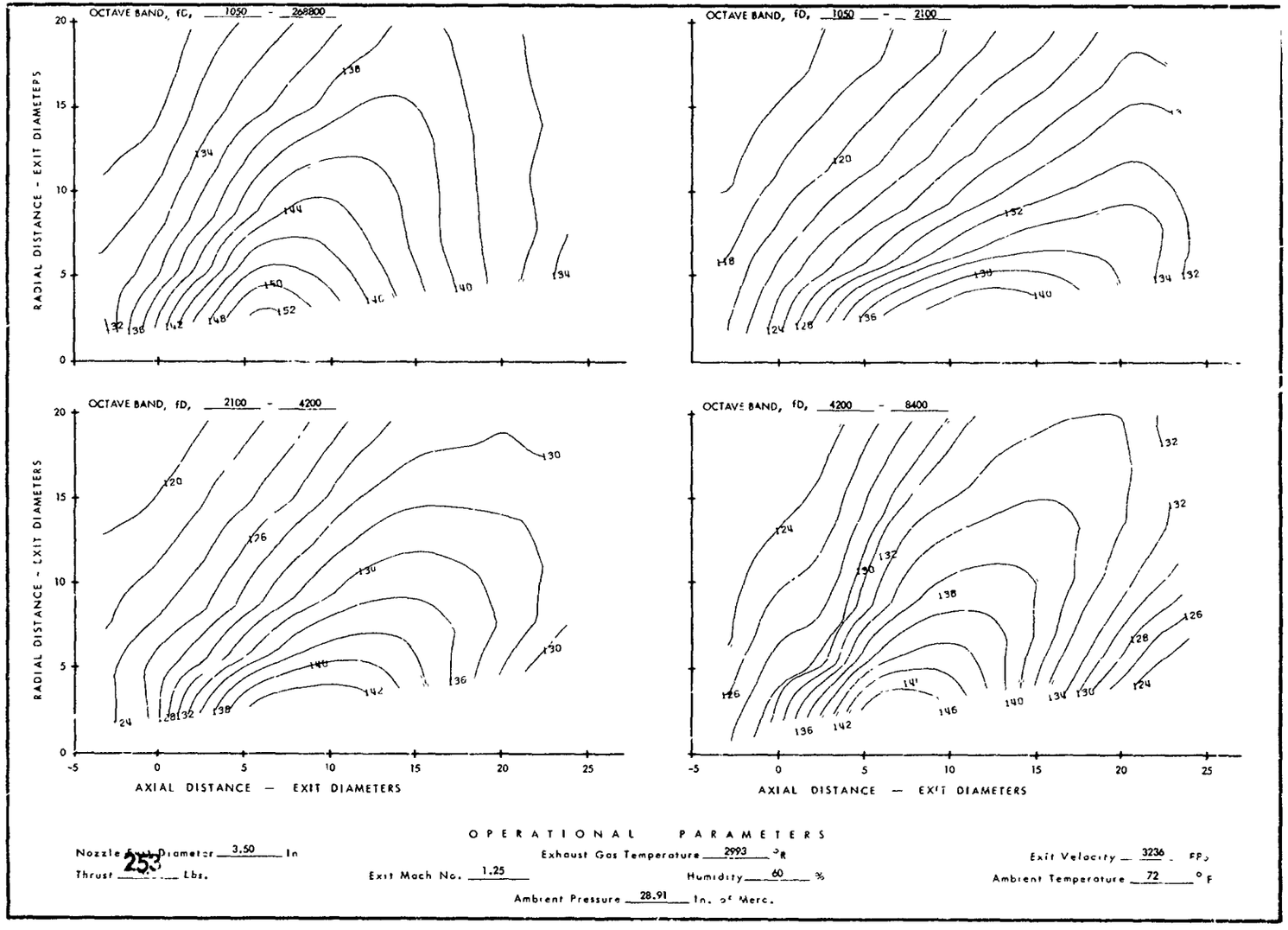

FIGURE 46 SPL CONTOURS FOR MACH 1.25 NOZZLE WITH EJECTOR, 2993°R

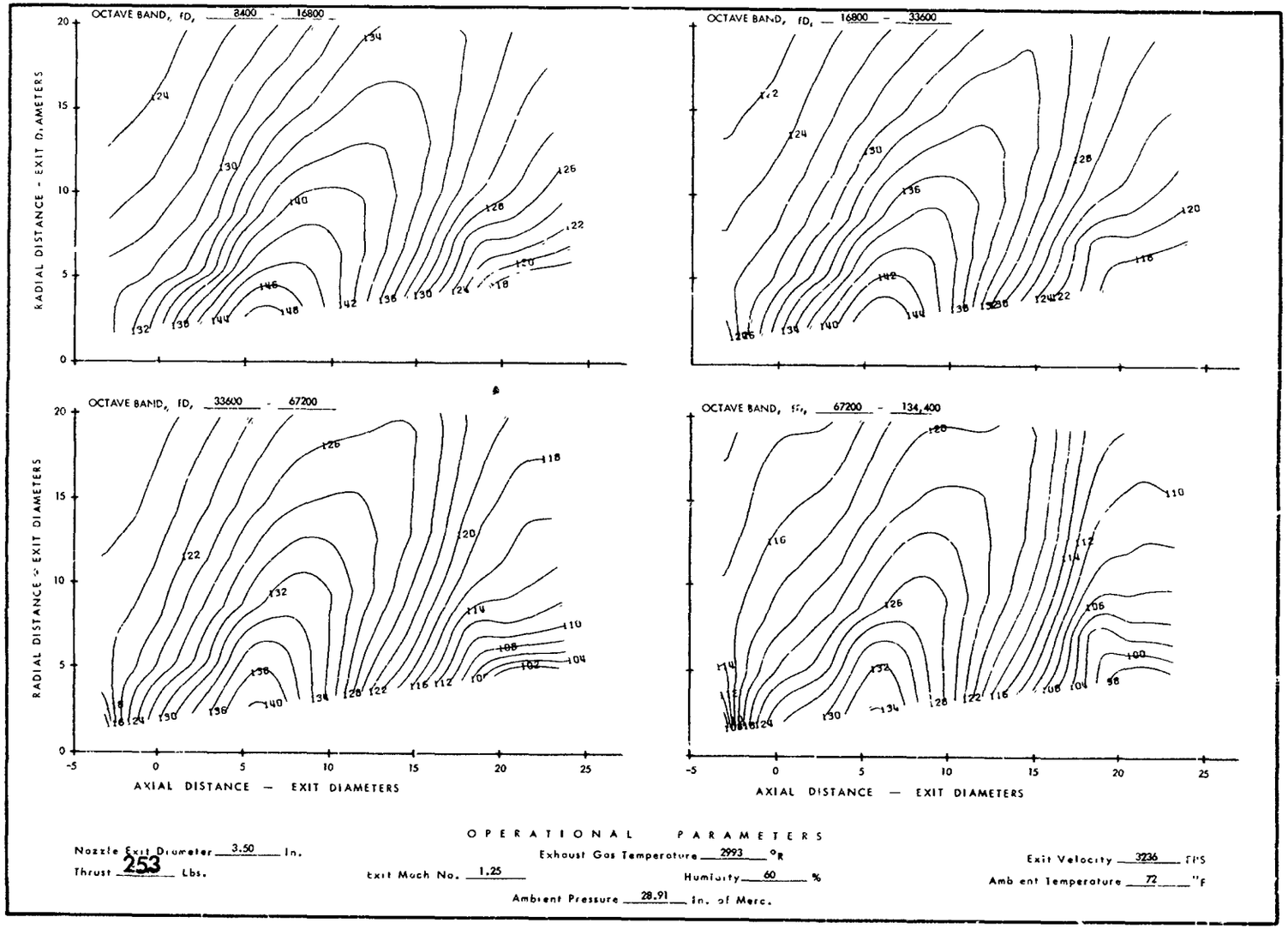

FIGURE 46 SPL CONTOURS FOR MACH 1.25 NOZZLE WITH EJECTOR, 2993°R (Cont'd)

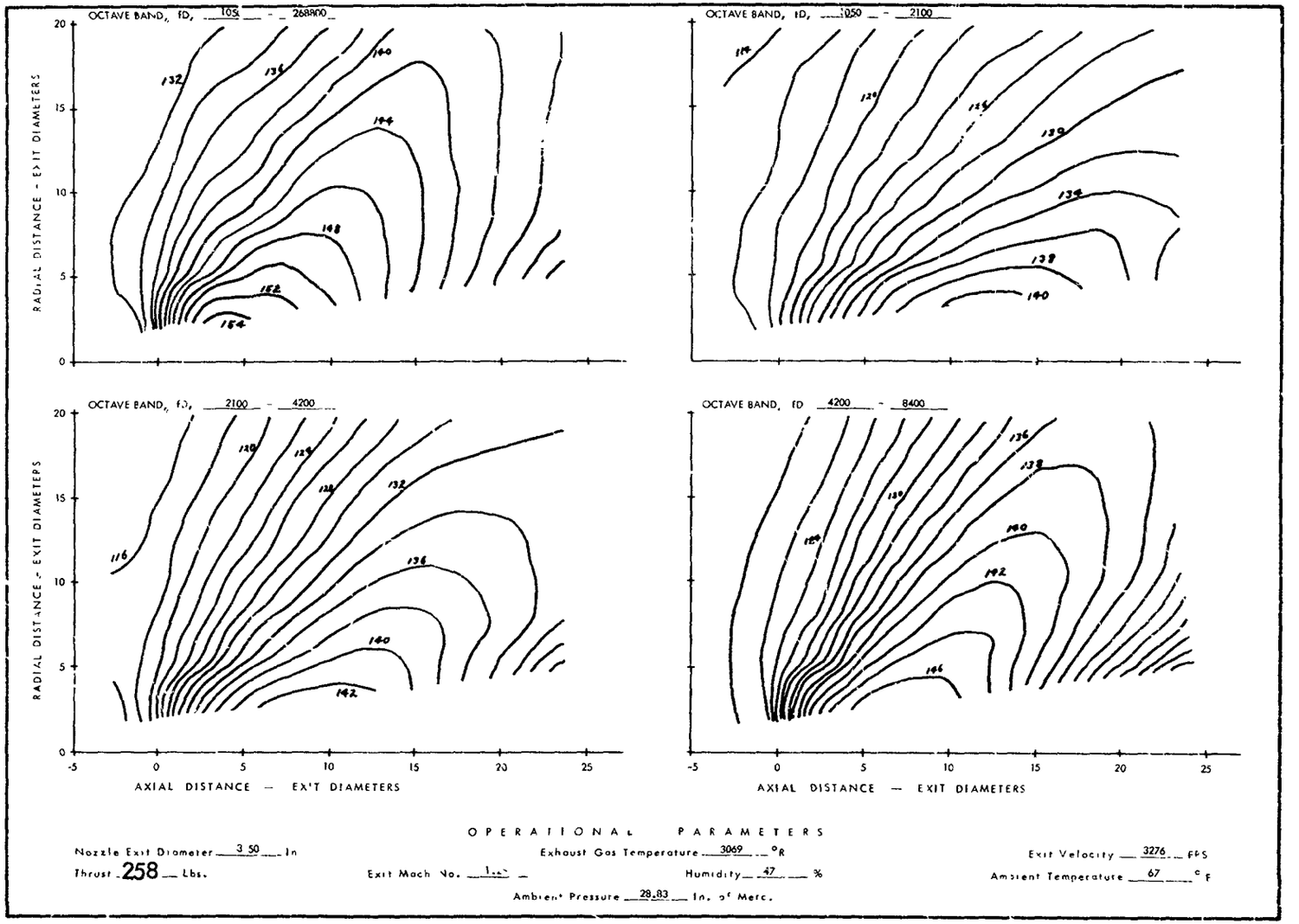

FIGURE 47 SPL CONTOURS FOR MACH 1.25 NOZZLE, 3069°R

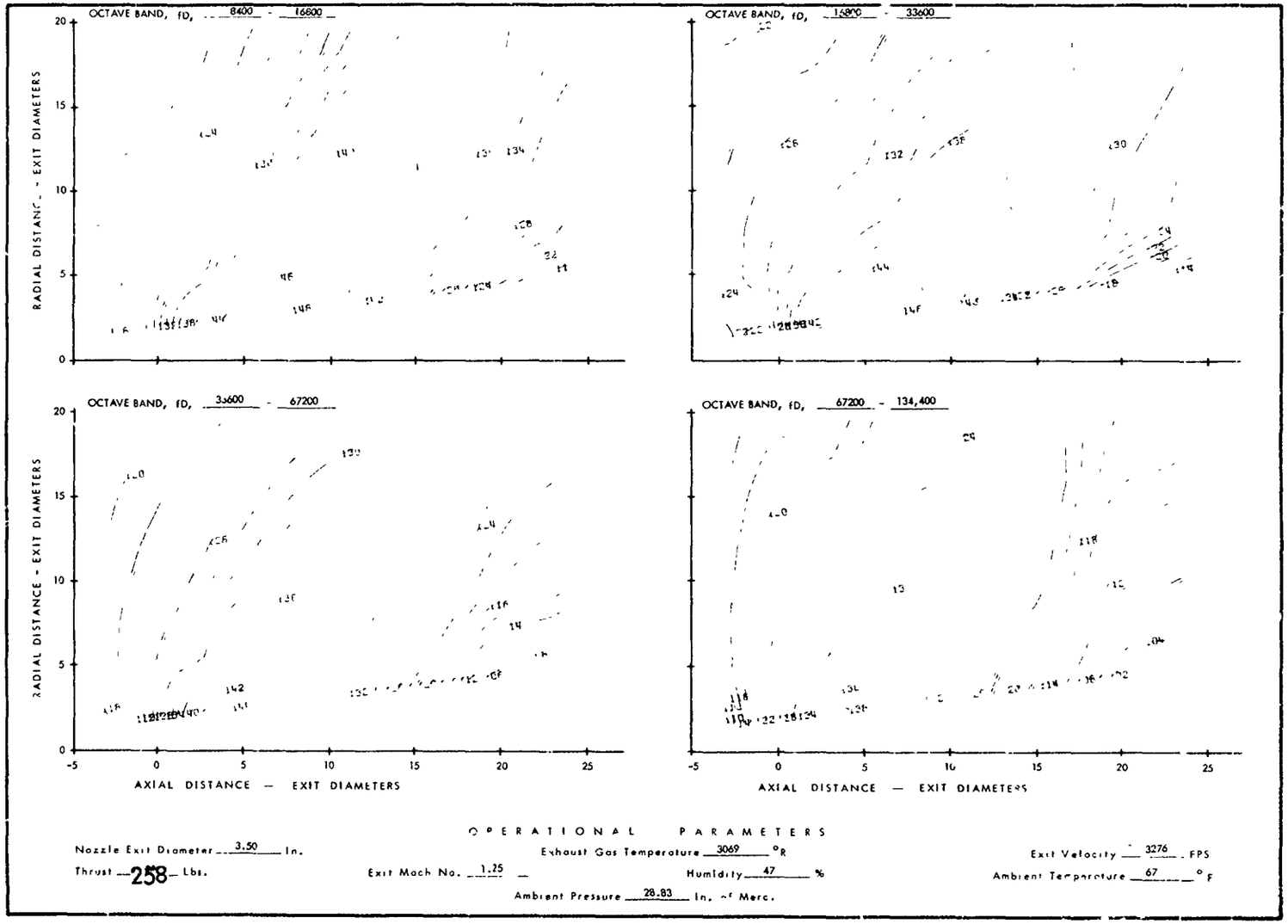

FIGURE 47 SPL CONTOURS FOR MACH 1.25 NOZZLE, 3069°R (Cont'd)

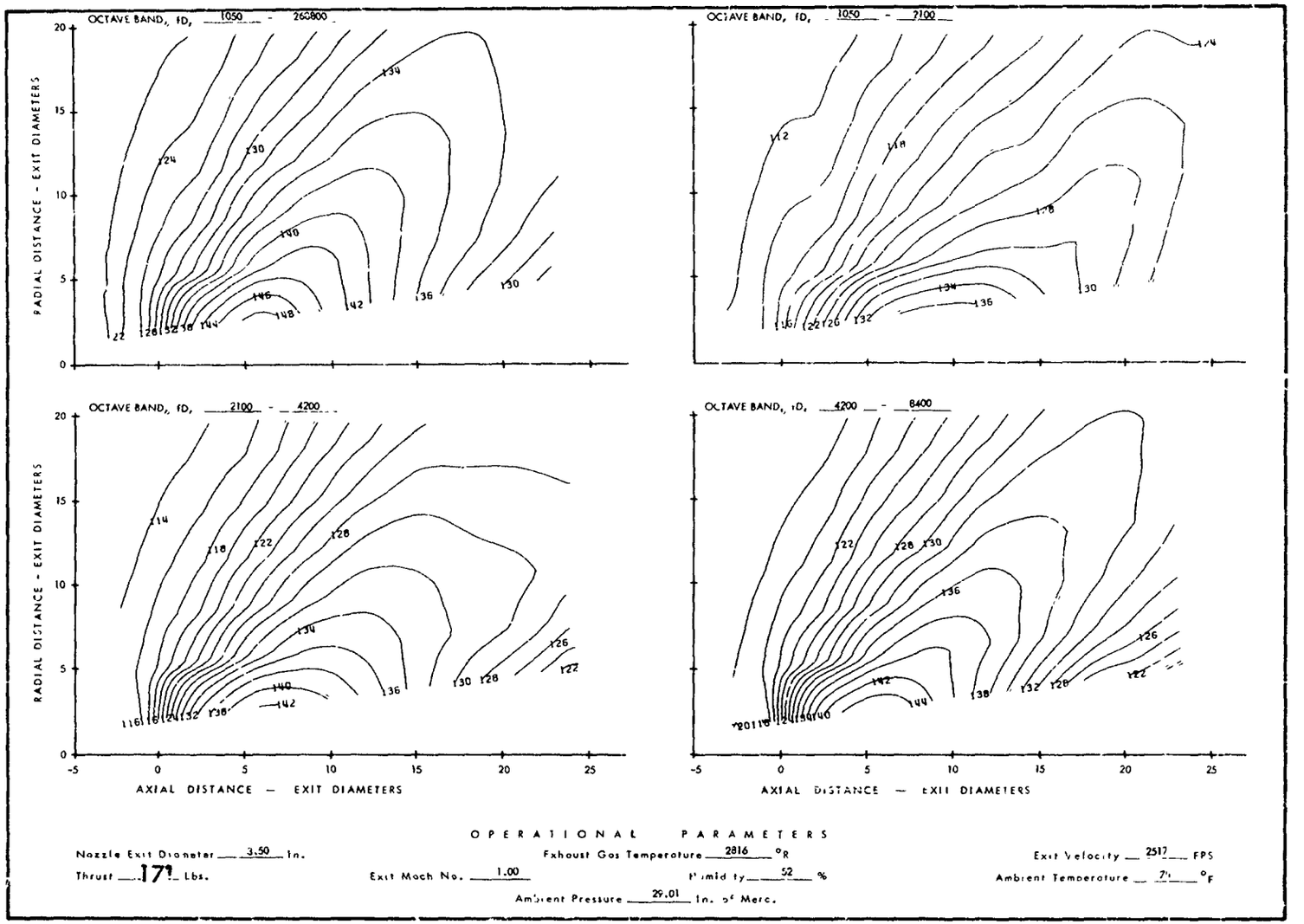

FIGURE 48 EFFECT OF GROUND PLANE ON BASIC JET: GROUND PLANE 5 DIAMETERS FROM C.L. MACH NO. = 1.00 TEMP. = 2816°R

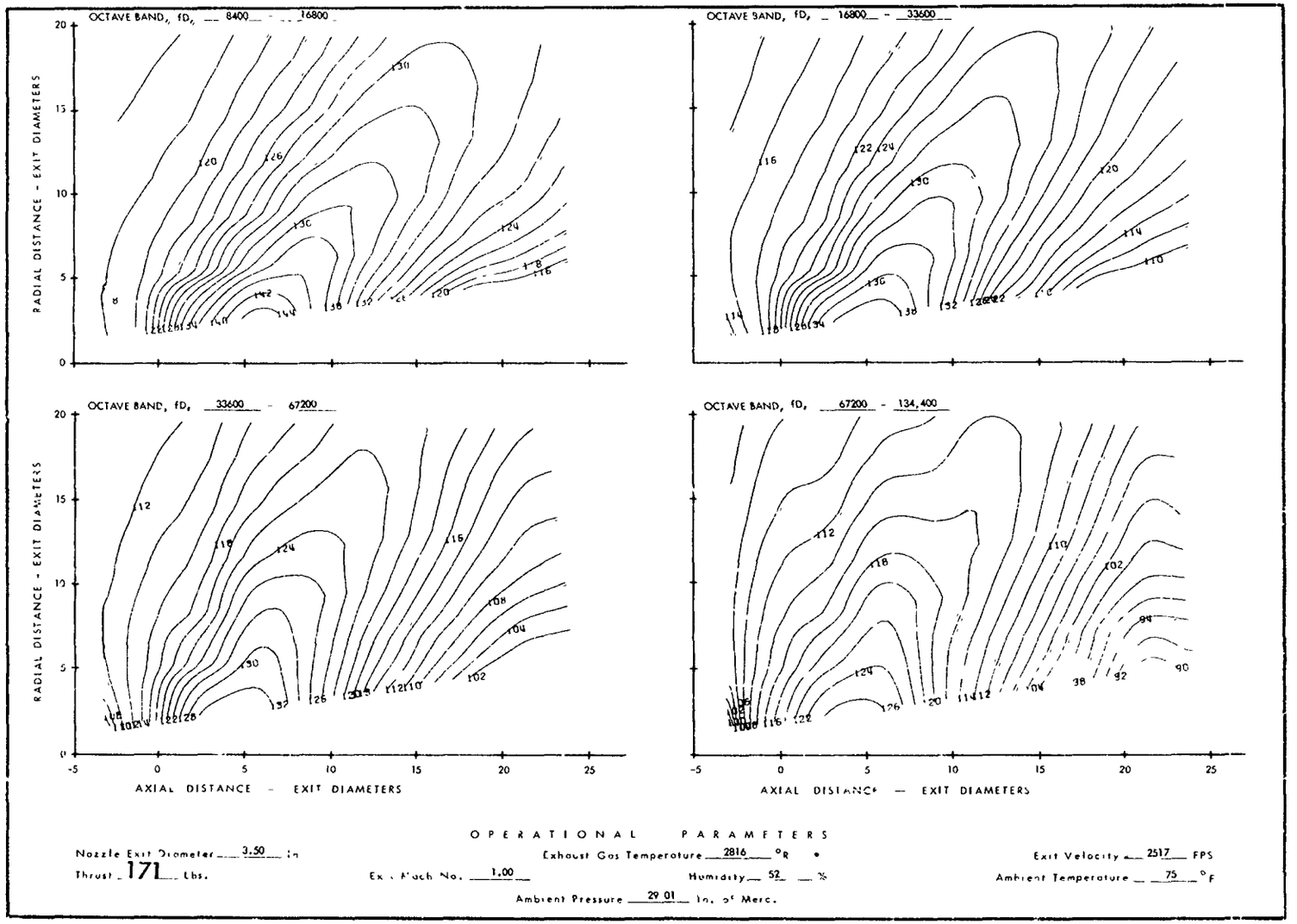

FIGURE 48 EFFECT OF GROUND PLANE ON BASIC JET GROUND PLANE 5 DIAMETERS FROM C.L. MACH NO. = 1.00 TEMP. = 2816°R (CONT'D)

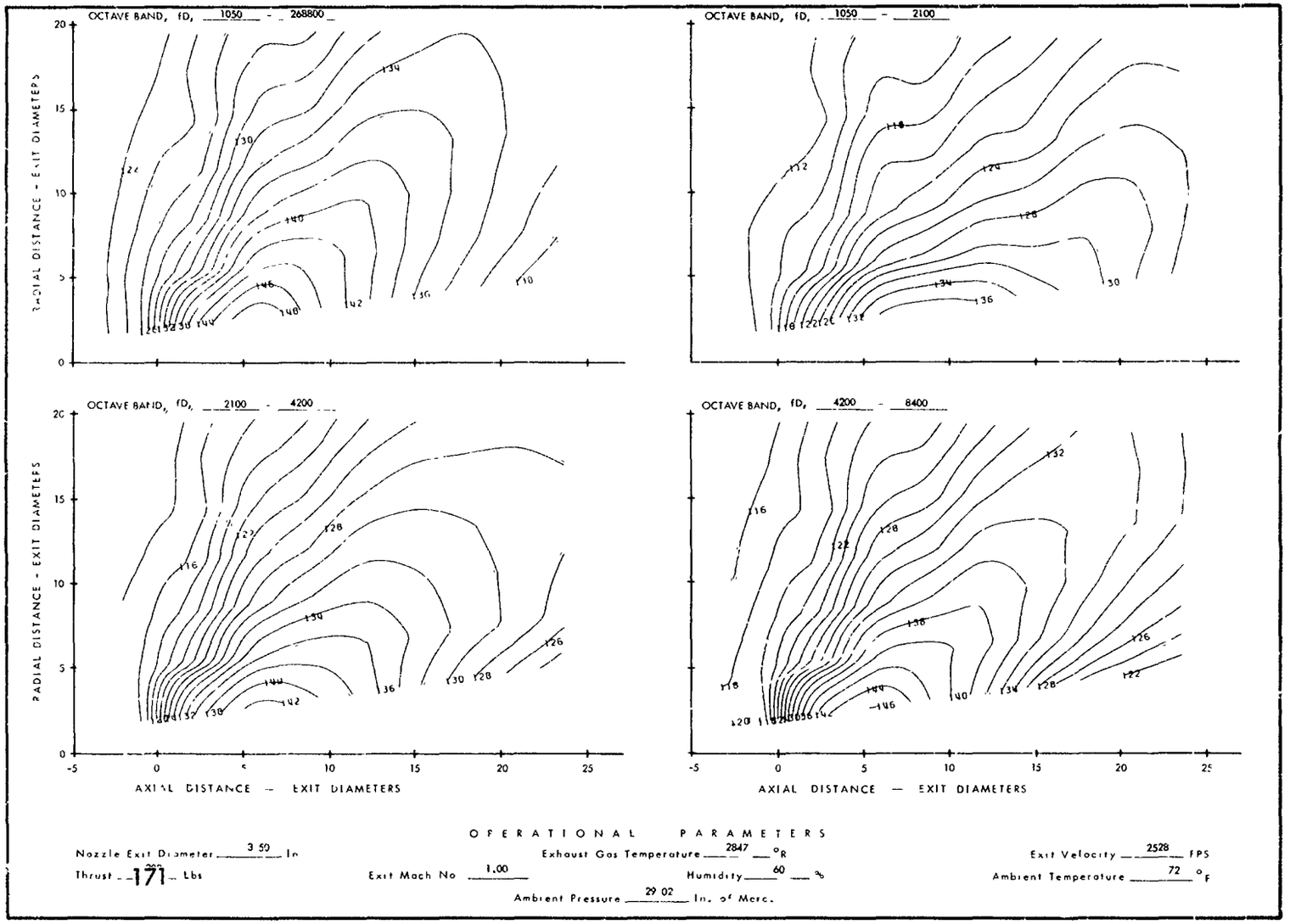

FIGURE 49 EFFECT OF GROUND PLANE ON BASIC JET GROUND PLANE 10 DIAMETERS FROM C. L. MACH NO. = 1.00 TEMP. = 2847°R

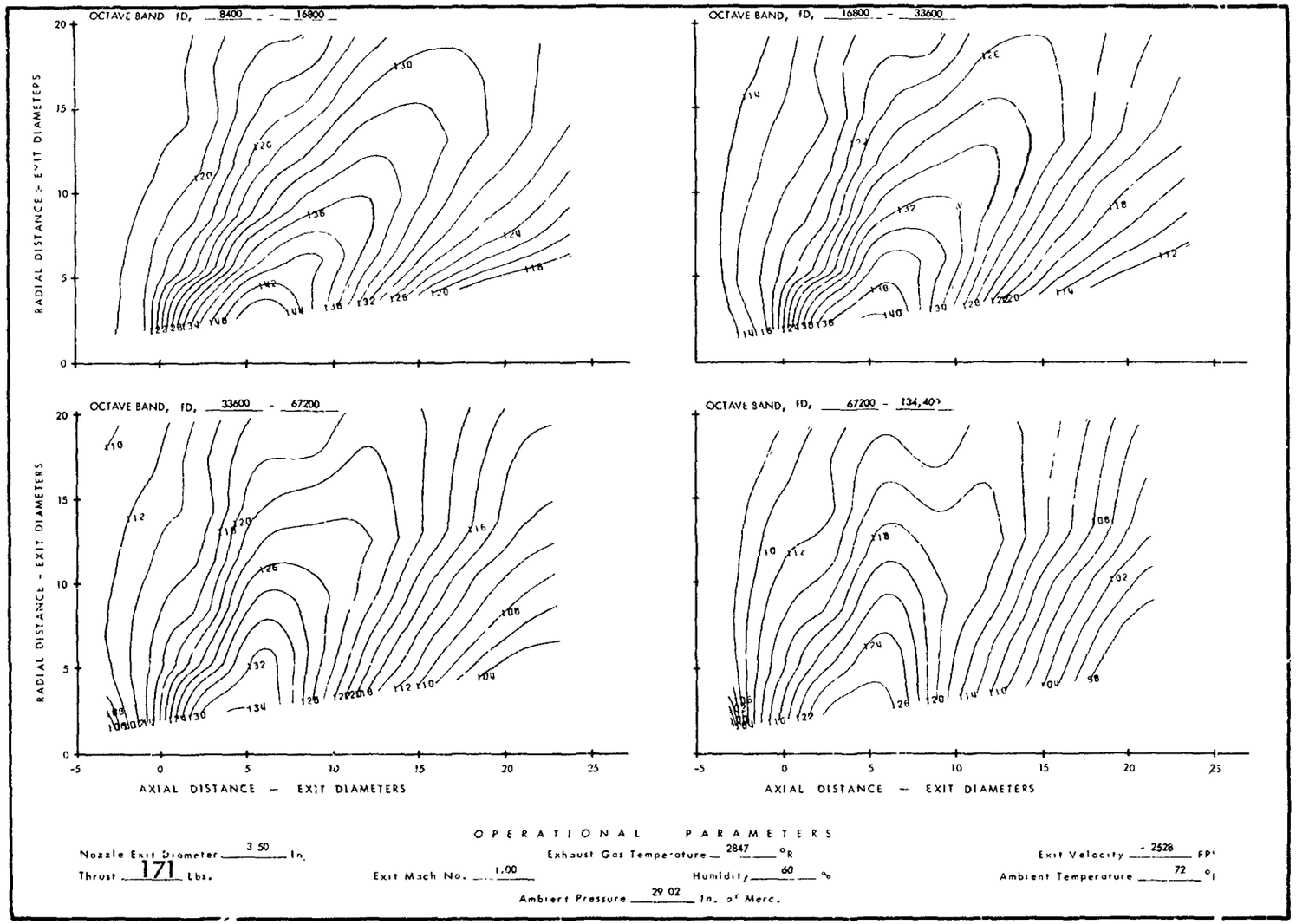

FIGURE 49 EFFECT OF GROUND PLANE ON BASIC JET GROUND PLANE 10 DIAMETERS FROM C. L. MACH NO. = 1.00 TEMP. = 2847°R (CONT'D)

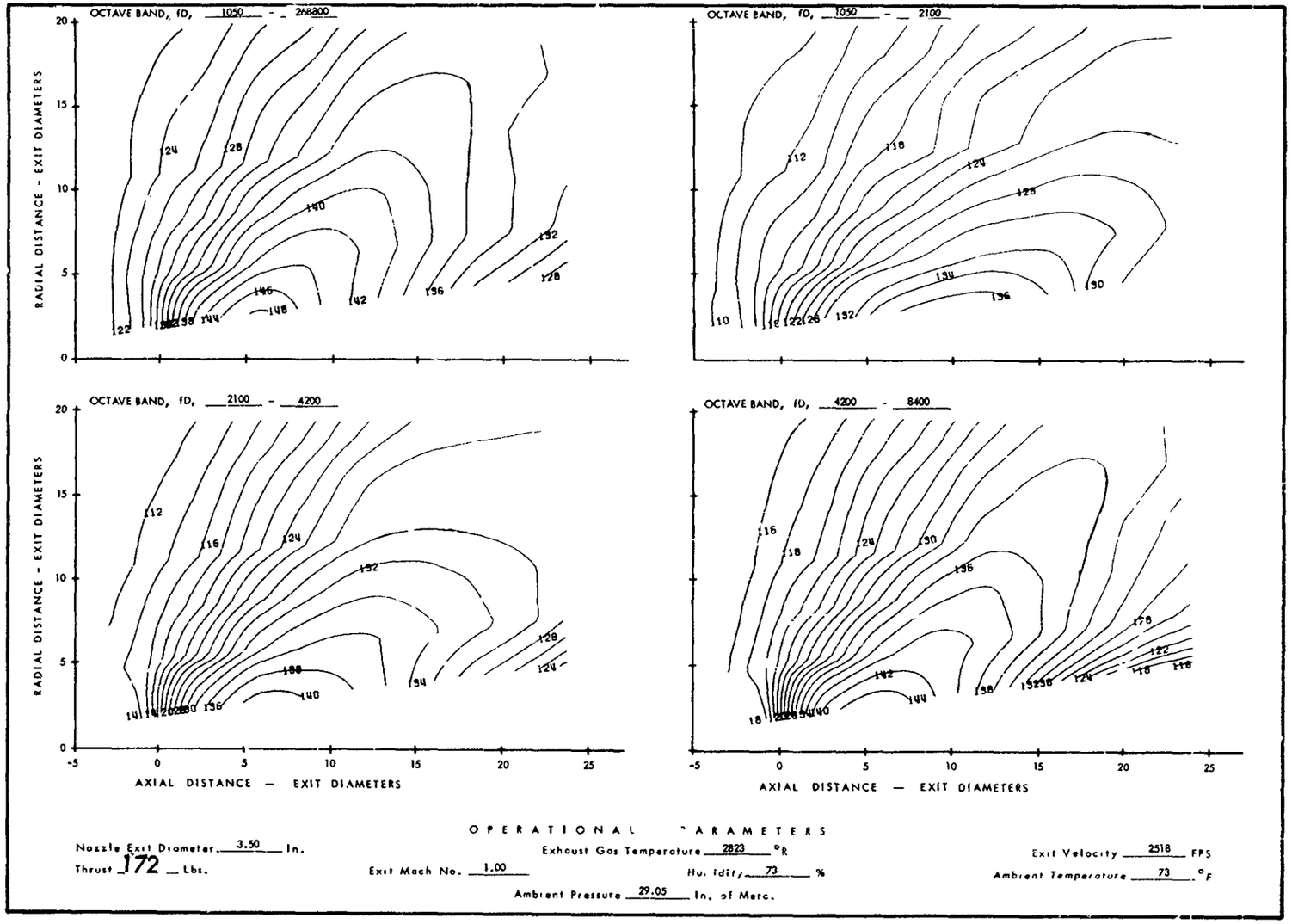

FIGURE 50 BASIC JET, MACH NO. = 1.00, TEMP. = 2823°R

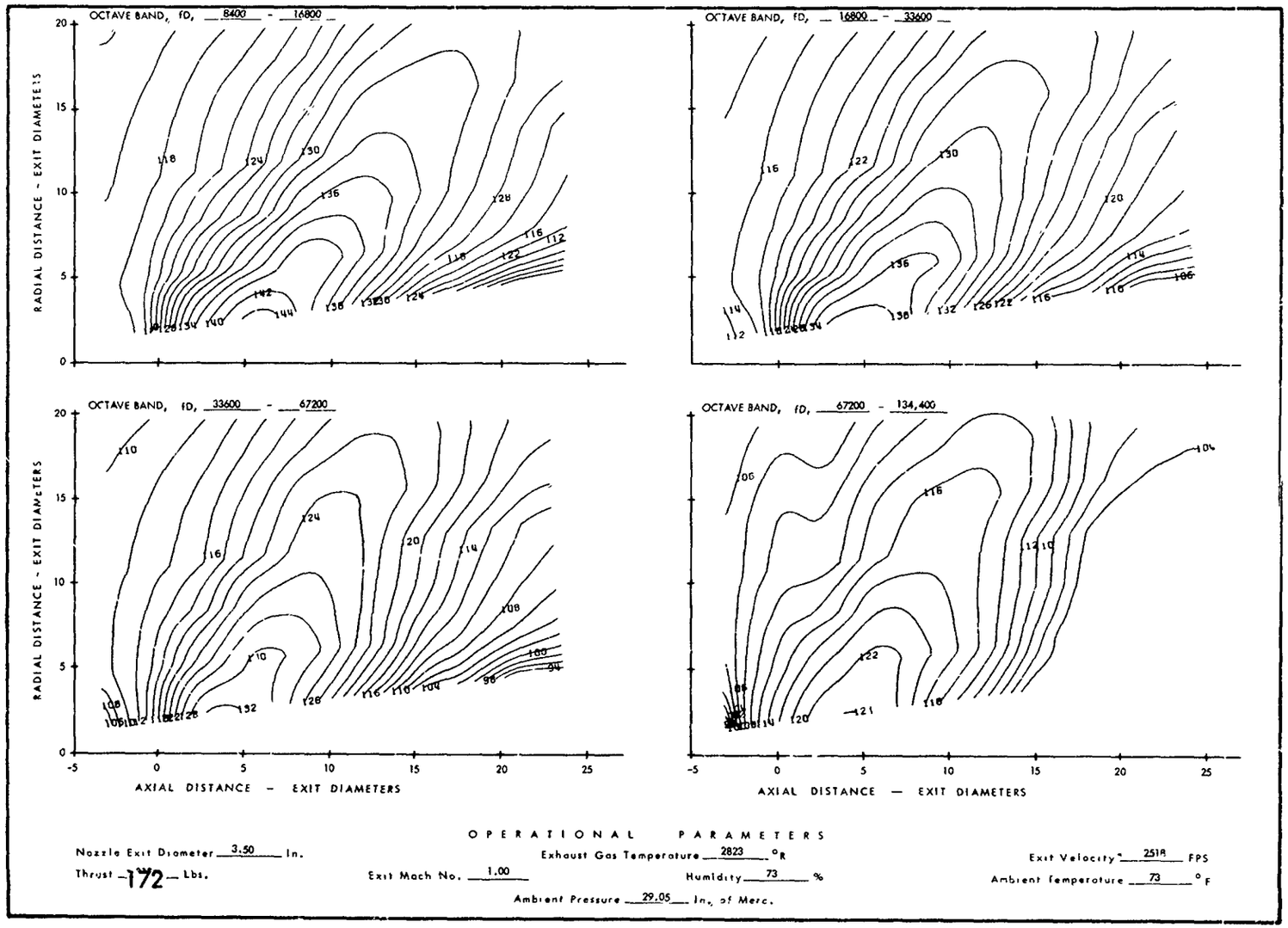

FIGURE 50 BASIC JET, MACH NO. = 1.00, TEMP. = 2823°R (CONT'D)

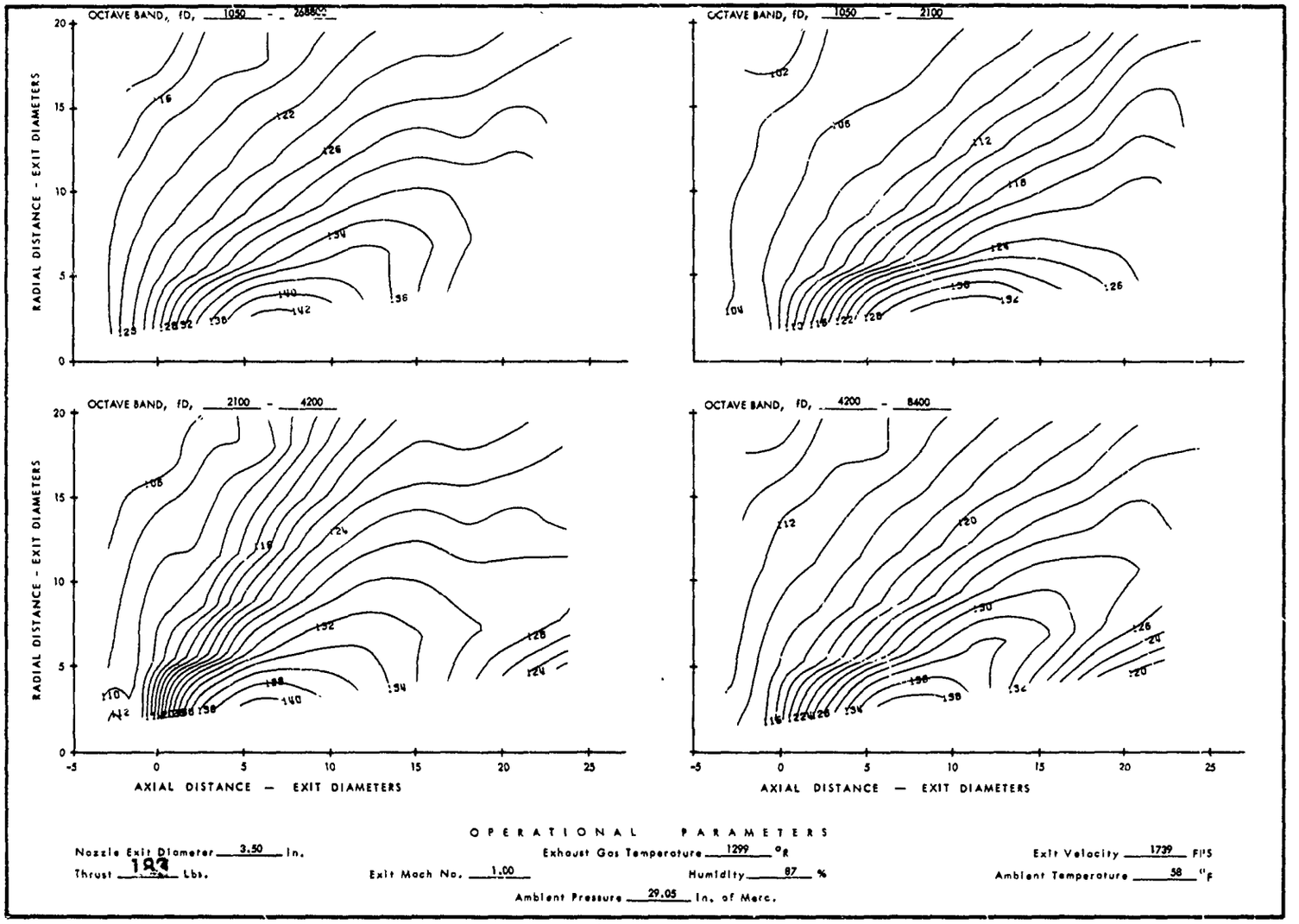

FIGURE 51 EFFECT OF GROUND PLANE ON BASIC JET, GROUND PLANE 5 DIAMETERS FROM C.L. MACH NO. = 1.00 TEMP. = 1299°R

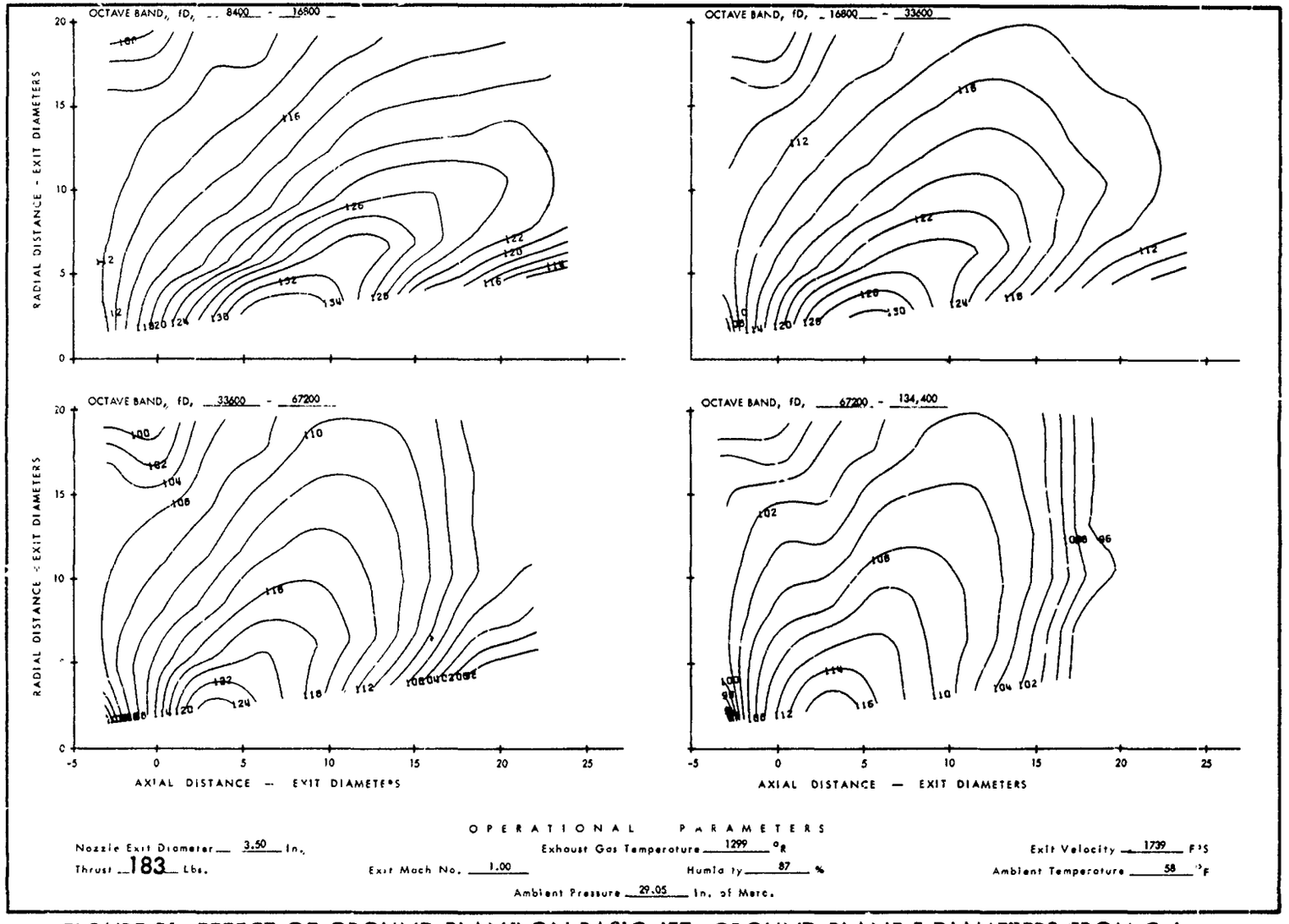

FIGURE 51 EFFECT OF GROUND PLANE ON BASIC JET GROUND PLANE 5 DIAMETERS FROM C.L. MACH NO. = 1.00 TEMP. = 1299°R (CONT'D)

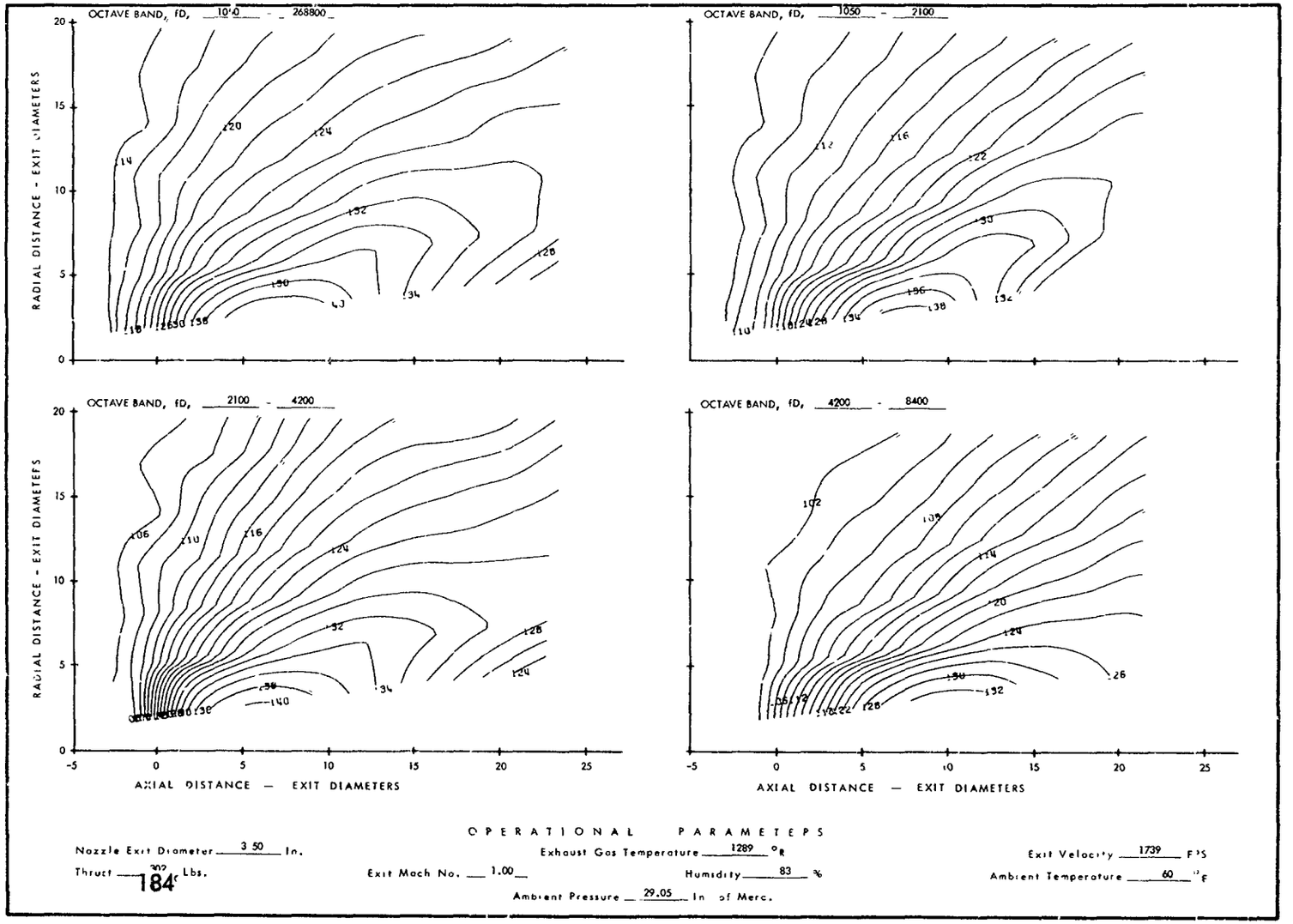

FIGURE 52 BASIC JET, MACH NO. = 1.00, TEMP. = 1289°R

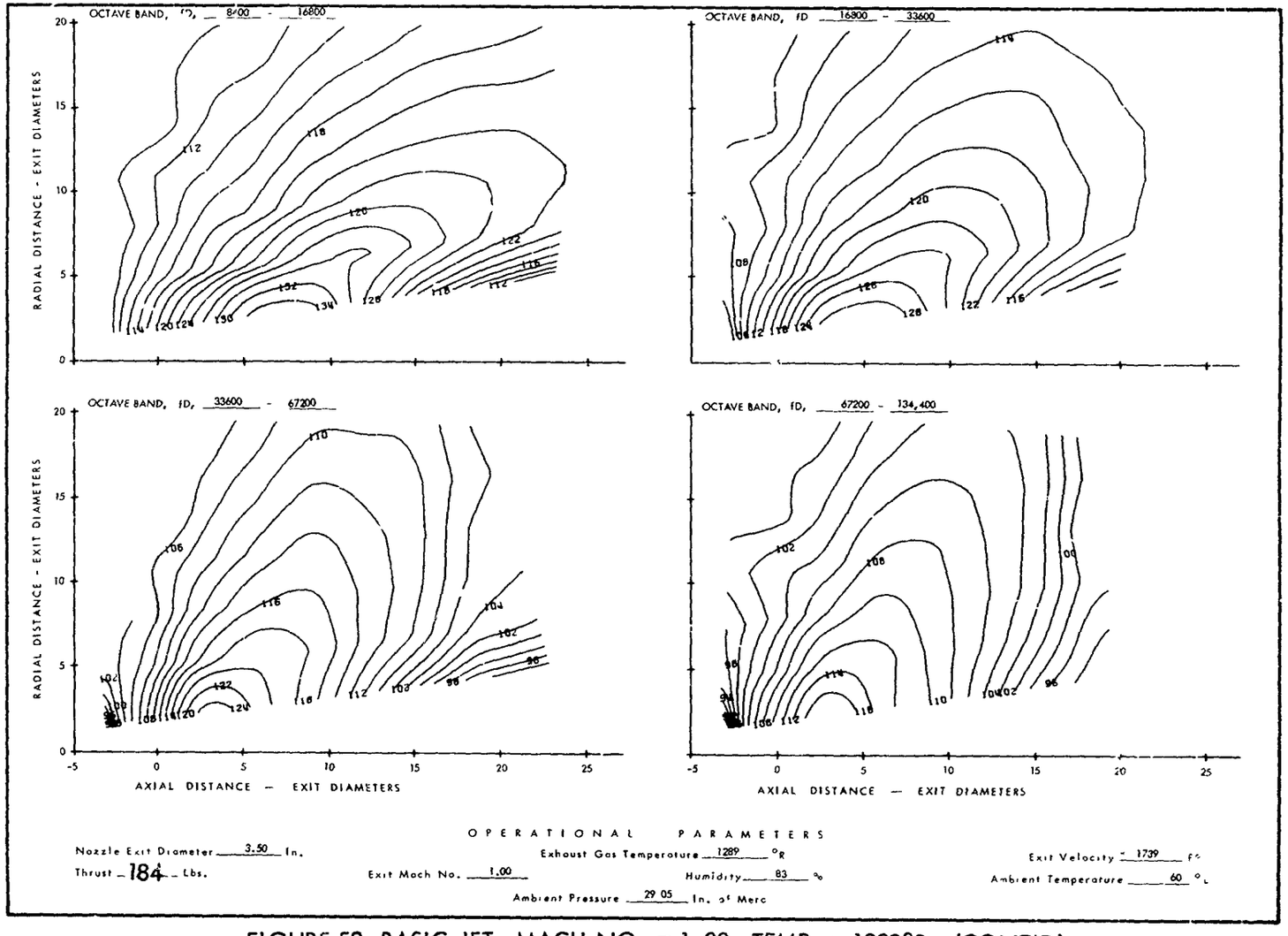

FIGURE 52 BASIC JET, MACH NO. = 1.00, TEMP. = 1289°R (CONT'D)

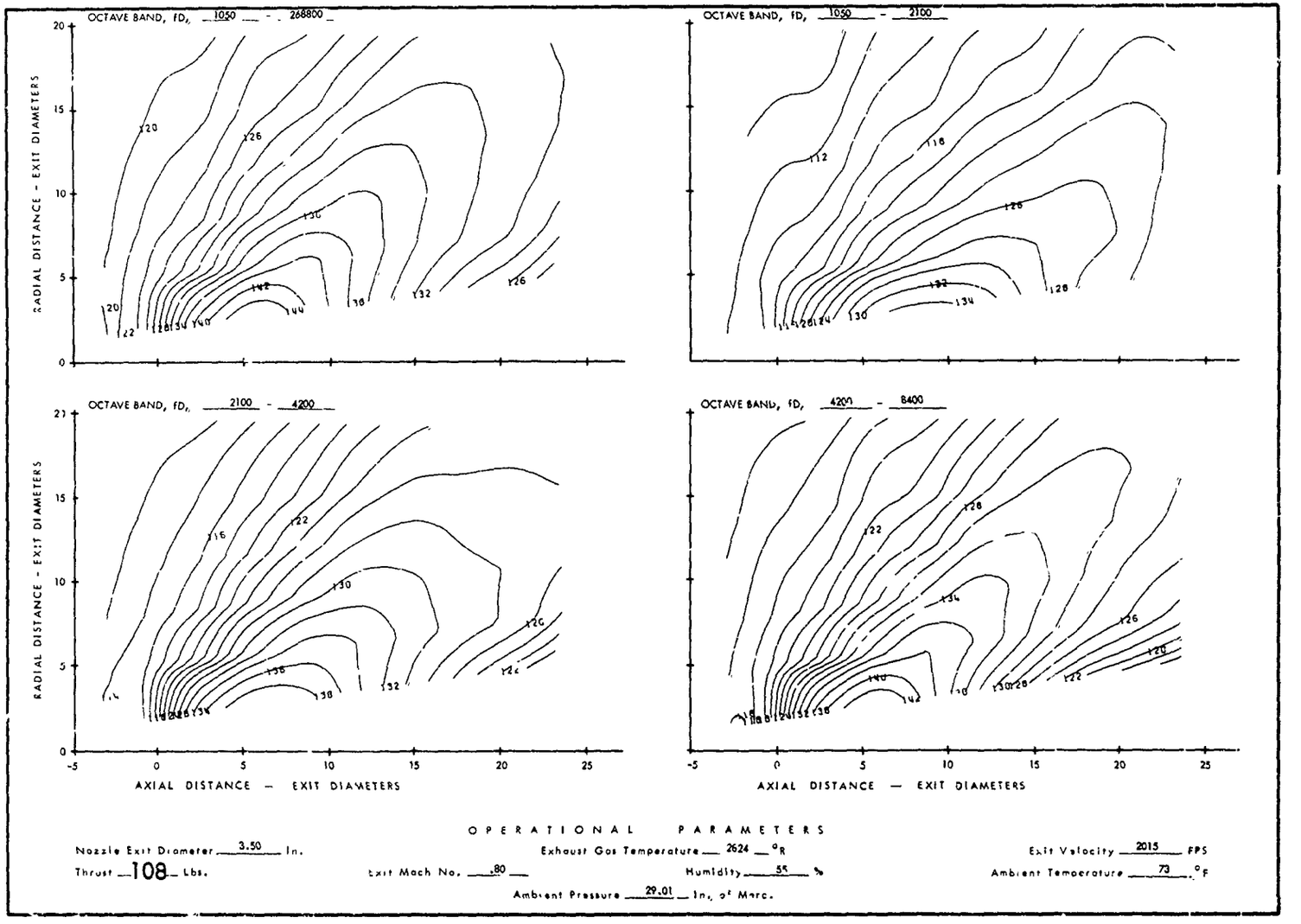

FIGURE 53 EFFECT OF GROUND PLANE ON BASIC JET GROUND PLANE 5 DIAMETERS FROM C.L.
MACH NO. = .80, TEMP. = 2824°R

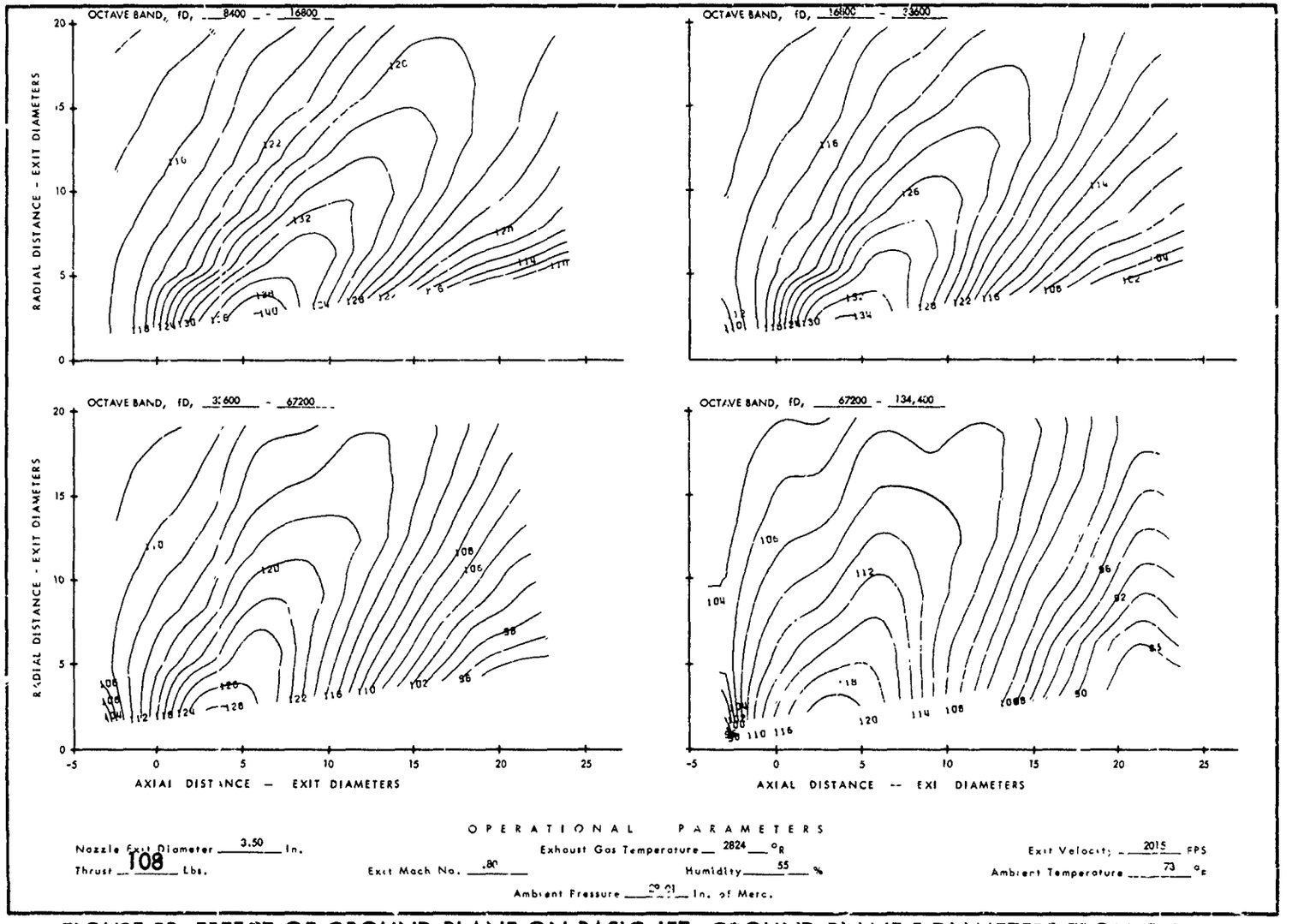

FIGURE 53 EFFECT OF GROUND PLANE ON BASIC JET · GROUND PLANE 5 DIAMETERS FROM C.L. MACH NO. = .80, TEMP. = 2824°R (CONT'D)

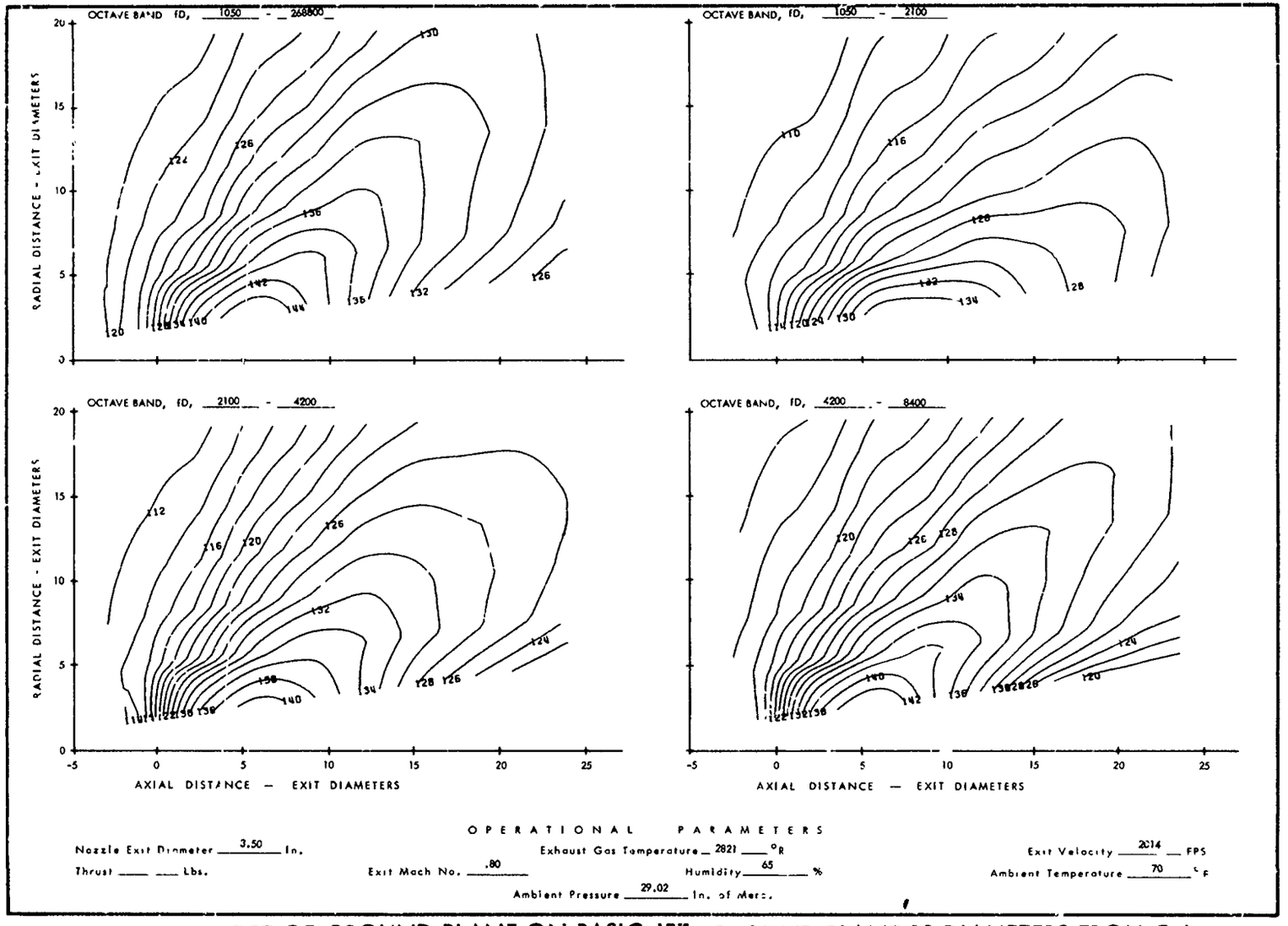

FIGURE 54 EFFECT OF GROUND PLANE ON BASIC JET GROUND PLANE 10 DIAMETERS FROM C.L. MACH NO. = .80, TEMP. = 2821°R

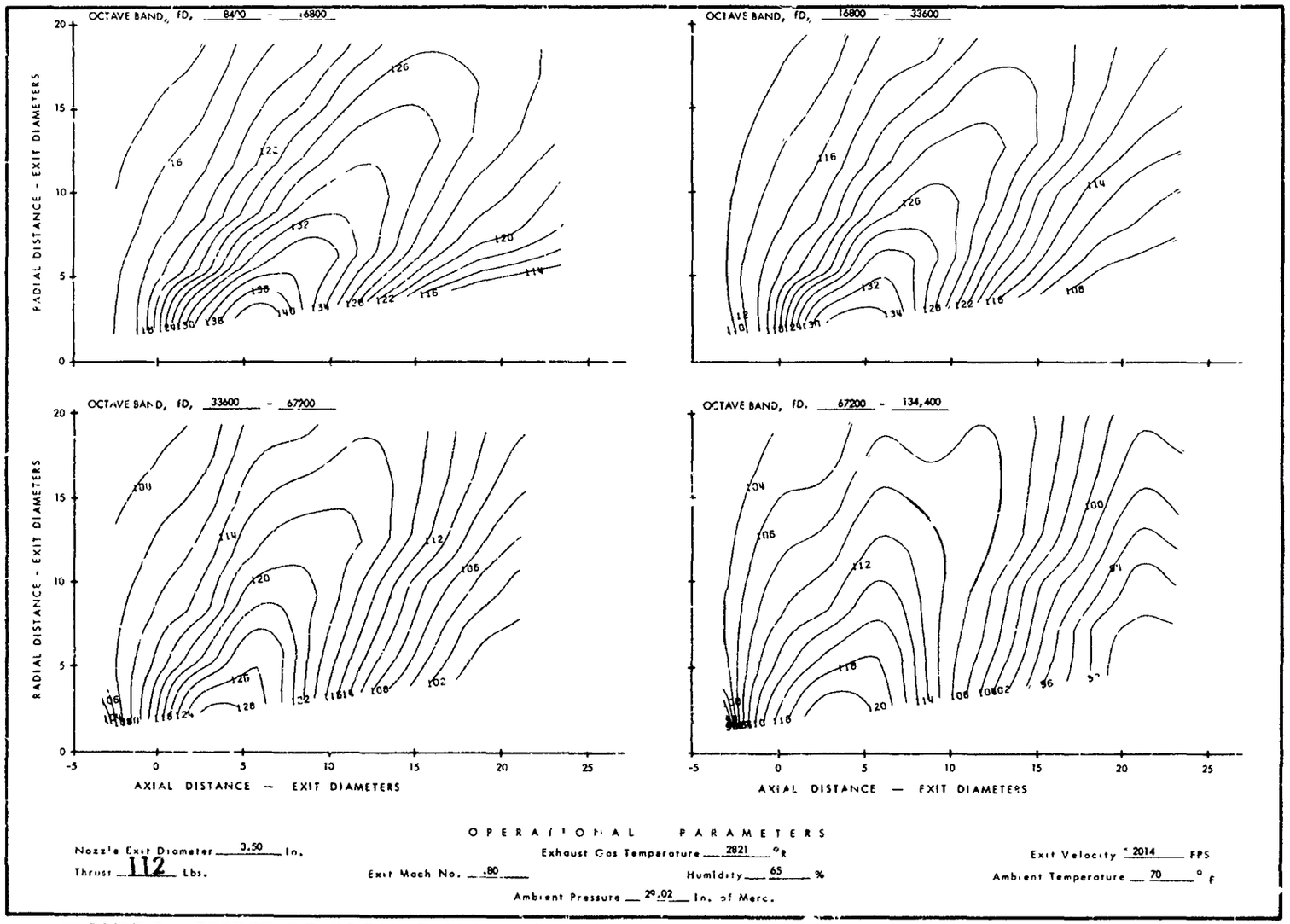

FIGURE 54 EFFECT OF GROUND PLANE ON BASIC JET GROUND PLANE 10 DIAMETERS FROM C.L. MACH NO. = .80, TEMP. = 2821°R (CONT'D)

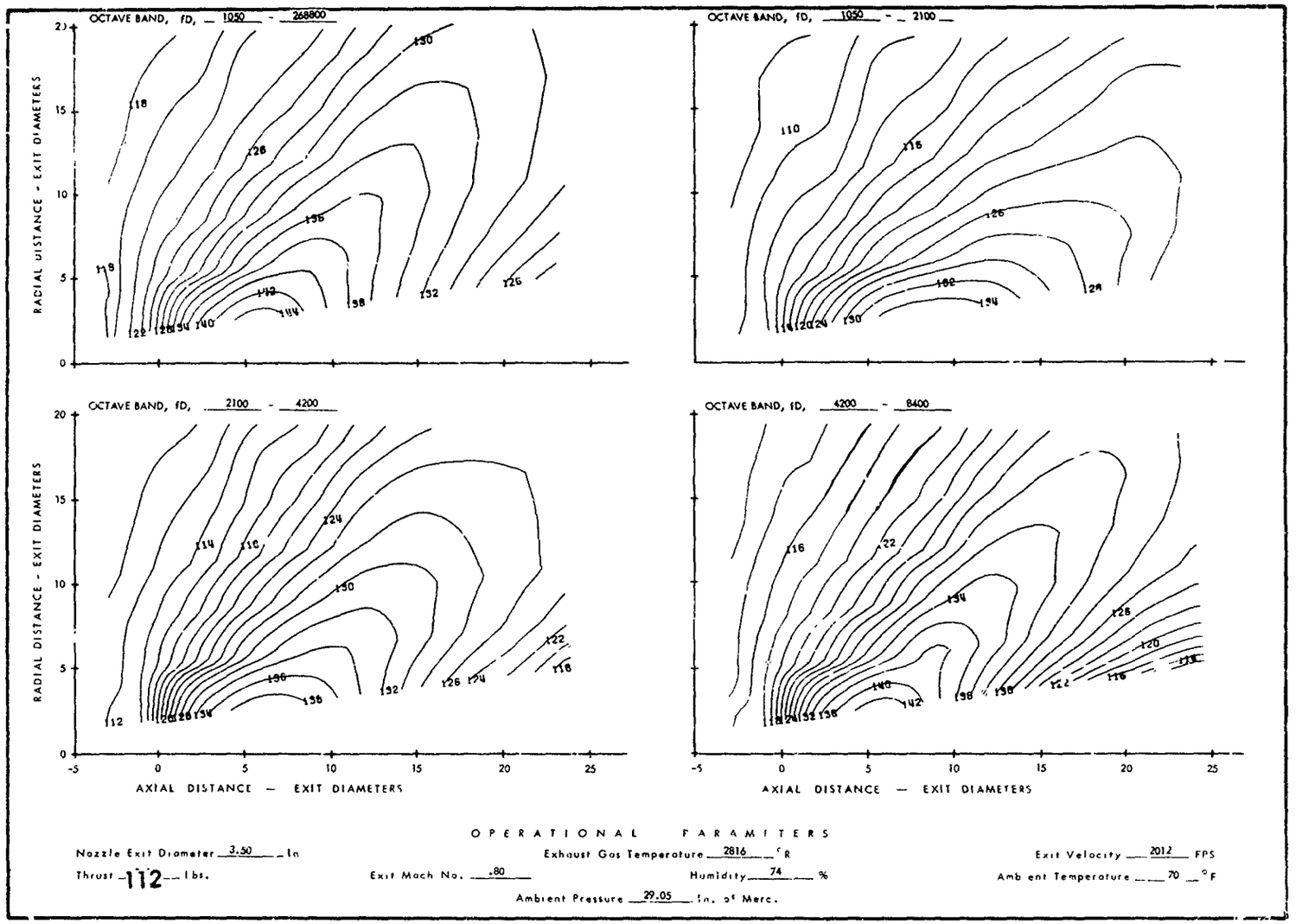

FIGURE 55 BASIC JET, MACH NO. = .80, TEMP. = 2816°R

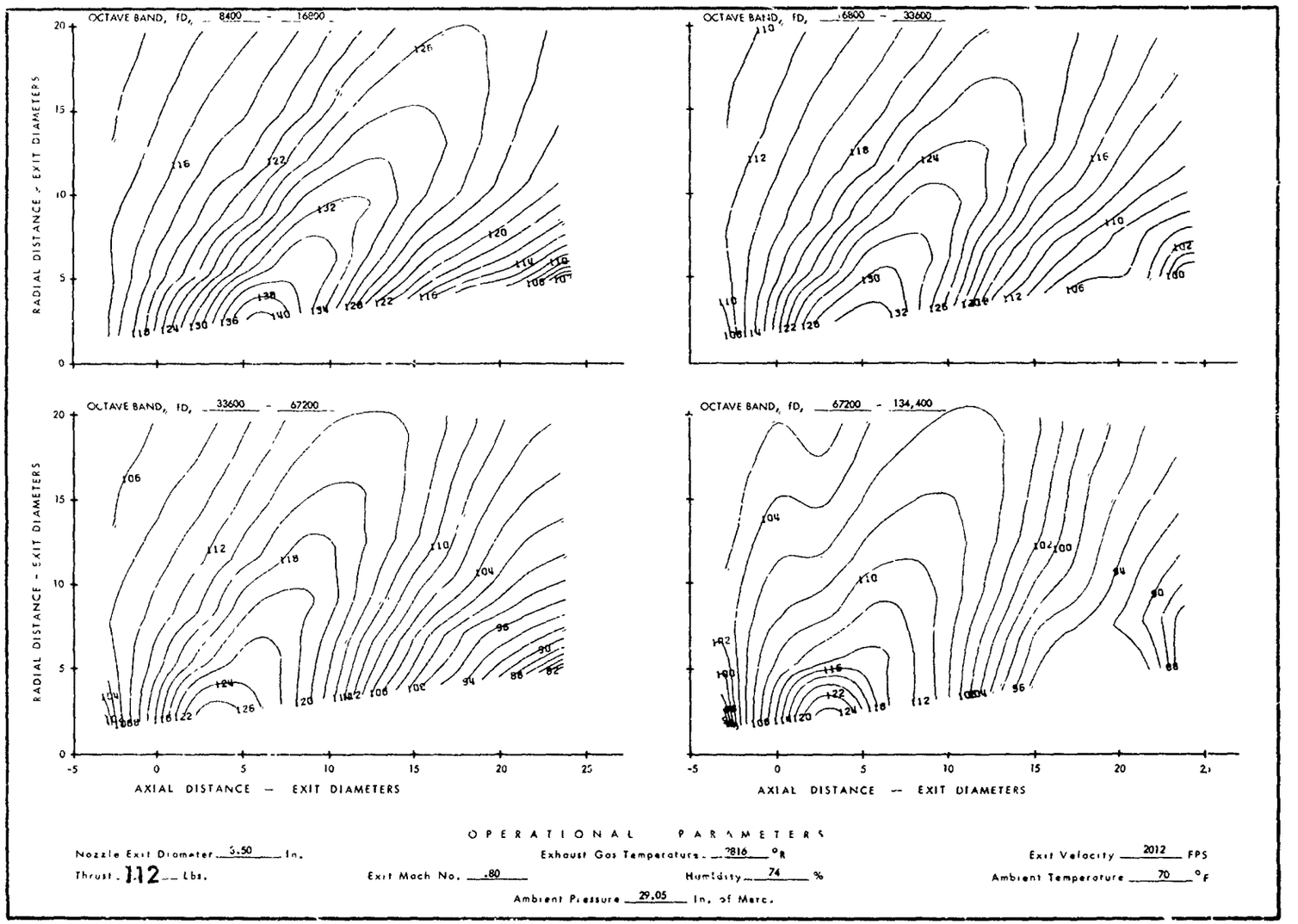

FIGURE 55 BASIC JET, MACH NO. = .80, TEMP. = 2816°R (CONT'D)

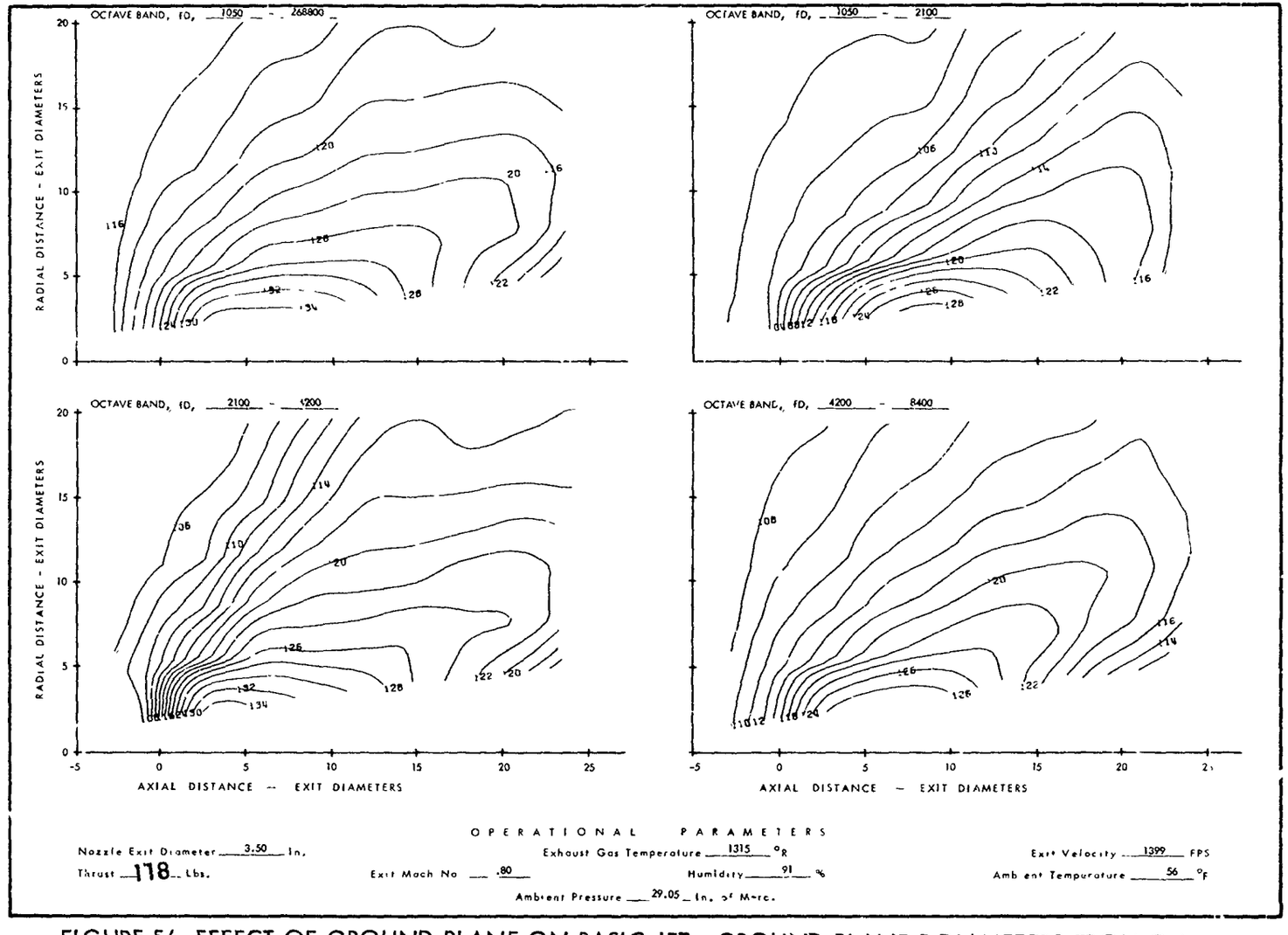

FIGURE 56 EFFECT OF GROUND PLANE ON BASIC JET GROUND PLANE 5 DIAMETERS FROM C.L. MACH NO. = .80, TEMP. = 1315°R

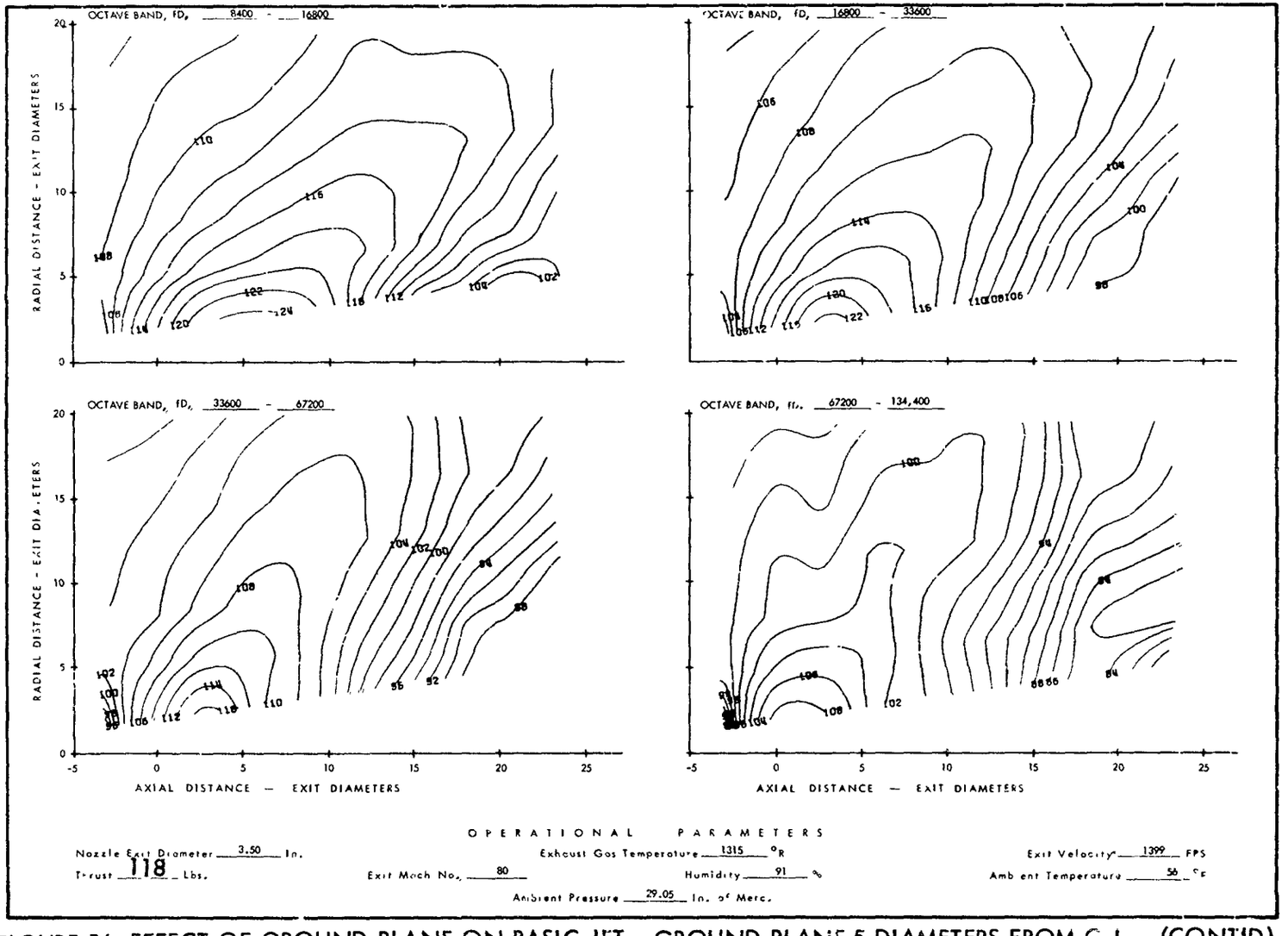

FIGURE 56 EFFECT OF GROUND PLANE ON BASIC JET GROUND PLANE 5 DIAMETERS FROM C.L. (CONT'D)
MACH NO. = .80, TEMP. = 1315°R

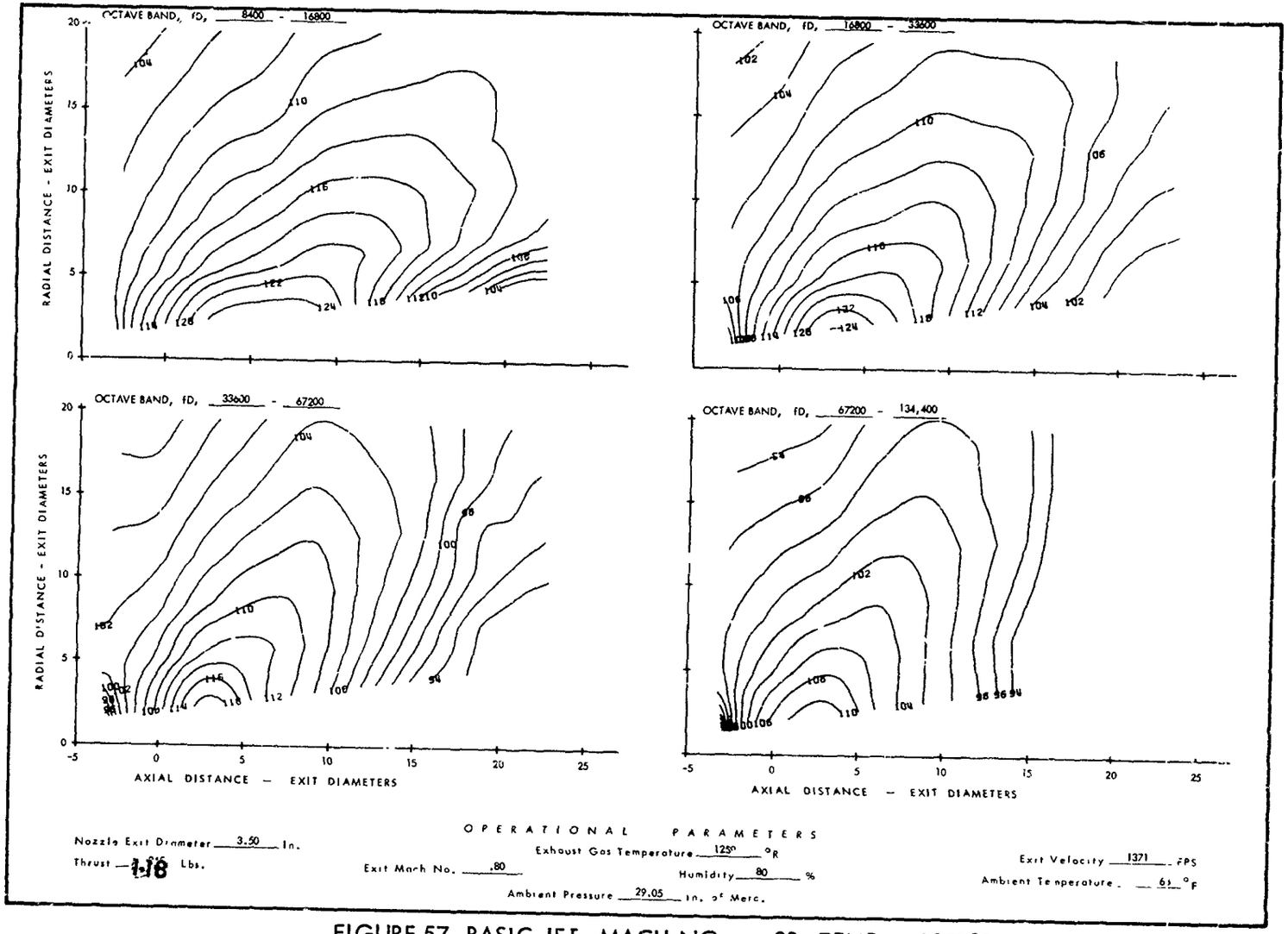

FIGURE 57 BASIC JET, MACH NO. = .80, TEMP. = 1259°R

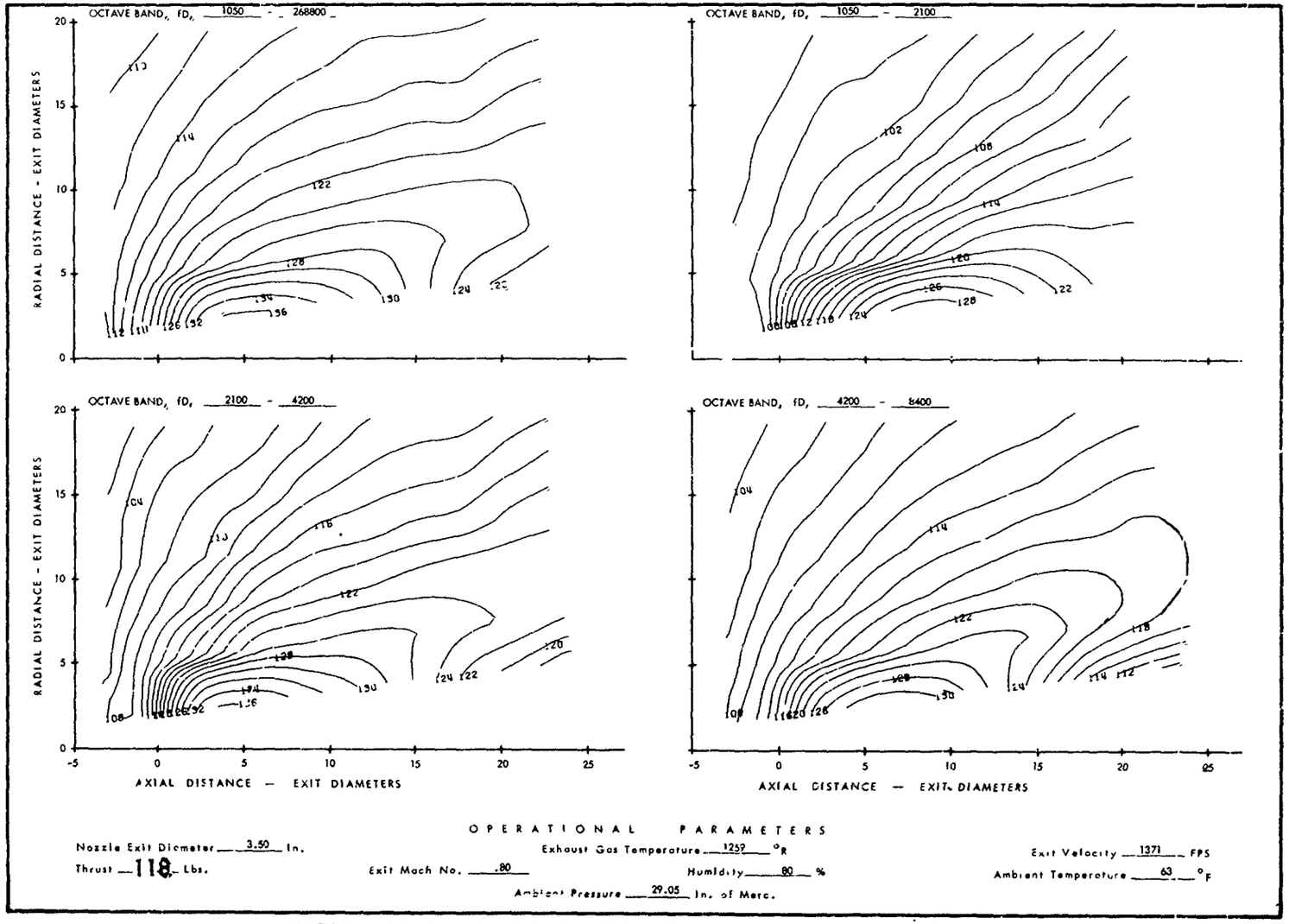

FIGURE 57 BASIC JET, MACH NO. = .80, TEMP. = 1259°R (CONT'D)

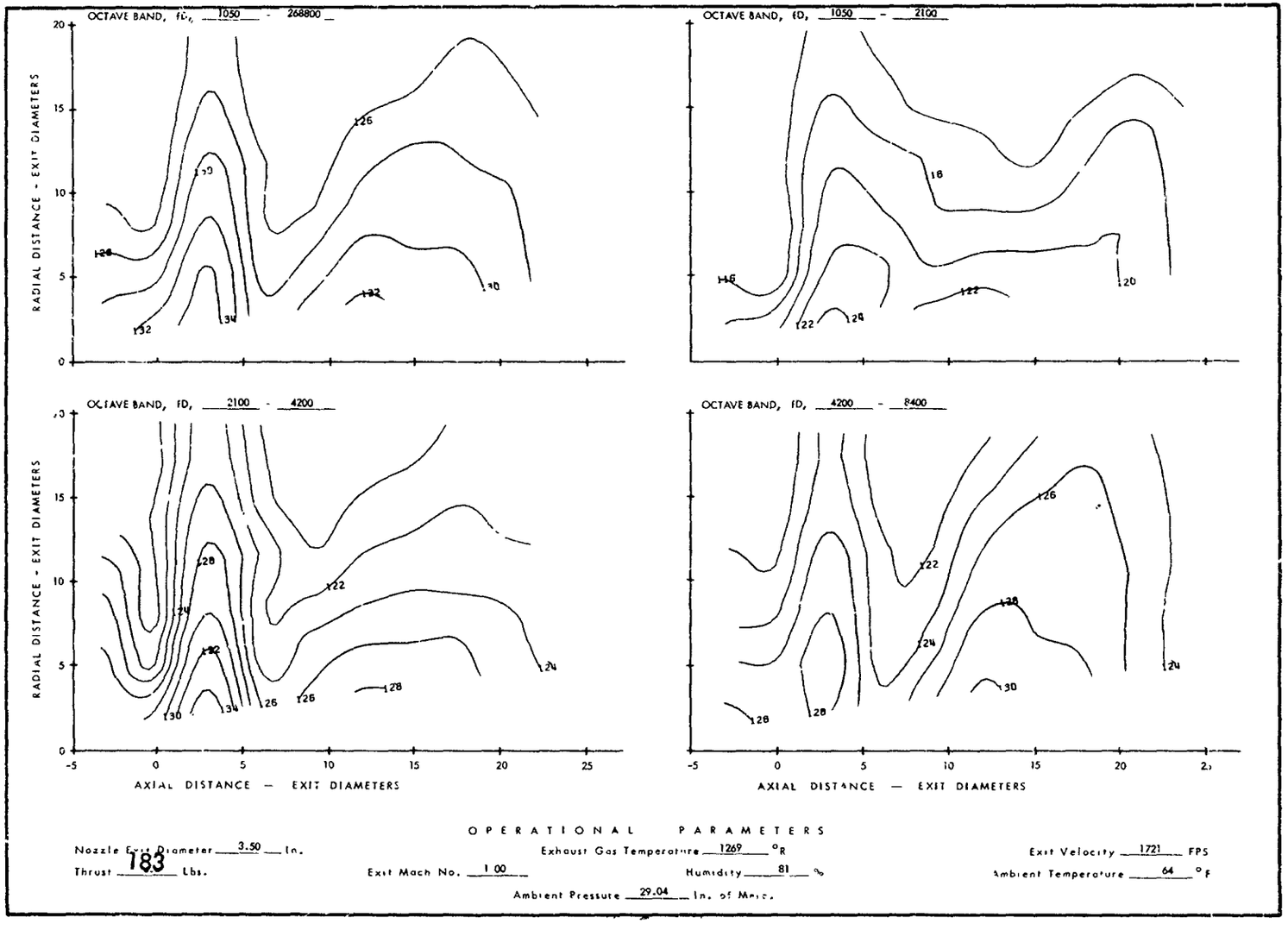

FIGURE 58 BASIC JET WITH 45° DEFLECTING VANE AND GROUND PLANE 5 DIAMETERS FROM JET C.L., MACH NO. = 1.00, TEMP. = 1269°R

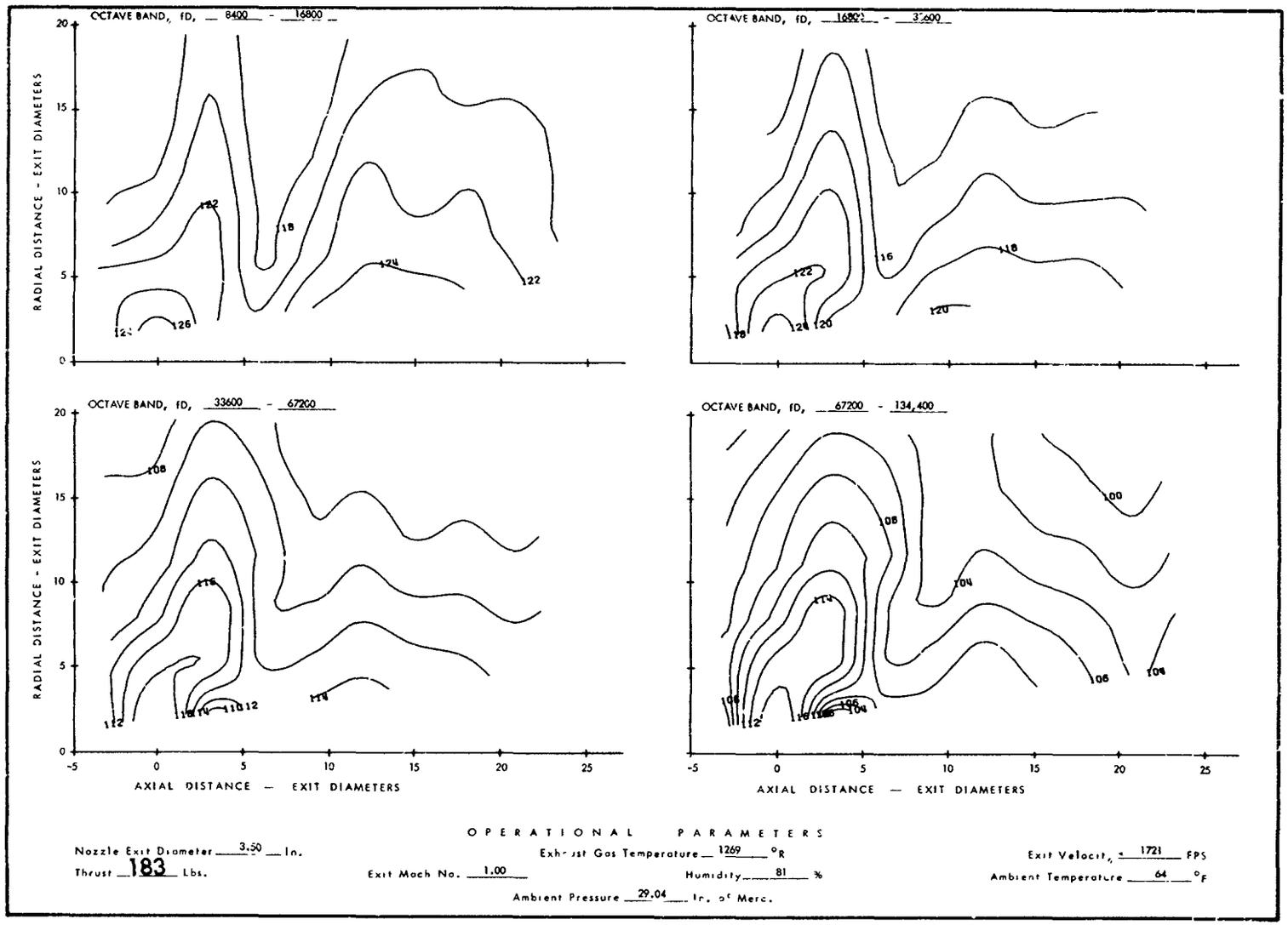

FIGURE 58 BASIC JET WITH 45° DEFLECTING VANE AND GROUND PLANE 5 DIAMETERS FROM JET C.L., MACH NO. = 1.00, TEMP. = 1269°R (CONT'D)

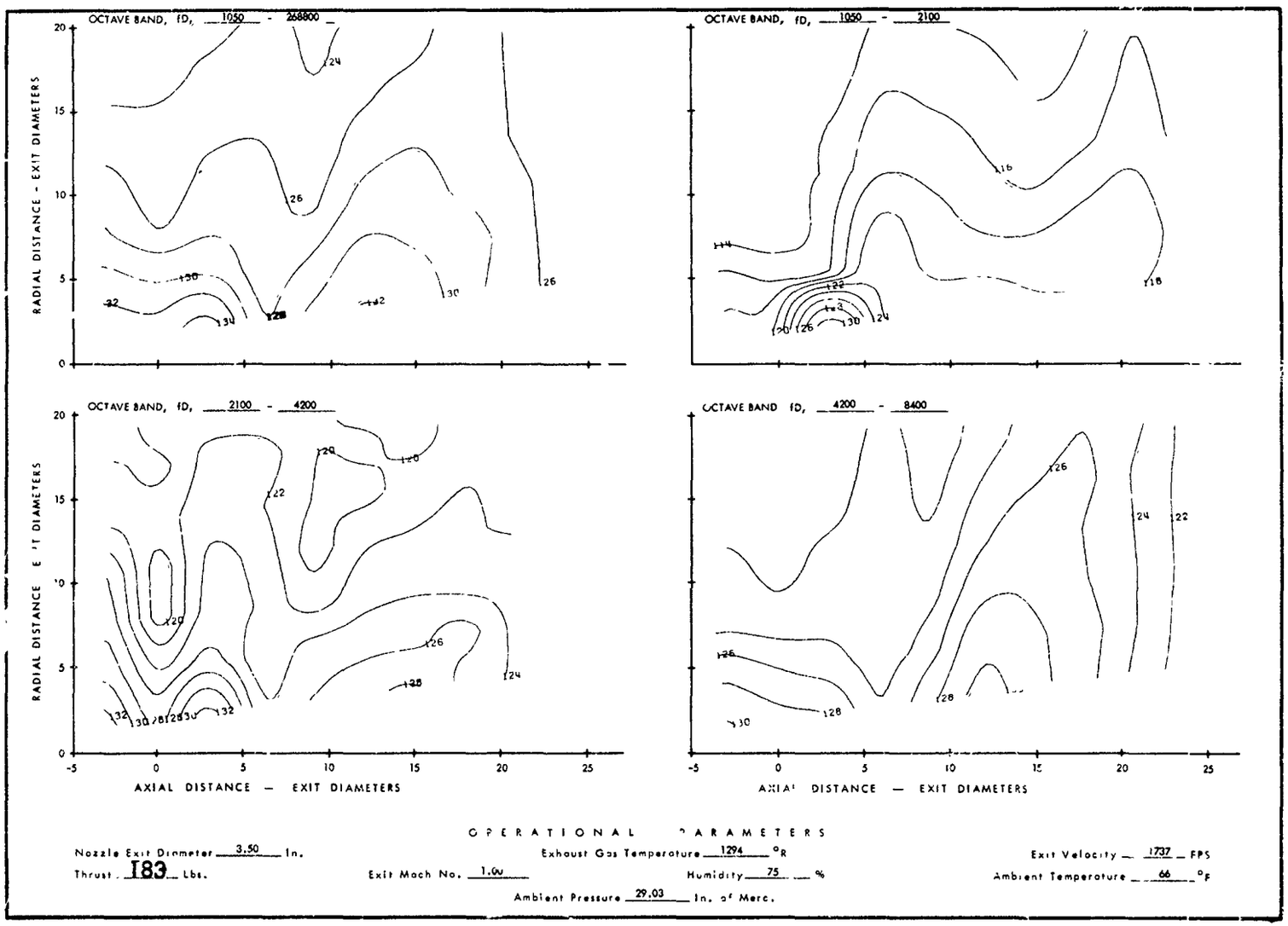

FIGURE 59 BASIC JET WITH 45° DEFLECTING VANE AND GROUND PLANE 10 DIAMETERS FROM JET C.L., MACH NO. = 1.00, TEMP. = 1294°R

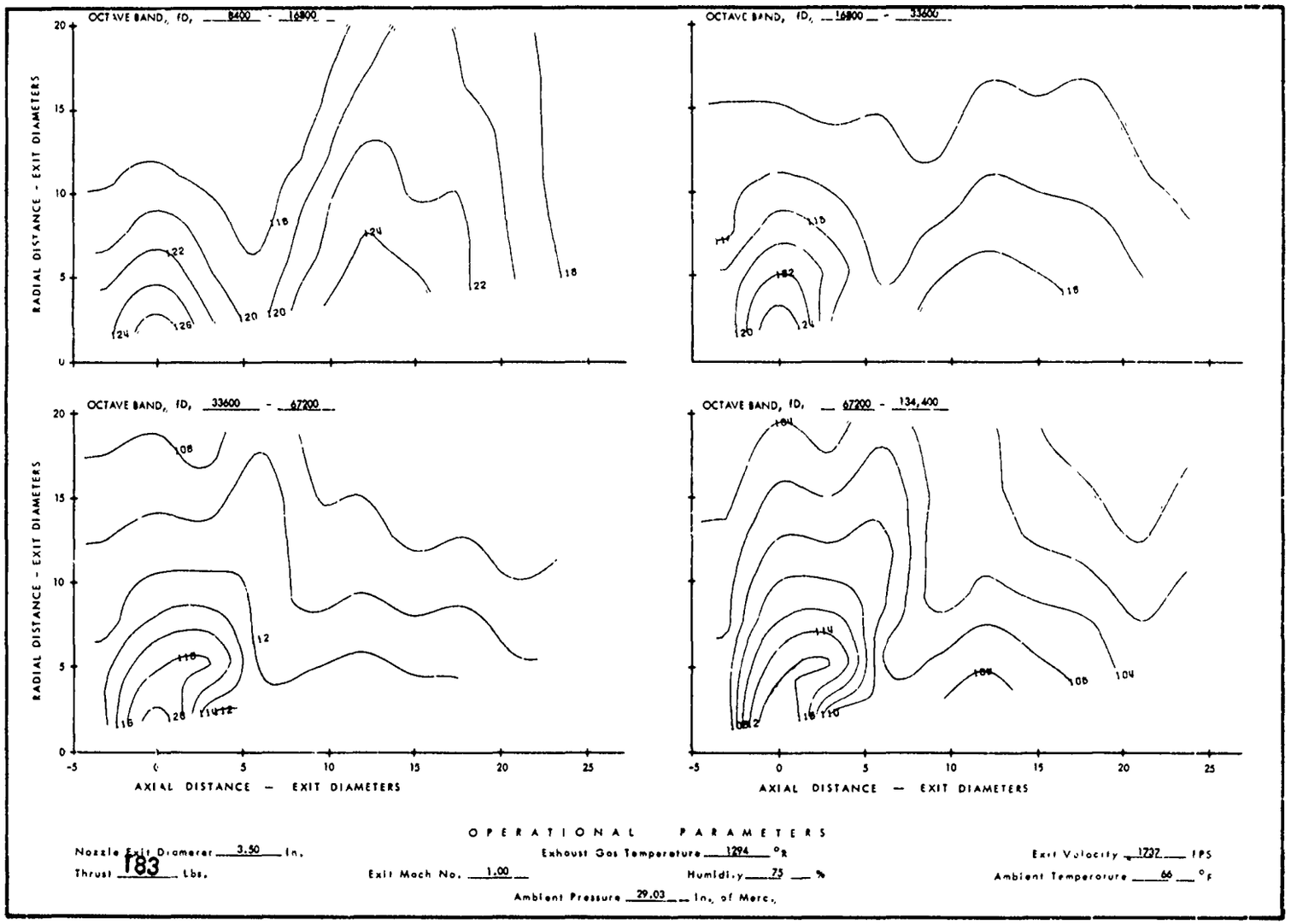

FIGURE 59 BASIC JET WITH 45° DEFLECTING VANE AND GROUND PLANE 10 DIAMETERS FROM JET C.L., MACH NO. = 1.00, TEMP. = 1294°R (CONT'D)

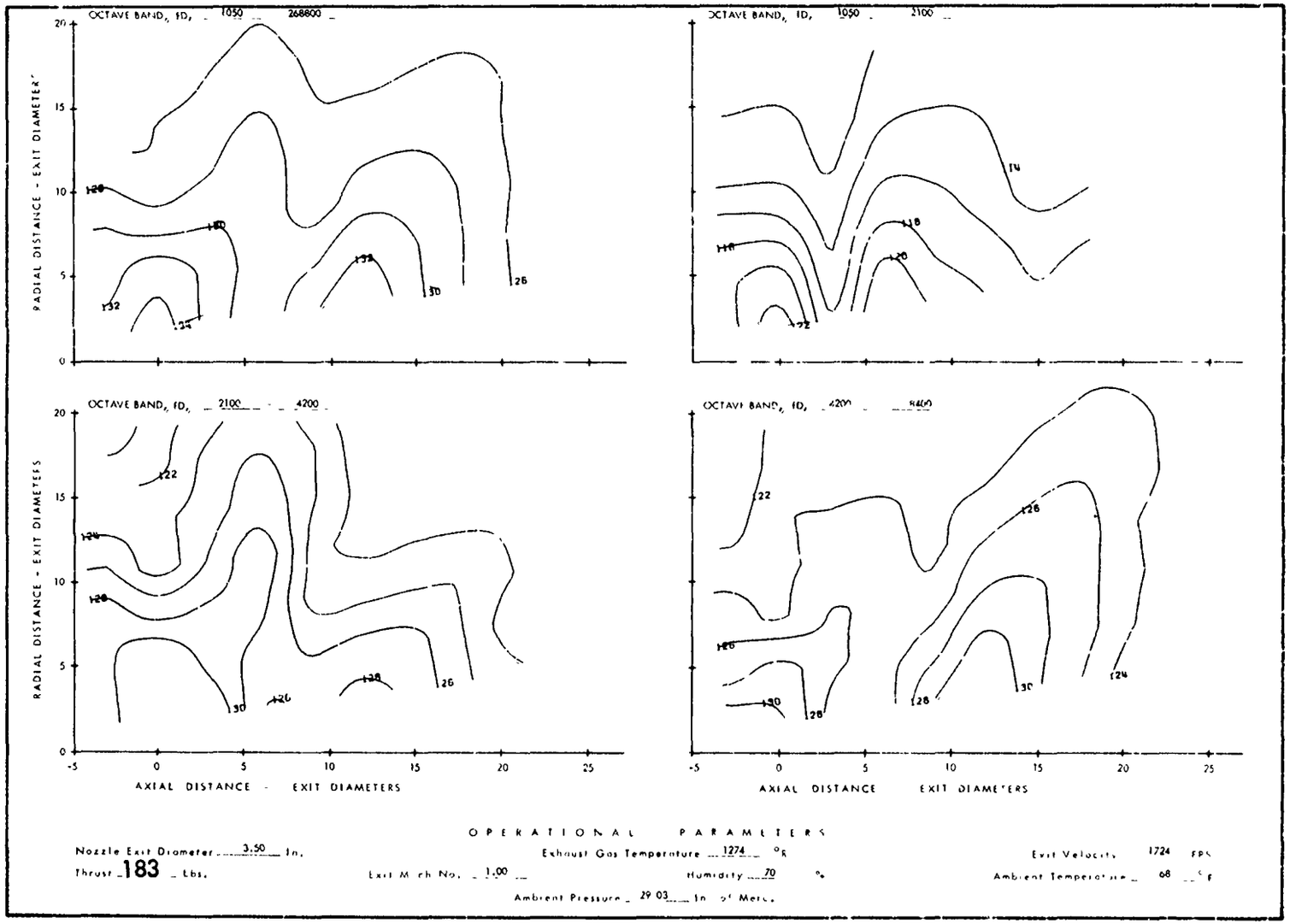

FIGURE 60 BASIC JET WITH 30° DEFLECTING VANE AND GROUND PLANE 10 DIAMETERS FROM C.L. MACH NO. = 1.00, TEMP = 1269°R

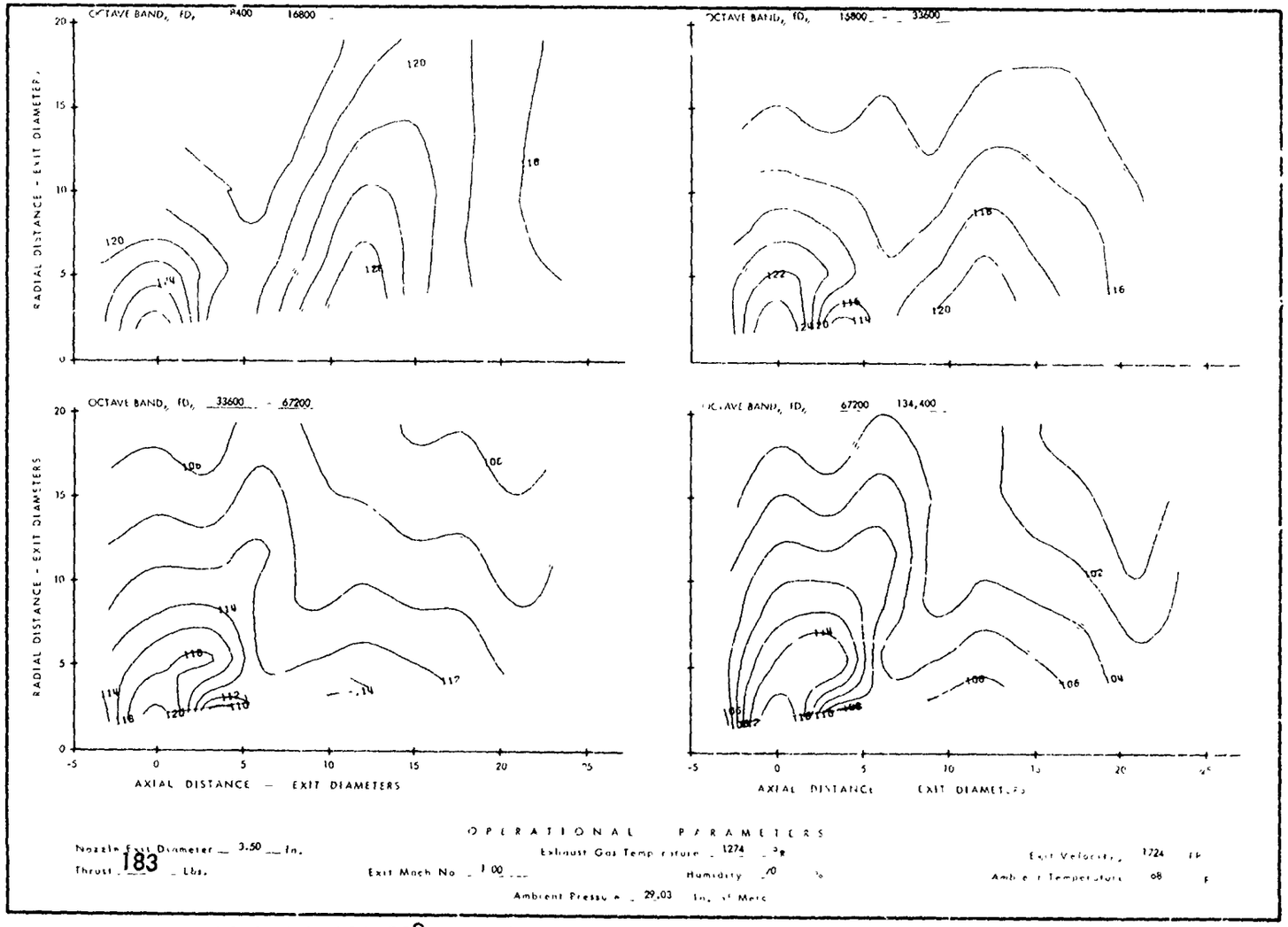

FIGURE 60 BASIC JET WITH 30° DEFLECTING VANE AND GROUND PLANE 10 DIAMETERS FROM C.L. MACH NO. = 1.00, TEMP = 1269°R (Cont'd)

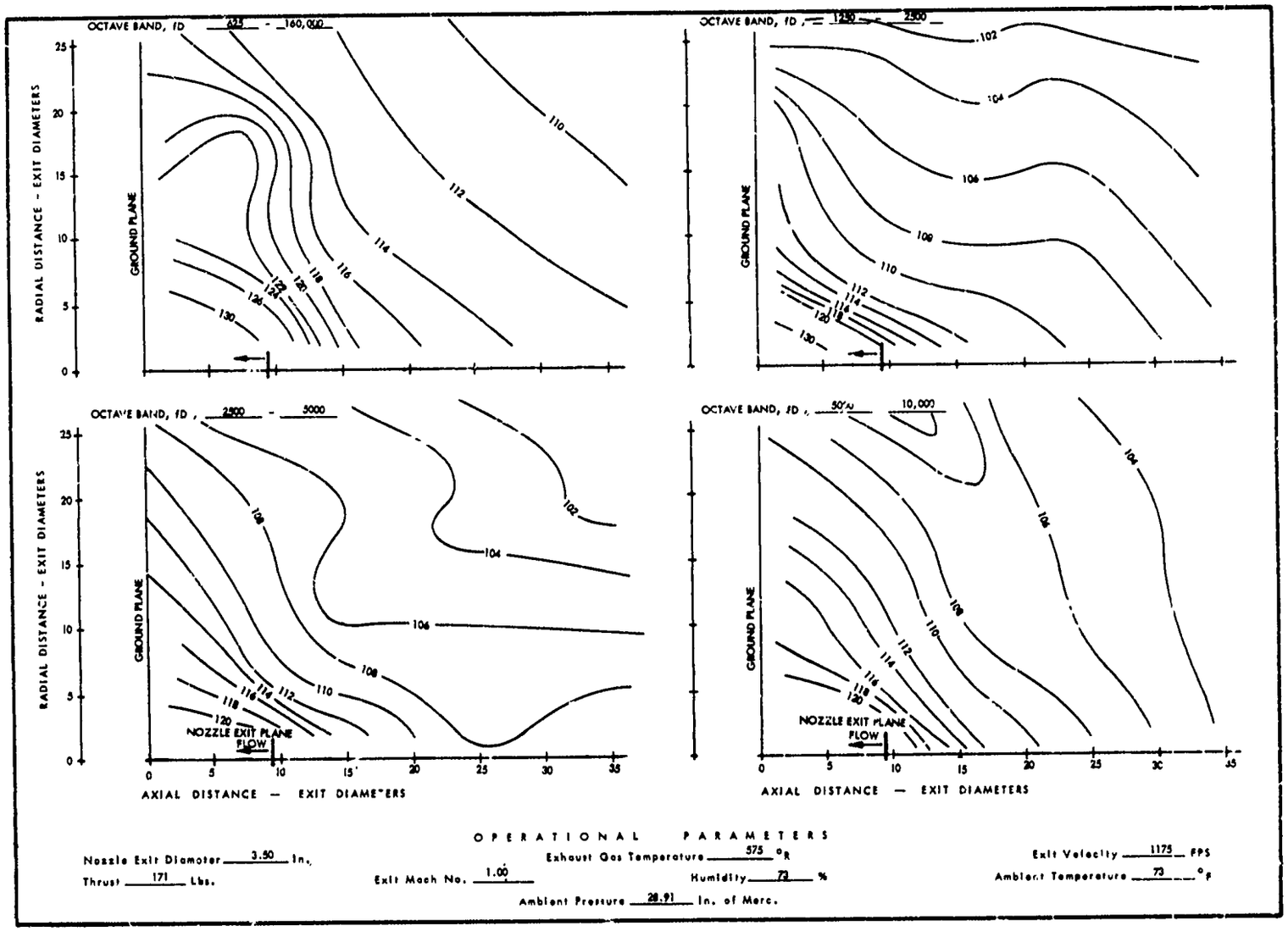

FIGURE 61 EFFECT OF GROUND PLANE DISTANCE ON VTOL JET SPL - GROUND PLANE @ 9 EXIT DIAMETERS

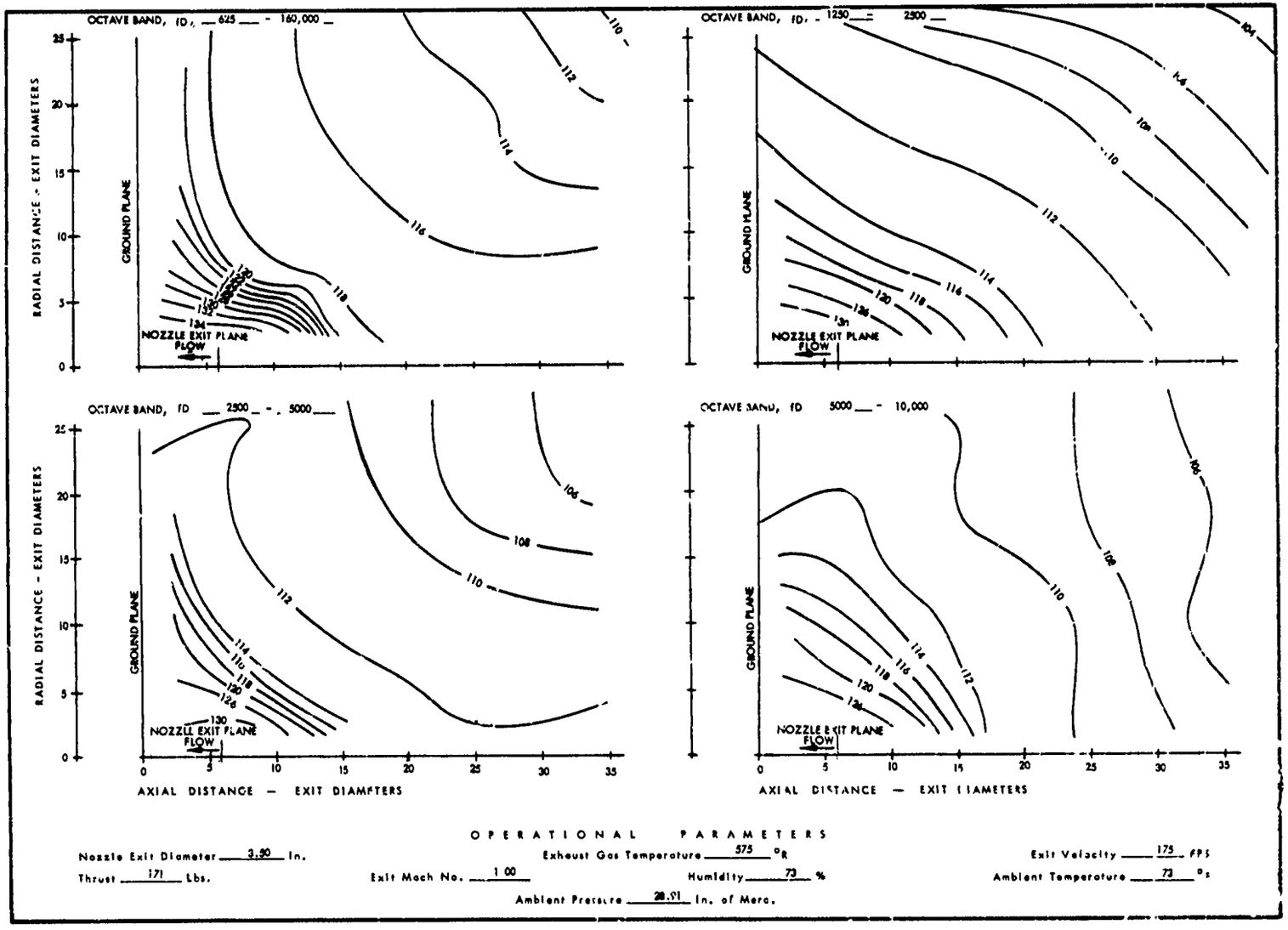

FIGURE 62 EFFECT OF GROUND PLANE DISTANCE ON VTOL JET SPL - GROUND PLANE @ 6 EXIT DIAMETERS

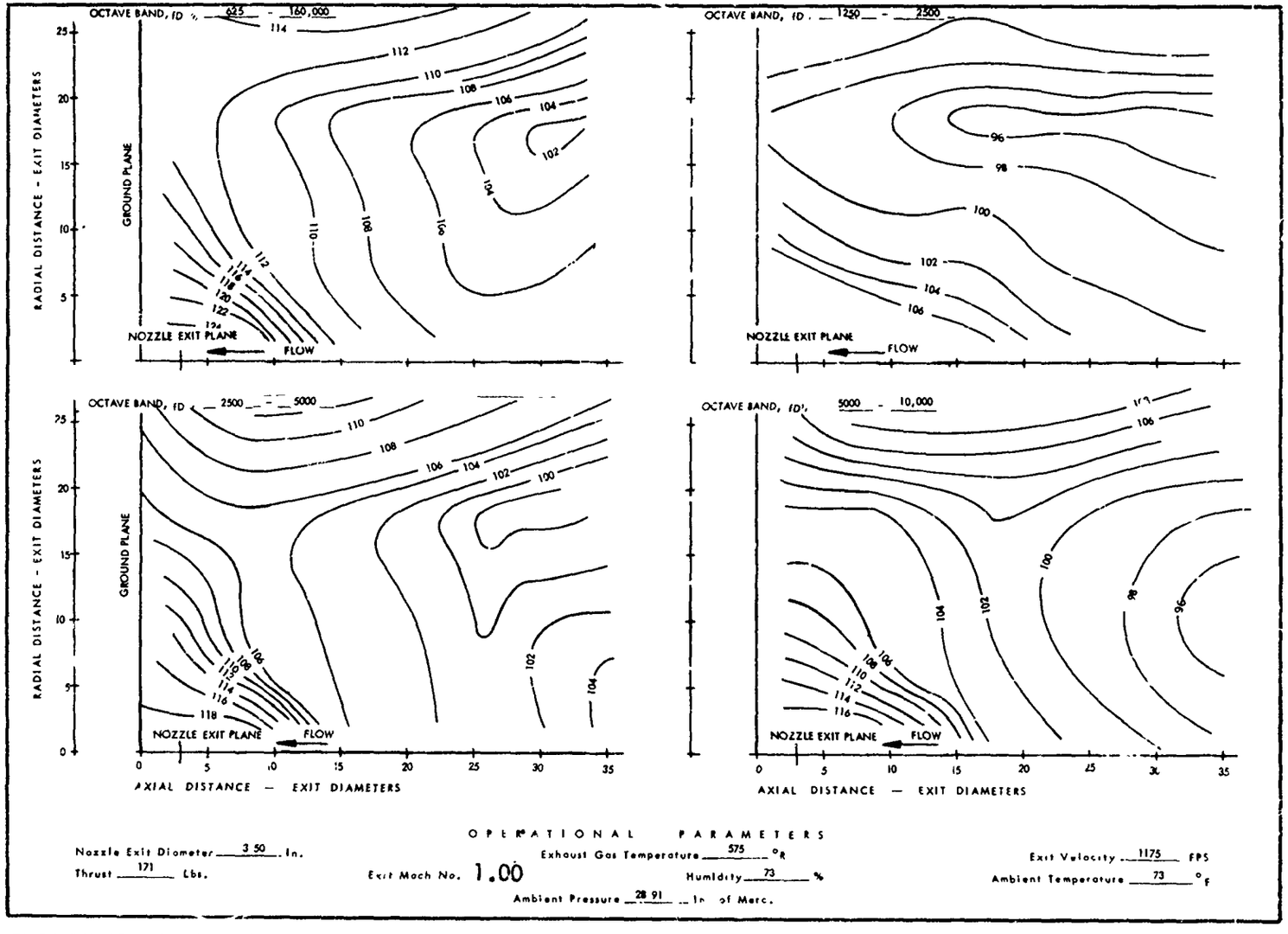

FIGURE 63 EFFECT OF GROUND PLANE DISTANCE ON VTOL JET SPL - GROUND PLANE @ 3 EXIT DIAMETERS

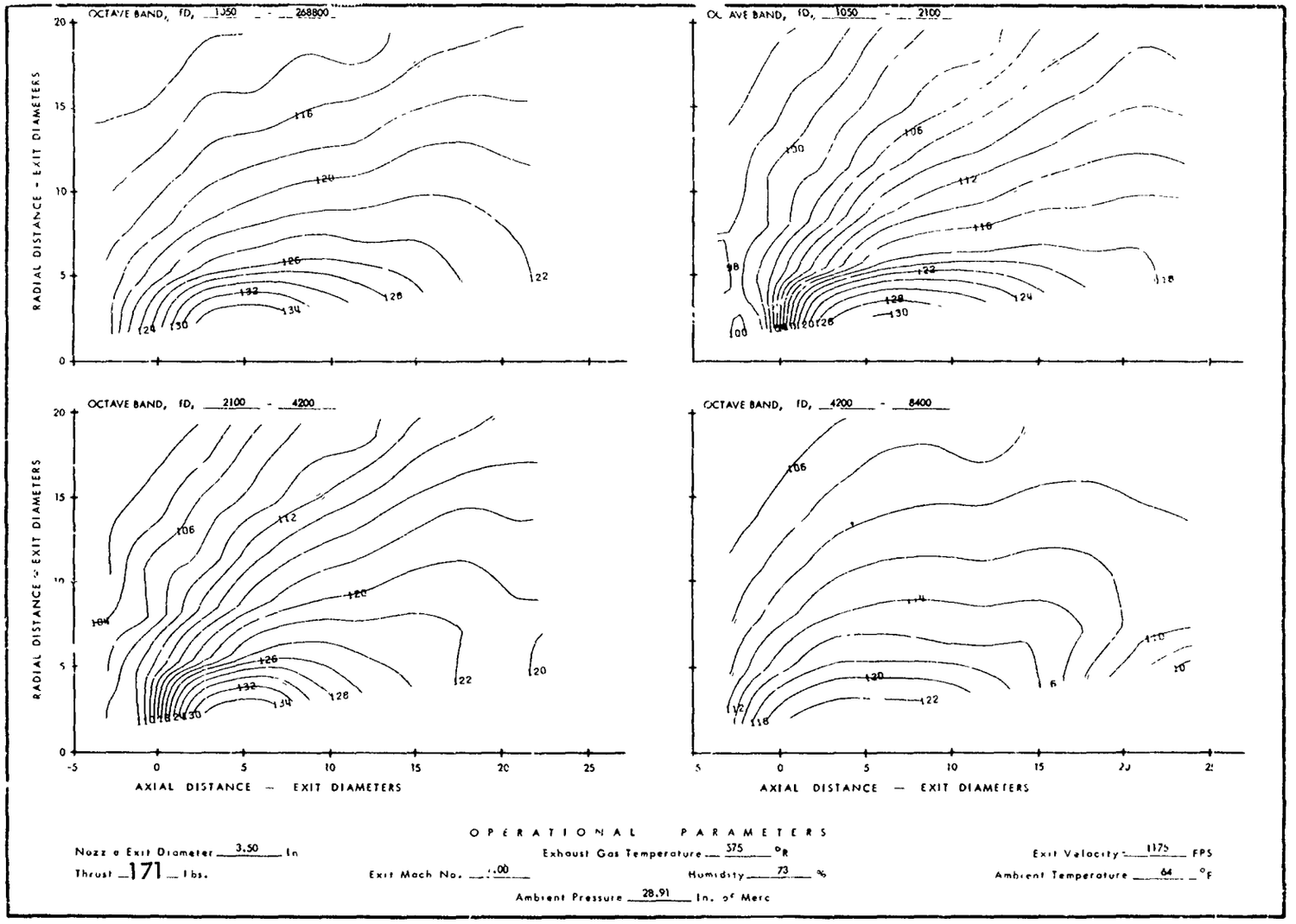

FIGURE 64 BASIC JET: MACH NO. = 1.00, TEMP. = 575°R

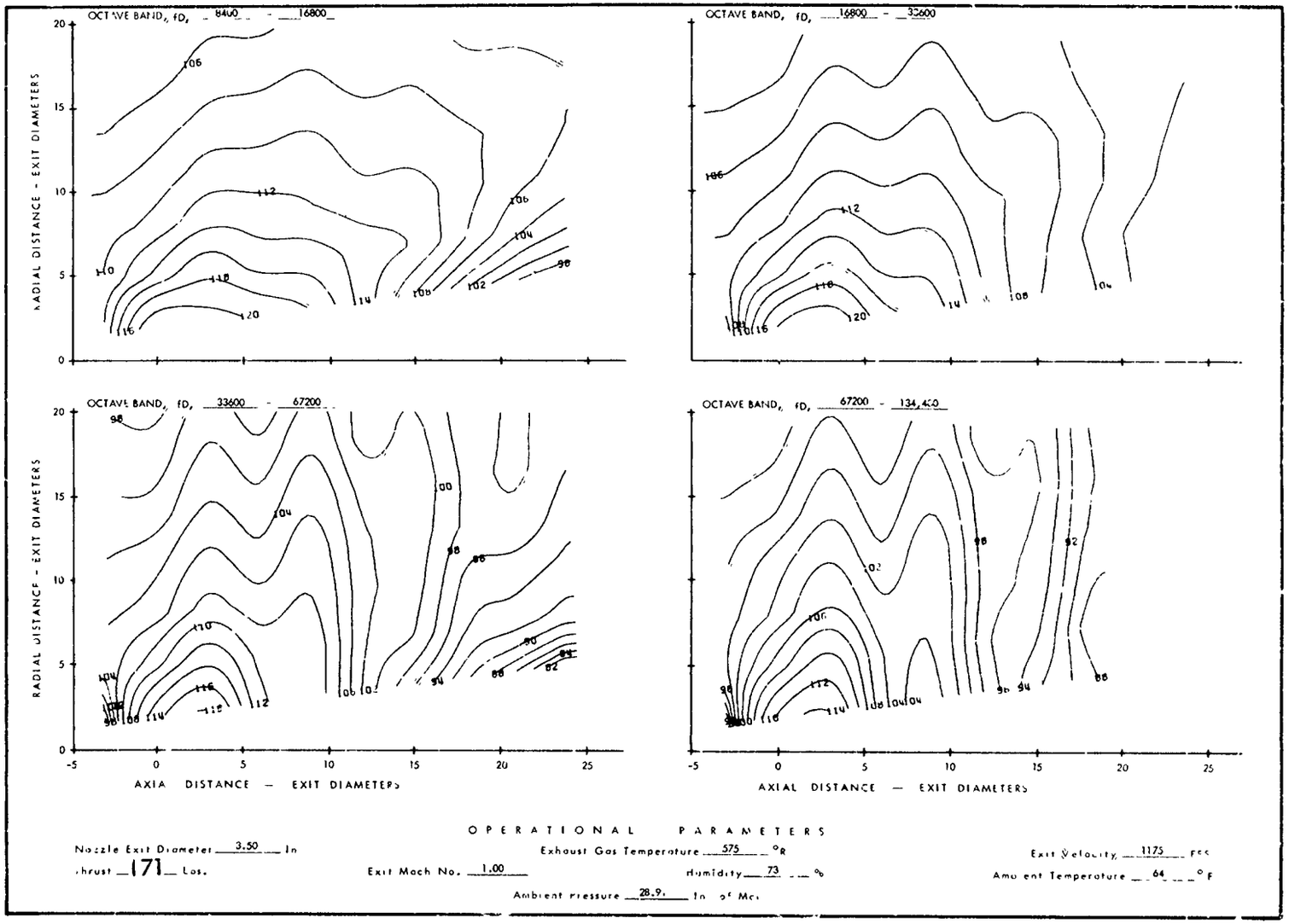

FIGURE 64 BASIC JET: MACH NO. = 1.00, TEMP. = 575°R (CONT'D)

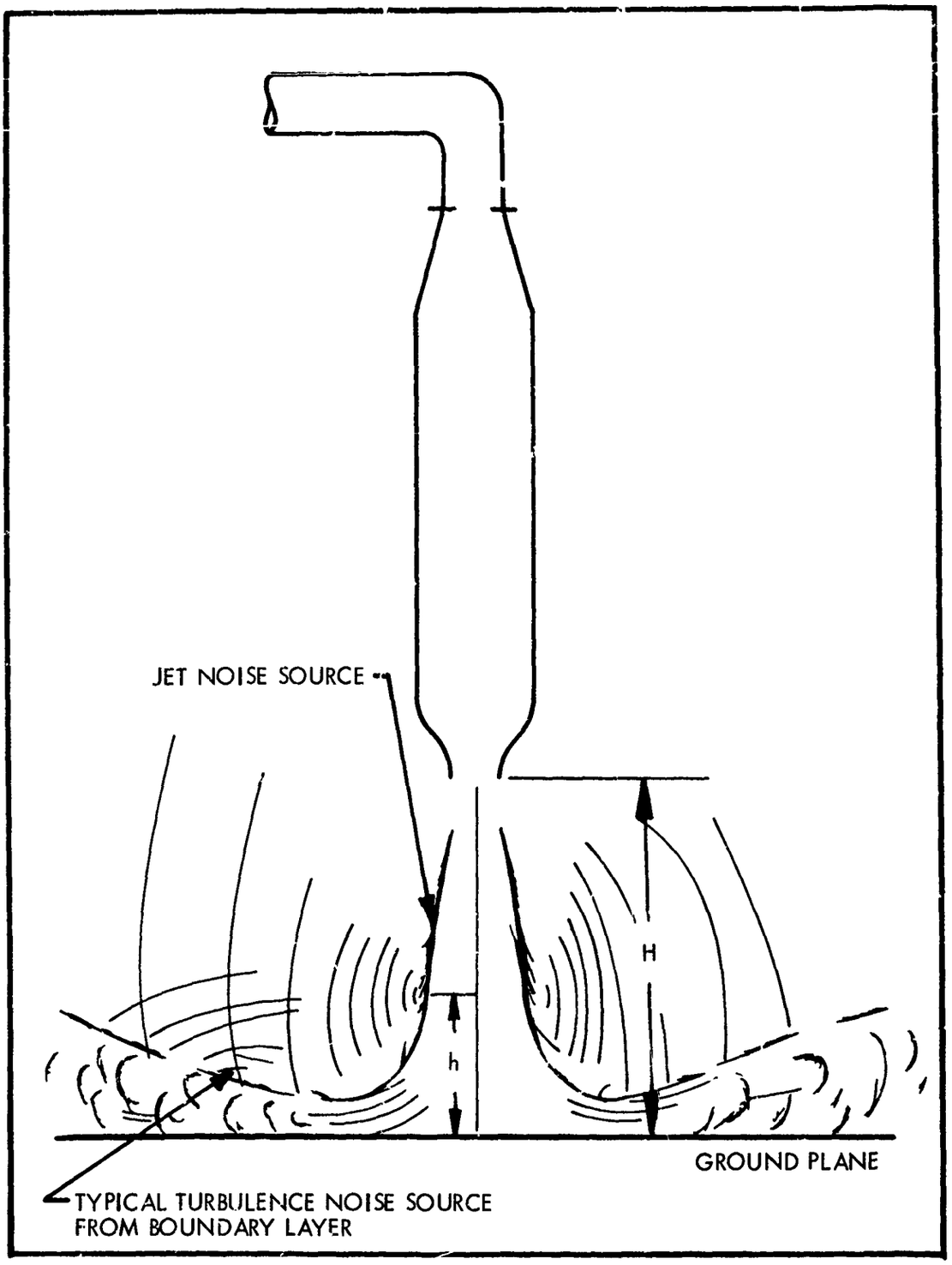

FIGURE 65. SHOWING SOURCES OF SOUND FOR VTOL JET

SECTION IV

NOISE CHARACTERISTICS OF FAN ENGINES

A. Introduction

Propeller and fan noise have been studied for more than 50 years. During this time the near pressure field has been studied by Hubbard and Regier (Reference 21) and others (References 22, 23, and 24). The almost universal adoption of the gas turbine engine aircraft power plant has reemphasized the problem of noise generated by propellers and fans. Specific attention is now returning to the mechanism of noise generated by fans, particularly as applied to axial-flow compressors, ducted-fan engines, and lift-fan engines for VTOL aircraft.

Methods of predicting fan and blade noise have resulted from the research accomplished in recent years. Lowson (Reference 25) has described the chain of cause and effect which leads to sound radiated by compressors. The chain comprises unsteady compressor flow components, fluctuating blade forces, blade noise radiation, inlet and outlet duct modes and duct-radiated sound. Once the forces on the blade rows are defined, the prediction of the discrete frequency noise radiation is relatively straightforward. Theories by Kemp and Sears (References 26 and 27) give blade forces due to interactions. Hetherington (Reference 28) and Lowson (Reference 29) used these results to predict the noise radiation due to blade interactions. Methods described by Tyler and Sofrin (Reference 30) can be used to show how the spinning property of the higher-order modes in inlet and outlet ducts are coupled to the pressure patterns induced by rotor-stator interactions. The radiation pattern from the end of a flanged circular duct due to a specified spinning mode has also been calculated by Tyler and Sofrin.

In summary, considerable research has been accomplished in the past few years in blade, fan, and axial flow compressor noise, and some promising methods of reducing this type of noise have been devised(see Reference 31). However, although tip-turbine fans offer promising uses as lift and cruise fans for VTOL aircraft, very little has been done in analyzing the noise from tip-turbine fans. Rentzepis (Reference 32) made a theoretical study of the acoustic field of a tip-turbine fan, but this study was primarily concerned with the far field. The tip-turbine fan noise field as regards ground effects is ill defined. In addition, the jet noise contribution to the whole noise field of the tip-turbine fan needs better definition. Consequently, the purpose of this portion of the research investigation was to gain a better definition of the noise fields from a tip-turbine for models including both lift and cruise configurations.

B. The Physical Aspects

As shown in Figure 66, a tip-turbine fan consists of a turbine section that occupies the outer ring of a concentric assembly. The fan section occupies the middle ring and is separated from the turbine section by a sealing device. A core fills the remaining space. Each of two annuli is made of a rotor and a stator section. Hot gases enter through a scroll to the tip-turbine section, supplying the power to drive the fan. This motion of the tip-turbine fan causes variations in pressure of the medium in which it is immersed, and these fluctuations cause the generation of sound. The rotation of the blades gives rise to various sources of sound such as rotational noise, pressure fluctuations due to interaction of the rotor-stator assembly on the rotating pressure patterns, interference on stator wakes

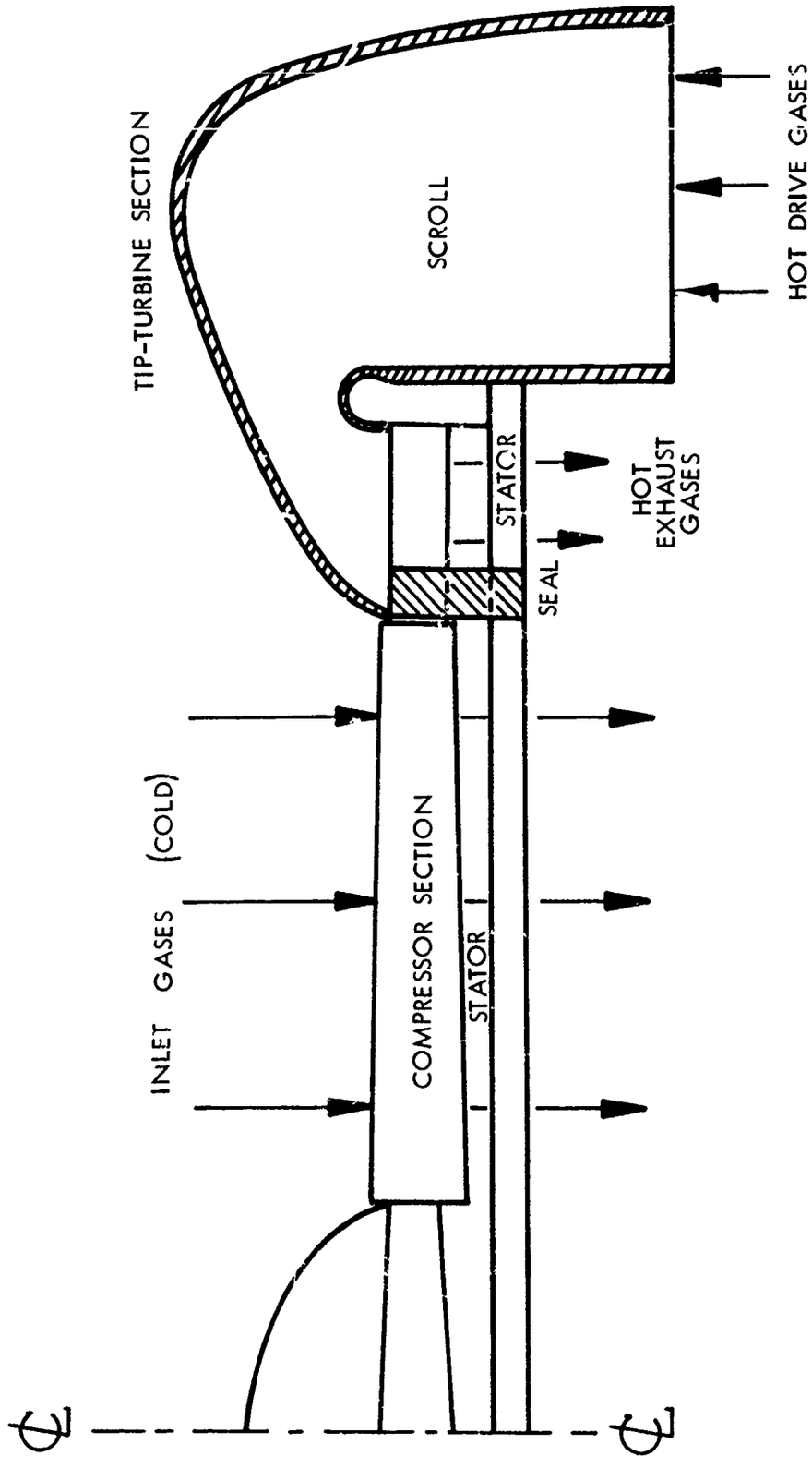

FIGURE 66 TIP-TURBINE FAN FLOW SCHEMATIC

by the rotor, rotor wakes cut by the stator, aerodynamic vortices causing impulses of periodic nature, and jet noise generated by the hot gases emitting from the tip-turbine ring.

C. Model Tip-Turbine Fan Description

The model used for this investigation is an air-driven, tip-turbine fan designed to simulate lift and cruise fan propulsion (Figure 67). It has the following specifications:

Outer Scroll Diameter	14.16 in.
Fan Blade Diameter	8.00 in.
Spinner Diameter	4.90 in.
Maximum Thrust	300 lbs.
Operating Temperature Range	70° to 1000°F
Low-Temperature Rotational Velocity	Up to 5000 rpm
High-Temperature Rotational Velocity	5000 - 22,900 rpm
Number of Fan Blades	22
Number of Vanes	24

D. Test Description

Lift and cruise tip-turbine fans are basically similar except for ducting and guide or vector vanes. The complete working model for this program was built as described in Section C. Tests were made with the model tip-turbine fan in three configurations: shroud mount, cruise fan, and wing mount.

1. Shroud Mount

The shroud-mount test arrangement is shown in Figure 68. As indicated by the photograph, the shroud-mount configuration was set up with the tip-turbine fan exhaust impinging upon a ground plane at normal incidence. Ground-plane effects were determined by recording noise levels at each field point in a grid pattern. Seven microphones were mounted on a mobile frame, as shown in Figure 69. The steel frame was set at a 7.5° line to a new position behind the former position for each test run. The microphone locations formed the grid shown in Figure 70, which was located just forward of the fan inlet and to the side of the tip-turbine centerline. Sound pressure levels were recorded with the ground plane set at three positions relative to the tip-turbine fan inlet. Table IV lists the test conditions.

TABLE IV

TEST CONDITIONS - SHROUD MOUNT CONFIGURATION

Test No.	Inlet driving air		Ground plane position		Rotational velocity, rpm	Total microphones
	Temp., °F	Press., psig	Inches	Diameters		
1	952	61	48	6	22,700	70
2	949	61	32	4	22,550	70
3	959	61	18	2.25	22,750	70
4	948	49	18	2.25	19,050	70
5	914	29	18	2.25	15,300	70
6	728	61	18	2.25	22,500	70

FIGURE 67 MODEL TIP-TURBINE FAN

FRONT VIEW

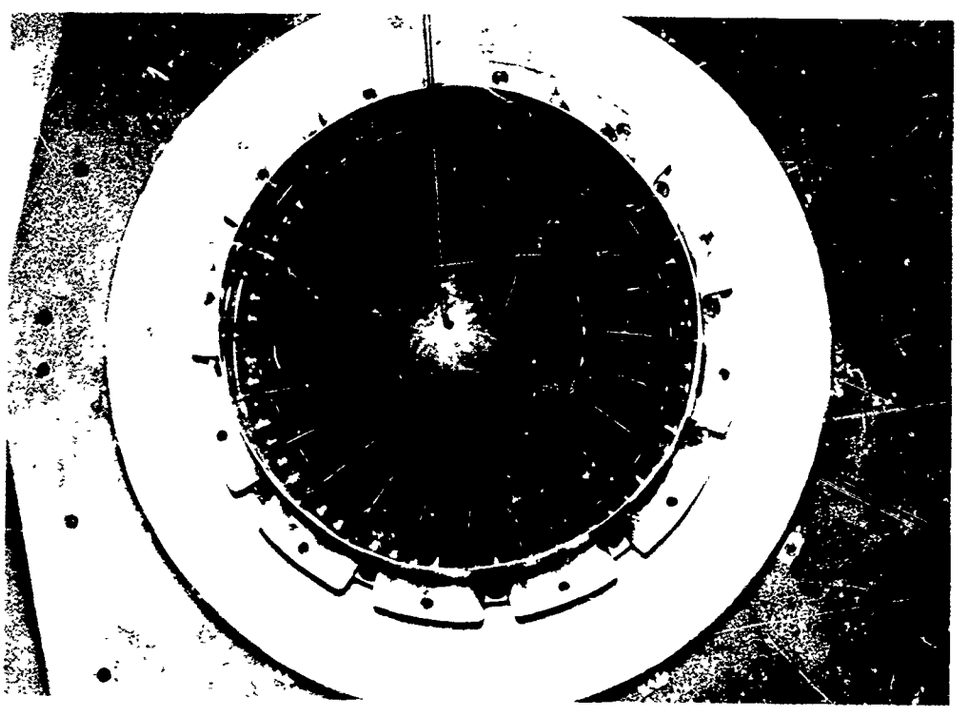

REAR VIEW

FIGURE 67. MODEL TIP-TURBINE FAN (CONT'D)

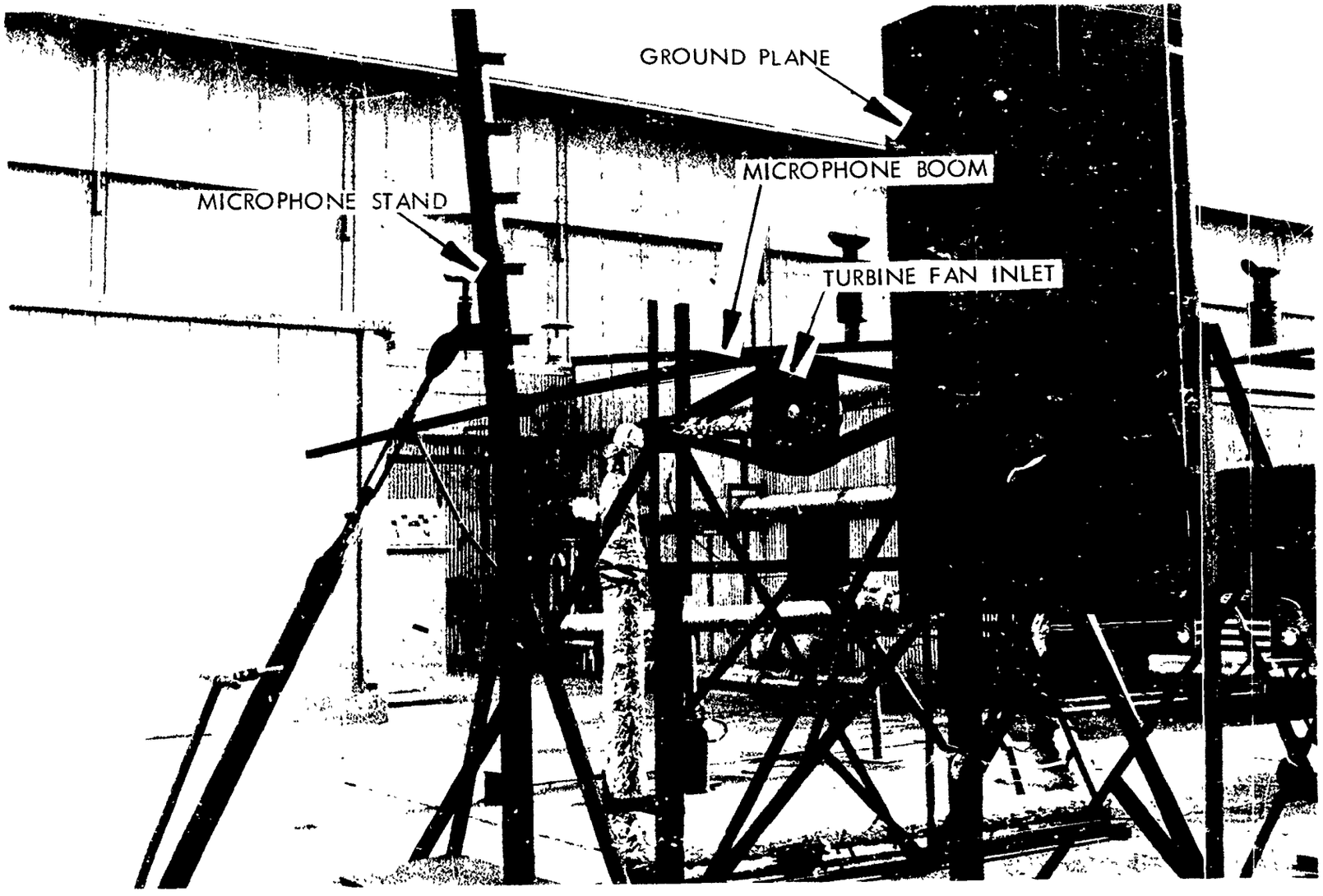

FIGURE 68 SHROUD MOUNT TEST SET-UP

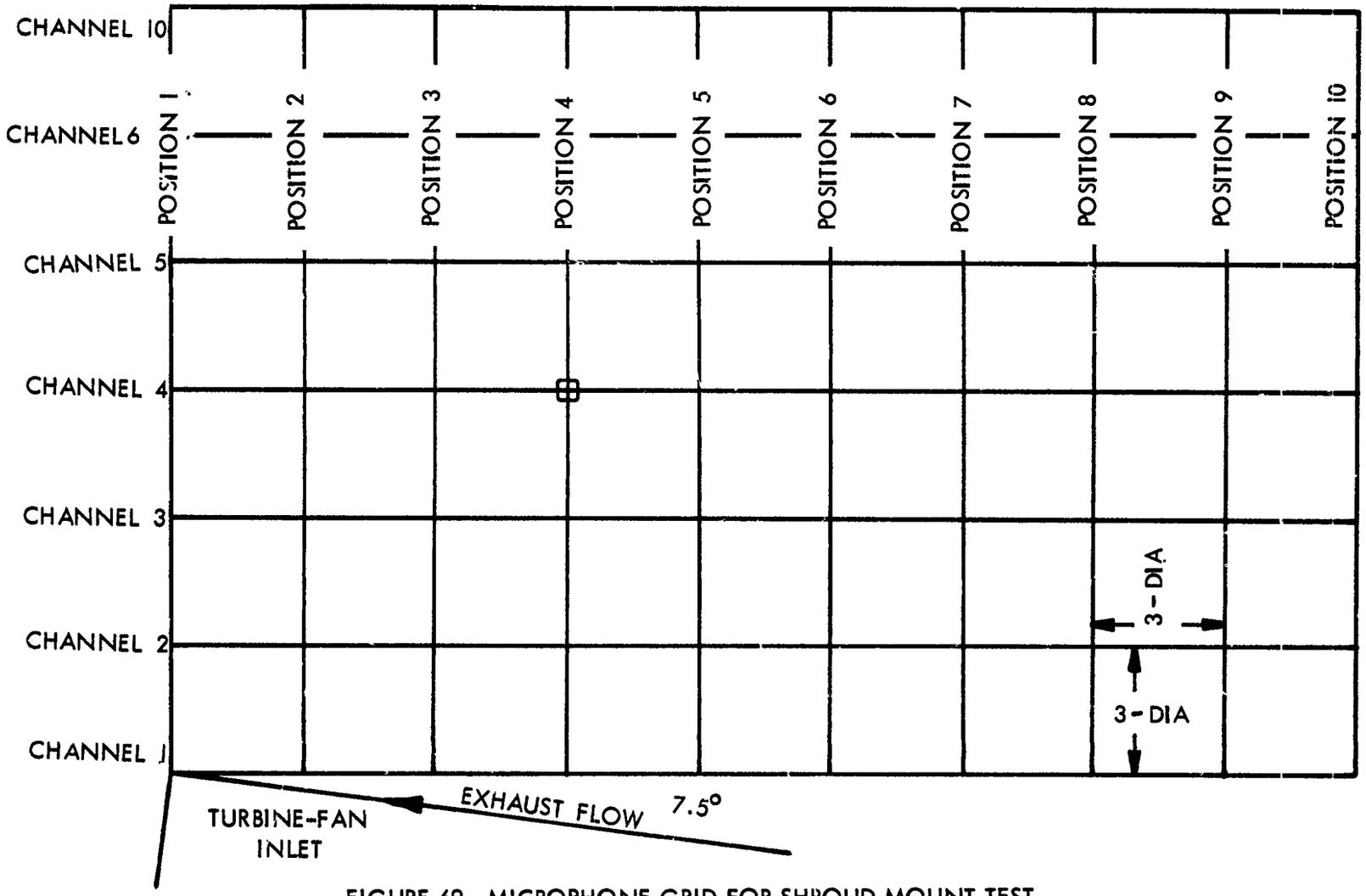

FIGURE 69 MICROPHONE GRID FOR SHROUD MOUNT TEST

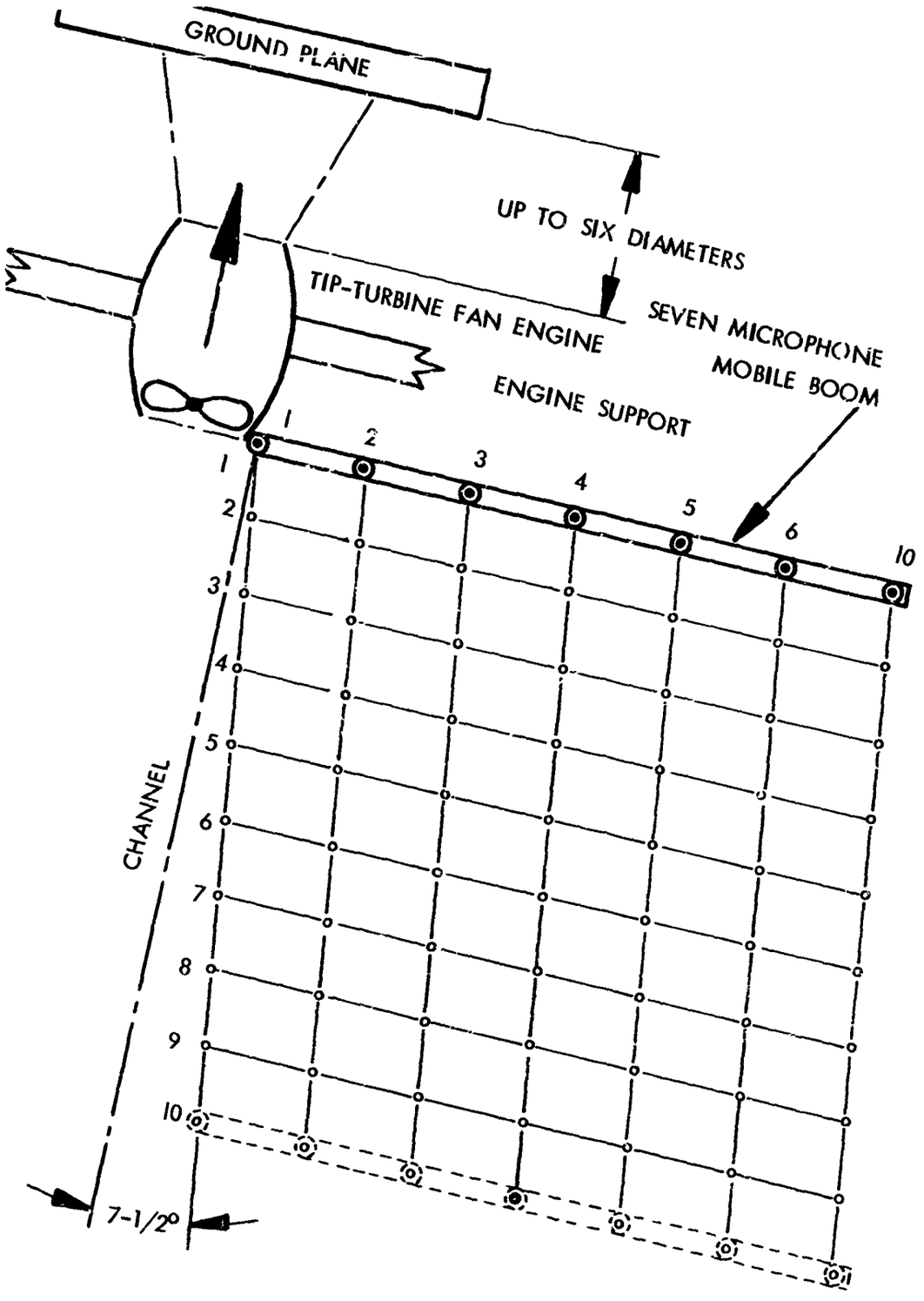

FIGURE 70. SCHEMATIC OF SHROUD MOUNT CONFIGURATION

2. Cruise Fan

Figure 71 is a schematic diagram of the test arrangement for the cruise-fan configuration with ground plane, and Figure 72 shows the test arrangement without ground plane. The microphone array used for sampling the sound field was positioned just aft of the tip-turbine exit plane at a 7.5° angle to the centerline (see Figures 71 and 72). Ground-plane effects were determined by sampling the noise field in the grid pattern shown in Figure 71 and with the movable ground plane set at two positions relative to the tip-turbine fan exit plane. Table V below is a list of test conditions for the cruise fan configuration.

TABLE V

TEST CONDITIONS - CRUISE FAN CONFIGURATION

Test No.	Inlet driving air		Ground plane position		Rotational velocity, rpm	Total microphones
	Temp., °F	Press., psig	Inches	Diameters		
7	960	66	18	2.25	22,890	49
8	958	66	48	6	22,850	49
9*	955	66	None	None	22,850	49
10*	708	68	None	None	22,800	49
11*	959	47	None	None	19,050	49
12*	942	30	None	None	15,000	49

*Ground plane was removed for runs 9 through 12.

3. Wing Mount

This configuration consisted of a wing-mounted tip-turbine fan (see Figure 73). Seven flush-mounted microphones are attached to the simulated wing to measure the spanwise distribution of sound pressure level. A movable ground plane was located in the exit flow at three positions to determine the ground plane effects. Figure 74 is a schematic diagram of the microphone grid pattern for measuring chordwise and spanwise sound pressure distribution. Table VI lists the test conditions for this configuration.

TABLE VI

TEST CONDITIONS - WING MOUNT CONFIGURATION

Test No.	Inlet driving air		Ground plane position		Rotational velocity, rpm	Total microphones
	Temp., °F	Press., psig	Inches	Diameters		
13	963	62	None	None	22,930	7
14	975	63	48	6	22,800	7
15	976	63	32	4	22,880	7
16	968	64	18	2.25	22,930	7
17	958	45	18	2.25	19,000	7
18	1000	29	18	2.25	15,100	7

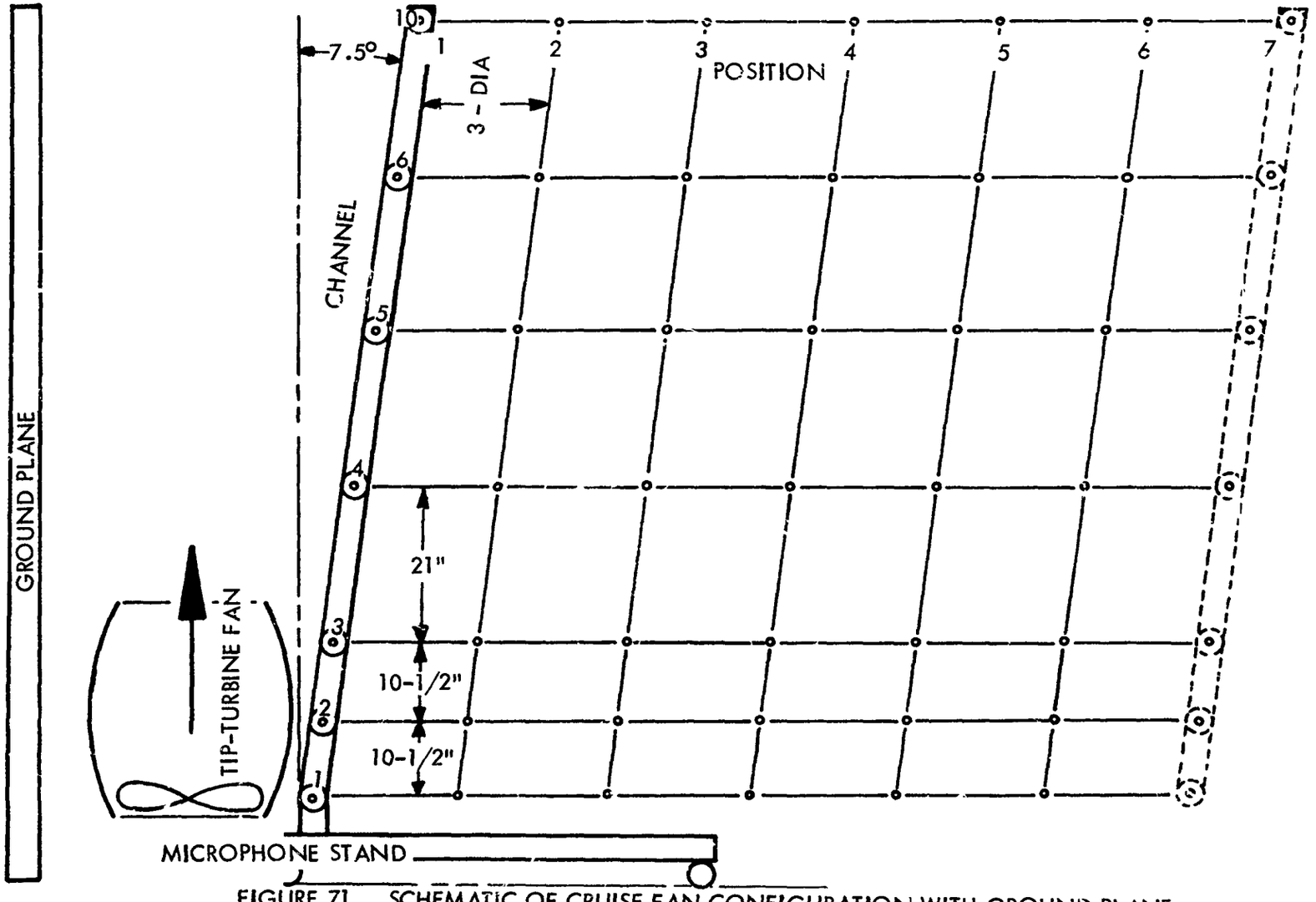

FIGURE 71. SCHEMATIC OF CRUISE FAN CONFIGURATION WITH GROUND PLANE

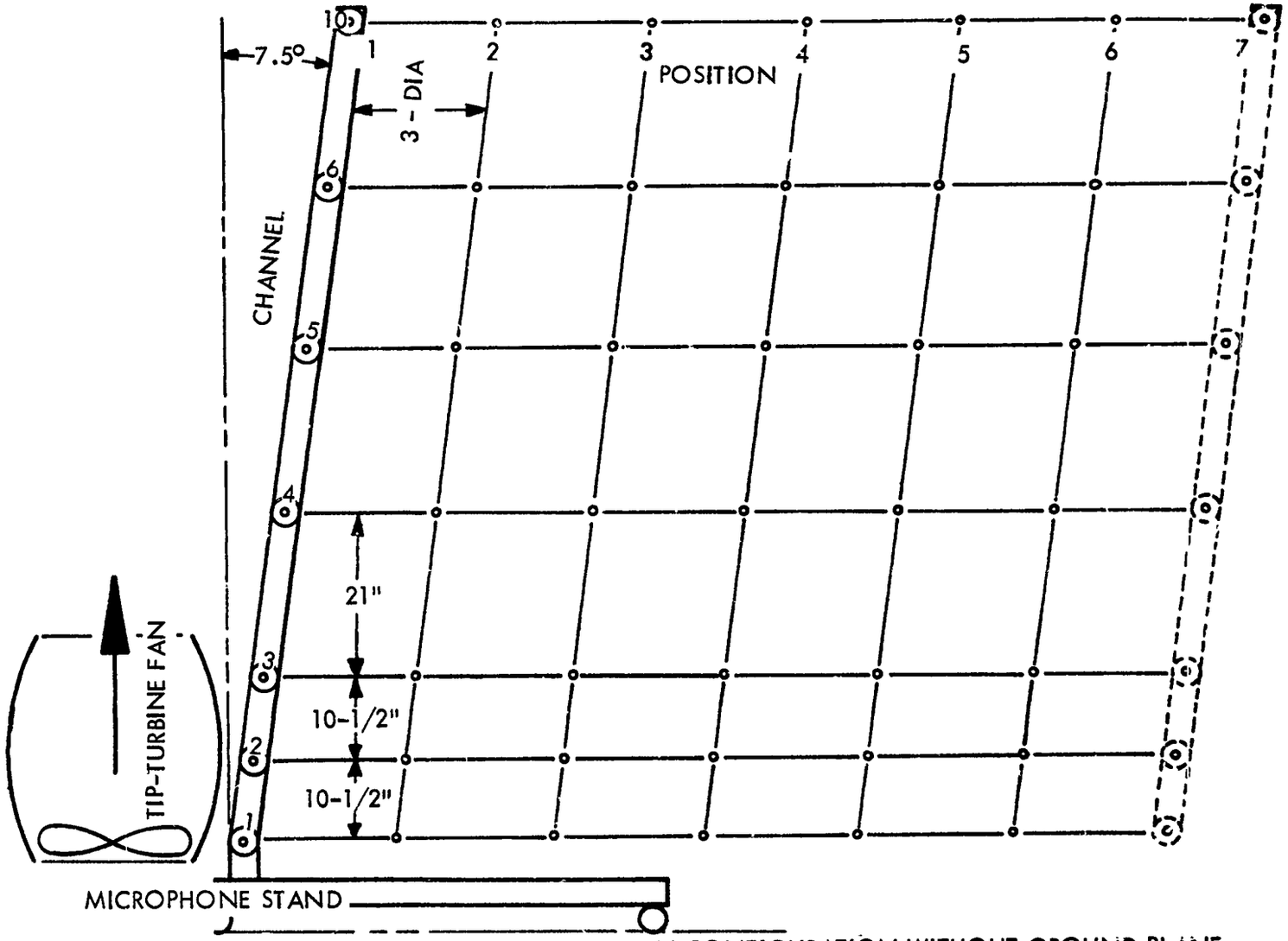

FIGURE 72. SCHEMATIC OF CRUISE FAN CONFIGURATION WITHOUT GROUND PLANE

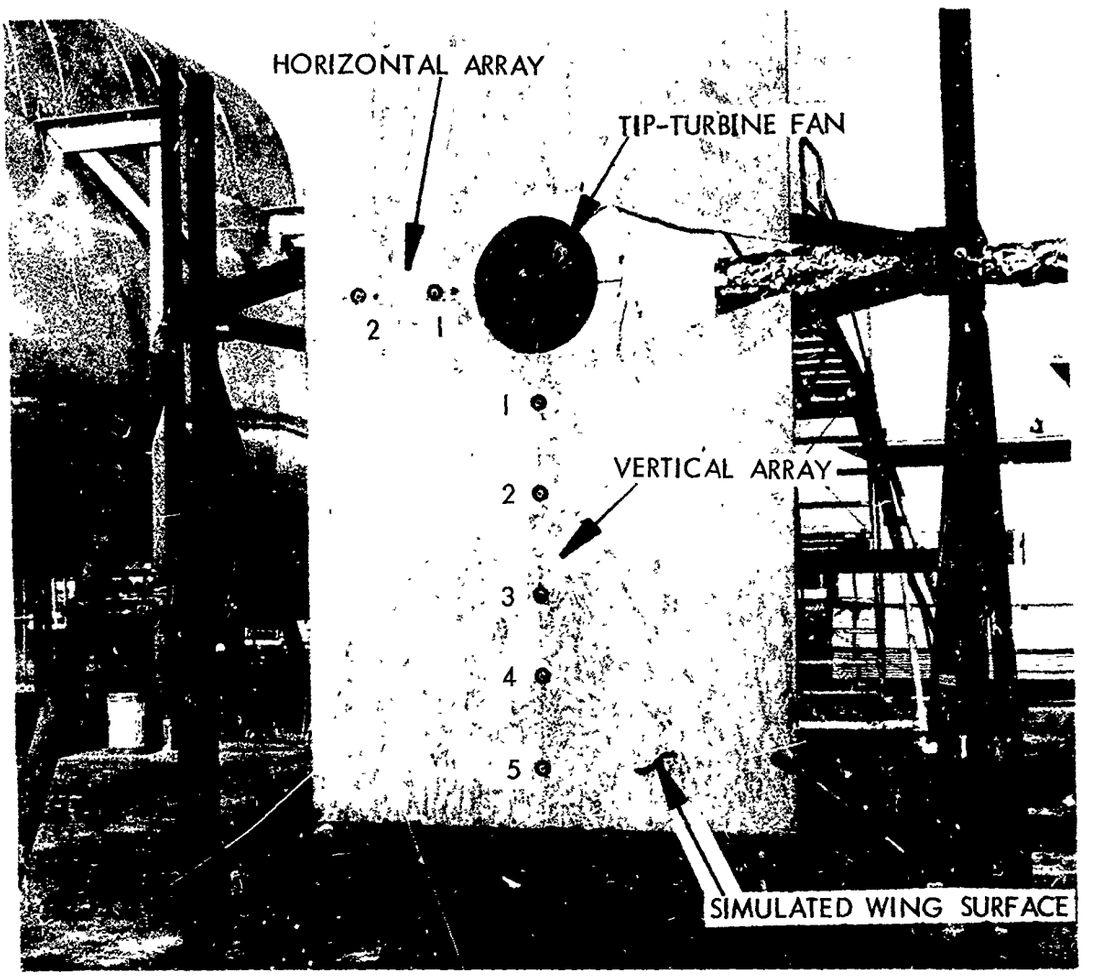

FIGURE 73 WING MOUNT TEST CONFIGURATION

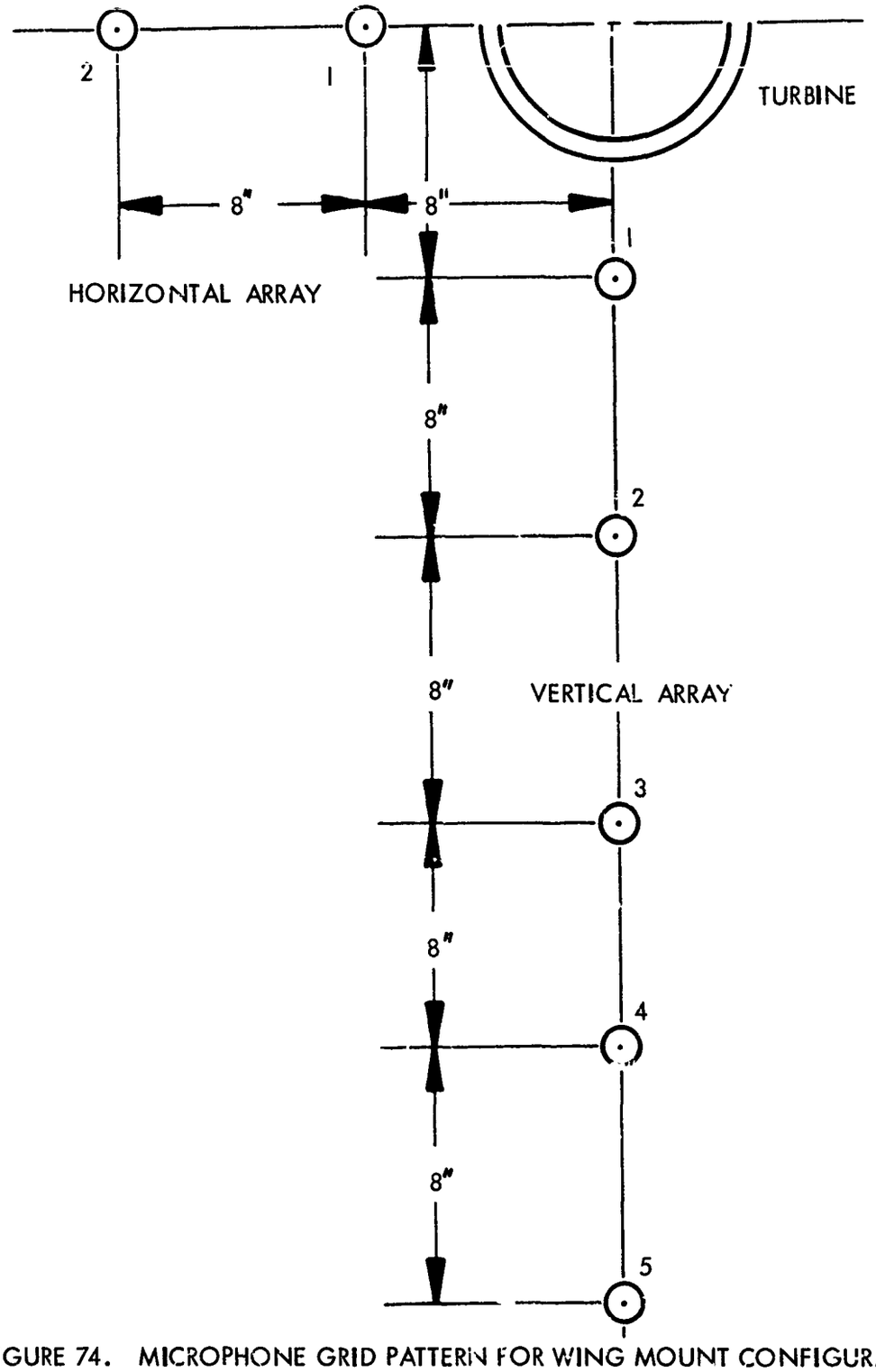

FIGURE 74. MICROPHONE GRID PATTERN FOR WING MOUNT CONFIGURATION

E. Test Results

1. Introduction

The microphone data recorded for the various phases of the tip-turbine fan tests were analyzed using one-third octave band filters and then transformed into sound pressure level contours and other required plots. During the course of the data analysis, it was discovered that a number of frequencies resulting from blade and stator vane combinations were prevalent. The noise at these frequencies was associated with either the rotational blade passage or with the overlap pattern between blades and stator vanes. In general, frequencies were found which correlated with the relationship mBn, where B is the number of blades, n is the rotational velocity in rps, and m is an integer 1, 2, 3, ... The spectra also exhibited components of frequency which correlated with the expression $m(B \pm G)n$, where G is the number of stator vanes.

2. Shroud Mount

Two important rotational blade passage frequencies, 8,400 Hz and 26,000 Hz, were present for this configuration. The former corresponds to the fundamental frequency, and the latter corresponds to the third harmonic. Figures 75a, 75b, and 75c are sound pressure level contours for 8,400 Hz frequency and Figures 76a, 76b, 76c are contours for 26,000 Hz. These contours represent the sound pressure level distribution for each frequency with the tip-turbine fan in a shroud mount and the ground plane positioned 48, 32, and 18 inches, respectively, aft of the fan exit plane (see Figure 70). The microphones were positioned in an array located just forward of the fan inlet, as shown in Figure 69.

A comparison of the contour plots in Figures 75a, 75b, and 75c, or Figures 76a, 76b, and 76c, reveals that influence of proximity of the ground plane on the sound field. It can be seen that pressure buildup resulting from the ground plane nearby was relieved by blow-by around the turbine shroud. This distorted the sound field forward of the tip-turbine fan.

Consider a representative location in the blow-by distorted region of each plot. Position 4, channel 4, Figure 69, is centrally located in the grid and clearly reveals the effect of the ground plane. The data for this comparison are contained in Table VII.

TABLE VII

GROUND PLANE EFFECTS

Reference figure number	Ground plane location		One-third octave SPL at MIC position, db	Frequency Hz
	Inches	Diameters		
75a	48	6	104	8,400
75b	32	4	110	8,400
75c	18	2.25	112	8,400
76a	48	6	112	26,000
76b	32	4	116	26,000
76c	18	2.25	120	26,000

The contour plots, from which the figures shown in Table VII were taken, indicate that the inner one-third of the plot had virtually no distortion of the sound field. Maximum

distortion occurred, however, from 4 to 8 feet (6 to 12 diameters) outboard of the fan shroud, and in this region there was a considerable increase in sound pressure level as the ground plane was moved nearer to the tip-turbine fan.

Figures 77 and 78 are profiles of the sound pressure level contours along a constant microphone location line for three consecutive test runs. The location of the ground plane was changed for each run. Figure 77 is a plot of SPL versus X/D (distance from the tip-turbine fan in terms of diameters) for the 26,000 Hz noise. This profile plot clearly indicates the buildup of sound pressure as the ground plane was moved nearer to the tip-turbine fan. Figure 78 indicates the same dependence for the 8,400 Hz noise.

Figures 79a, 79b, and 79c are narrow-band analyses (2 Hz bandwidth) made to show the frequency content of the tip-turbine fan at microphone positions 1-1, as shown in Figure 69. Table VIII shows the calculated rotational blade passage and overlap pattern frequencies identified in the data.

TABLE VIII

IDENTIFICATION OF DOMINANT NOISE PEAKS

Test	RPM	Blade frequency	Overlap B-G frequency	Overlap B+G frequency	Third blade harmonic
3	22,750	8,200	760	16,400	24,600
4	19,050	7,000	635	14,000	21,000
5	15,300	5,700	510	11,700	17,000
10	22,800	8,600	750	26,000	17,500
11	19,050	7,200	635	14,600	21,900
12	15,000	5,450	500	11,000	16,500

3. Cruise Fan

Figures 80 and 81 are sound pressure level contour plots of the sound field measured under simulated cruise conditions. Comparison of Figures 80a, 80b, and 80c, or Figures 81a, 81b, and 81c showed no significant effect from relocating the ground plane. There was only a slight change in the sound field characteristics as the ground plane was moved away; at most there was a decrease in the field gradient at the outboard edge of the grid.

Figure 82 is a plot of the 26,000-Hz noise displayed as SPL versus X/D for the cruise fan configuration where the ground plane was oriented parallel to the exhaust flow direction. There was no evident influence of ground plane position on the measured sound pressure level. Figure 83 indicates the same characteristics for the 8400-Hz noise.

Contours on Figures 84a, 84b, 84c, and 84d are cruise-fan configuration sound pressure levels measured with a microphone array just off the fan exhaust flow field as indicated in Figure 71. The only parameter decidedly changed from the test conditions of Figures 80 through 83 was the turbine inlet temperature (see Table V). Evaluation of these data reveals no significant distortion of the sound field that might be related to the turbine fan inlet temperature. Jet noise appeared to be dominant only on channels 3, 4, and 5 in position 1; elsewhere the jet noise was highly attenuated or absent.

Figures 85a through 85d show representative noise measured from the cruise condition test. These are one-third octave band analyses representative of the data used for the foregoing

discussion. Both channel 1, position 1 (see Figure 71) of test 7 and test 8 show a predominance of turbine blade noise, while the plots from the same test runs taken from channel 4 show jet noise sound pressure levels almost of the same magnitude as the blade noise.

4. Wing Mount Configuration

Figures 86 and 87 present sound pressure levels measured on the simulated wing surface at the positions shown on Figure 74. Judging from the data of Figures 86 and 87, the spanwise and chordwise distribution was fairly uniform and there was no noticeable effect from relocating or removing the ground plane. Figure 87 shows that there was some shadowing effect on the simulated wing due to the tailpipe (see Figure 73). Figure 88 displays three plots similar to Figures 86 and 87, where only the engine rpm was changed. It appears that a more severe noise environment was formed for the 15,000-rpm configuration.

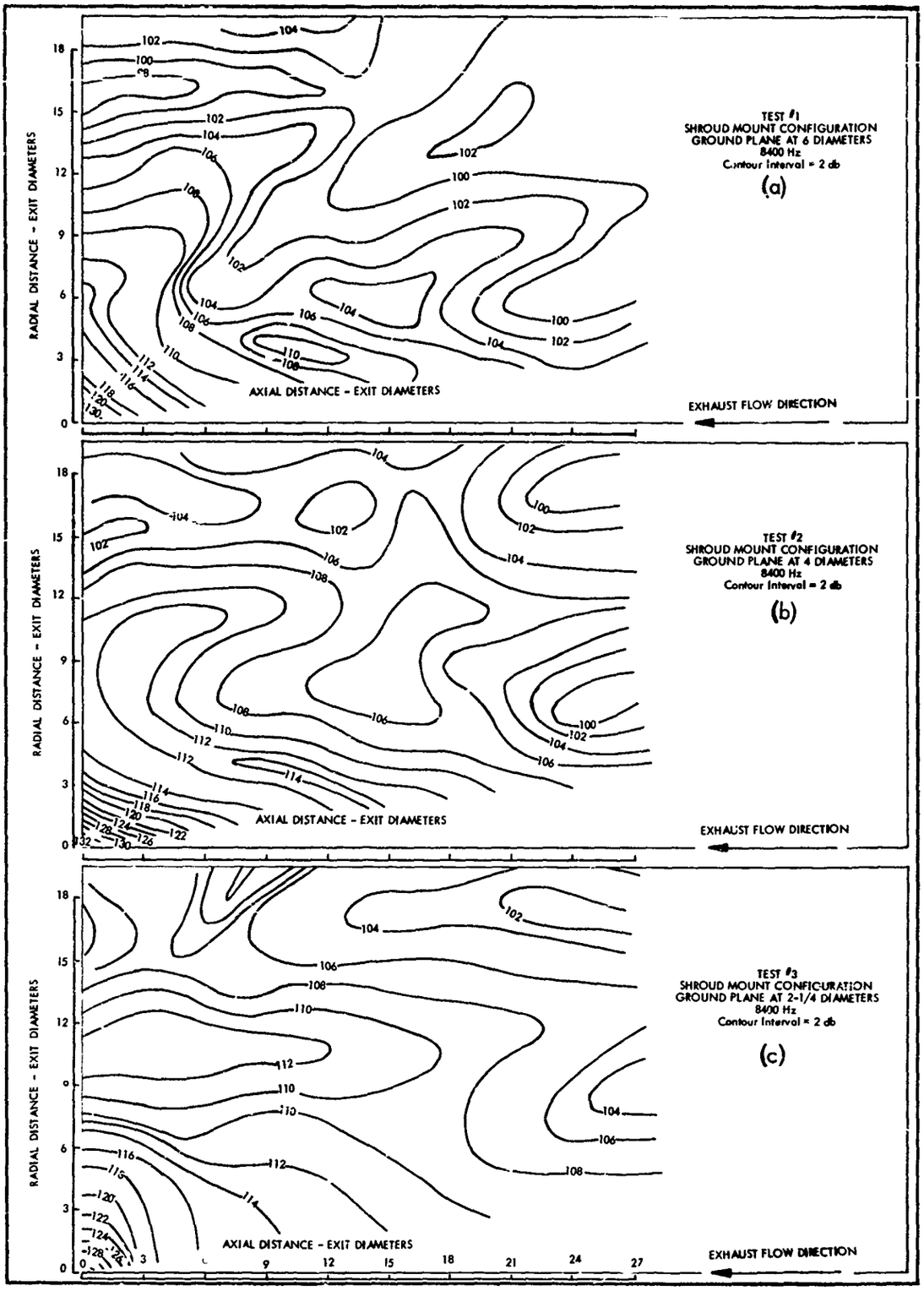

FIGURE 75 NEAR FIELD CONTOURS IN FRONT OF TIP-TURBINE FAN SHROUD MOUNT SHOWING EFFECT OF RELOCATING THE GROUND PLANE, 8,400 Hz

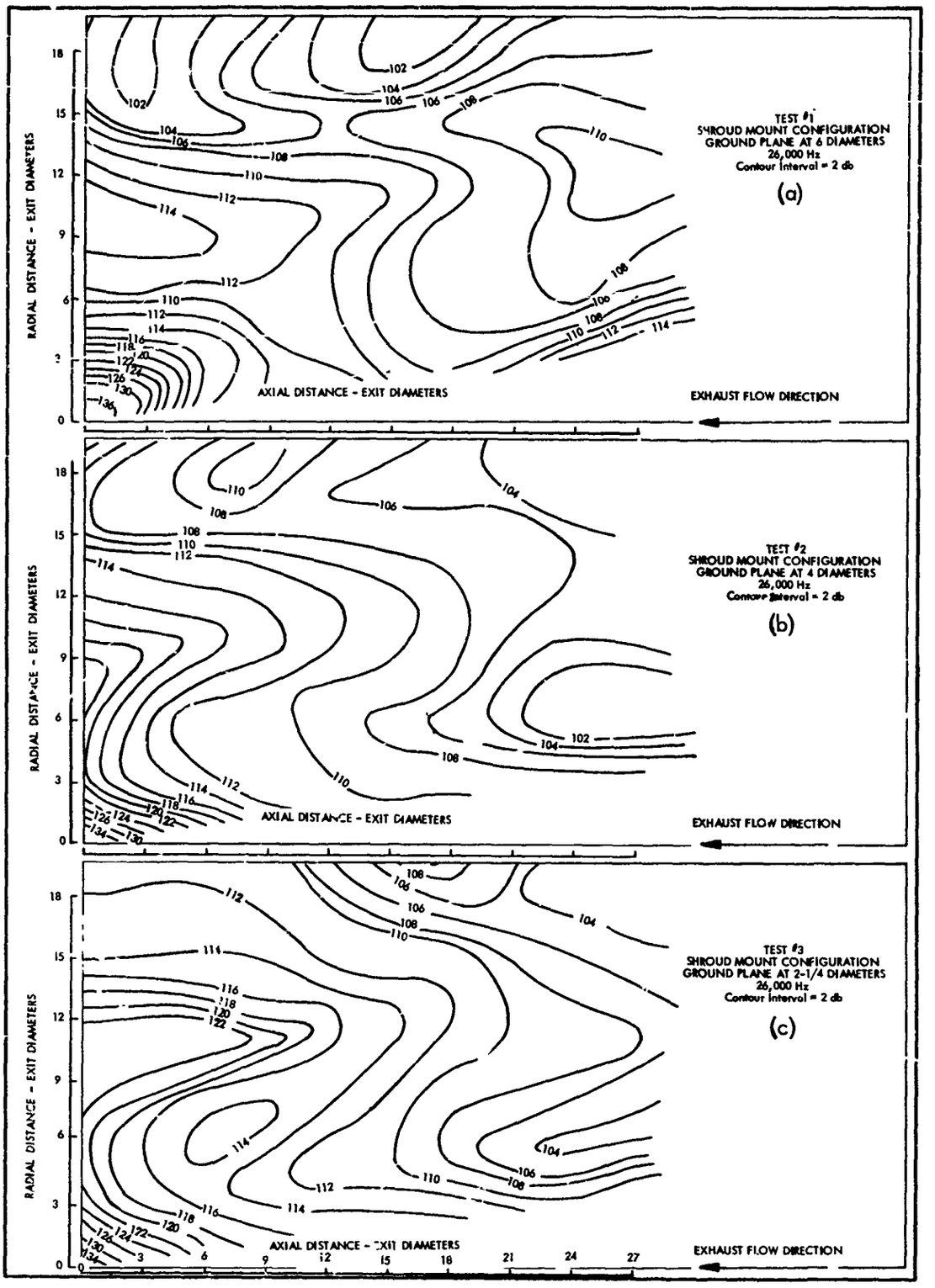

FIGURE 76 NEAR FIELD CONTOURS IN FRONT OF TIP-TURBINE FAN SHROUD MOUNT SHOWING EFFECT OF RELOCATING THE GROUND PLANE, 26,000 Hz

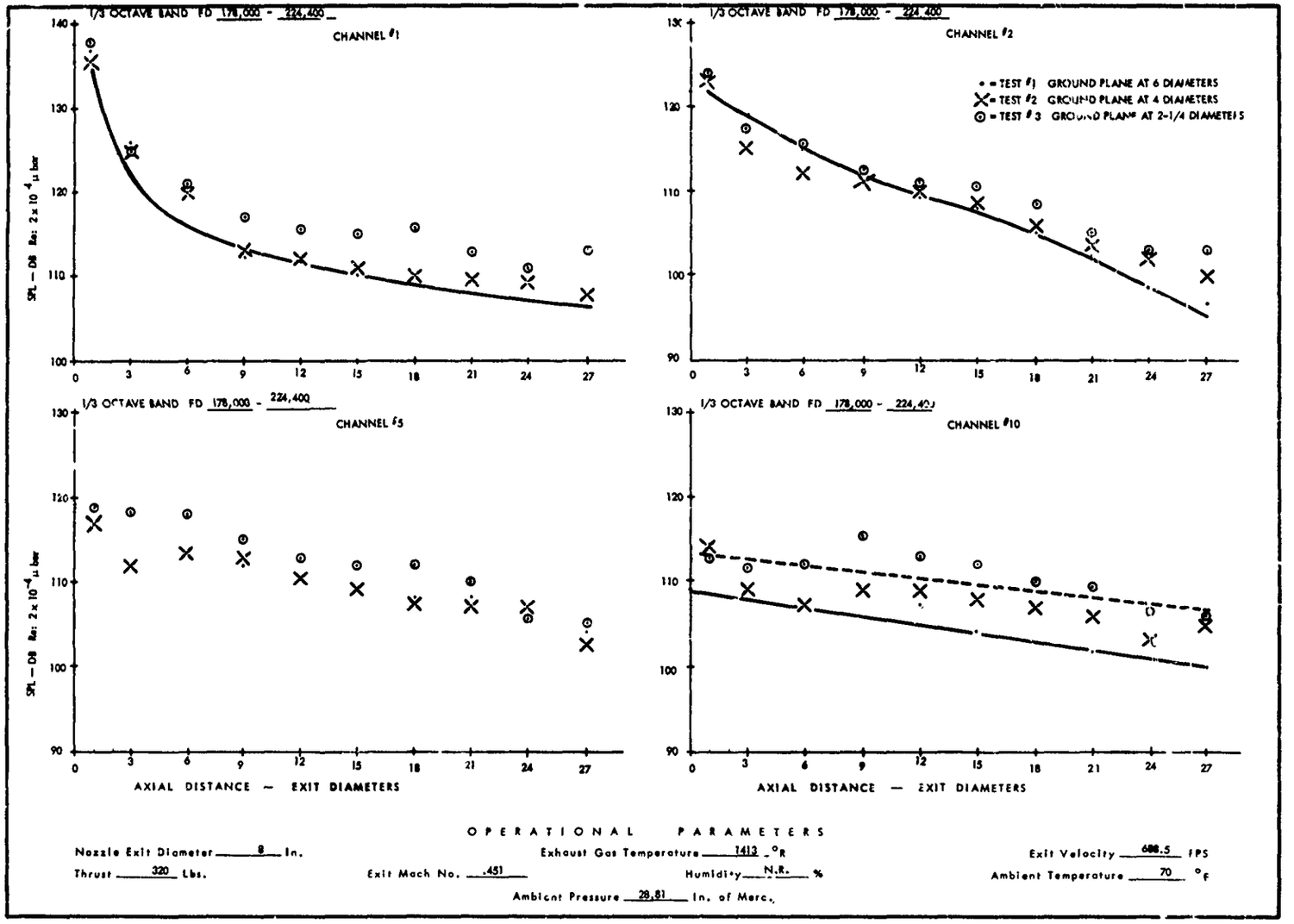

FIGURE 77 SPL VS. AXIAL DISTANCE FOR VARIOUS GROUND PLANE POSITIONS, SHROUD MOUNTED FAN, 26,000 Hz

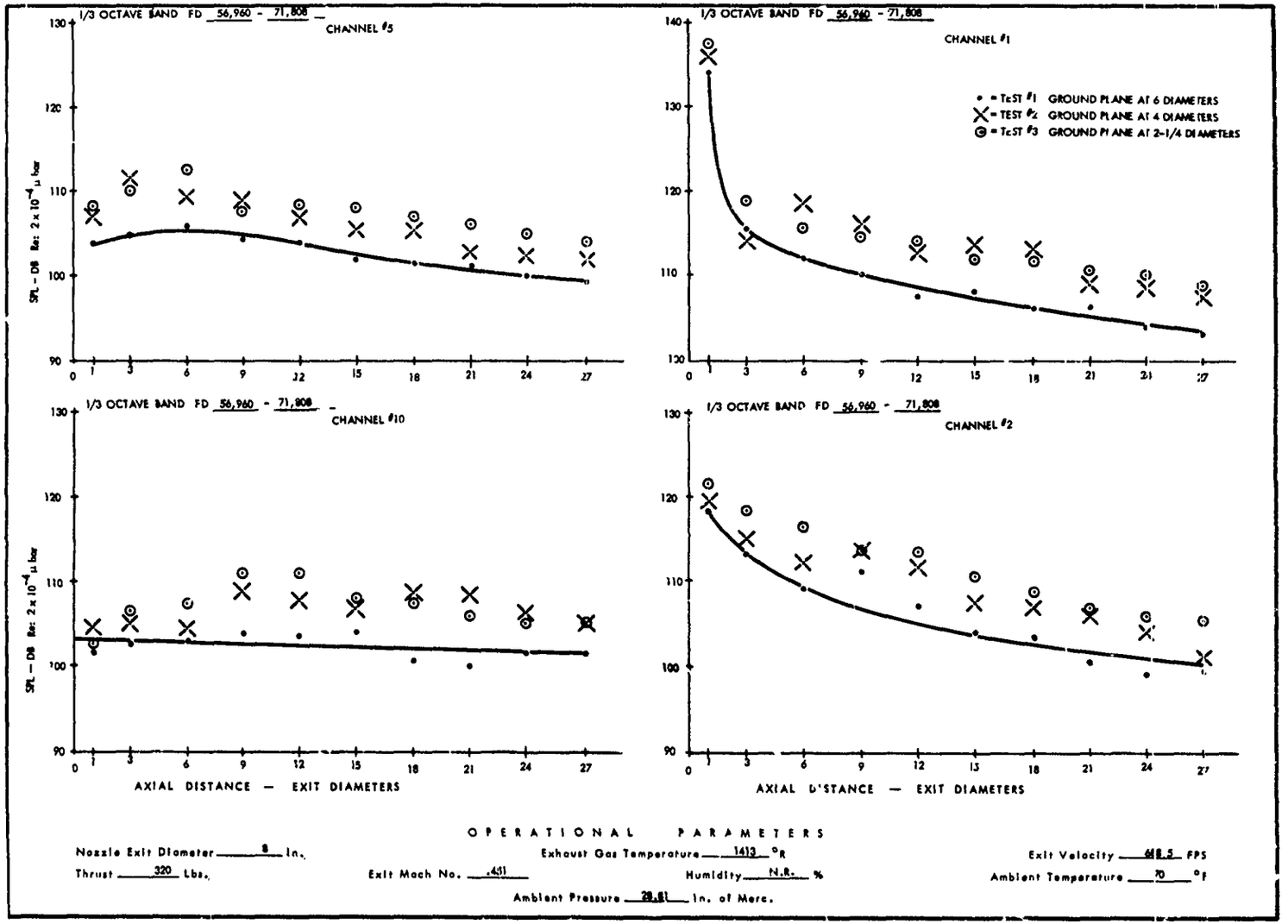

FIGURE 78 SPL VS. AXIAL DISTANCE FOR VARIOUS GROUND PLANE POSITIONS, SHROUD MOUNTED FAN, 8,400 Hz

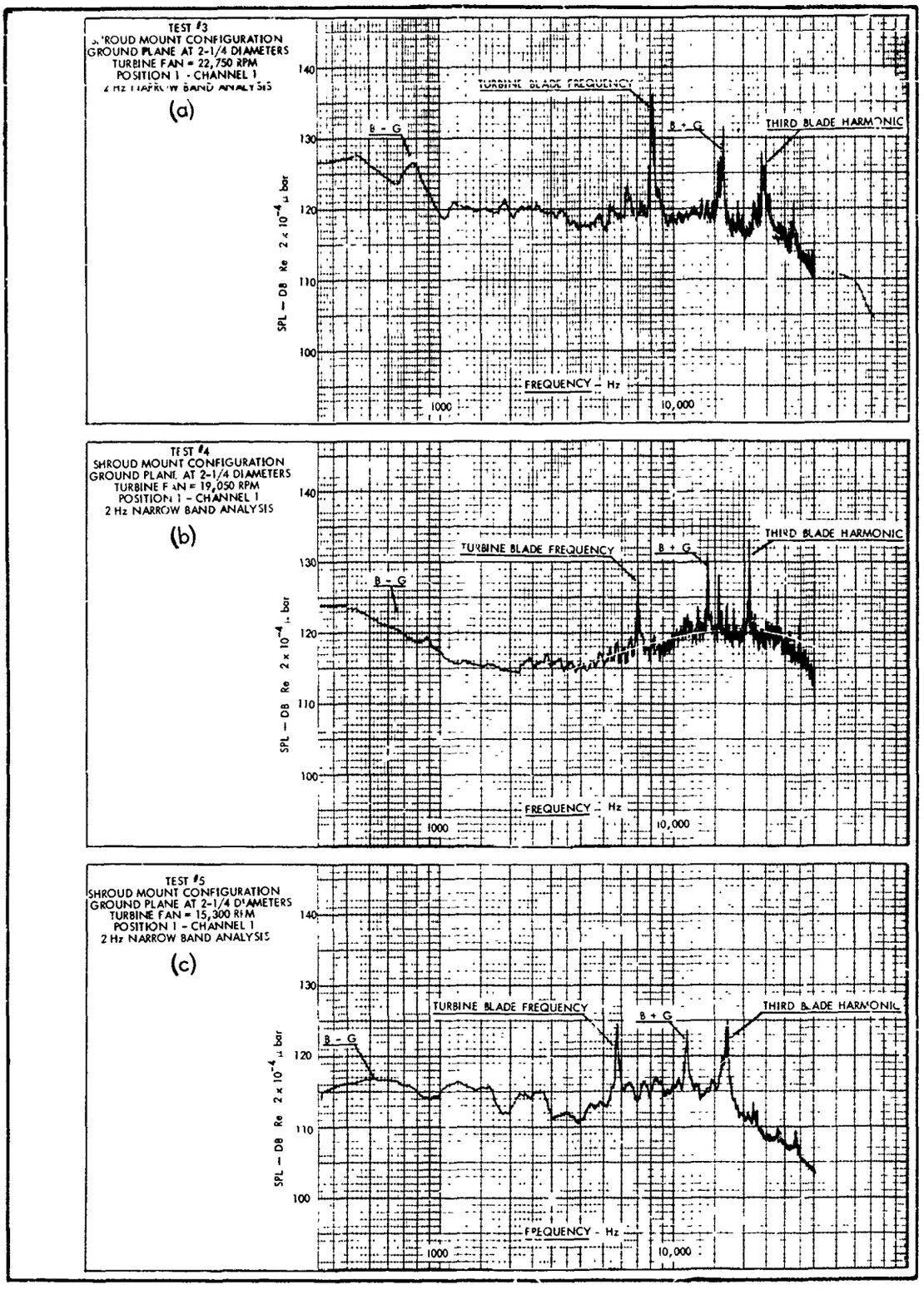

FIGURE 79 SHROUD MOUNT NARROW BAND SPECTRA FOR VARIOUS TURBINE RPM

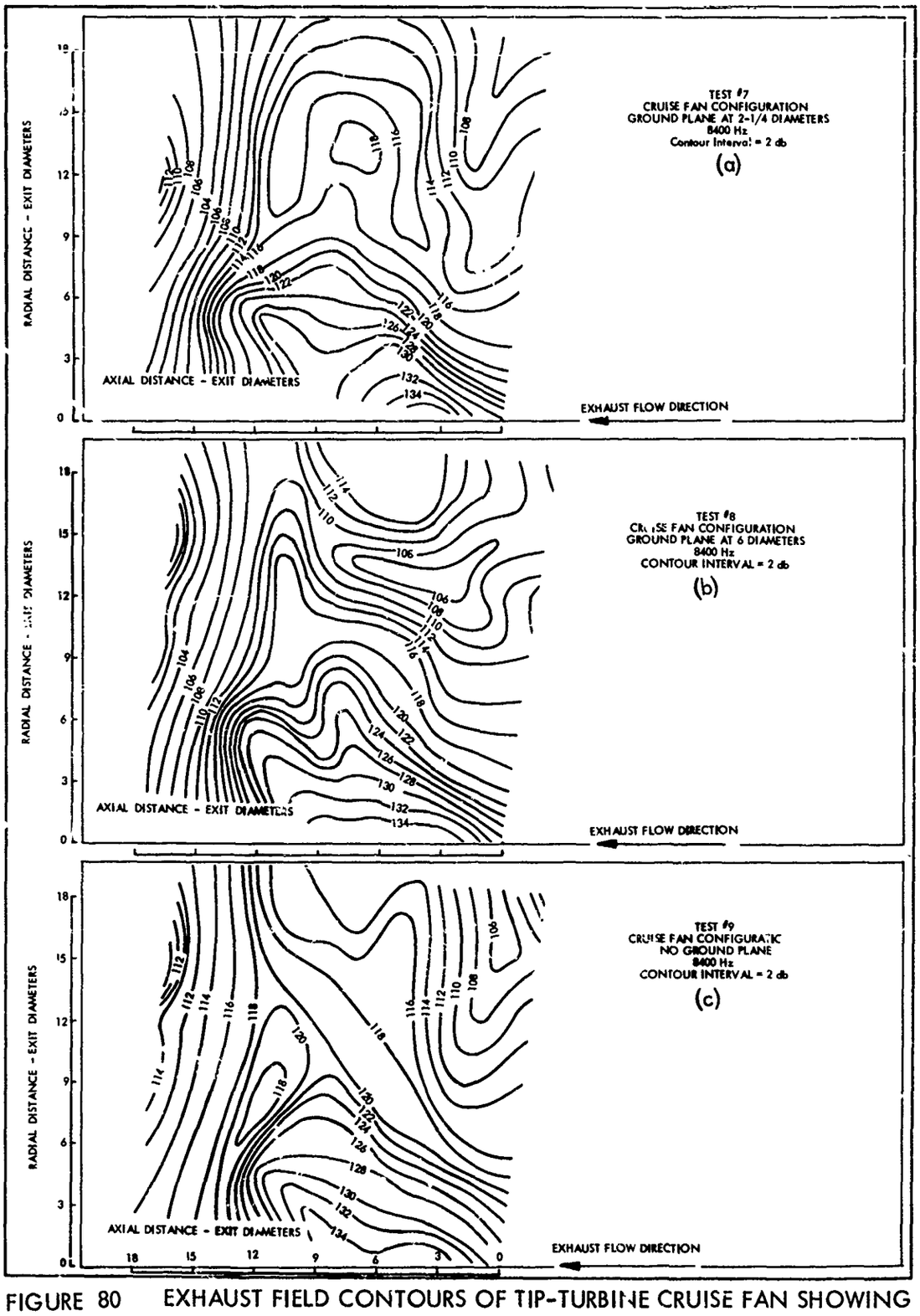

FIGURE 80 EXHAUST FIELD CONTOURS OF TIP-TURBINE CRUISE FAN SHOWING EFFECT OF RELOCATING THE GROUND PLANE, 8,400 Hz

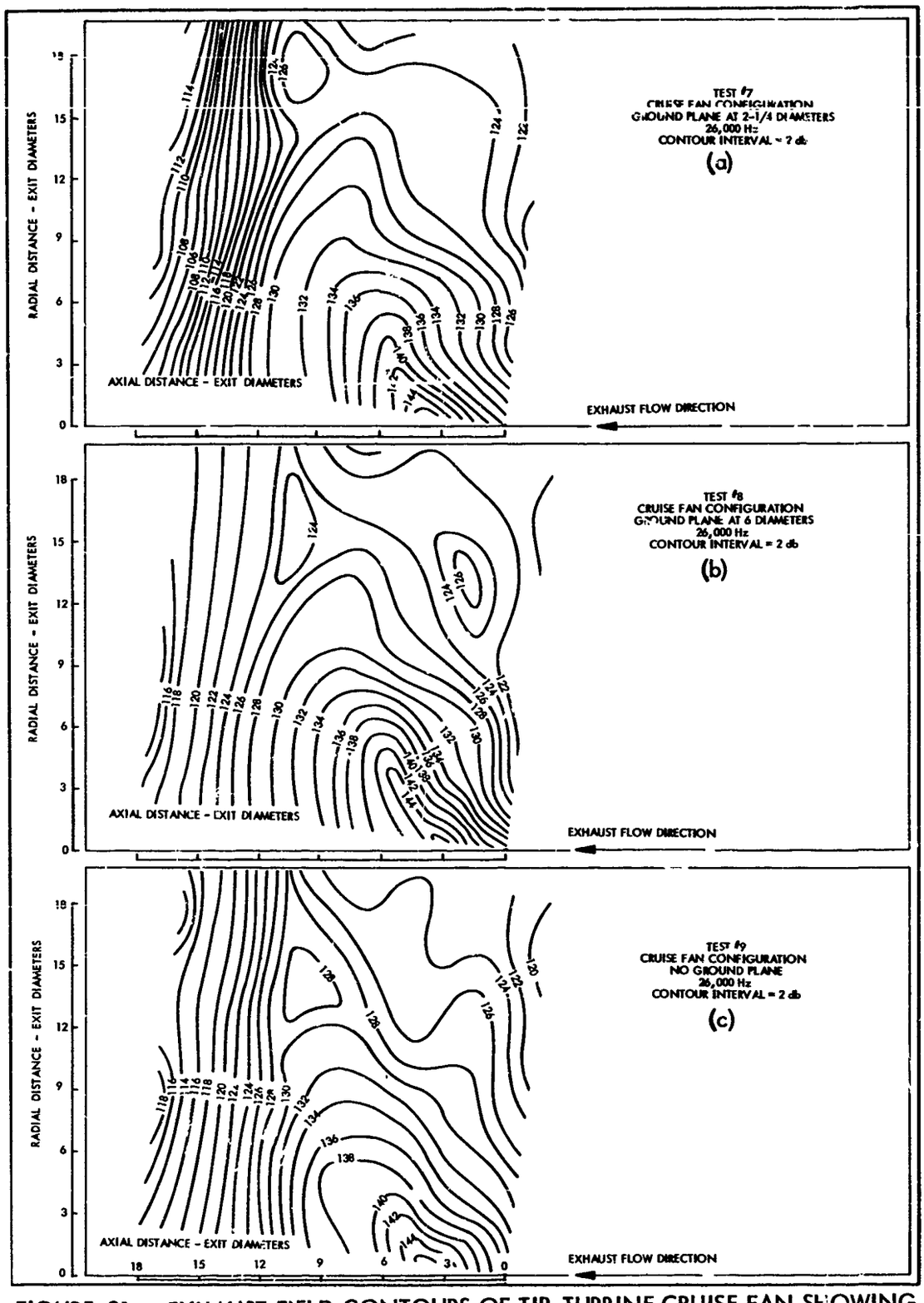

FIGURE 81 EXHAUST FIELD CONTOURS OF TIP-TURBINE CRUISE FAN SHOWING EFFECT OF RELOCATING THE GROUND PLANE, 26,000 Hz

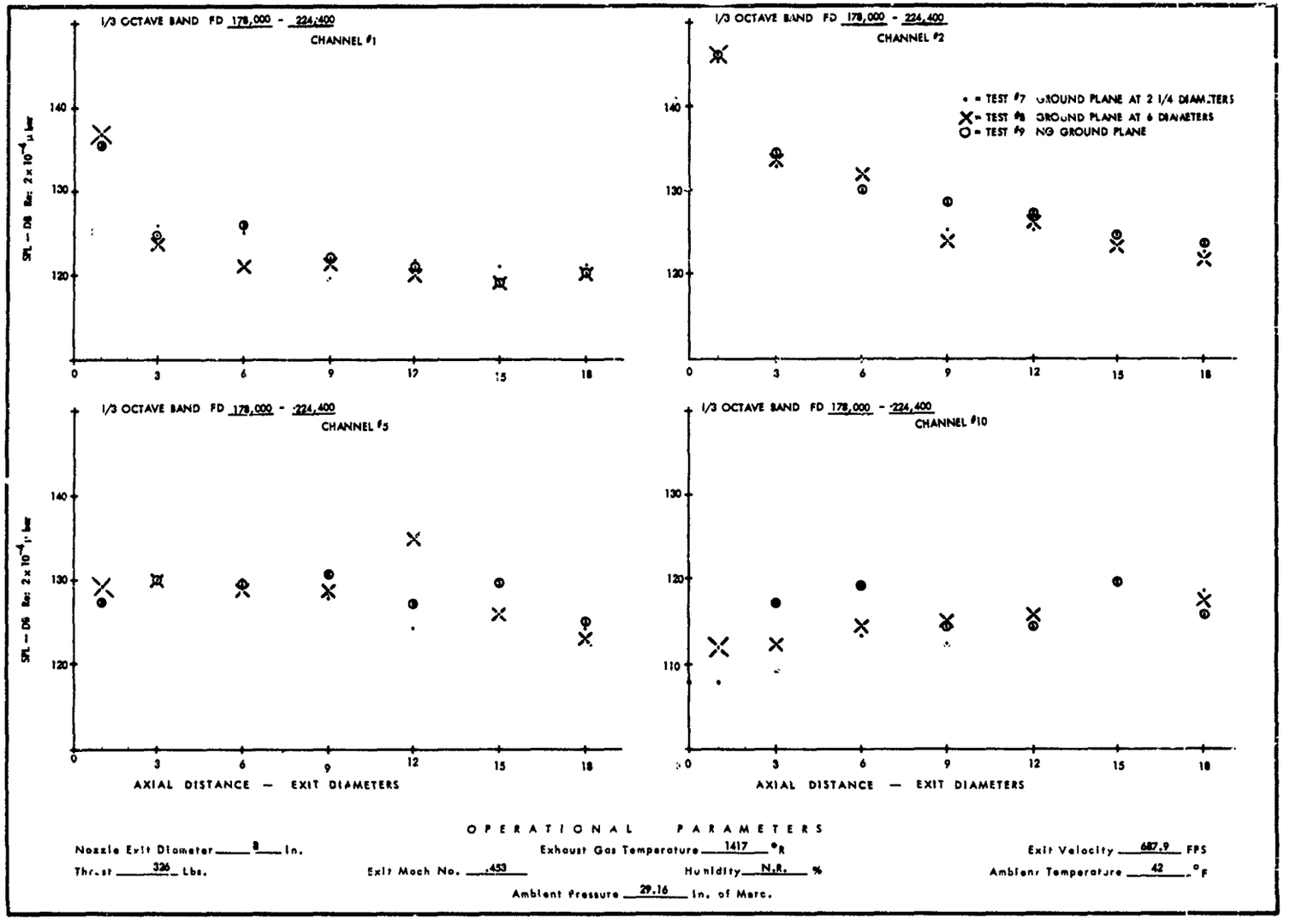

FIGURE 82 SPL VS. AXIAL DISTANCE FOR VARIOUS GROUND PLANE POSITIONS, CRUISE FAN TEST, 26,000 Hz

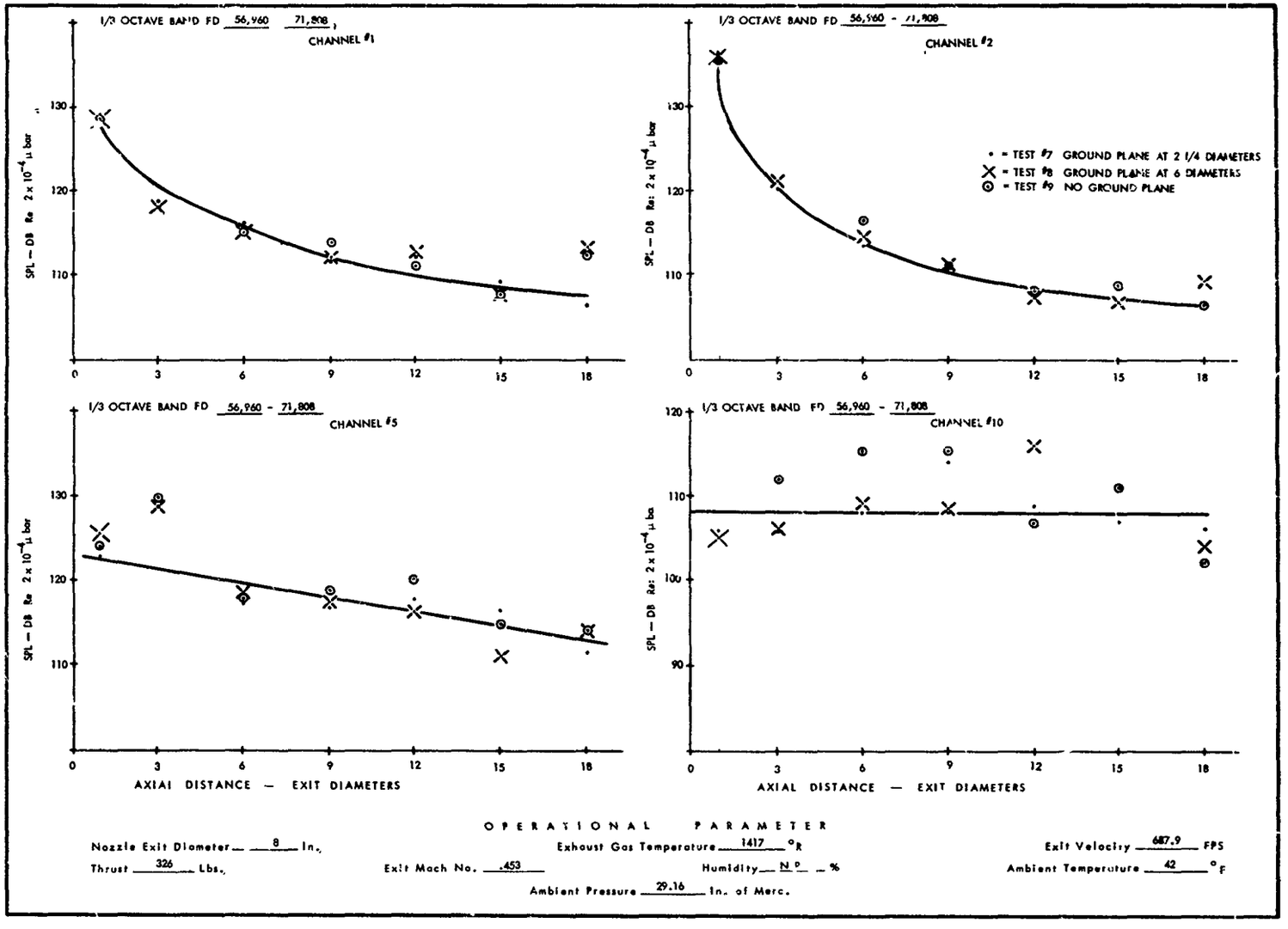

FIGURE 83 SPL VS. AXIAL DISTANCE FOR VARIOUS GROUND PLANE POSITIONS, CRUISE FAN TEST, 8,400 Hz

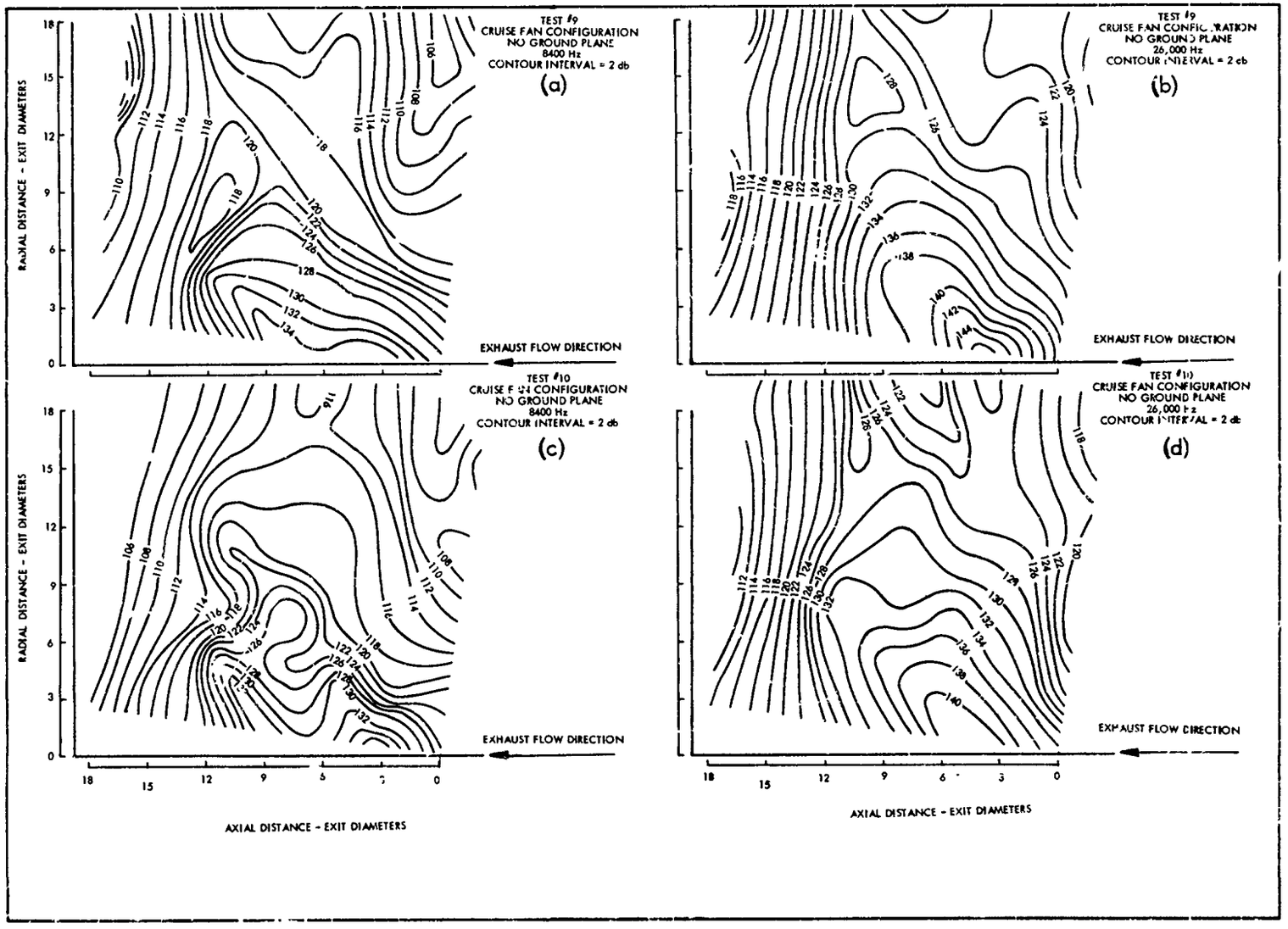

FIGURE 84 EXHAUST FIELD CONTOURS OF TIP-TURBINE CRUISE FAN FOR VARYING INLET TEMPERATURE

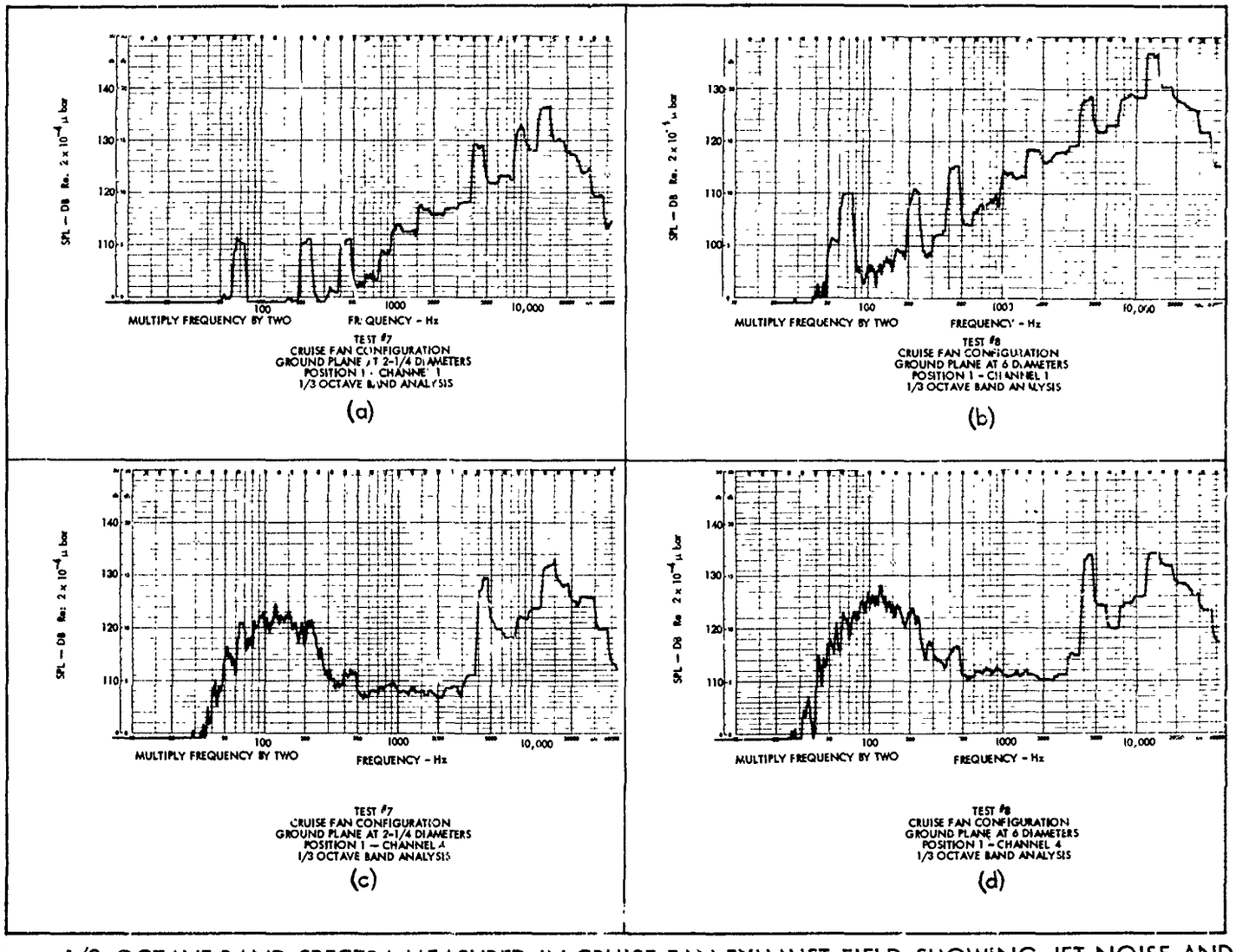

FIGURE 85 1/3-OCTAVE BAND SPECTRA MEASURED IN CRUISE FAN EXHAUST FIELD SHOWING JET NOISE AND BLADE PASSAGE NOISE CHARACTERISTICS

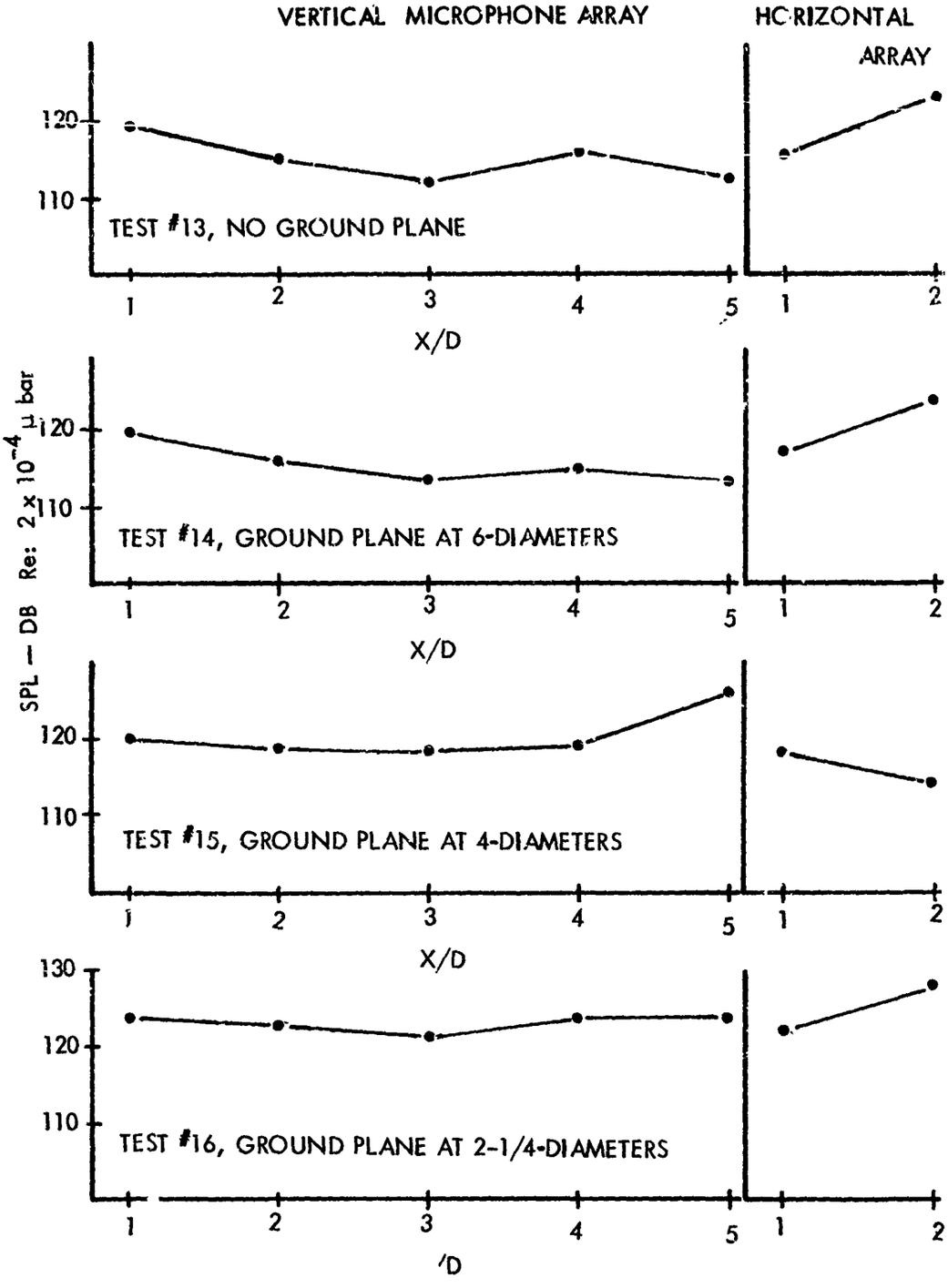

FIGURE 86 SPL VS. AXIAL DISTANCE FOR VARIOUS GROUND PLANE POSITIONS, WING MOUNT TEST, 8,400 Hz

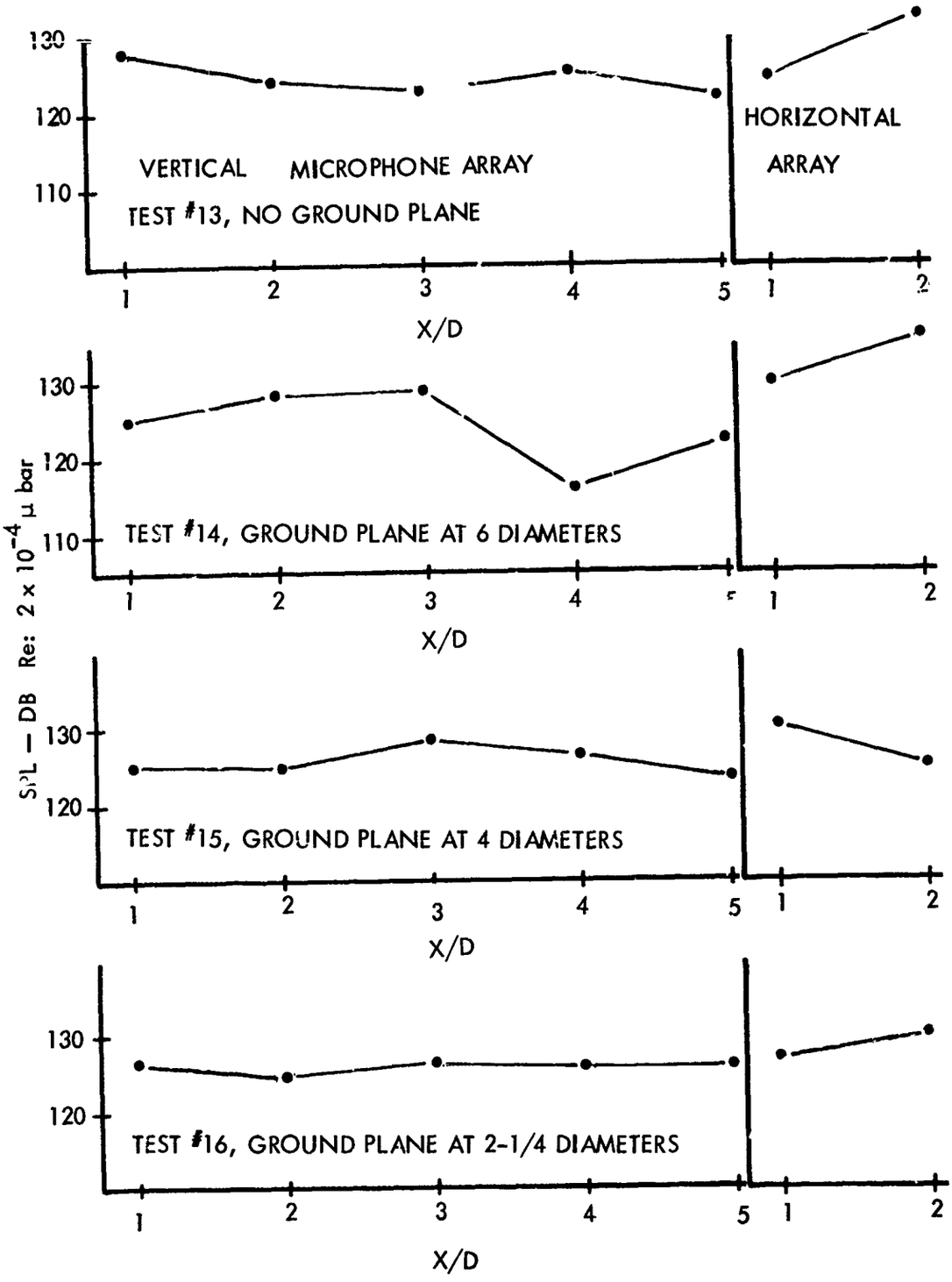

FIGURE 87. SPL VS. AXIAL DISTANCE FOR VARIOUS GROUND PLANE POSITIONS, WING MOUNT TEST, 26,000 Hz

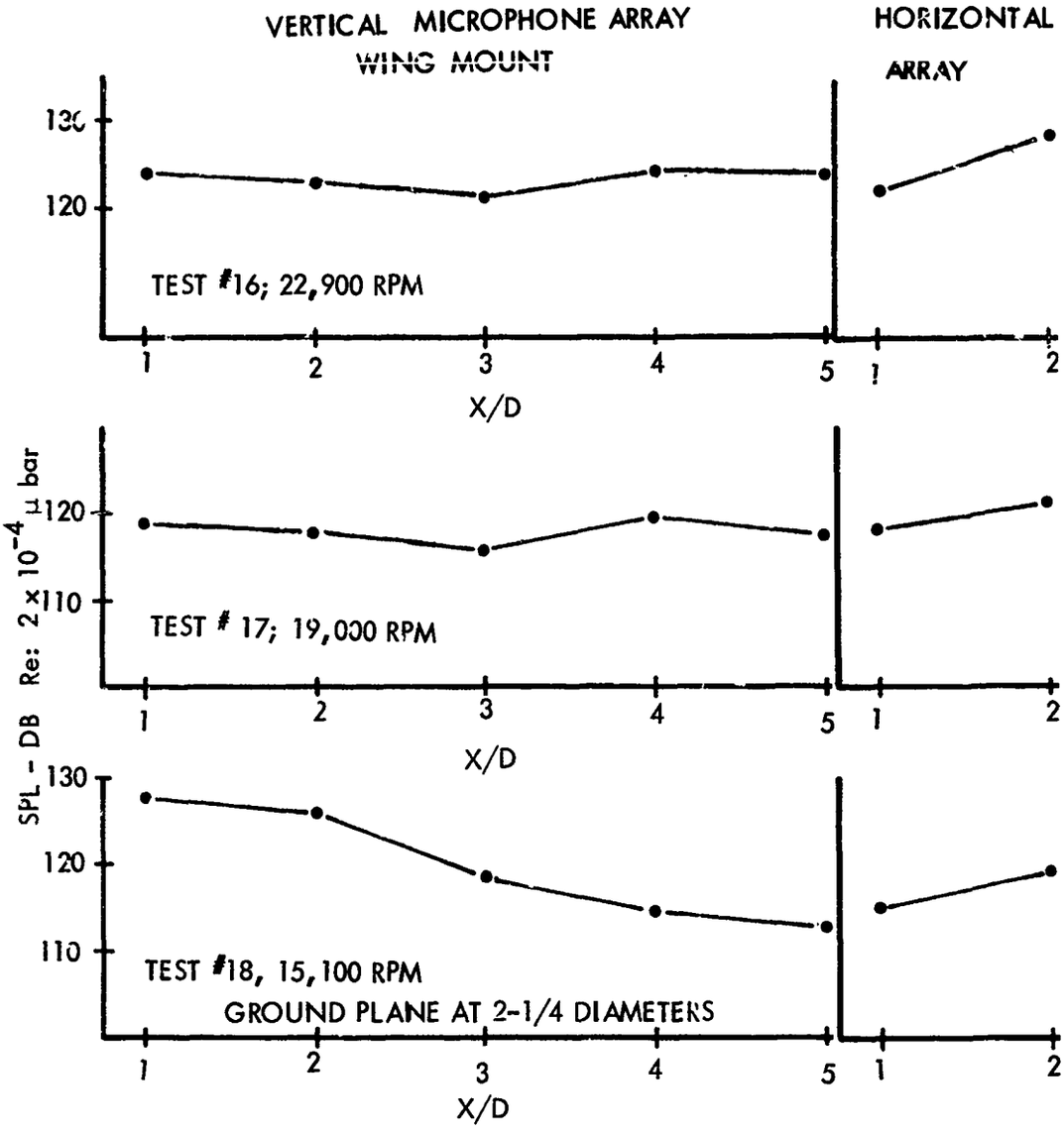

FIGURE 88. SPL VS. AXIAL DISTANCE FOR VARIOUS TURBINE RPM, WING MOUNT TEST

SECTION V

CONCLUSIONS

The following conclusions are drawn from this research investigation:

A. Sound pressure level contours have been measured and automatically plotted for a range of exhaust Mach numbers and exhaust plane temperatures, which encompasses the expected operational range of engines planned for use through 1977.

B. A prediction method and a digital computer program were derived which yield sound pressure level contours for the overall and 3 octave bands. The predicted contours compare quite well with model and full-scale data.

C. A relationship was derived which indicates a method of reducing jet engine SPL in the far field by increasing operating temperature and decreasing nozzle Mach number.

D. VTOL jets were tested to determine the effect of distance to the ground plane on near-field sound pressure level. It was found that, as the jet approaches the ground, the maximum SPL first increases and then is drastically reduced. The level never exceeds the maximum level of a free-field jet at the same operational conditions.

E. A typical ejector configuration was tested. If the pressure ratio and temperature are in the correct range, sound pressure level is not affected by installation of the ejector (this conclusion concerns a short ejector). In certain operational regimes, a flow resonance can occur, resulting in increased sound pressure level. A distinct tone is emitted.

F. It was shown that a reflecting ground plane has no effect on sound pressure levels in the jet near field opposite the ground plane.

G. A deflected jet shows two distinct source locations, but near-field noise levels are reduced when compared to a free-field jet.

H. Sound intensities measured forward of a VTOL fan are directly related to the proximity of a reflecting surface (such as the ground plane used in the shroud-mount fan test). Noise in this region consists of the various blade-passage frequencies and their harmonics.

I. Jet noise generated by the tip-turbine fan exhaust was detected only in the exhaust flow field and only for limited locations. About 3 to 6 diameters aft of the exit plane and just to the side of the flow, the jet noise was found at levels almost as high as the blade noise.

J. For the cruise-fan configuration, there was no significant increase or change in the acoustic field measured aft of the VTOL fan for varying ground-plane distance. For the wing-mounted fan there also was no noticeable change in the sound field for change in location of the ground plane. Apparently the sound field along the wing surface is subject to turbulence and eddys, especially near the fan itself, with a rather uniform average level along the wing.

APPENDIX I

MODEL ENGINE DESIGN CRITERIA

It was required that the model jet engine be able to simulate existing jet power plants as well as those being considered for the next decade. The parameters to be simulated across the exit nozzles were pressure ratios, temperatures, and Mach number (exit velocity). A parametric study revealed that pressure ratios of 3.67 across the exit nozzles would be required to yield the maximum Mach number requirements (Mach 1.50). In addition, gas temperatures in excess of 3000°F were needed, with 3500°F being a desirable level. Based on the above parameters and an assumed air supply of 5 pounds per second, the operating envelope shown in Figure I-1 was established. Note that this envelope is based on a given nozzle and will change slightly for other nozzle configurations.

A variable-area exit nozzle was considered but not adopted because of its complexity. Three different nozzles were designed which yielded a range of Mach numbers from subsonic to Mach 1.50.

DESCRIPTION OF MODEL JET ENGINE DESIGN

1. Air Inlet

The design considerations for this section (see Figure I-2) involved such factors as flow separation, turbulence level, and associated pressure losses. Judgment was required to fix the maximum allowable inlet air velocity consistent with the requirements. A maximum Mach number of M = 0.20 at the gas generator inlet was chosen. This resulted in an inlet diameter of 4.0 inches. The length of the inlet was also set at 4.0 inches, which allowed enough space for the installation of instrument probes (temperature and pressure).

> Note: If, due to unusual piping (such as flexible hose), highly turbulent flows are introduced to the gas generator, it is recommended that the length of the inlet section be increased to about 10 inches, allowing for the installation of flow straighteners and turbulence-reducing screens.

Stainless steel (316, 321, or 341) was selected for the inlet duct to accommodate the 1000°F hot-air inlet temperature and to provide protection against oxidation.

2. Diffuser

To keep the system compact, a diffuser was used with an included diffusion angle of 20 degrees. A conical centerbody with four fins was then incorporated inside the diffuser to prevent flow separation and to further reduce turbulence. The centerbody also serves as the fuel manifold. The material of the diffuser and the centerbody is the same as that for the inlet.

3. Fuel System

The fuel system uses JP-4 fuel and consists of a reservoir, filter, pump, throttle, fuel manifold, and fuel nozzle (Figure I-3).

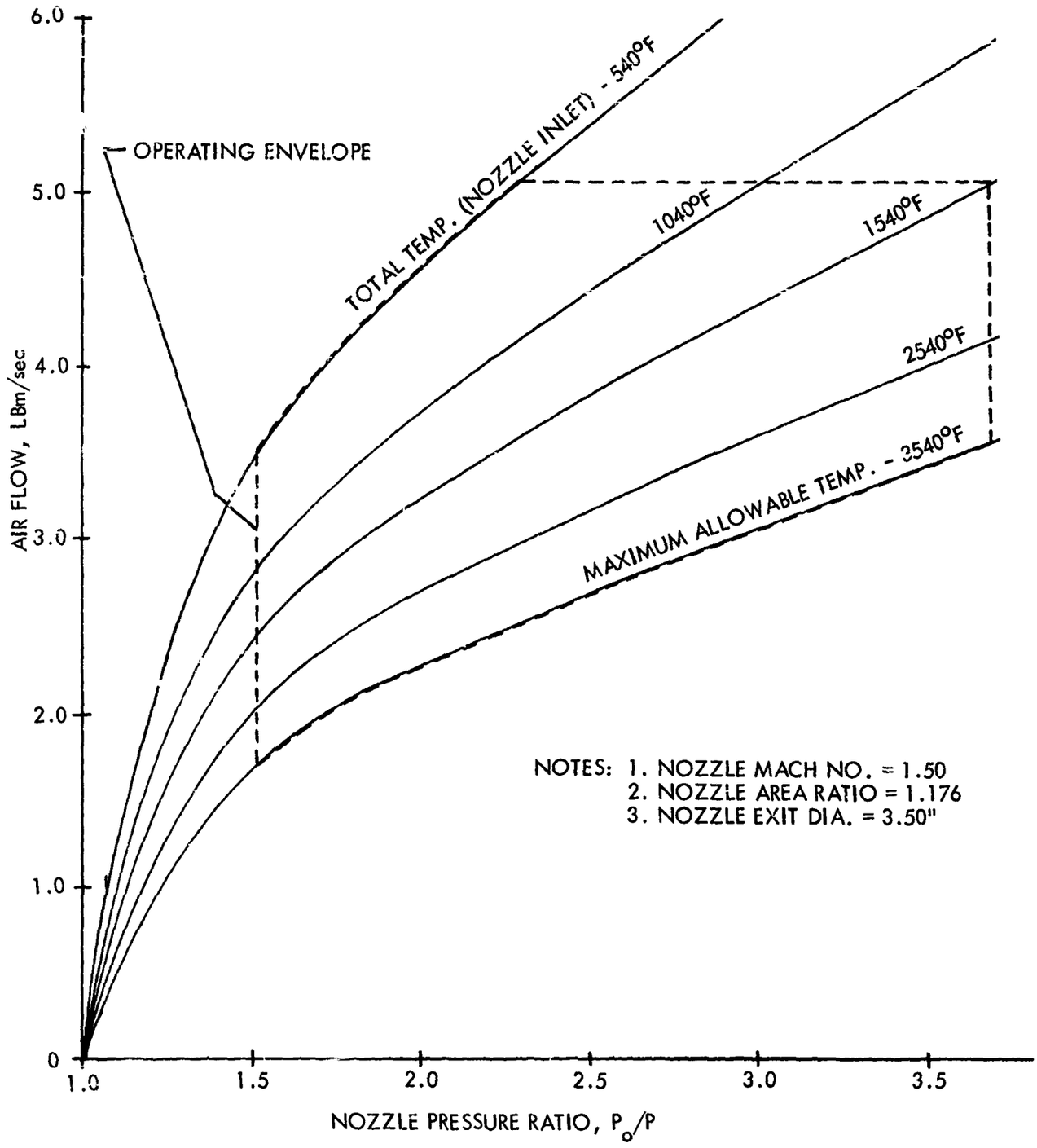

FIGURE I-1. OPERATING ENVELOPE FOR MODEL JET ENGINE

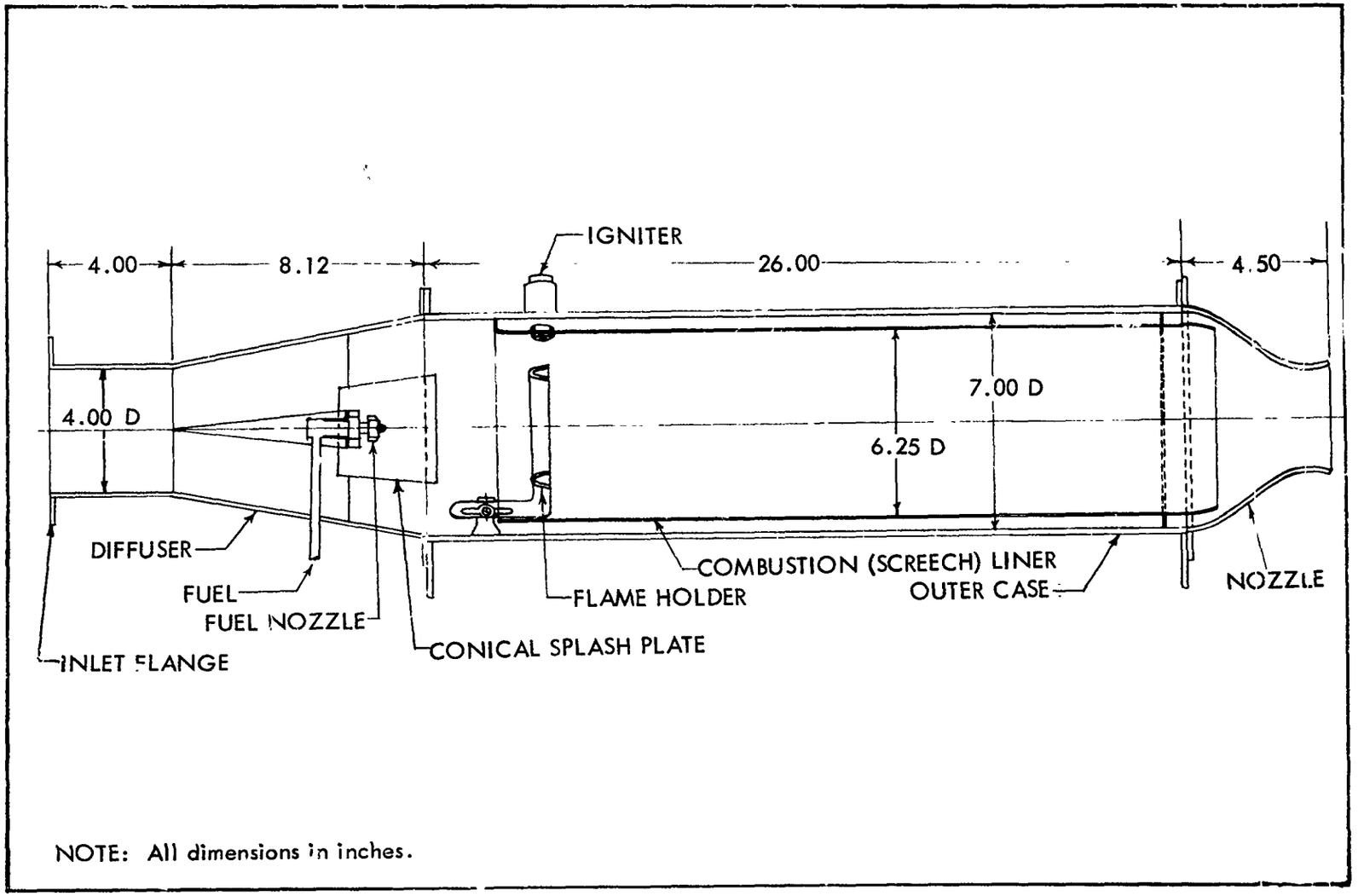

FIGURE I-2. MODEL ENGINE INTERNAL ARRANGEMENT

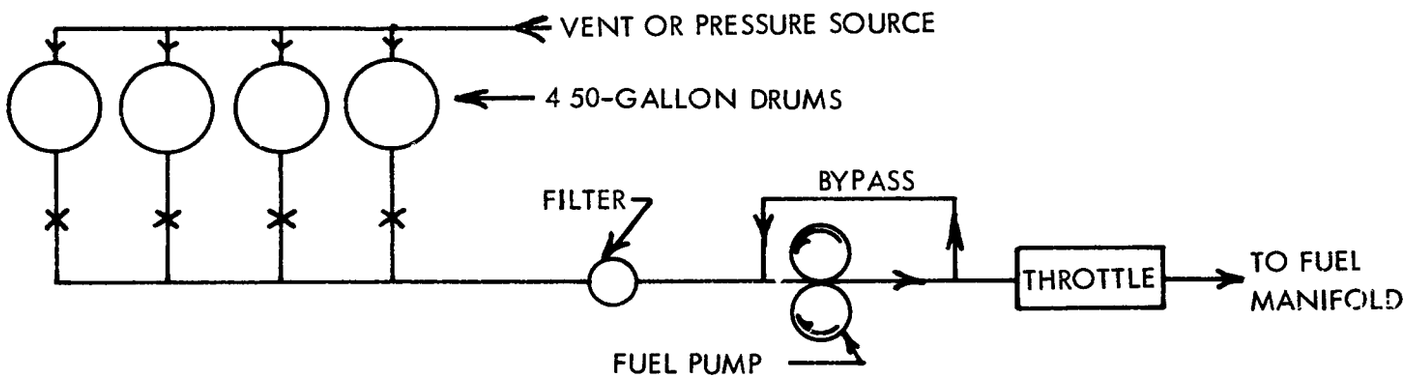

FIGURE I-3. MODEL JET ENGINE FUEL SYSTEM

a. Reservoir - To keep refueling operations to a minimum, a 200-gallon system was chosen. This consists of four 50-gallon drums interconnected with a common manifold. For safety reasons the fuel tanks are located at least 50 feet from the gas generator. The system provided for approximately 2 hours of uninterrupted running at maximum fuel flow conditions.

b. Fuel Filter - The filter was required for the protection of the fuel pump and also the fuel nozzle. A filter element of at least 20 microns was required with 10 microns being a desirable size. Caution must be exercised with a 10-micron filter, because high pressure losses may cause fuel pump cavitation problems. The filter requirements are 100 pounds per hour fuel flow at a maximum pressure drop of 10 psi.

c. Fuel Pump - A capability was required to pump JP-4 to 200 psig at a rate of 600 PPH. A jet engine fuel pump (Pratt & Whiteney JT-12) was adopted and was driven by a hydraulic power cart.

d. Throttle - A simple needle valve was used to control fuel flow. However, it is recommended that for future operation a more sophisticated system be adopted due to the unusual starting requirements of the gas generator (starts fuel rich, and after ignition, a rapid reduction in fuel flow is required to reduce thermal shock). It is suggested that an aircraft engine throttle system be adopted with preset starting and idle detent positions.

e. Fuel Manifold - The conical centerbody of the diffuser serves as the fuel manifold (see Figure I-2 and Figures I-6 to I-9).

f. Fuel Nozzle - It was desirable to use relatively low fuel pressures so that the fuel system and its components would not become complex. The resulting fuel nozzle flow-pressure relationship is shown in Figure I-4. The nozzle is comprised of six orifices, 0.030" diameter, discharging radially outward (perpendicular to the engine axis) into the air stream. Due to the low pressure drop across the orifices, a conical splash plate was installed over the nozzle to help atomize the fuel.

4. Flame Holder

The geometry of the flame holder determines to a large extent the flameout limits of the gas generator, the temperature profile of the hot gases, and pressure losses. The flame holder shown in Figure I-6 was designed for minimum downstream disturbance. This allowed a large portion of the combustion process to take place at the center of the gas generator, yielding a hot core and a relatively cool outer surface which simulates conditions consistent with turbofan configurations. Another flame holder, not shown on the drawings, was later designed to simulate afterburning turbojet systems. This flame holder was similar in geometry to the first one but larger in size. The flame holders were designed such that they could be moved upstream or downstream to locate their optimum position.

5. Ignition System

The ignition system was composed of standard aircraft jet engine components and included a 28-volt DC source, an exciter box (transformer), and a spark plug.

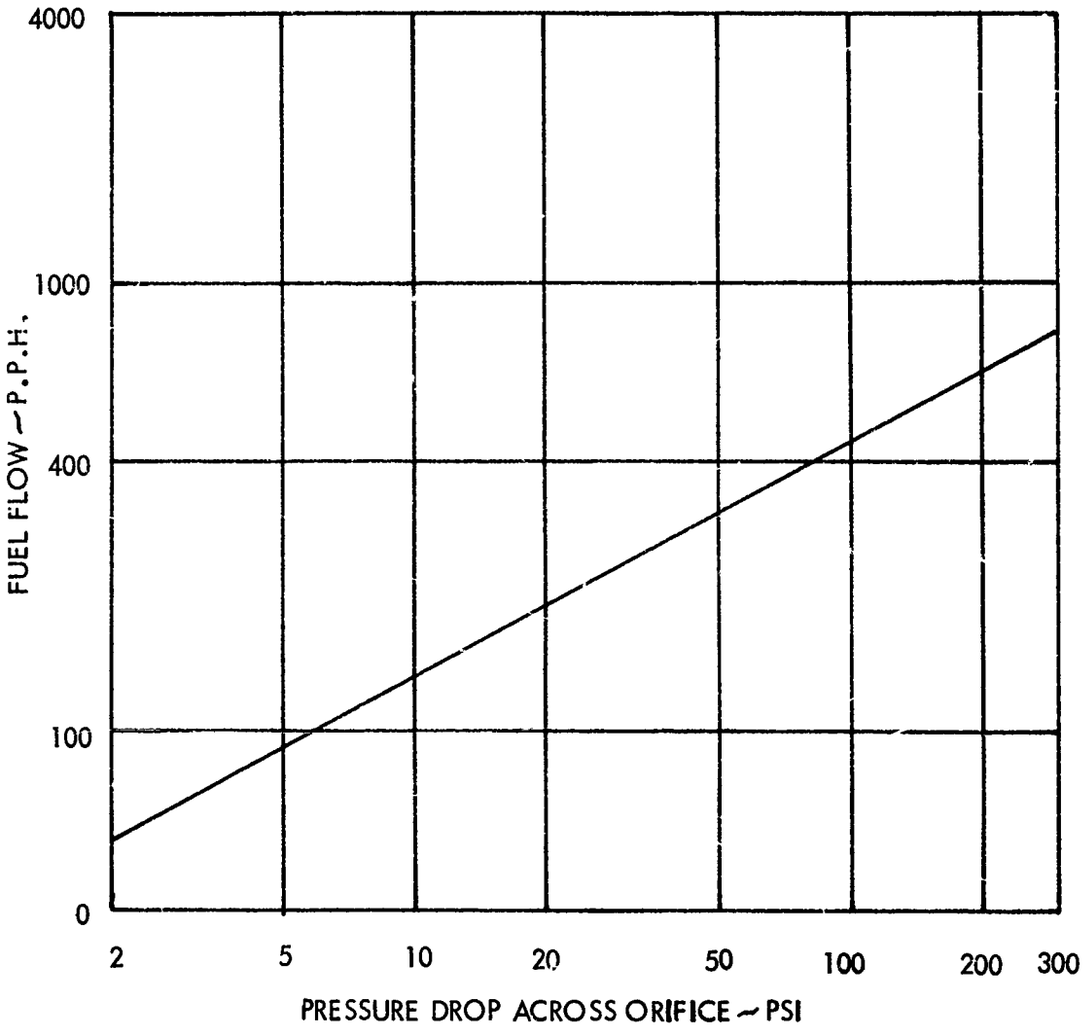

FIGURE I-4. FUEL NOZZLE THEORETICAL FLOW-PRESSURE CURVE

a. Electrical Source - A power cart was used. It contained an electric-motor-driven DC generator which delivered 28 volts DC. An alternate power supply using nickel-cadmium batteries rated at 28 volts DC could also be used.

b. Exciter (transformer) - This was a Pratt & Whitney JT 12 jet engine part.

c. Igniter Plug - A standard JT-12 combustor spark plug was used.

6. Duct (Outer Engine Case)

The duct diameter of 7.00 inches was dictated by the need to keep velocities inside the combustion chamber between Mach 0.125 and 0.150 so that reasonable combustion efficiencies, blowout limits, and pressure drops could be expected. A duct length of 26.00 inches was chosen. This was slightly shorter than that consistent with optimum combustion efficiency (about 35.00 inches is desirable), but the overriding factor was to keep the system compact. The design criteria for the type of material and wall thickness were 500°F, 60 psig, and a safety factor of four.

7. Combustion (Screech) Liner

The governing design criteria of the screech liner were combustion screech attenuation and heat-transfer considerations. Previous experience dictated that 18 percent open area through the combustion (screech) liner would be required to preclude combustion screech. In addition, the annular gap between the combustion liner and the outer duct is critical in that it acts as an attenuation chamber as well as a cooling air passage. Here again, previous experience dictated a gap dimension of 5/8 inch.

Transpiration cooling techniques were applied to the combustion liner, using 1/8-inch holes in a staggered geometric shape as shown in Figure I-8. Heat transfer calculations indicated the liner would be subjected to a temperature as high as 1800°F. Hestalloy material was first sought for this part, but as it was not available, Inconel was substituted.

8 Exhaust Nozzles

The design criteria for the nozzles were established after a survey indicated the pressure ratios and temperatures to be expected from powerplants of the next decade. The maximum required pressure ratio of 3.67 was established by setting the required nozzle exit Mach number to 1.50. This Mach number was anticipated to be the top limit expected from propulsion systems that would evolve within the next decade

A variable-area nozzle, considered briefly, was found to be too complex and expensive. It was decided to pick three pressure ratios and design a nozzle corresponding to each pressure. Each nozzle would then be tested at constant pressure ratio with a temperature variation. A single nozzle was designed to cover the subsonic speed range, including Mach 1.00. The other two nozzles were designed for Mach 1.25 and Mach 1.50, respectively.

It was desirable that all nozzles have the same exit diameter to facilitate the correlation of acoustic data. This necessitated that the throat area be varied for each nozzle to obtain the desired area ratio.

Isentropic flow conditions were assumed in the design of the nozzles, although it was acknowledged that this would result in a slight overexpansion. However, this was desirable, since an ejector was to be incorporated behind the nozzles for some of the test conditions.

The design philosophy for the contour of the nozzles was that of simulating, as closely as possible, the actual jet engine exit. For instance, to achieve nearly perfect expansion and optimum efficiency, the resulting nozzle would have been longer and heavier. The longer nozzles would have generated a cooling problem in that the film-cooling techniques used on nozzles are highly susceptible to length. In addition, "exotic" materials had to be employed for the nozzle due to the high-temperature requirements. This would have added to the fabrication problems of the part. Therefore, a compromise was accepted on the performance of the nozzle in order to partially satisfy the other conditions.

The following simple cosine function was chosen for the nozzle contour:

$$y = A + B \cos x \ .$$

Due to the requirement that the exit diameter was to remain constant for all three nozzles, constants A and B differ for each nozzle. (The nozzle shape is shown in Figure I-5 and I-9.)

Considering the area ratio requirement for each nozzle, the resulting contour equations were established as follows:

a) Mach = 1.50, $y = 2.557 + 0.944 \cos x$

b) Mach = 1.25, $y = 2.605 + 0.895 \cos x$

c) Mach = 1.00, $y = 2.625 + 0.875 \cos x$

The length of the nozzle was established by arbitrarily letting x = 4.00 inches when the argument of cos x is 180 degrees.

9. Ejectors

The ejector geometry is shown in Figure I-6. No attempt was made to control a specified thrust agumentation or other parameter. Its purpose was to assess the qualitative acoustical effects of a typical ejector. The geometry of the ejector was established by making arbitrary assumptions.

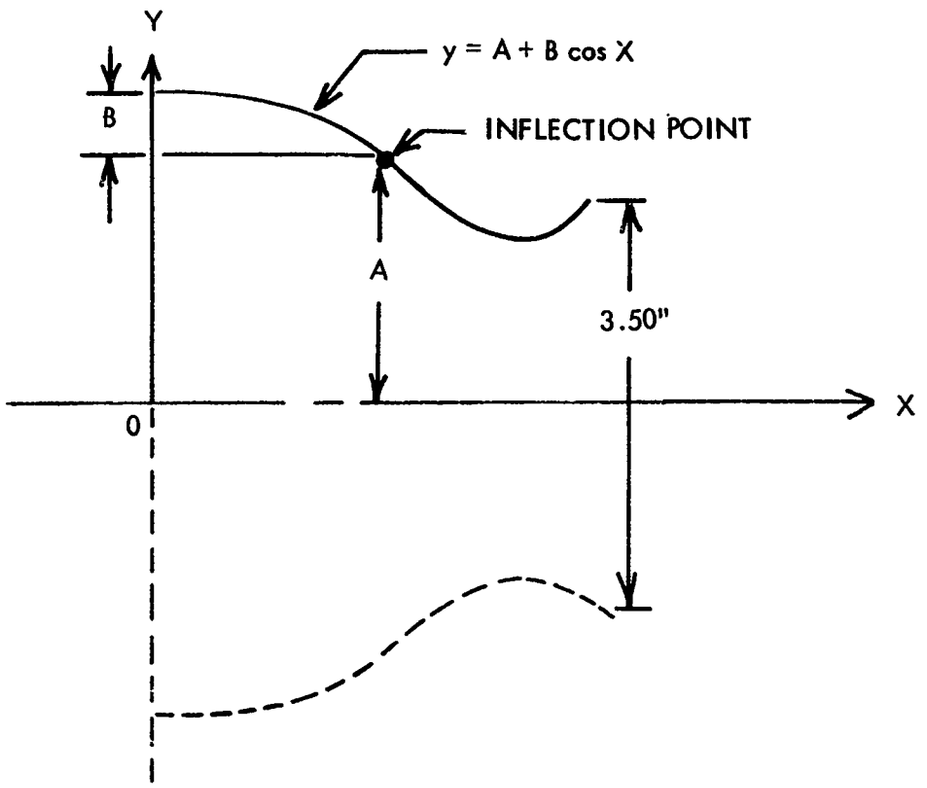

FIGURE I-5. NOZZLE SHAPE

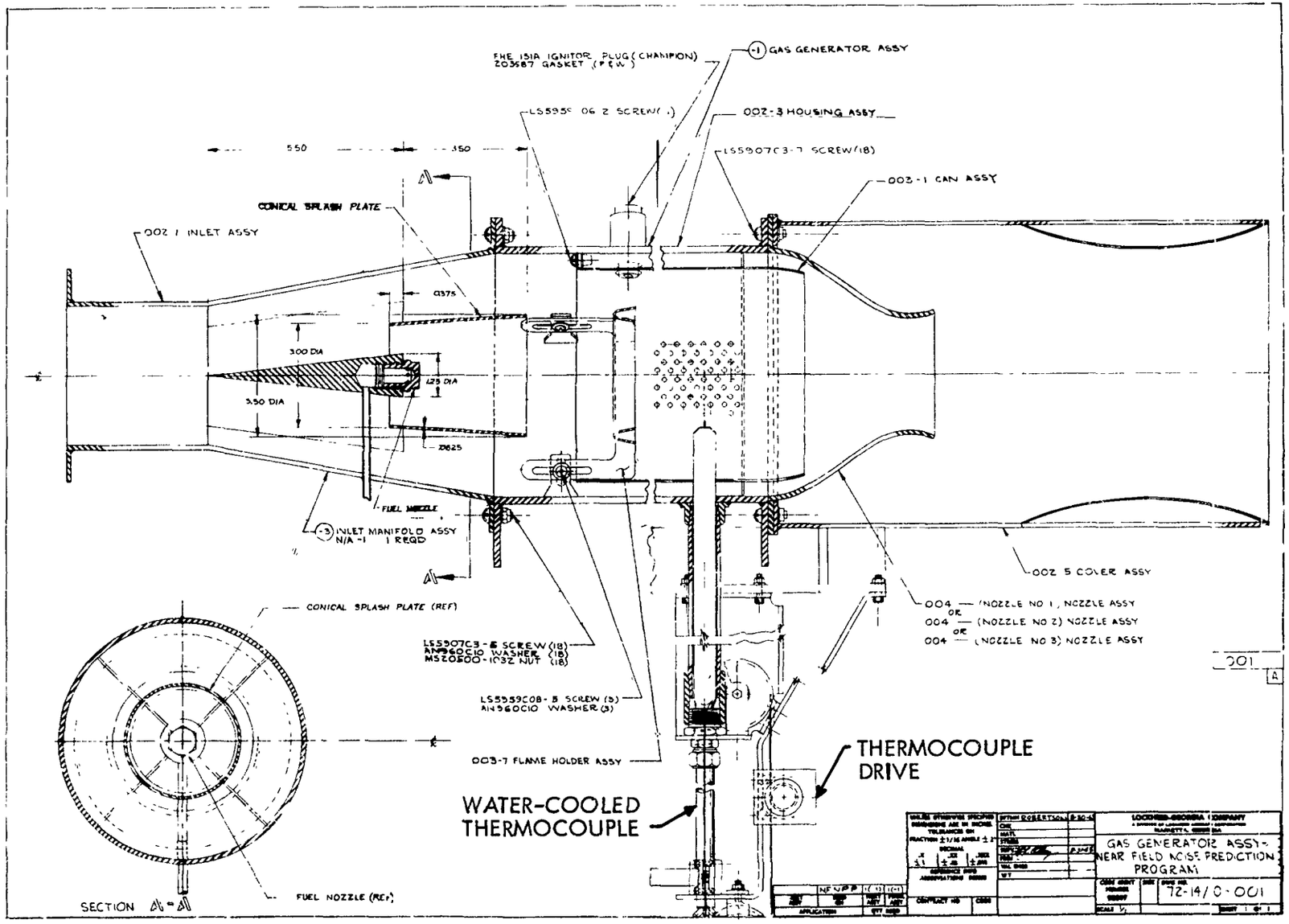

FIGURE 1-6. MODEL ENGINE ASSEMBLY

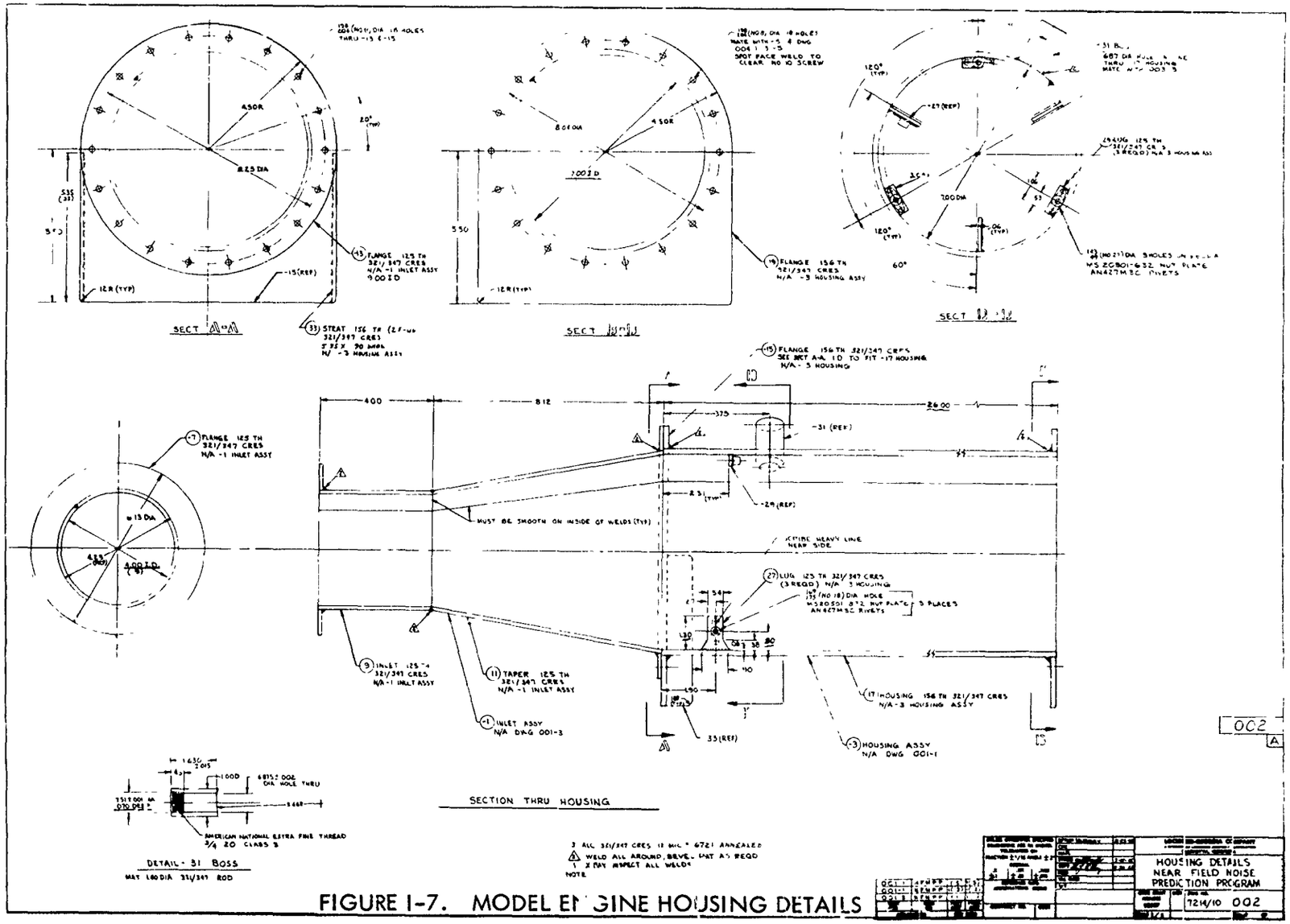

FIGURE I-7. MODEL ENGINE HOUSING DETAILS

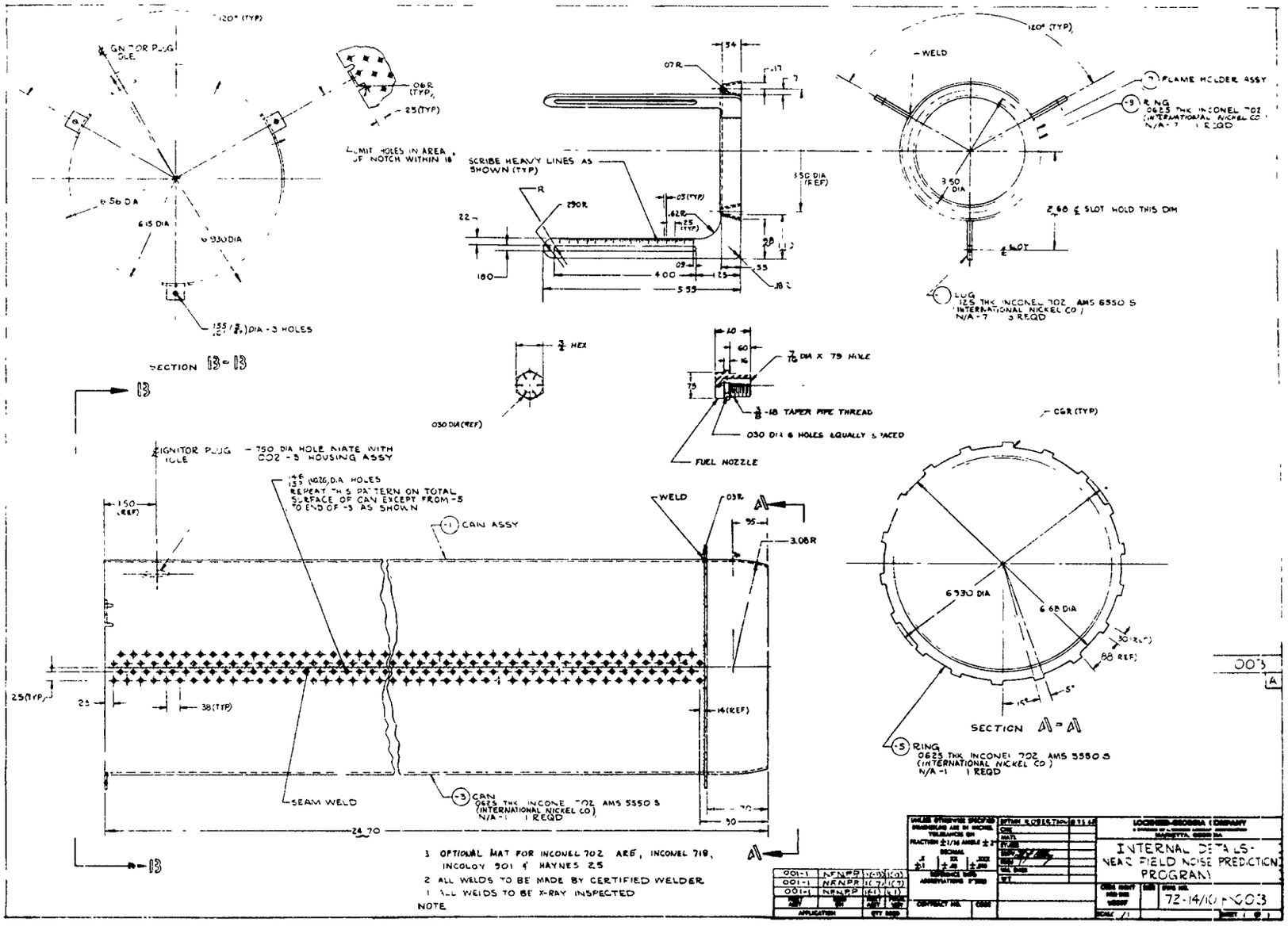

FIGURE 1-8. MODEL ENGINE INTERNAL DETAILS

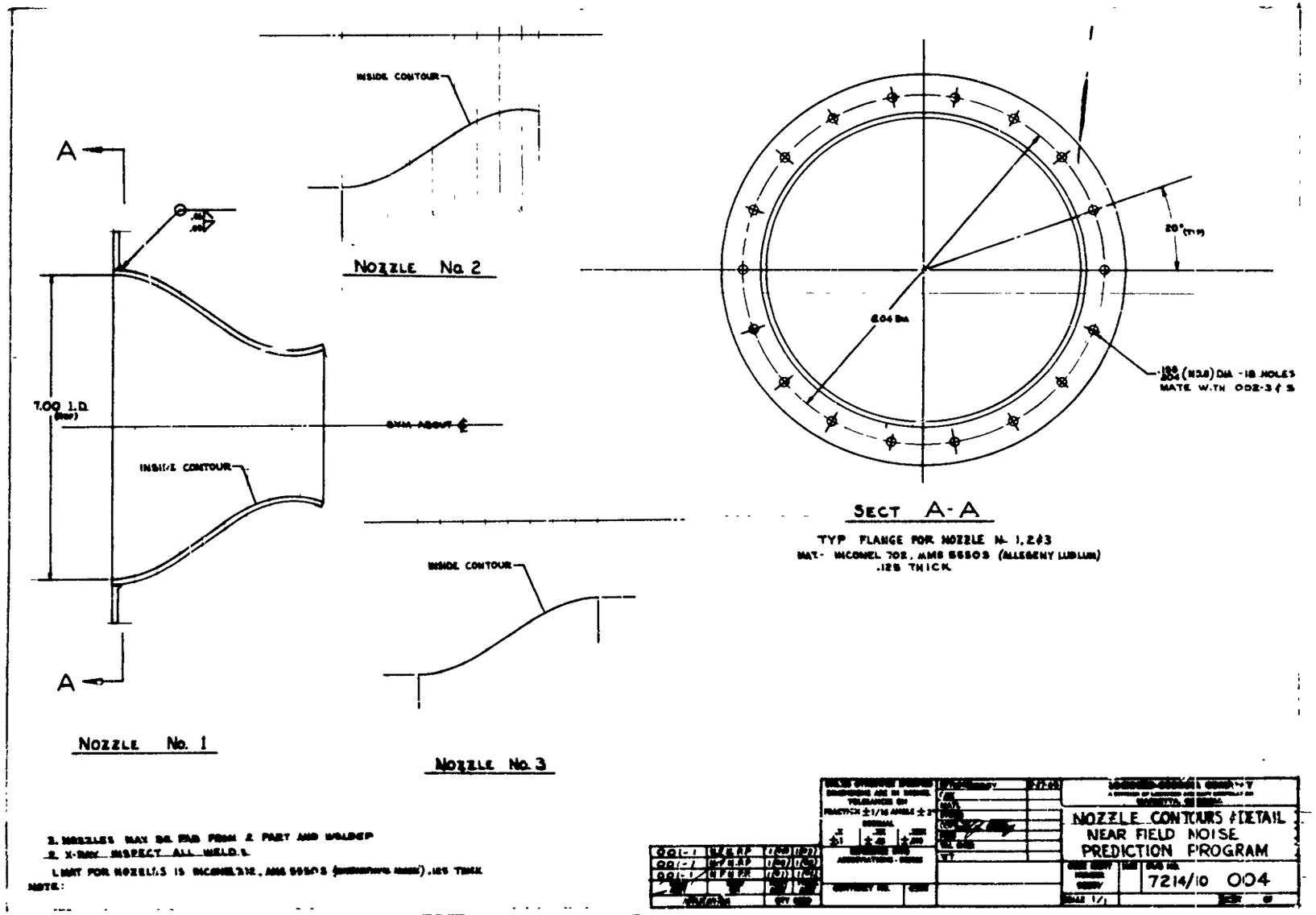

FIGURE 1-9. MODEL ENGINE NOZZLE CONTOURS

APPENDIX II

BASIC JET SPL CONTOURS

This appendix contains the contours for all the basic jet conditions listed in Table I. Some of these curves are used elsewhere in the report for comparison. All are reproduced here for ease of inspection.

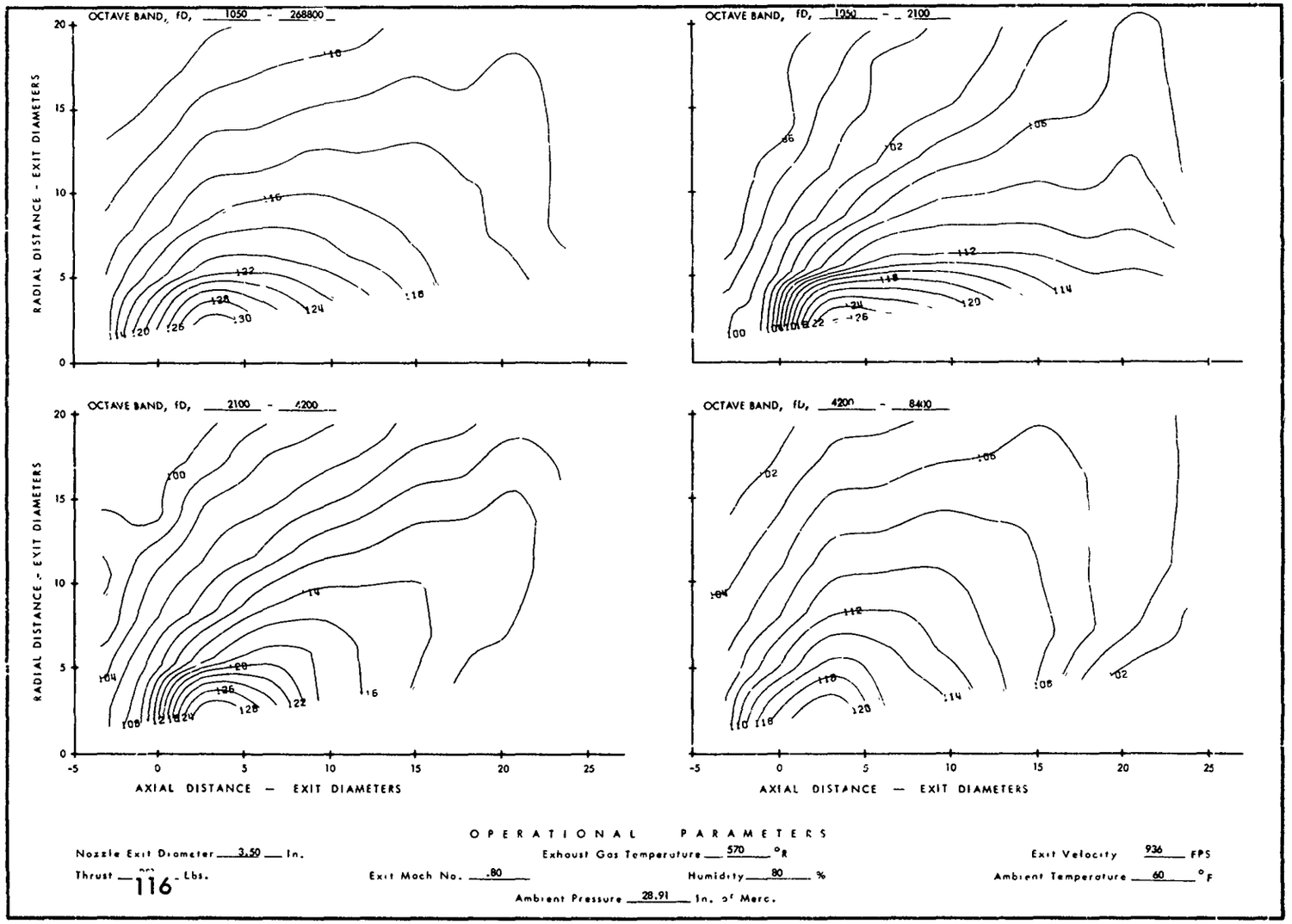

FIGURE II-1. BASIC JET SPL CONTOURS; MACH NO. = 0.80, TEMP. = 570°R

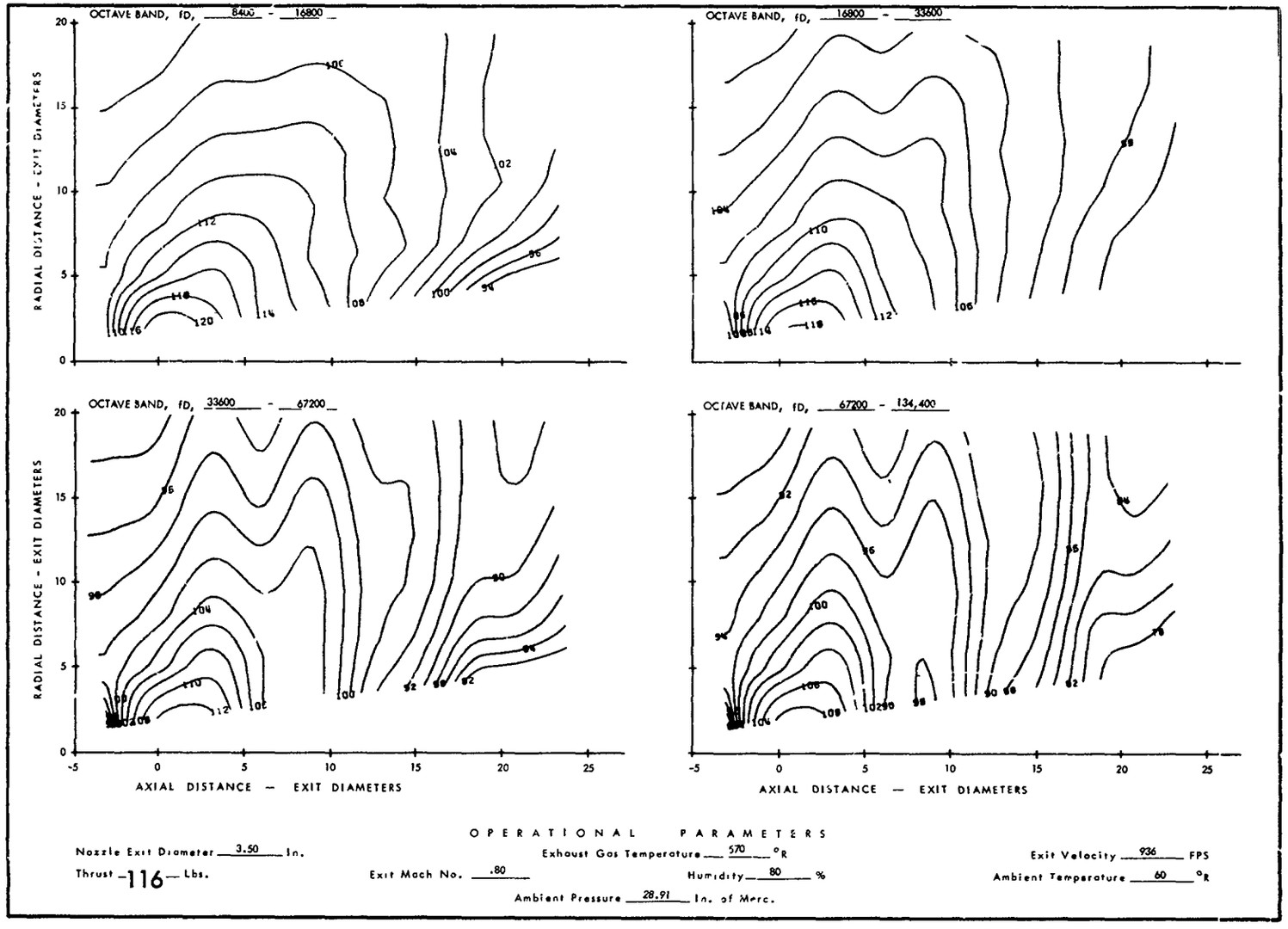

FIGURE II-1. BASIC JET SPL CONTOURS; MACH NO. = 0.80, TEMP. = 570°R (CONTINUED)

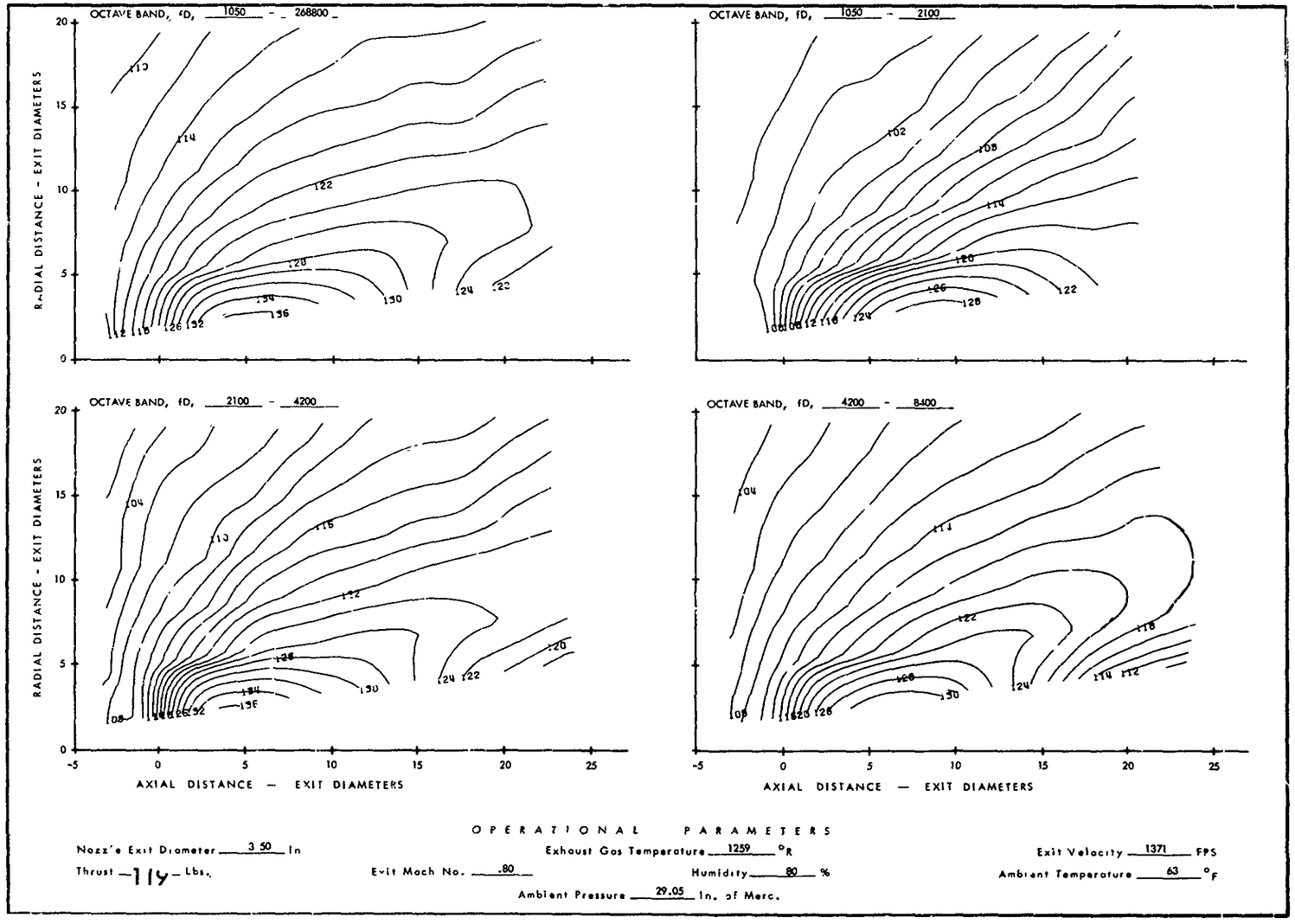

FIGURE II-2. BASIC JET SPL CONTOURS; MACH NO. = 0.80, TEMP. = 1260°R

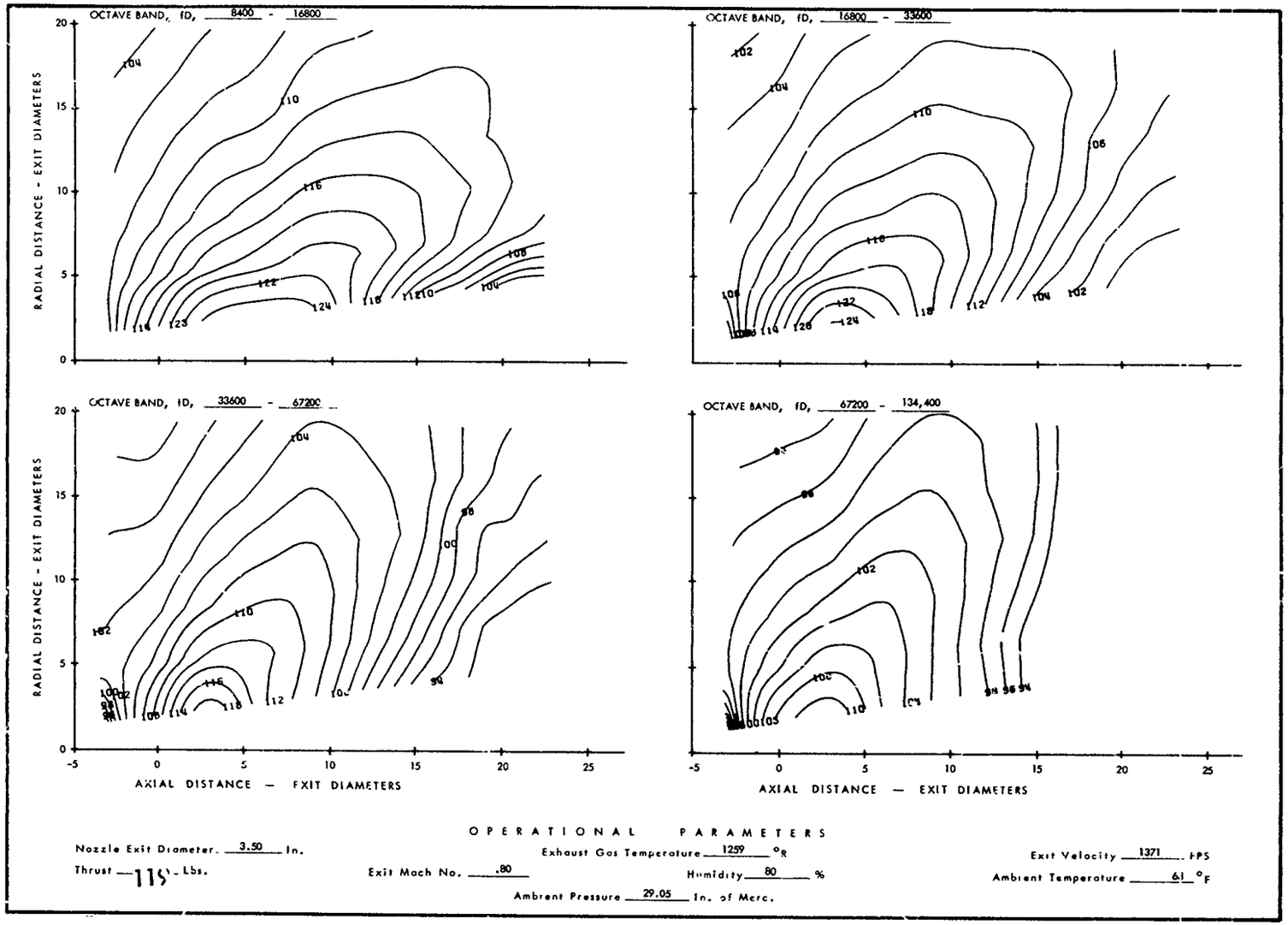

FIGURE II-2. BASIC JET SPL CONTOURS; MACH NO. = 0.80, TEMP. = 1260°R (CONTINUED)

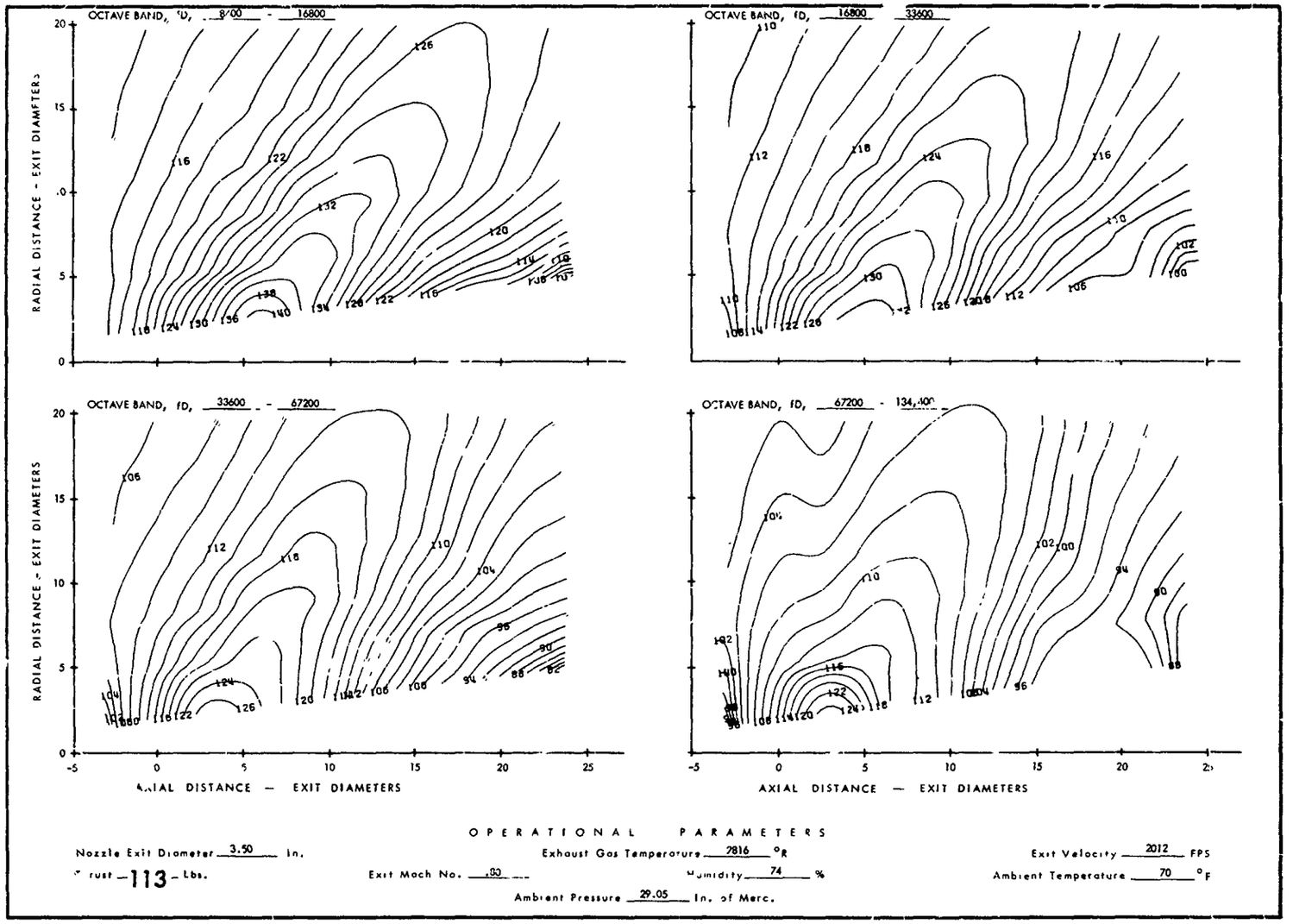

FIGURE II-3. BASIC JET SPL CONTOURS; MACH NO. = 0.80, TEMP. = 2817°R (CONTINUED)

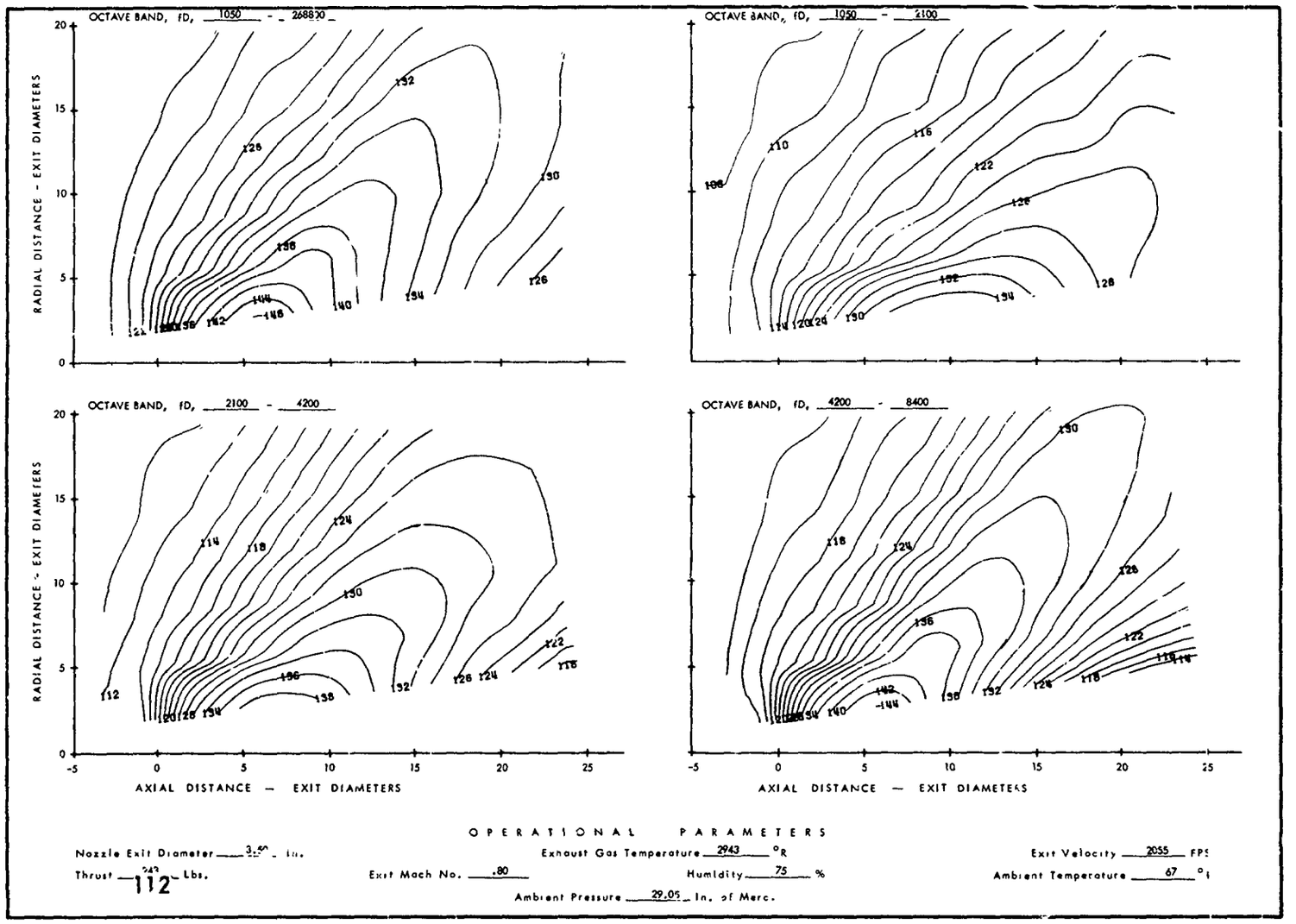

FIGURE II-4. BASIC JET SPL CONTOURS; MACH NO. = 0.80, TEMP. = 2943°R

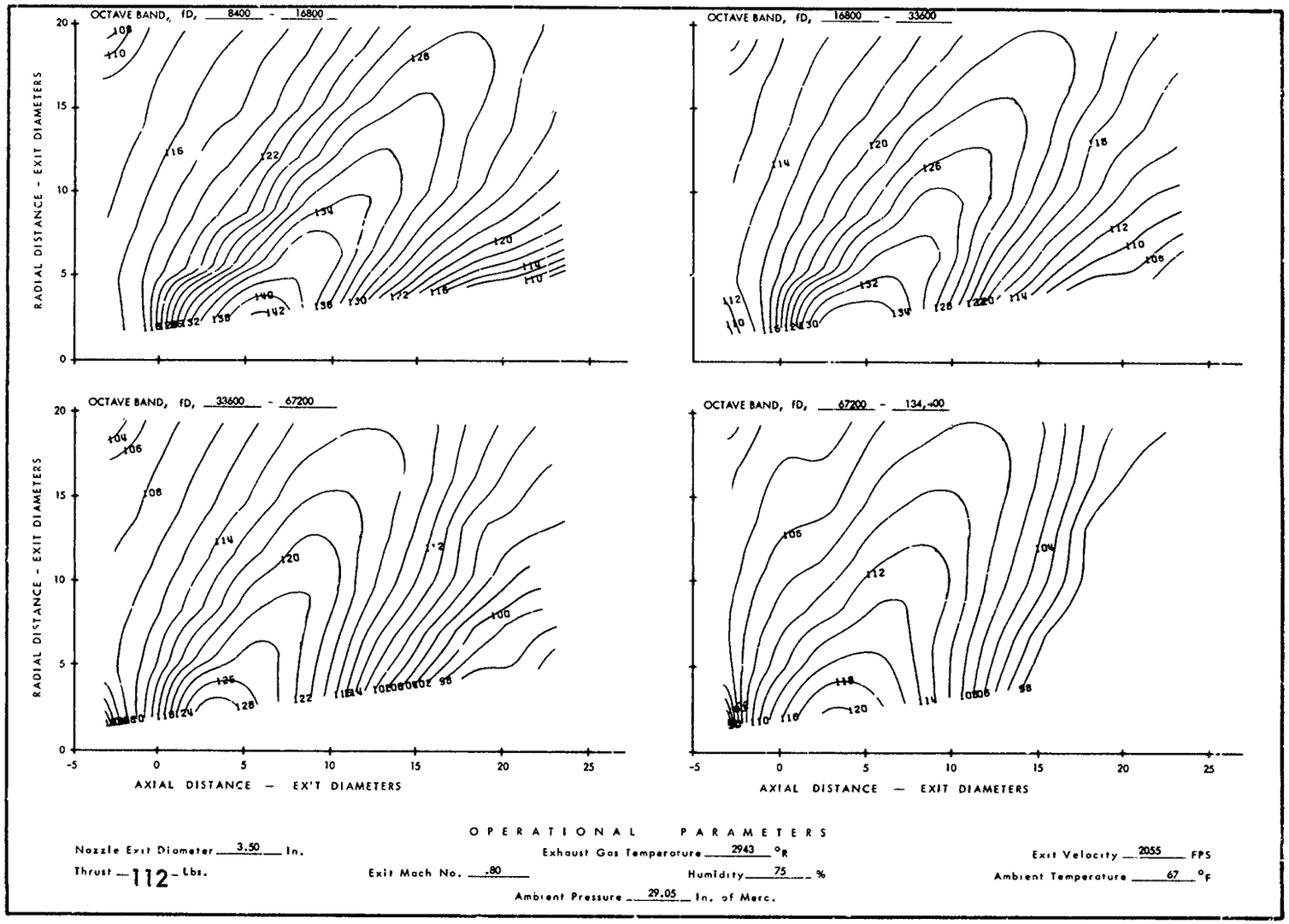

FIGURE II-4. BASIC JET SPL CONTOURS; MACH NO. = 0.80, TEMP = 2943°R (CONTINUED)

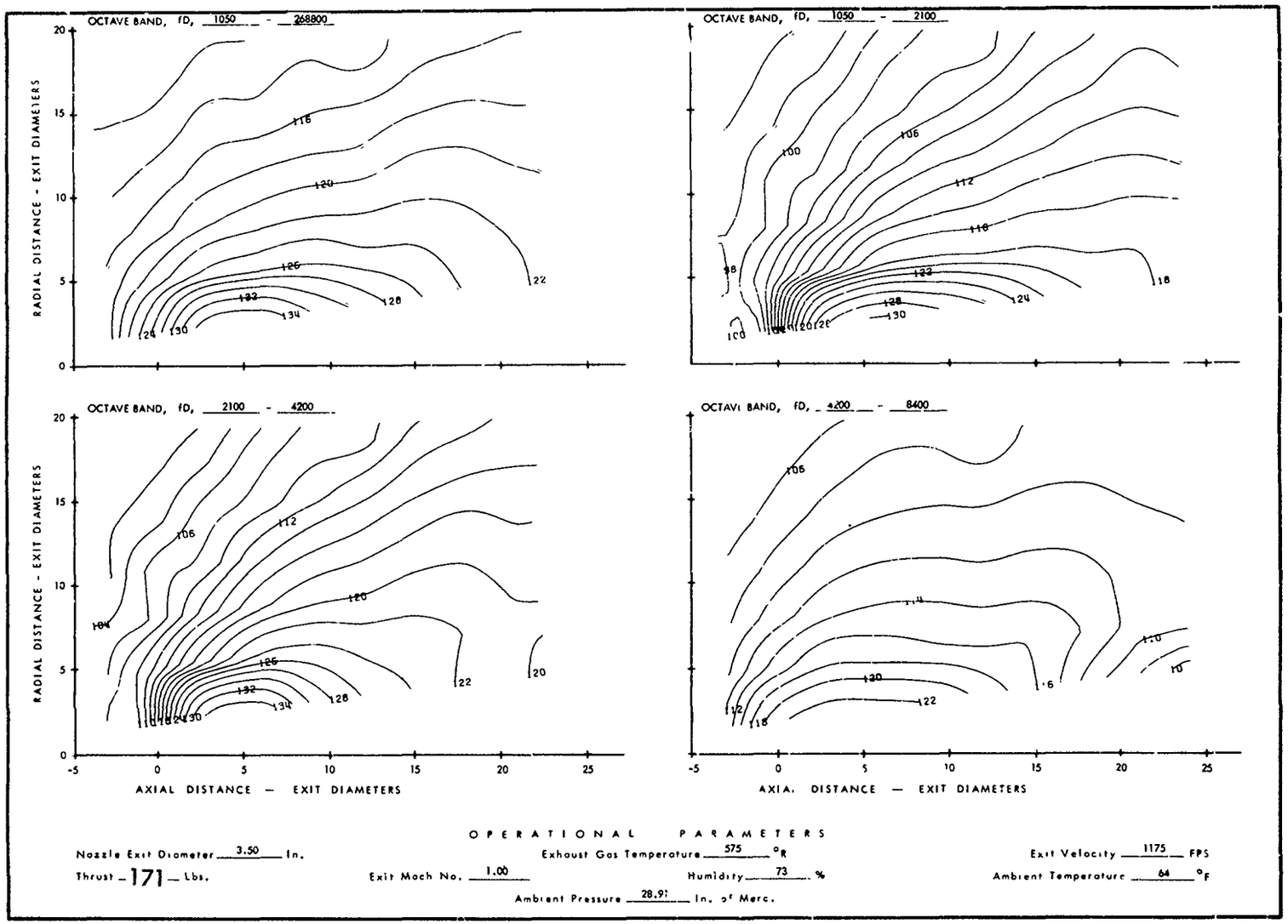

FIGURE II-5. BASIC JET SPL CONTOURS; MACH NO. = 1.00, TEMP. = 575°R

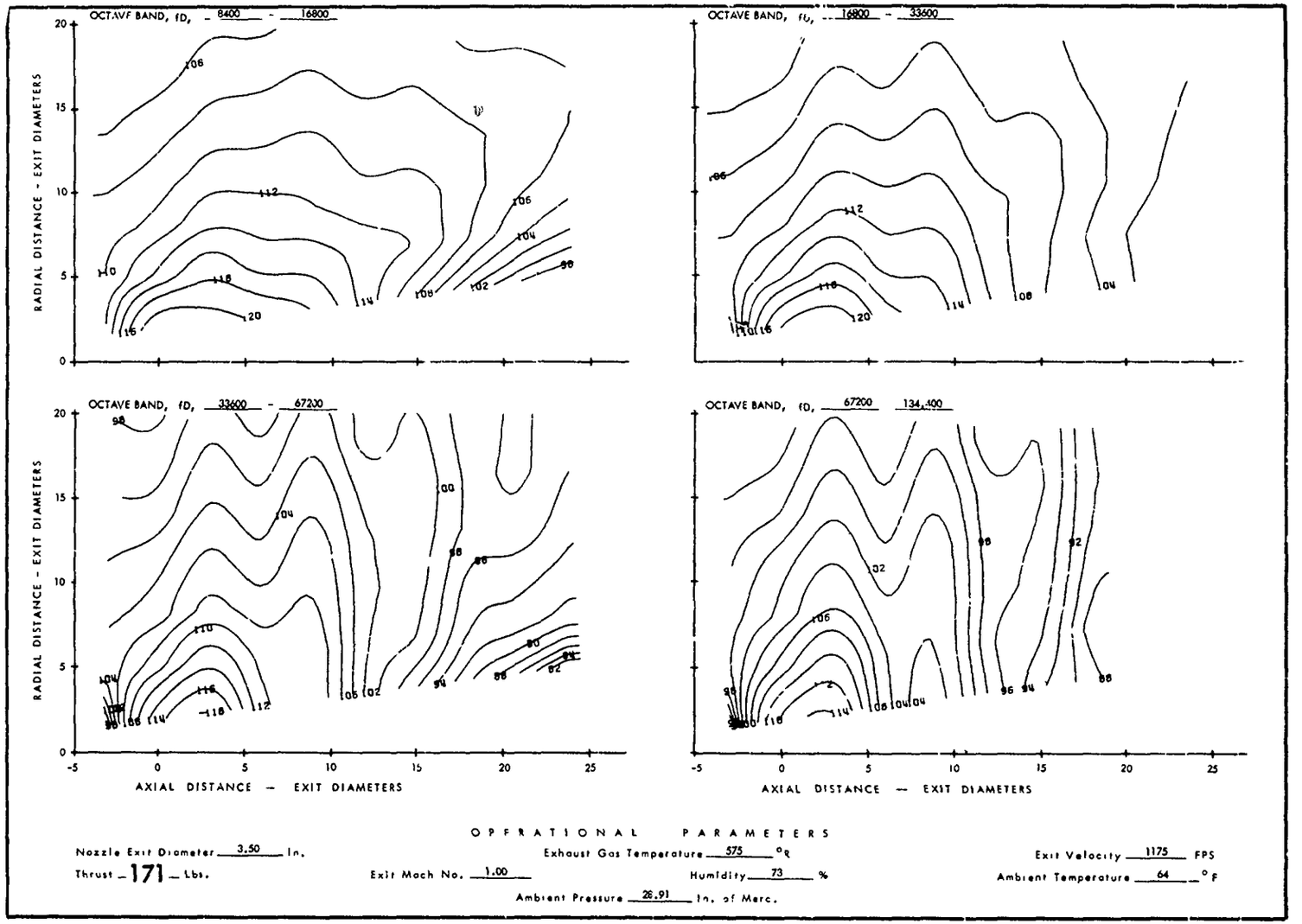

FIGURE II-5. BASIC JET SPL CONTOURS; MACH NO. = 1.00, TEMP. = 575°R (CONTINUED)

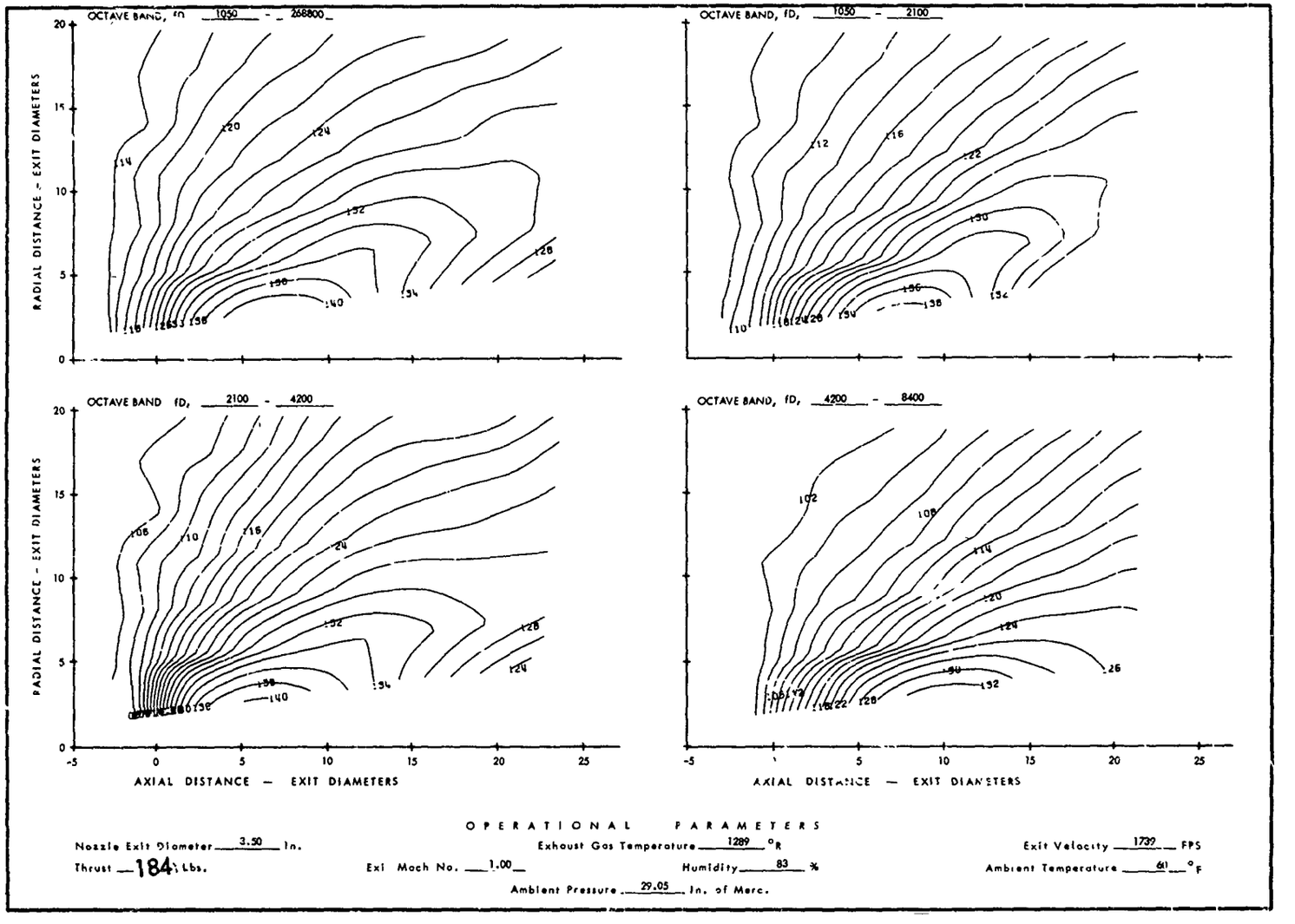

FIGURE 11-6. BASIC JET SPL CONTOURS; MACH NO. = 1.00, TEMP. = 1290°R

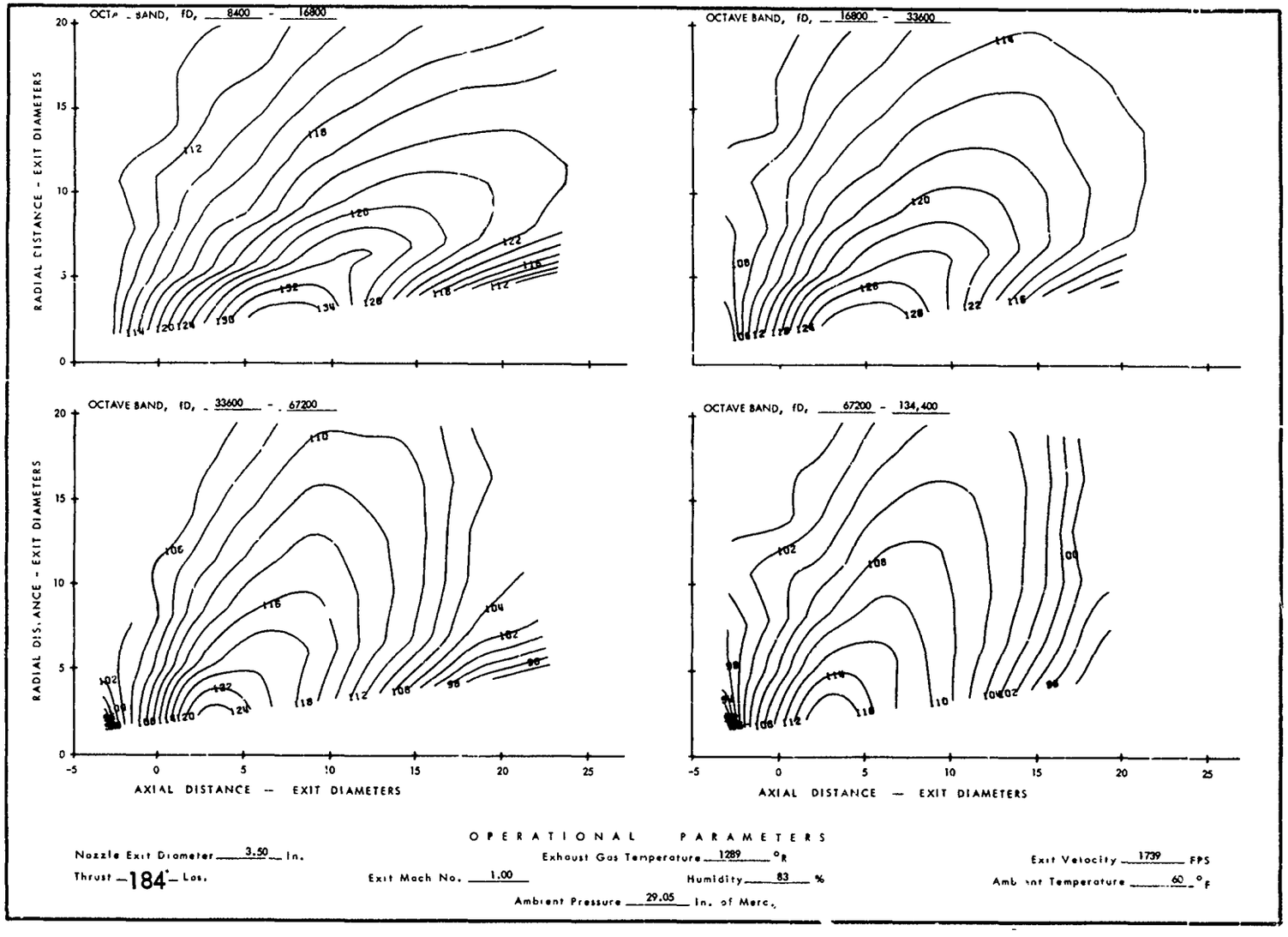

FIGURE II-6. BASIC JET SPL CONTOURS; MACH NO. = 1.00, TEMP. = 1290°R (CONTINUED)

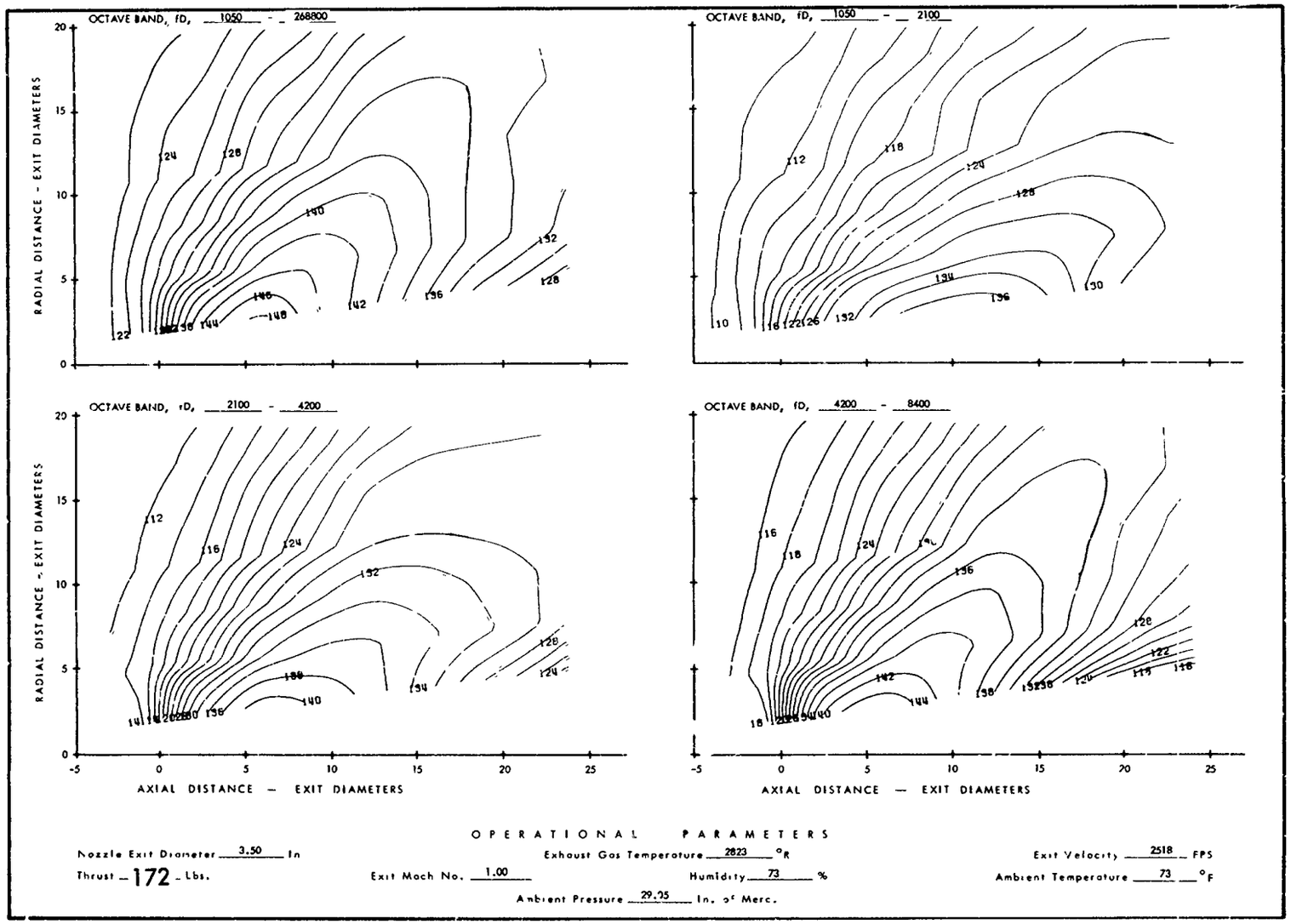

FIGURE II-7. BASIC JET SPL CONTOURS; MACH NO. = 1.00, TEMP. = 2823°R

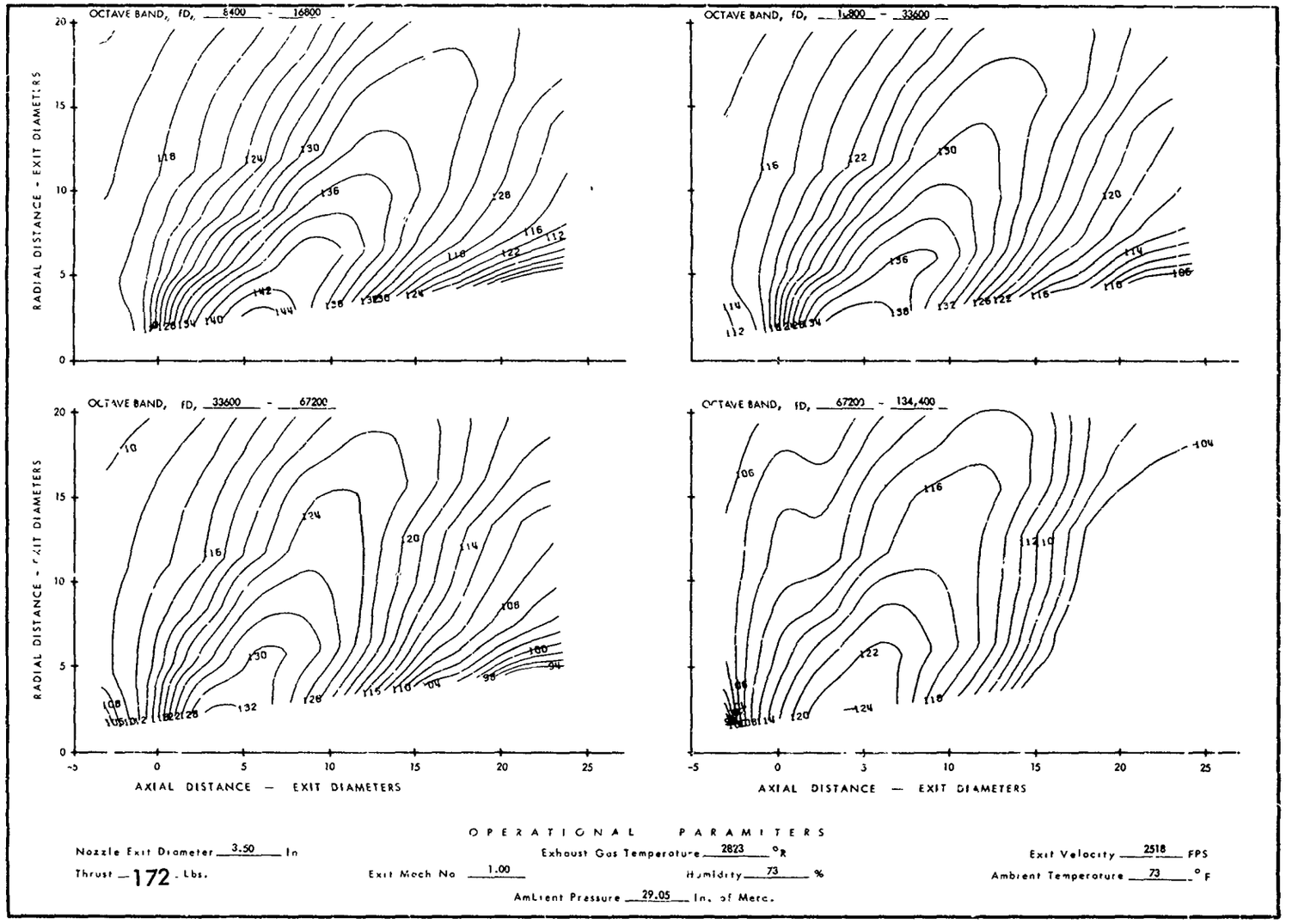

FIGURE II-7. BASIC JET SPL CONTOURS; MACH NO. = 1.00, TEMP. = 2823°R (CONTINUED)

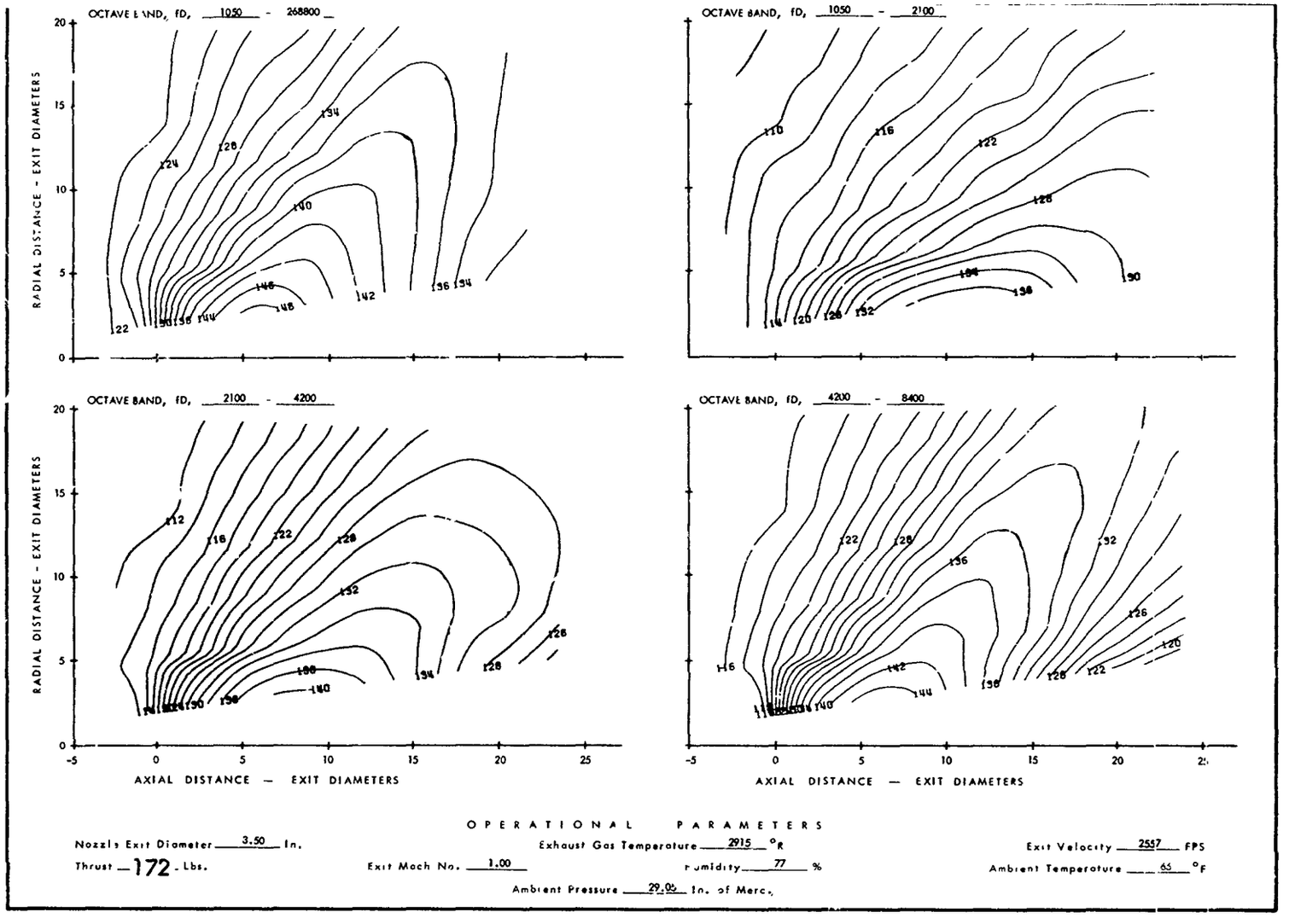

FIGURE II-8. BASIC JET SPL CONTOURS; MACH NO. = 1.00, TEMP. = 2915°R

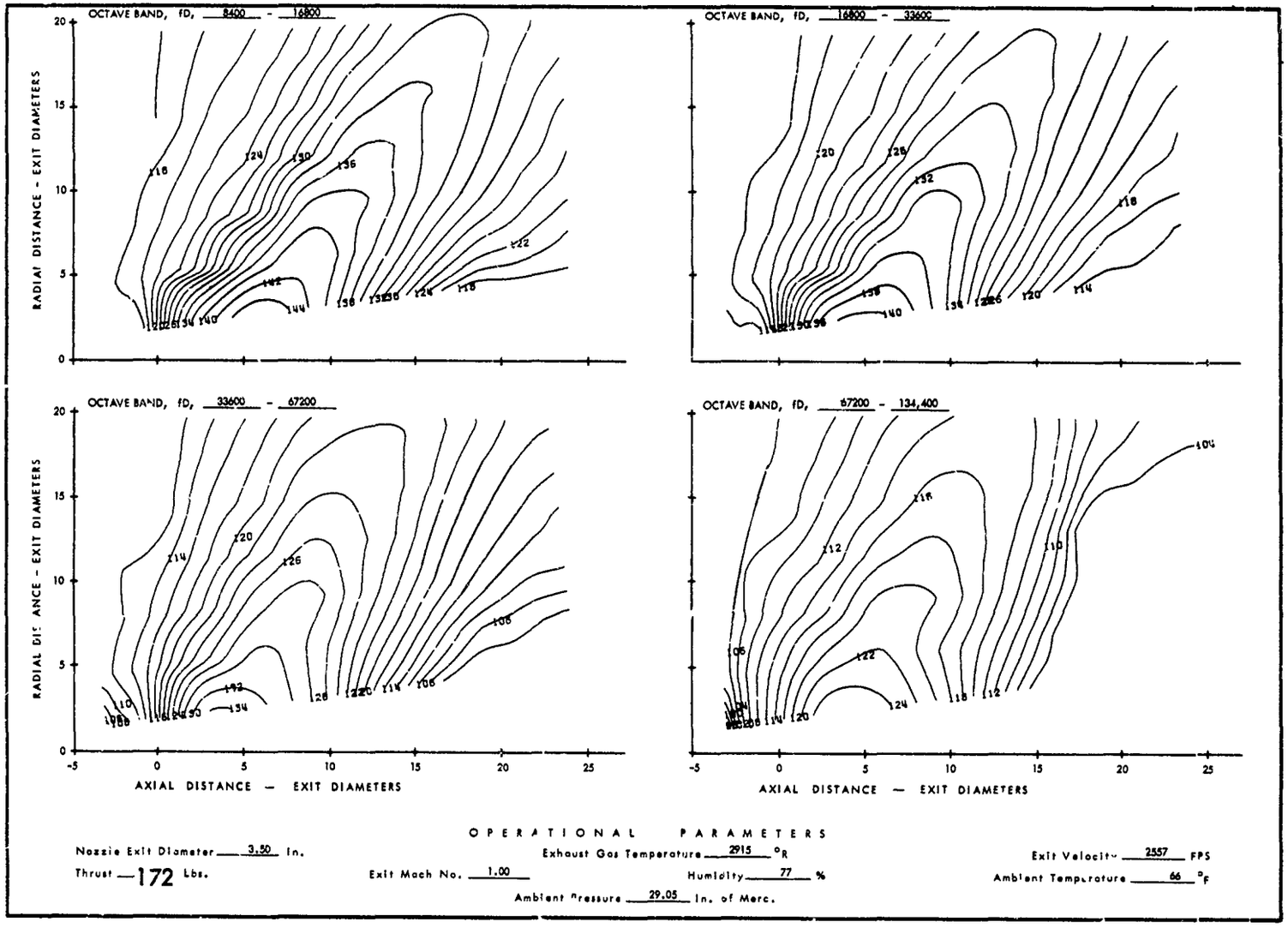

FIGURE II-8. BASIC JET SPL CONTOURS; MACH NO. = 1.00, TEMP. = 2915°R (CONTINUED)

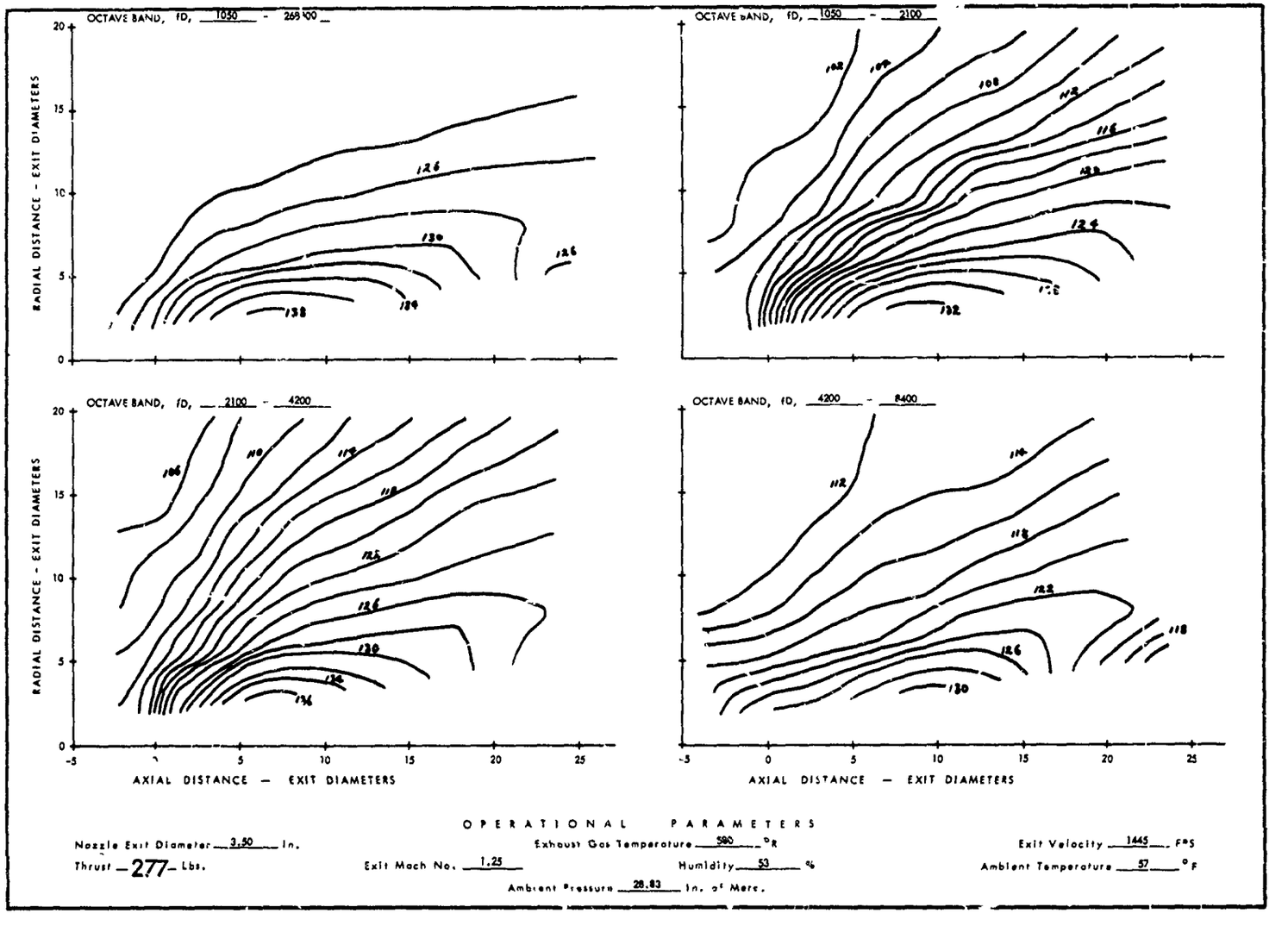

FIGURE II-9. BASIC JET SPL CONTOURS; MACH NO. = 1.25, TEMP. = 580°R

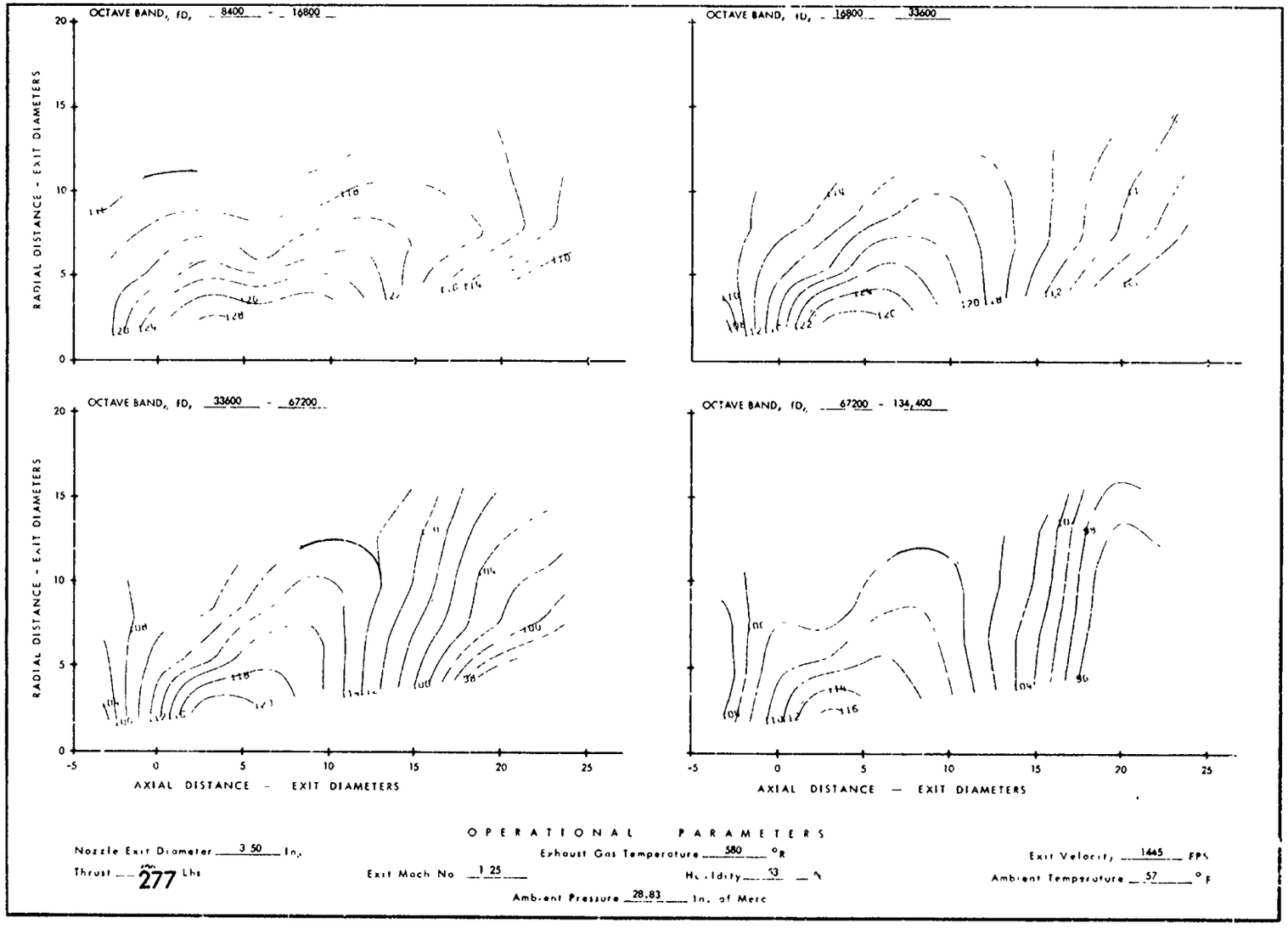

FIGURE II-9. BASIC JET SPL CONTOURS; MACH NO. = 1.25, TEMP. = 580°R (CONTINUED)

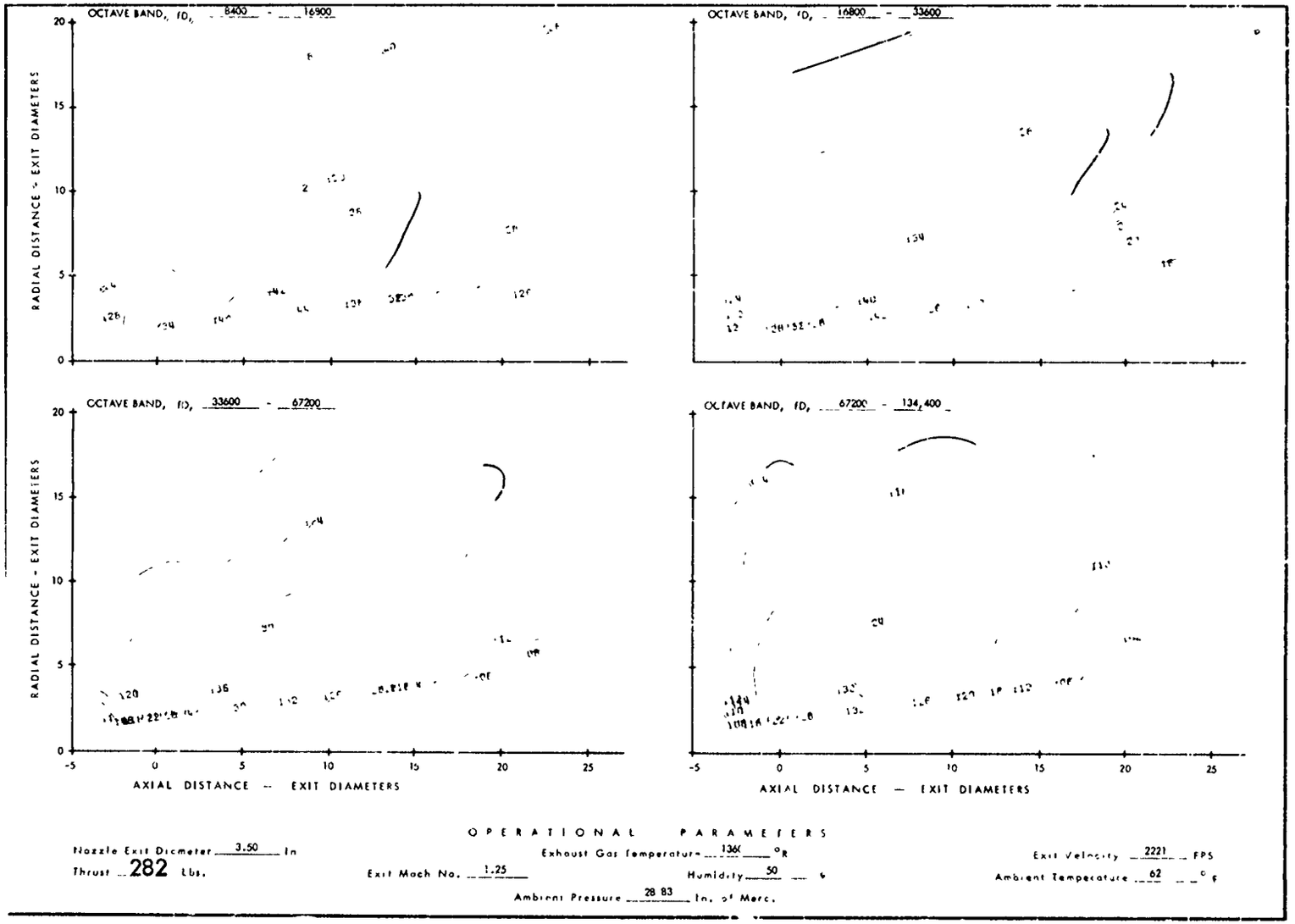

FIGURE II-10. BASIC JET SPL CONTOURS; MACH NO. = 1.25, TEMP. = 1360°R

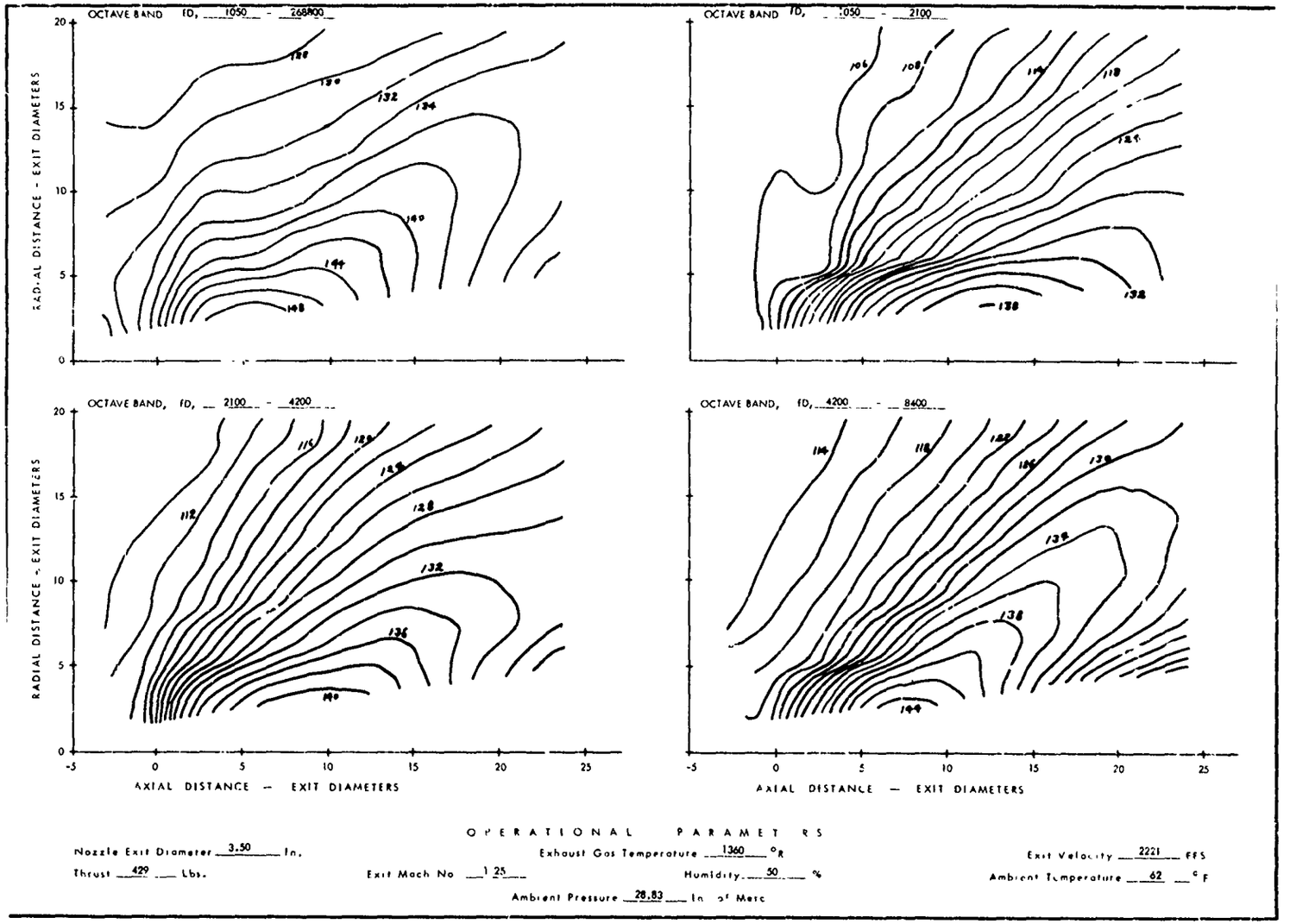

FIGURE II-10. BASIC JET SPL CONTOURS; MACH NO. = 1.25, TEMP. = 1360°R (CONTINUED)

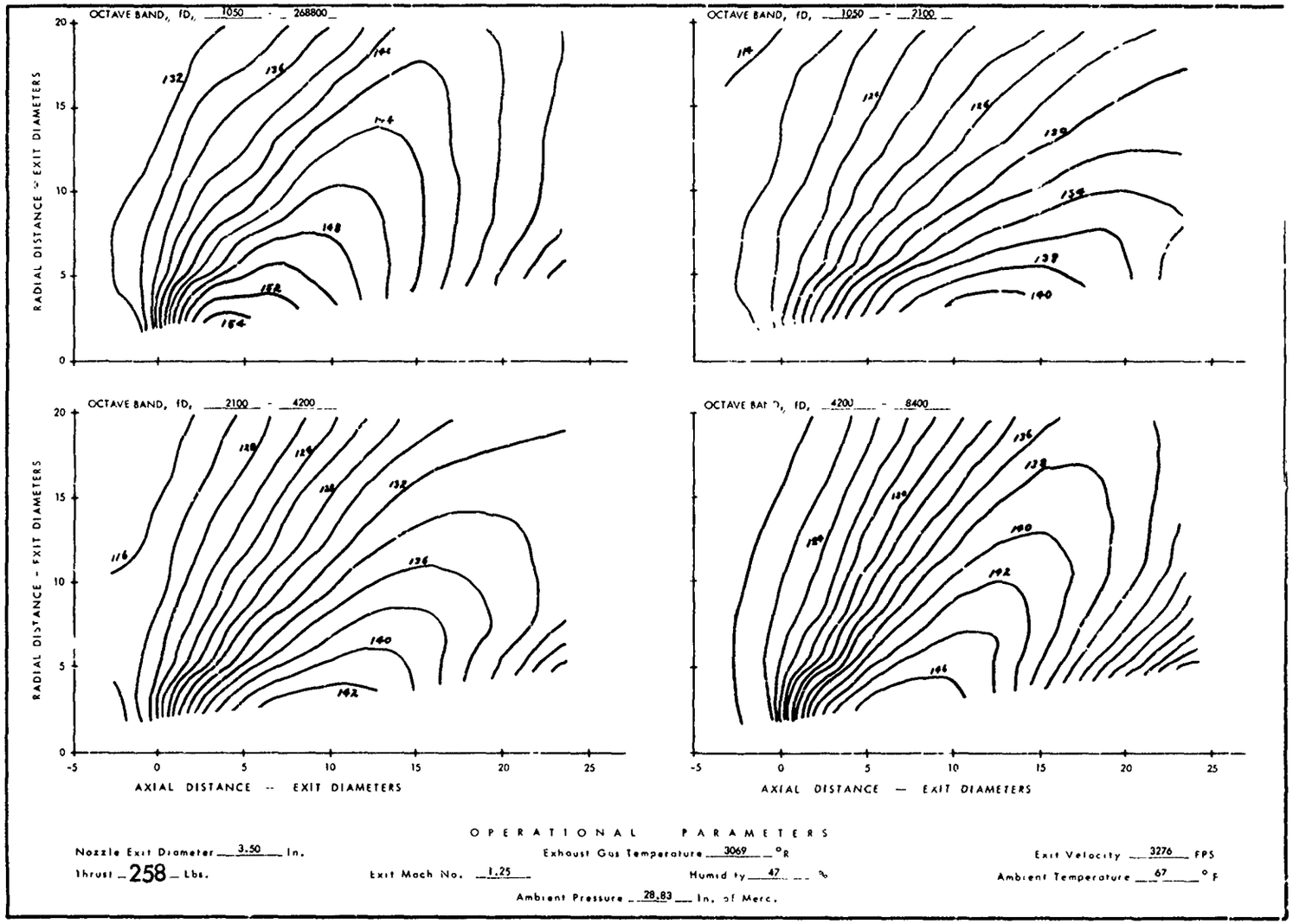

FIGURE II-11. BASIC JET SPL CONTOURS; MACH NO. = 1.25, TEMP. = 3069°R

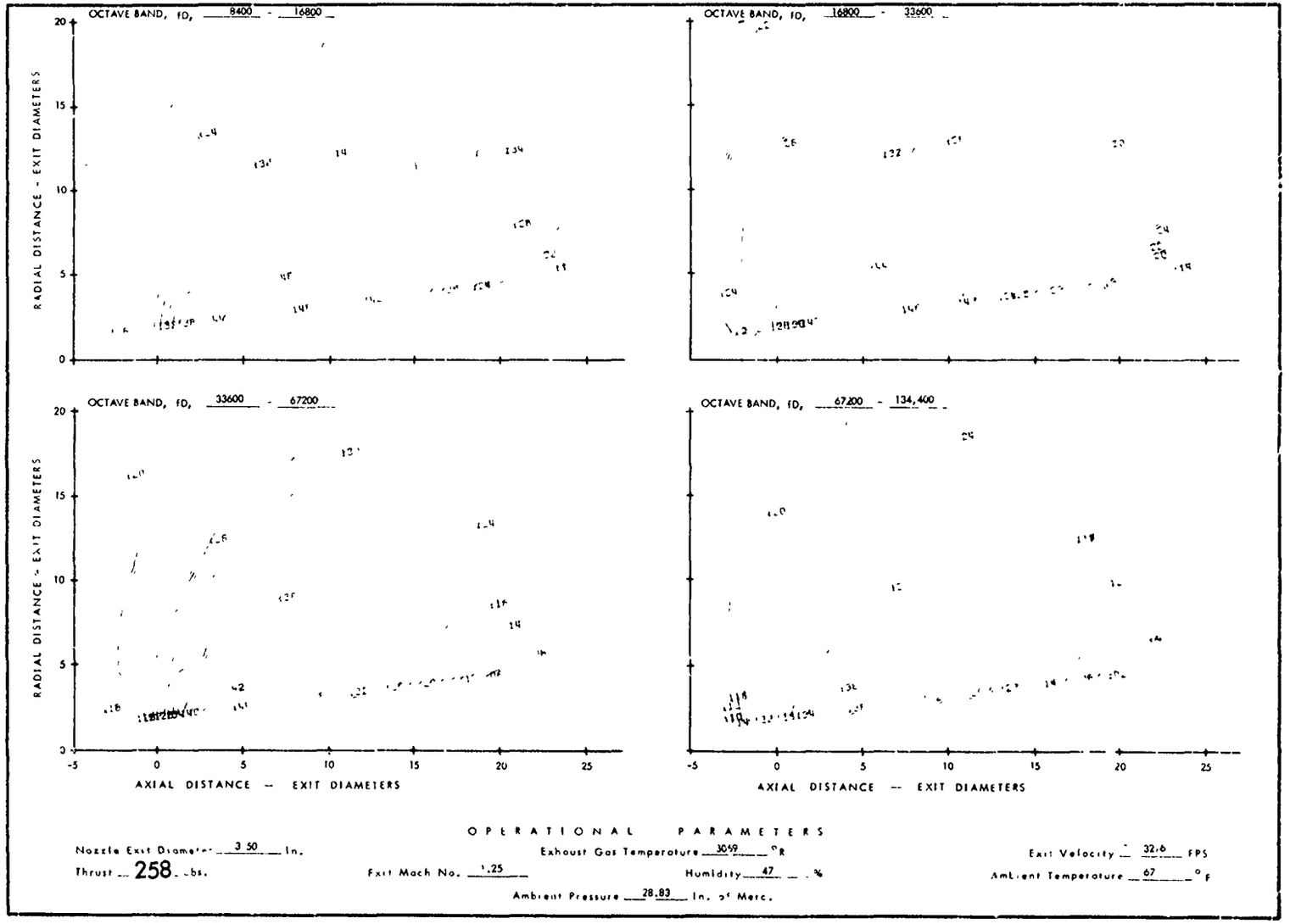

FIGURE II-11. BASIC JET SPL CONTOURS; MACH NO. = 1.25, TEMP. = 3069°R (CONTINUED)

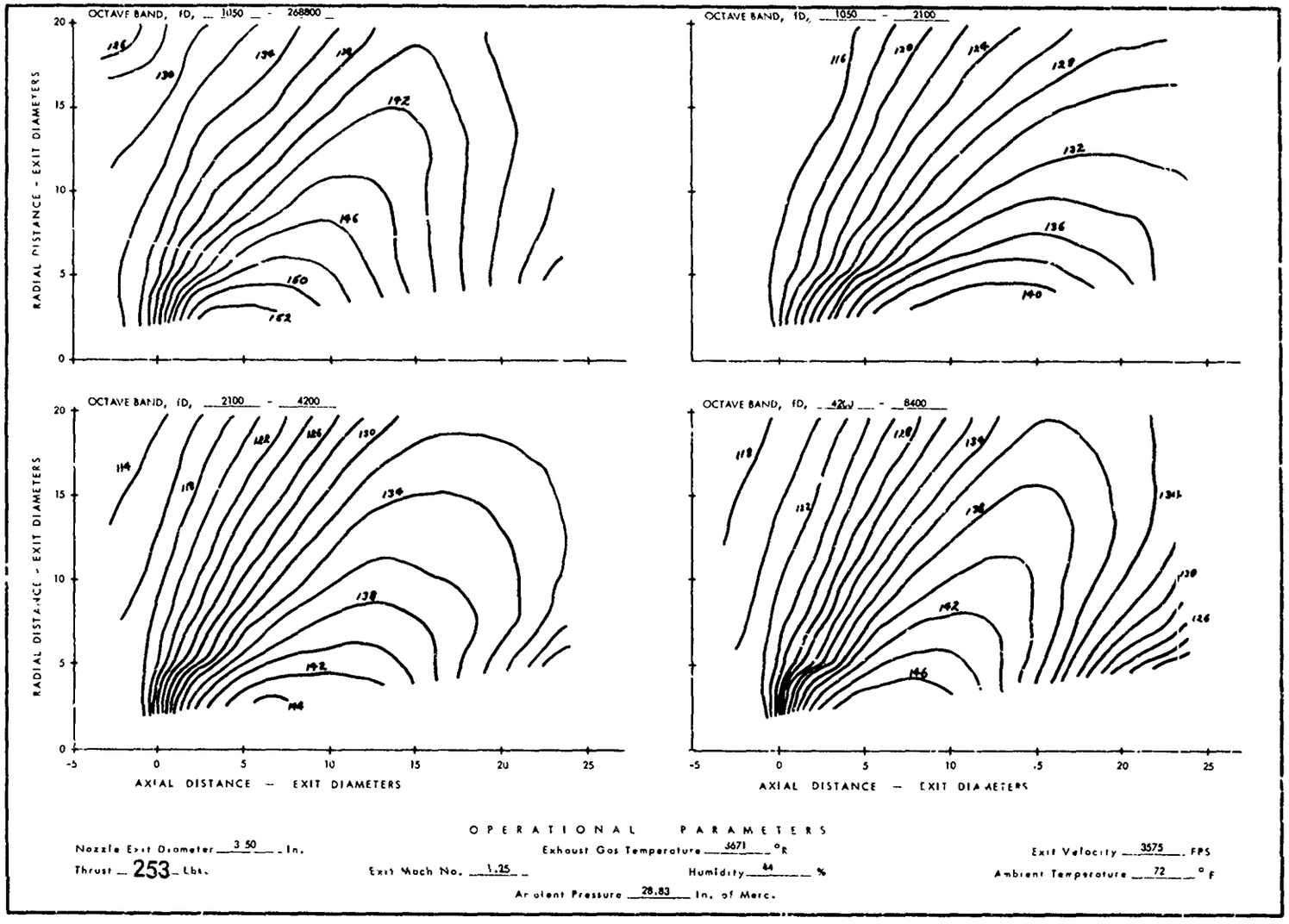

FIGURE II-12. BASIC JET SPL CONTOURS; MACH NO. = 1.25, TEMP. = 3671°R

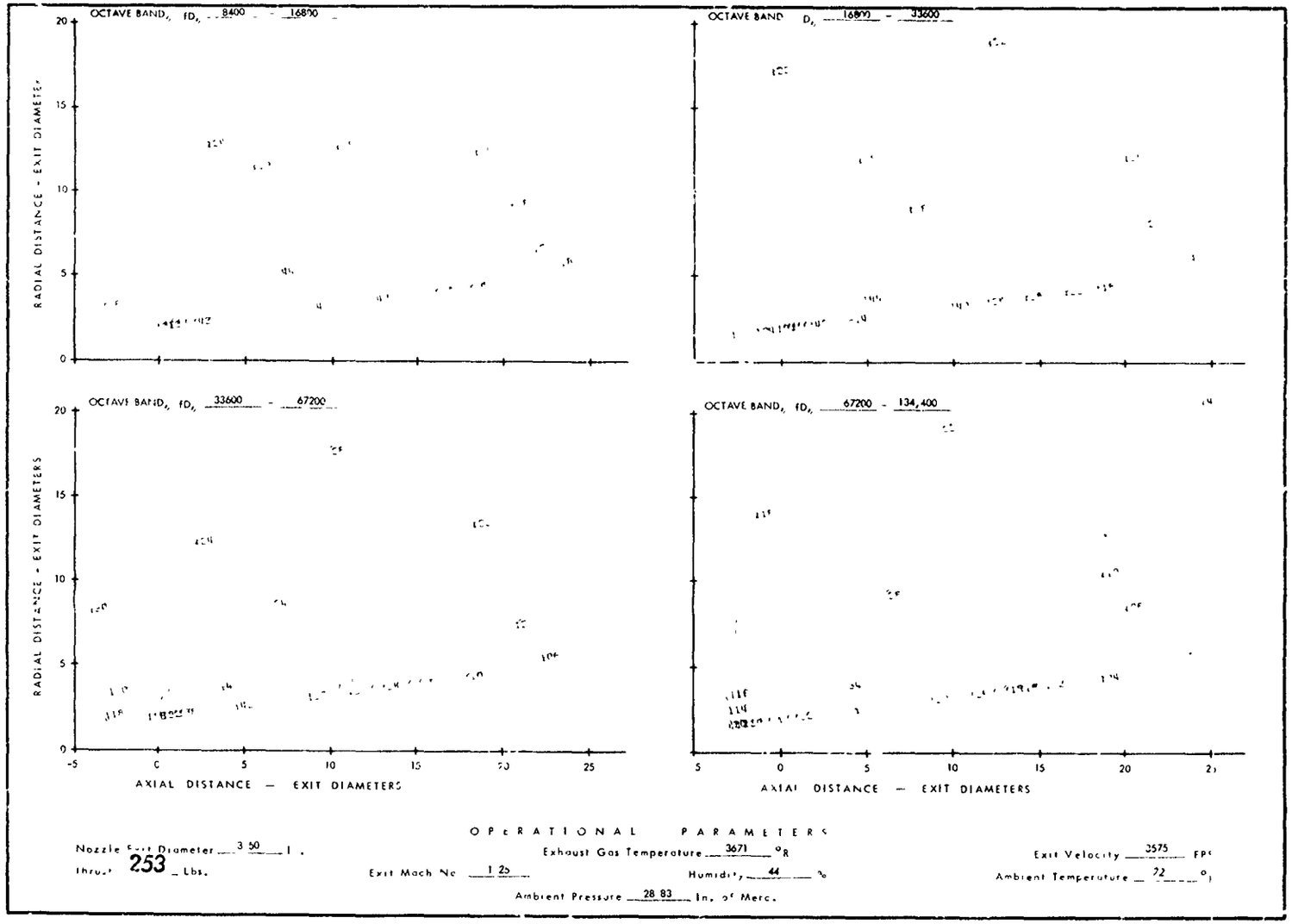

FIGURE II-12. BASIC JET SPL CONTOURS; MACH NO. = 1.25, TEMP. = 3671°R (CONTINUED)

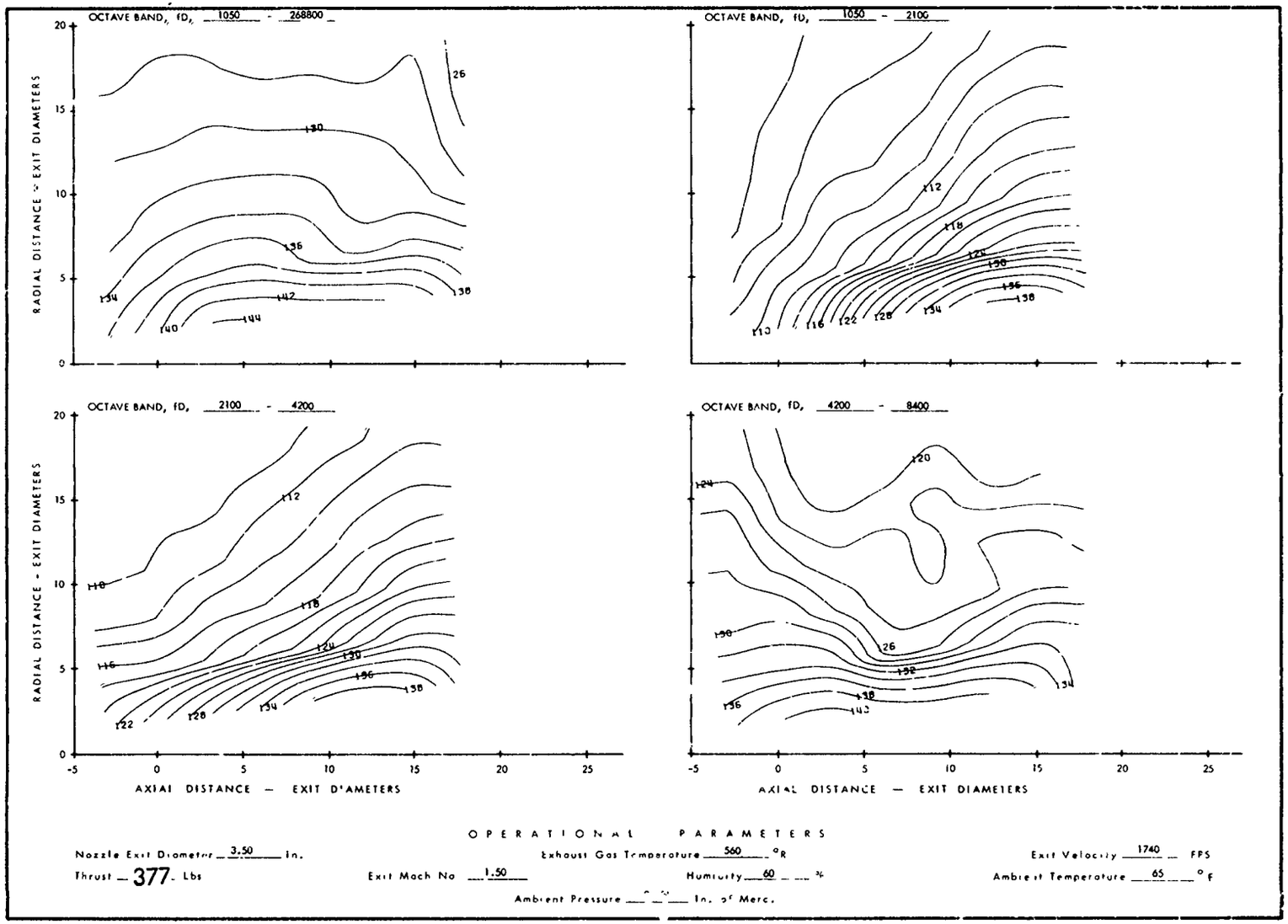

FIGURE II-13. BASIC JET SPL CONTOURS; MACH NO. = 1.49, TEMP. = 560°R

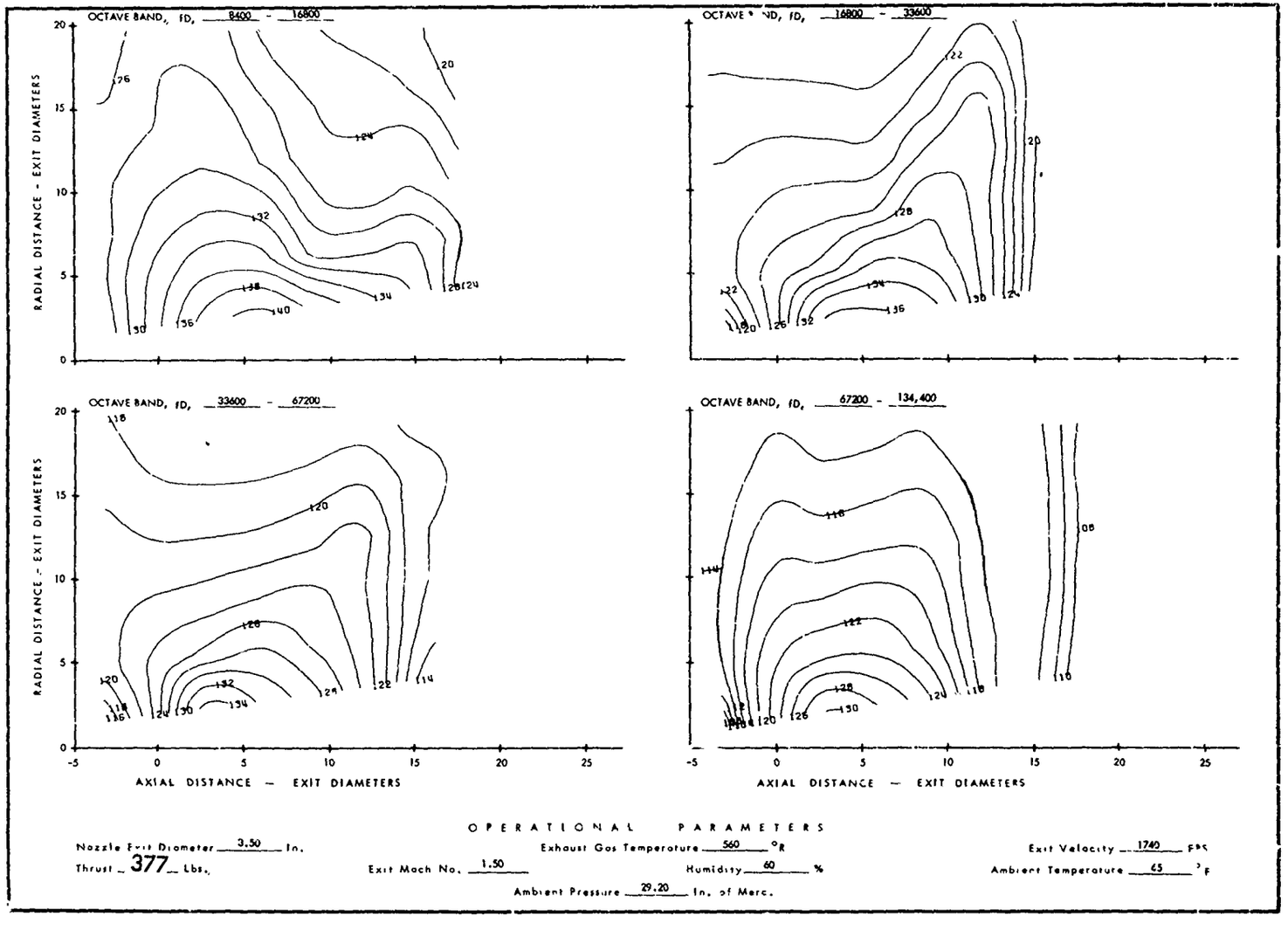

FIGURE II-13. BASIC JET SPL CONTOURS; MACH NO. = 1.49, TEMP. = 560°R (CONTINUED)

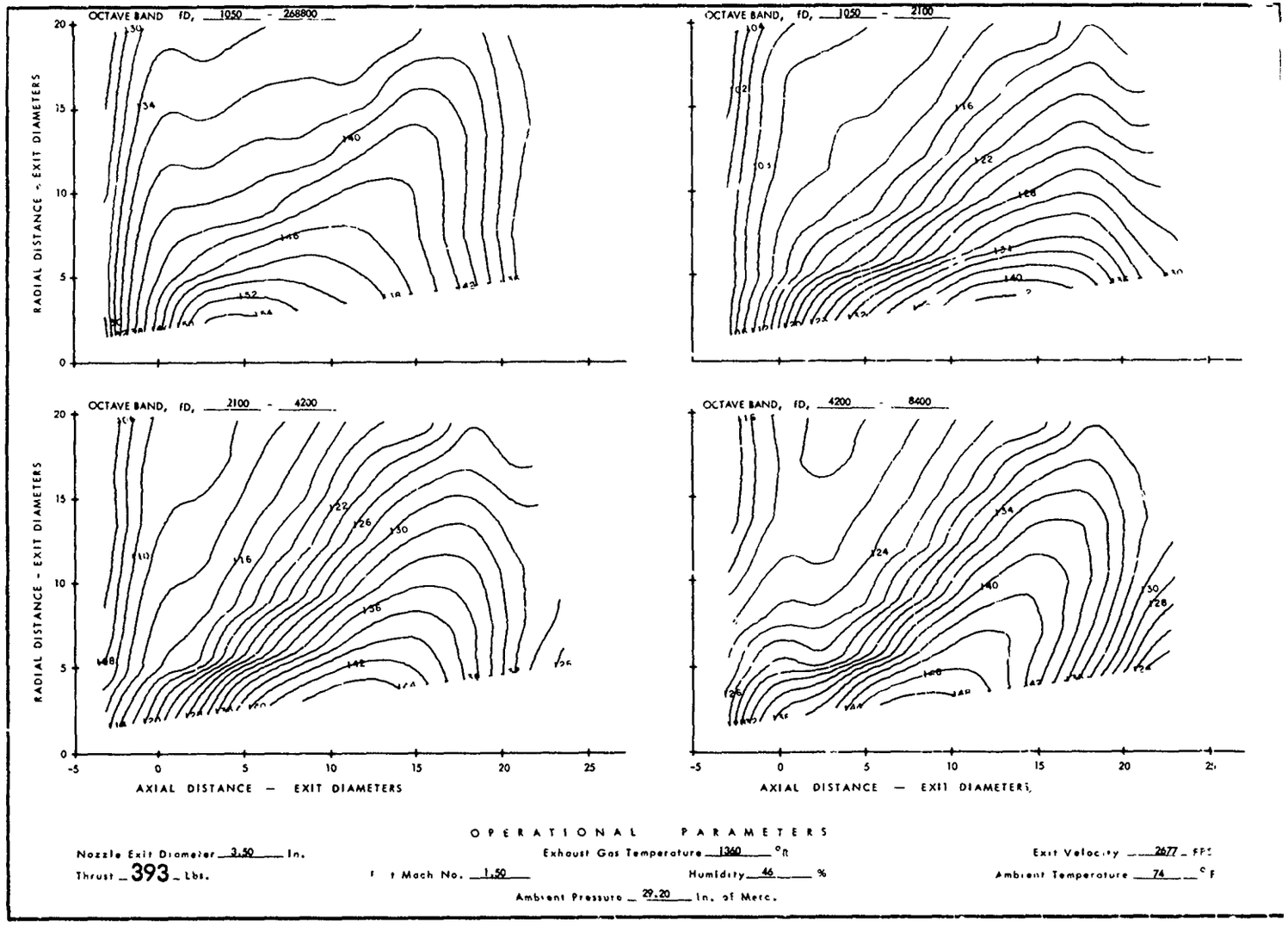

FIGURE II-14. BASIC JET SPL CONTOURS; MACH NO. = 1.51, TEMP. = 1360°R

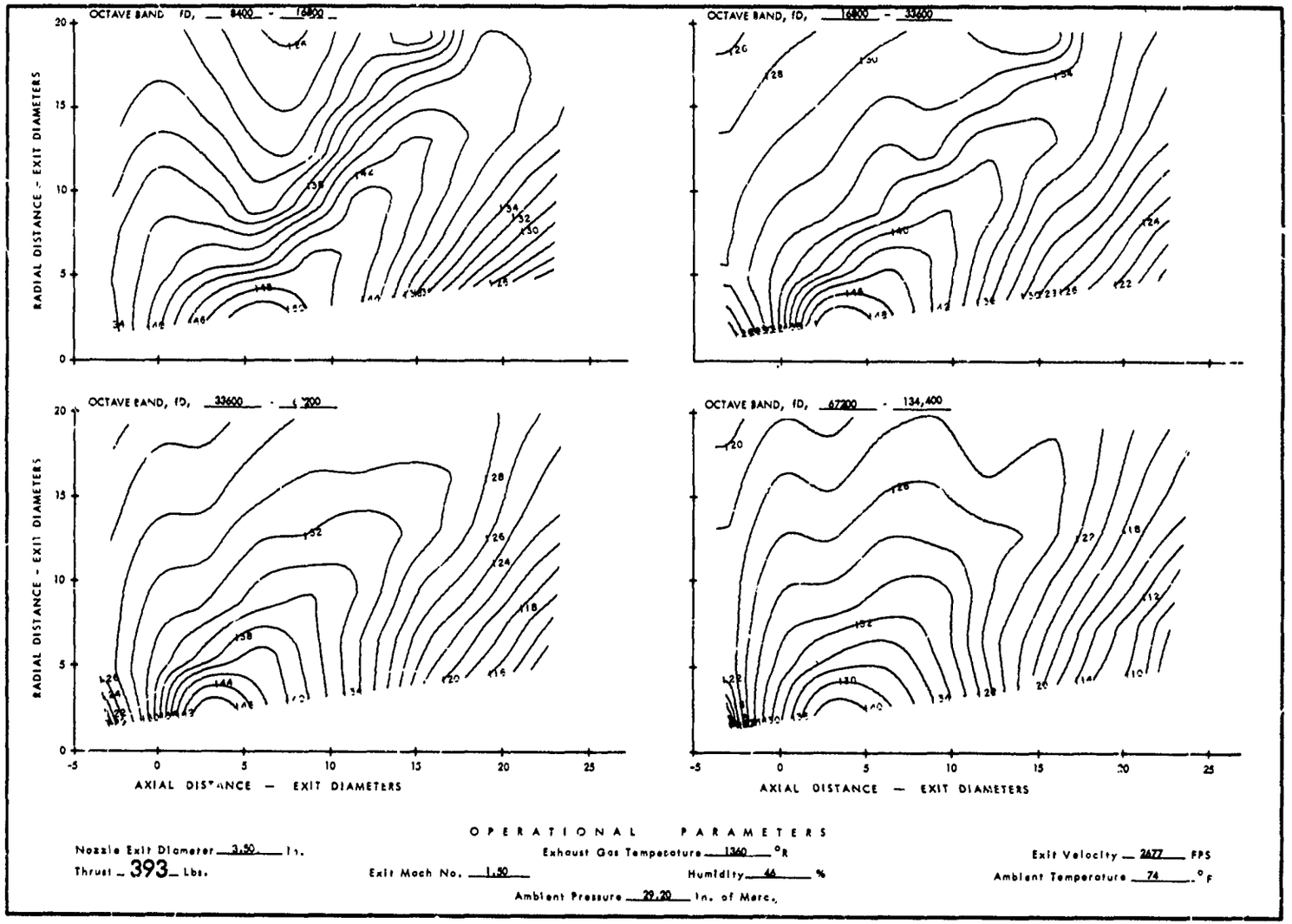

FIGURE II-14. BASIC JET SPL CONTOURS; MACH NO. = 1.51, TEMP. = 1360°R (CONTINUED)

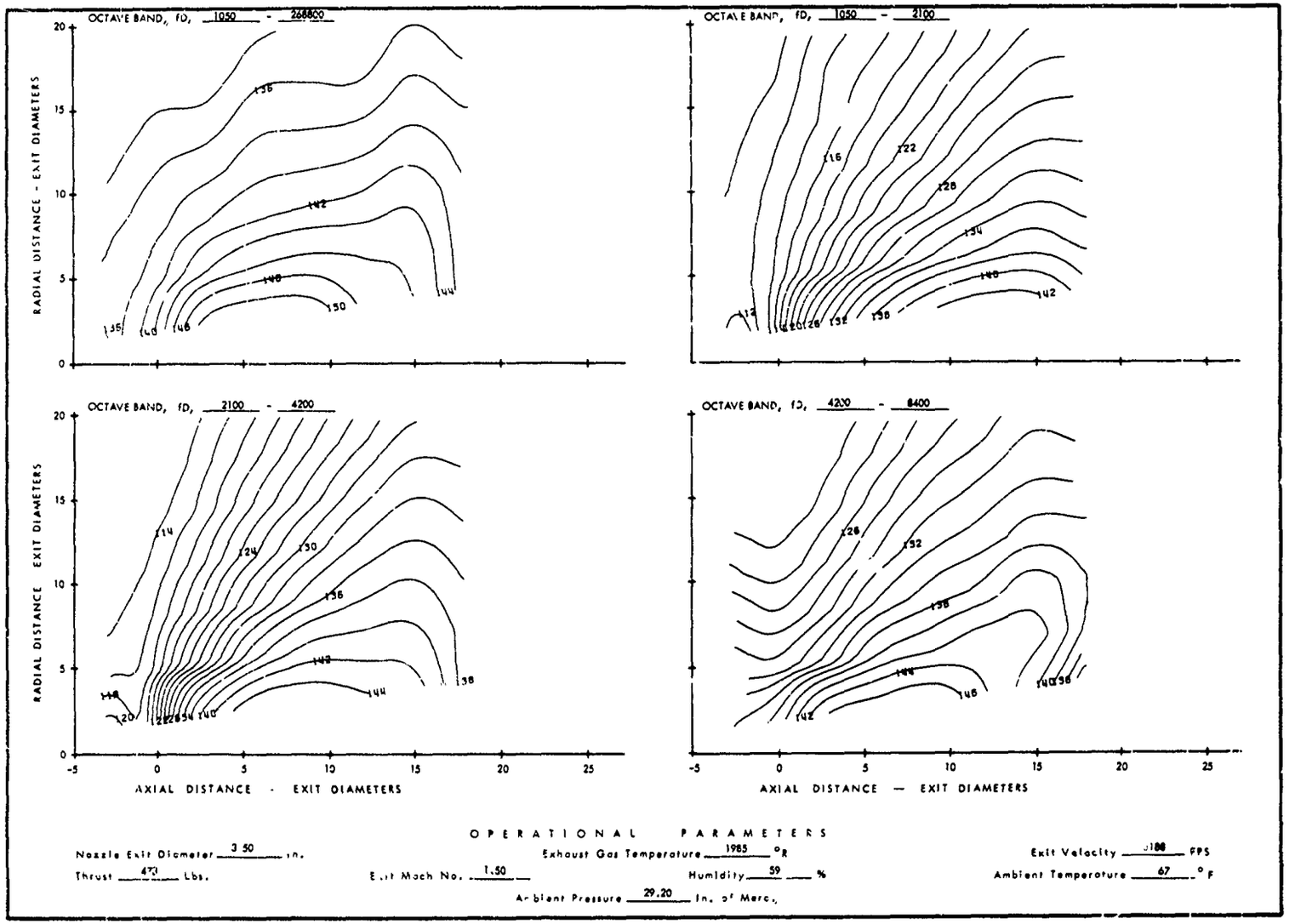

FIGURE II-15. BASIC JET SPL CONTOURS; MACH NO. = 1.49, TEMP. = 1985°R

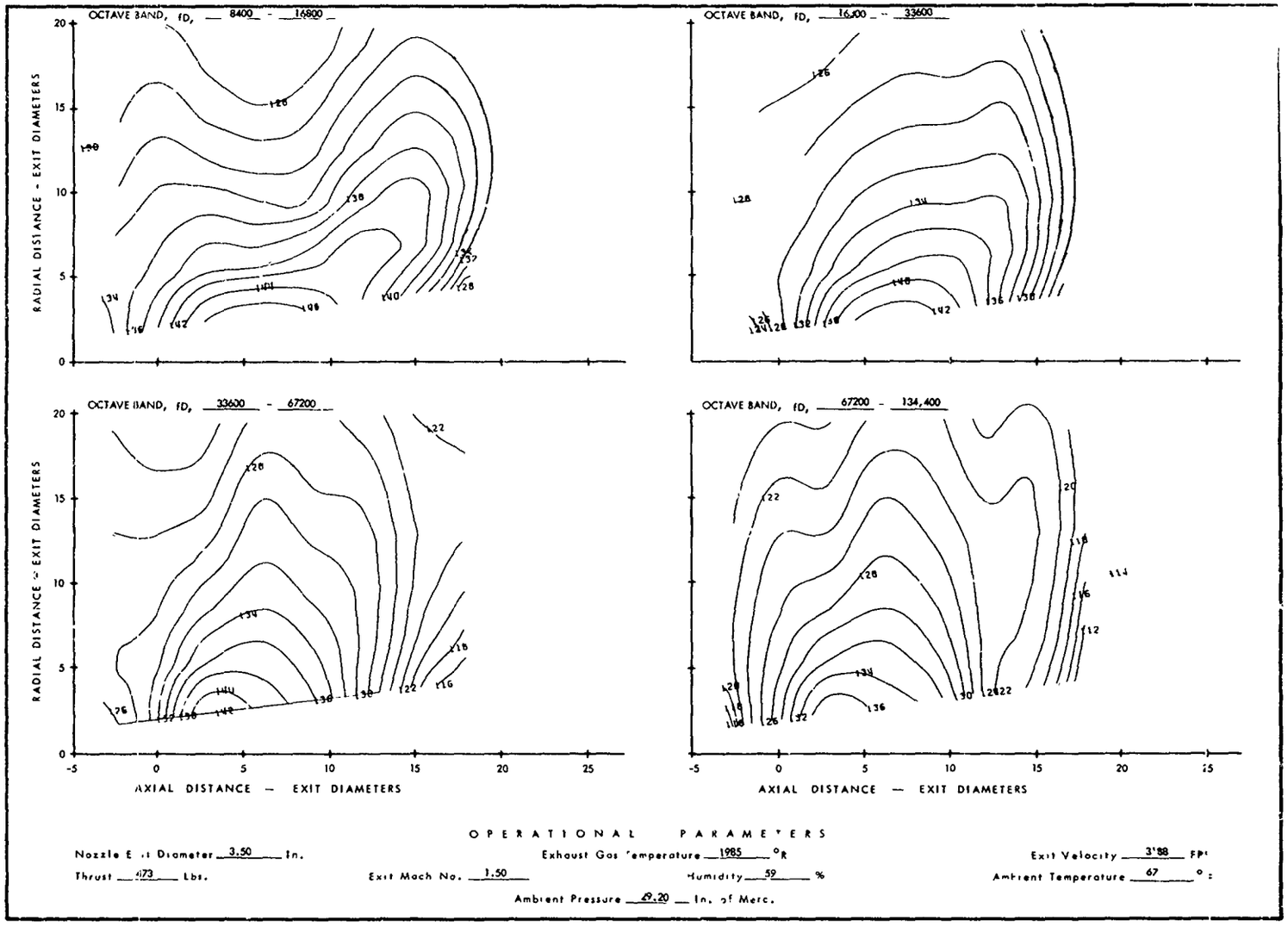

FIGURE II-15. BASIC JET SPL CONTOURS; MACH NO. = 1.49, TEMP. = 1985°R (CONTINUED)

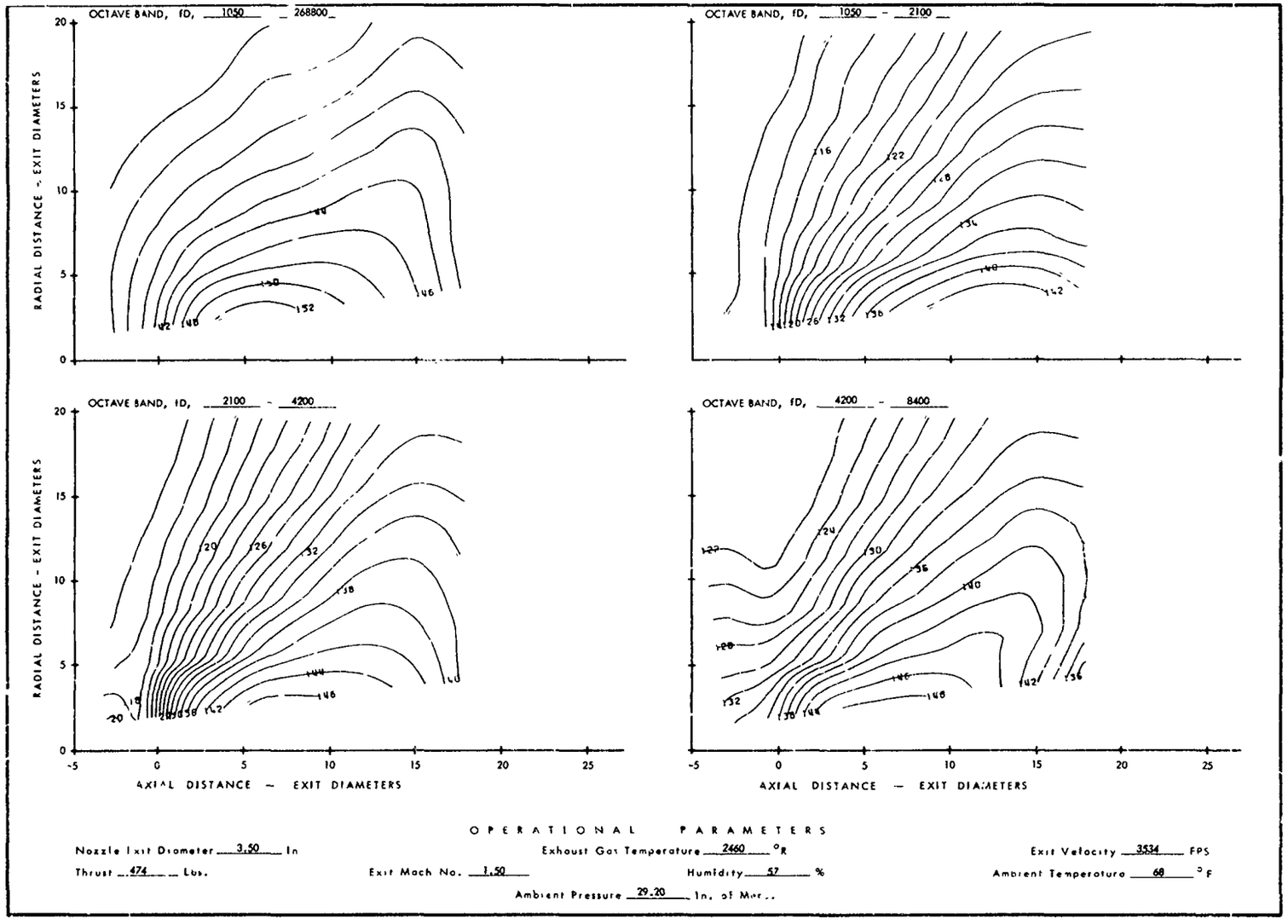

FIGURE II-16. BASIC JET SPL CONTOURS; MACH NO. = 1.51, TEMP. = 2460°R

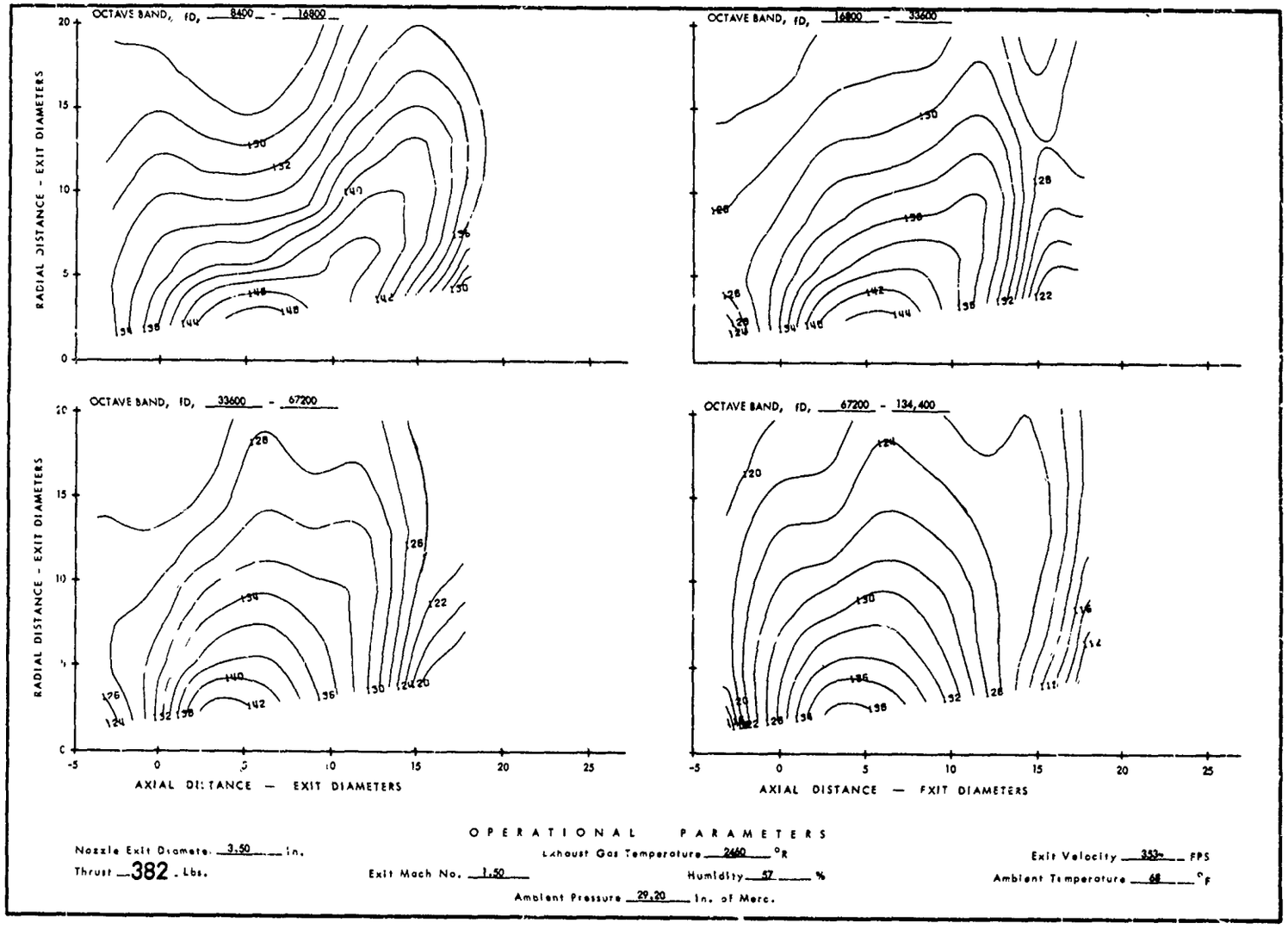

FIGURE II-16. BASIC JET SPL CONTOURS; MACH NO. = 1.51, TEMP. = 2460°R (CONTINUED)

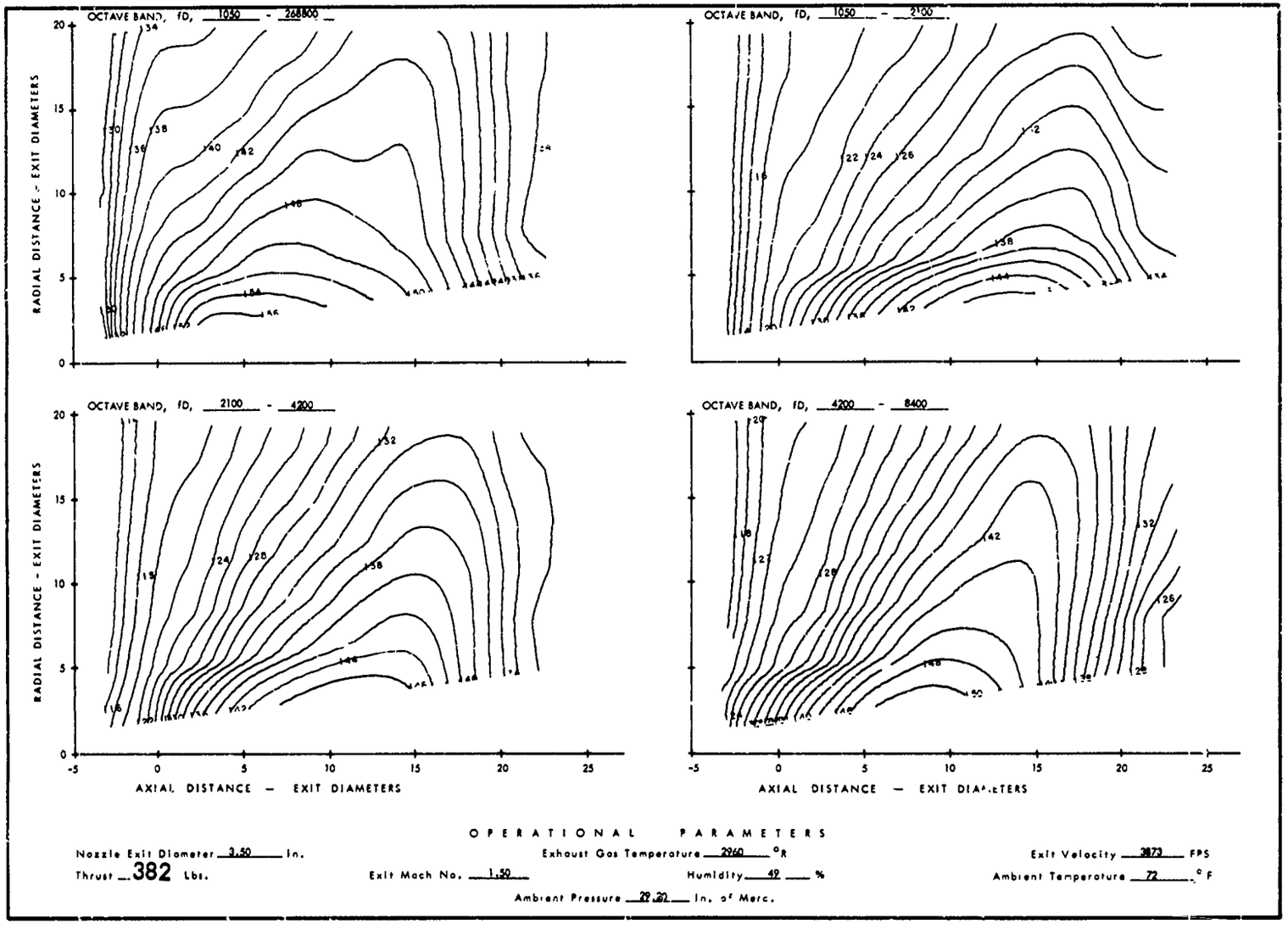

FIGURE II-17. BASIC JET SPL CONTOURS; MACH NO. = 1.50, TEMP. = 2960°R

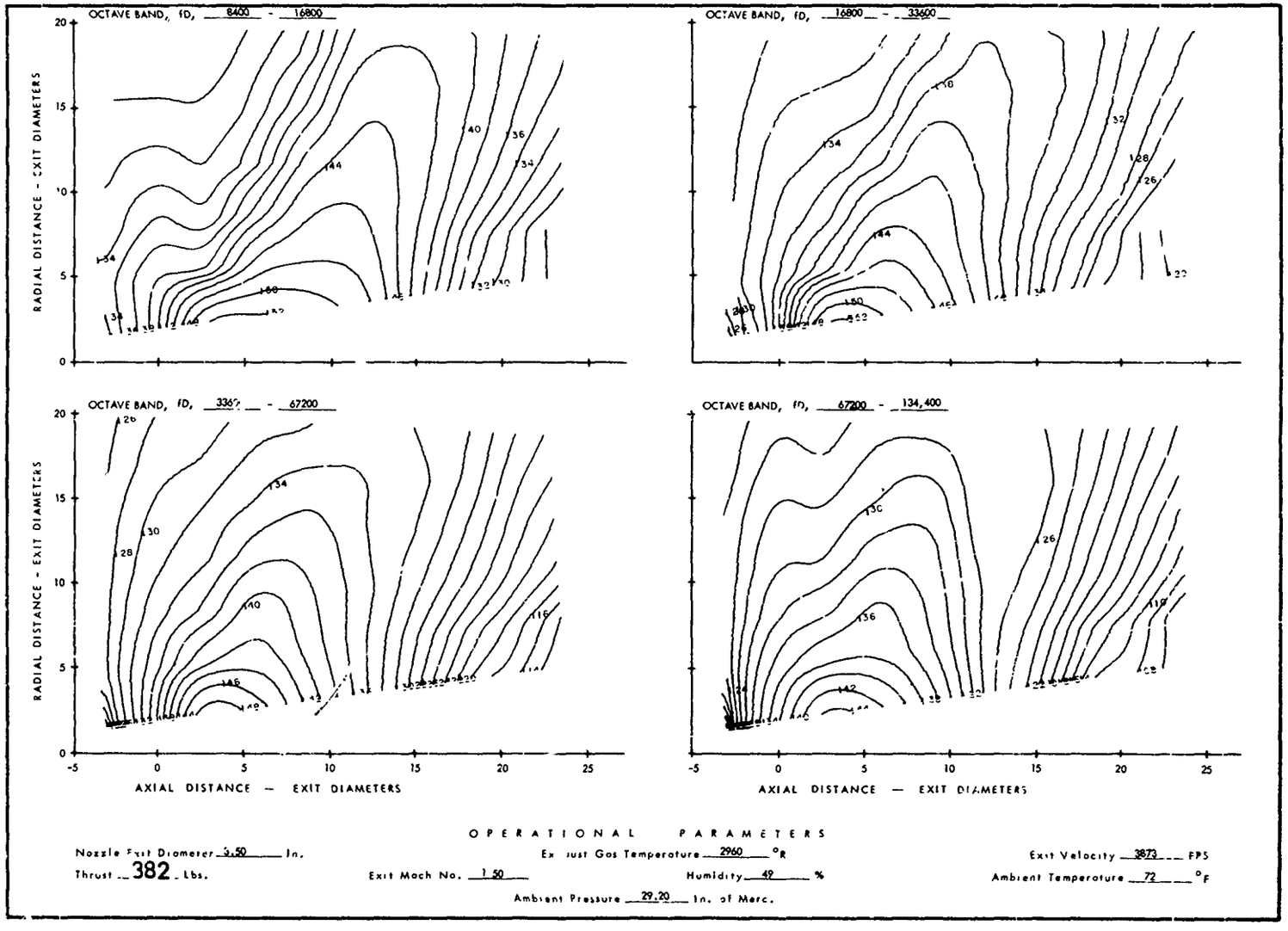

FIGURE II-17. BASIC JET SPL CONTOURS; MACH NO. = 1.50, TEMP. = 2960°R (CONTINUED)

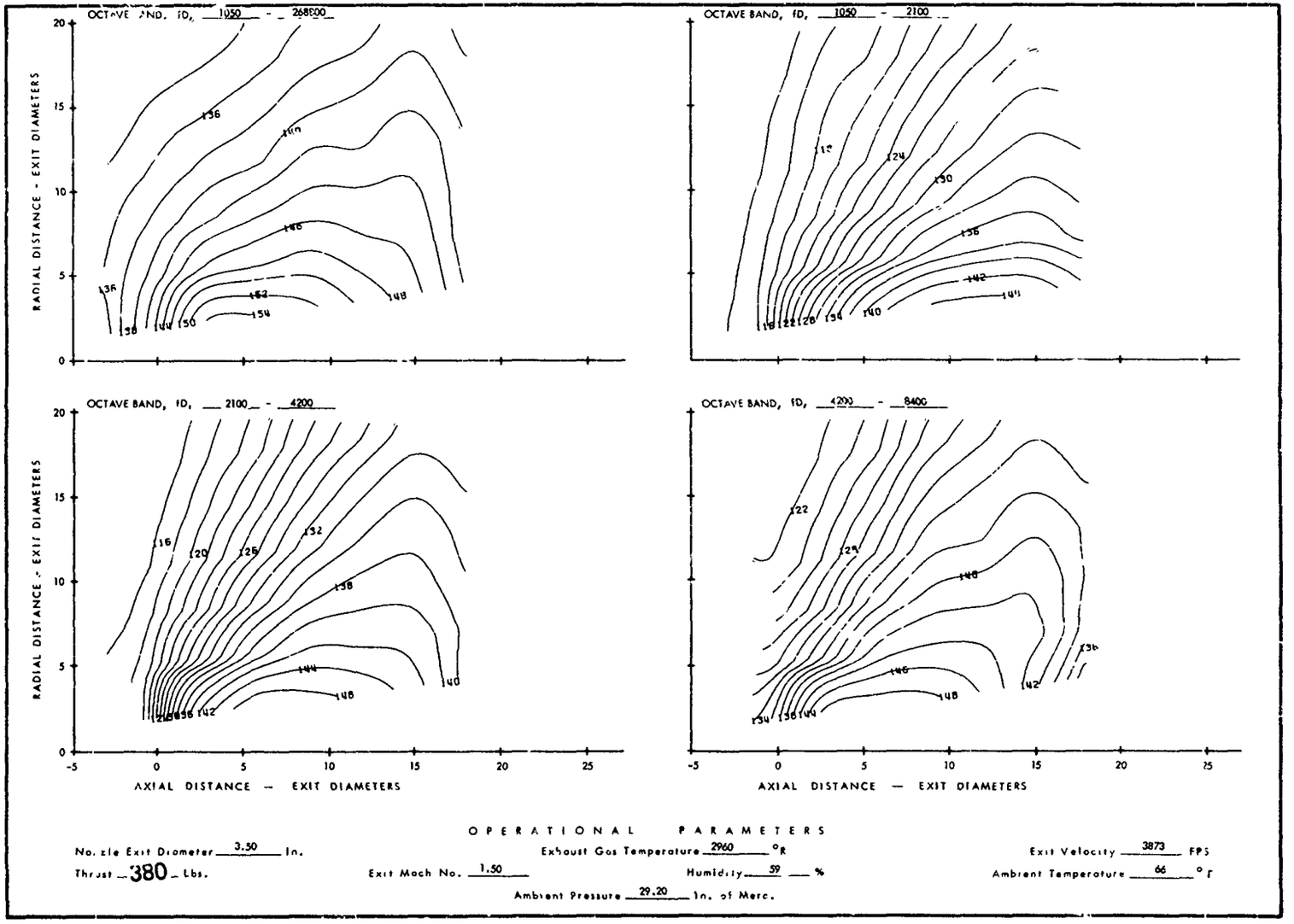

FIGURE II-18. BASIC JET SPL CONTOURS; MACH NO. = 1.50, TEMP. = 2960°R

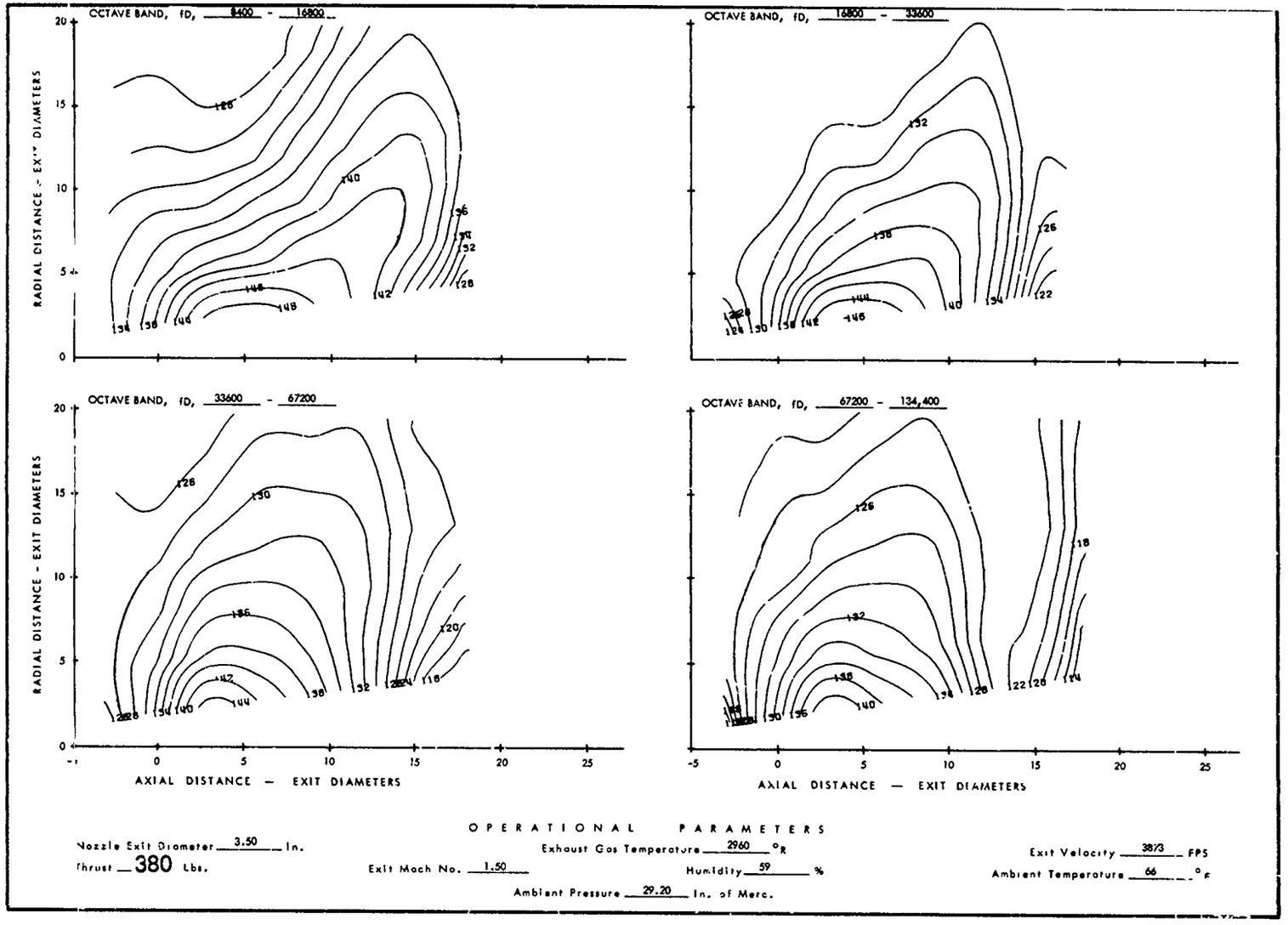

FIGURE II-18. BASIC JET SPL CONTOURS; MACH NO. = 1.50, TEMP. = 2960°R (CONTINUED)

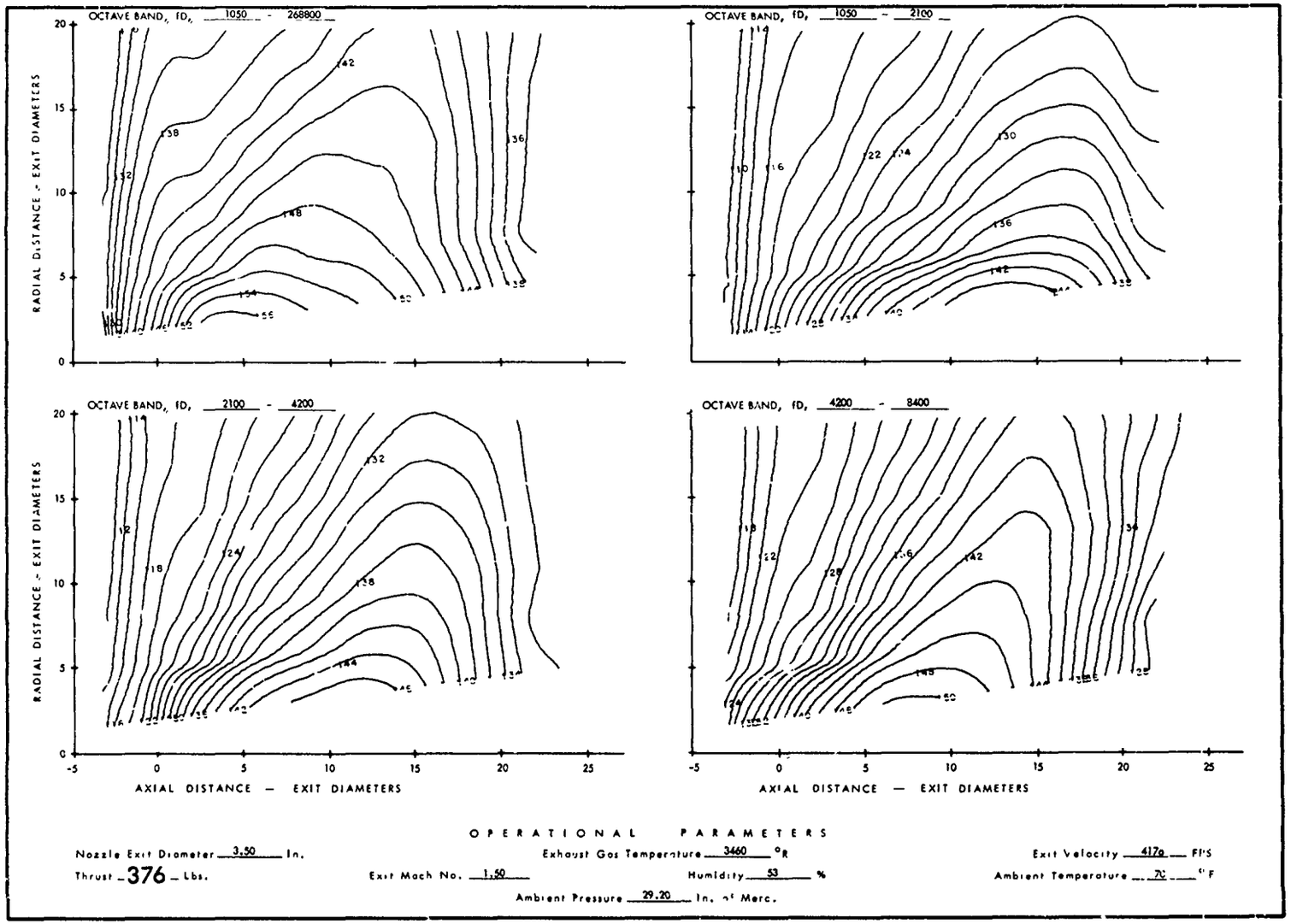

FIGURE II-19. BASIC JET SPL CONTOURS; MACH NO. = 1.52, TEMP. = 3460°R

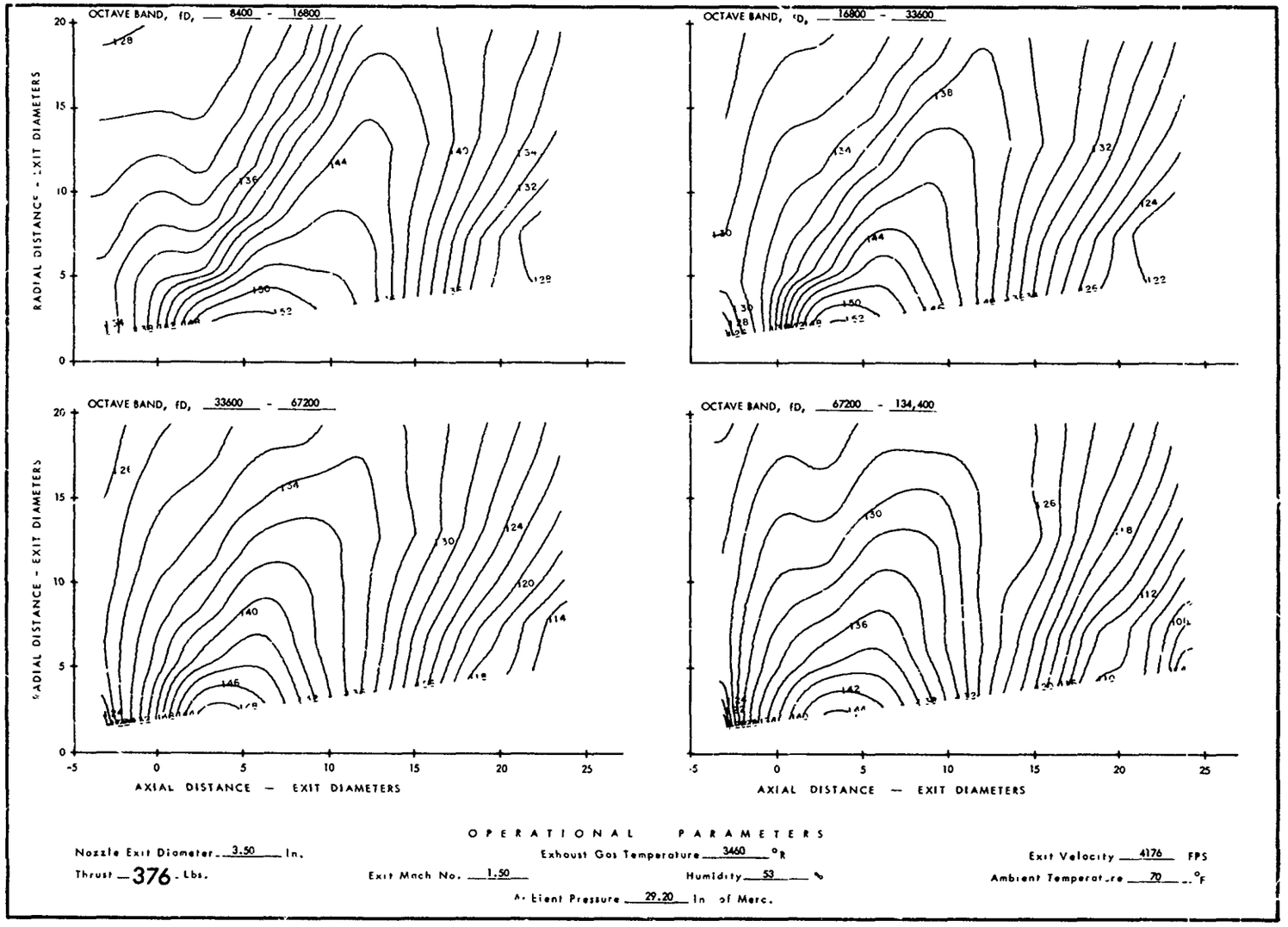

FIGURE II-19. BASIC JET SPL CONTOURS; MACH NO. = 1.52, TEMP. = 3460°R (CONTINUED)

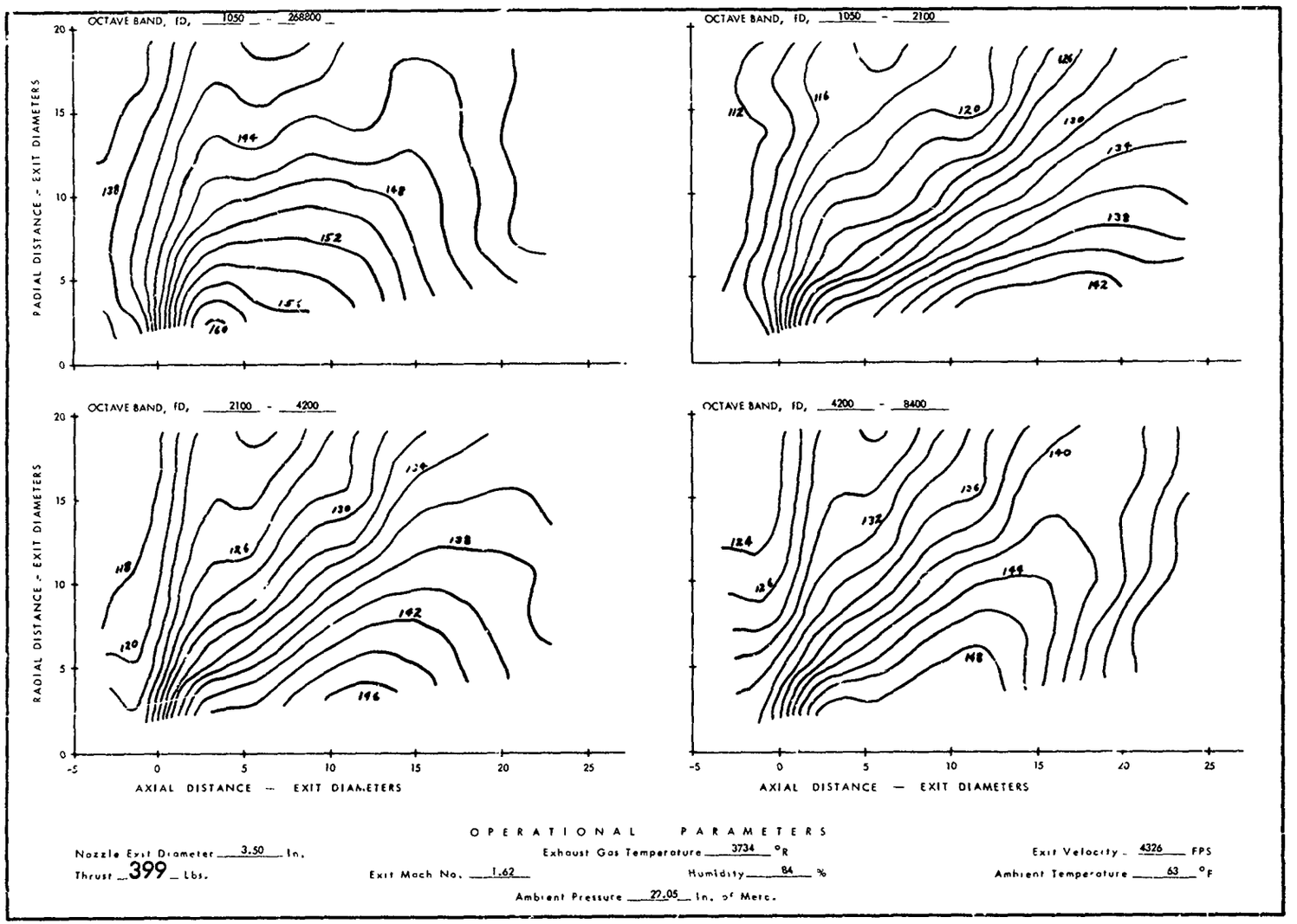

FIGURE II-20. BASIC JET SPL CONTOURS; MACH NO. = 1.59, TEMP. = 3735°R

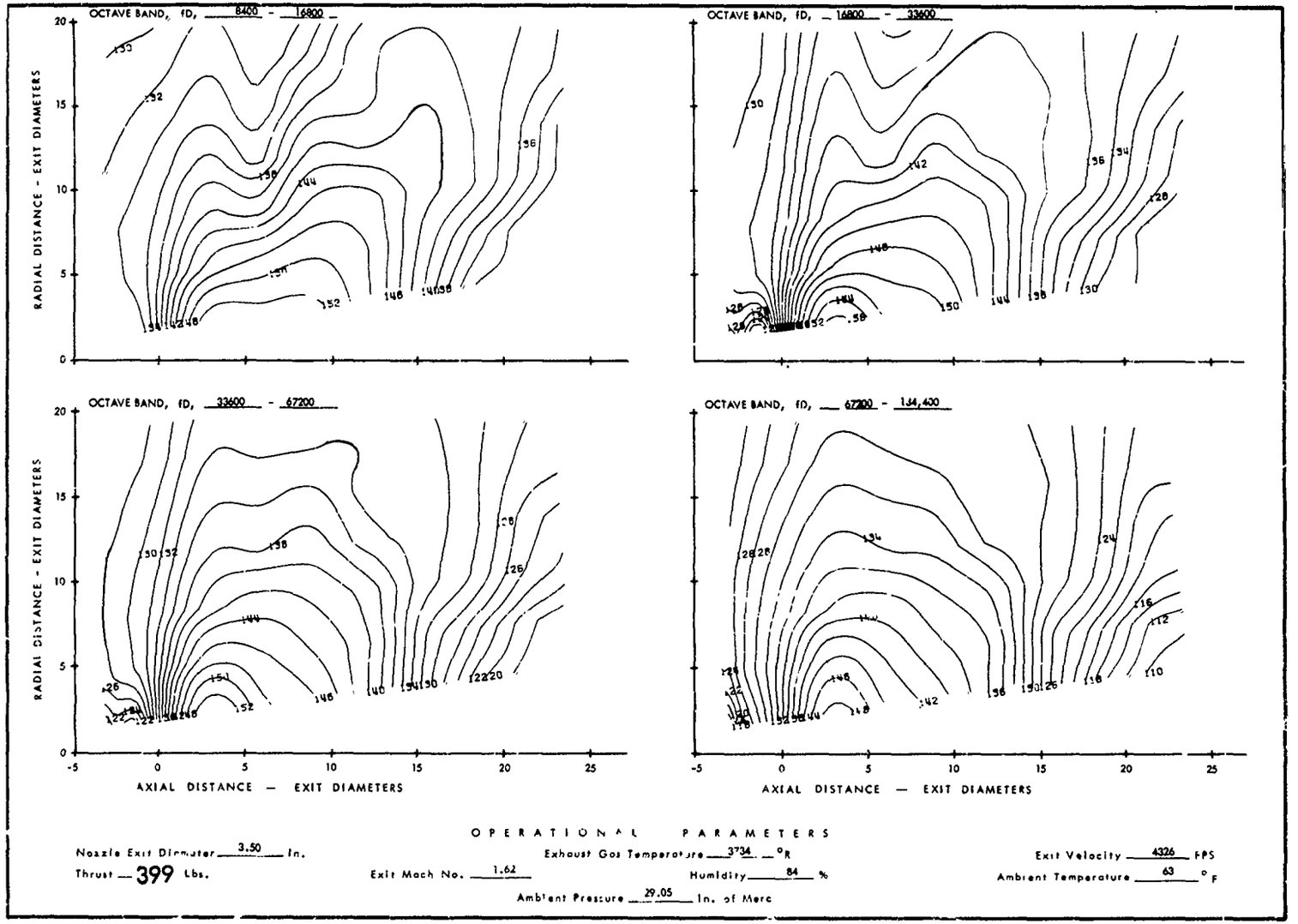

FIGURE II-20. BASIC JET SPL CONTOURS; MACH NO. = 1.59, TEMP. = 3735°R (CONTINUED)

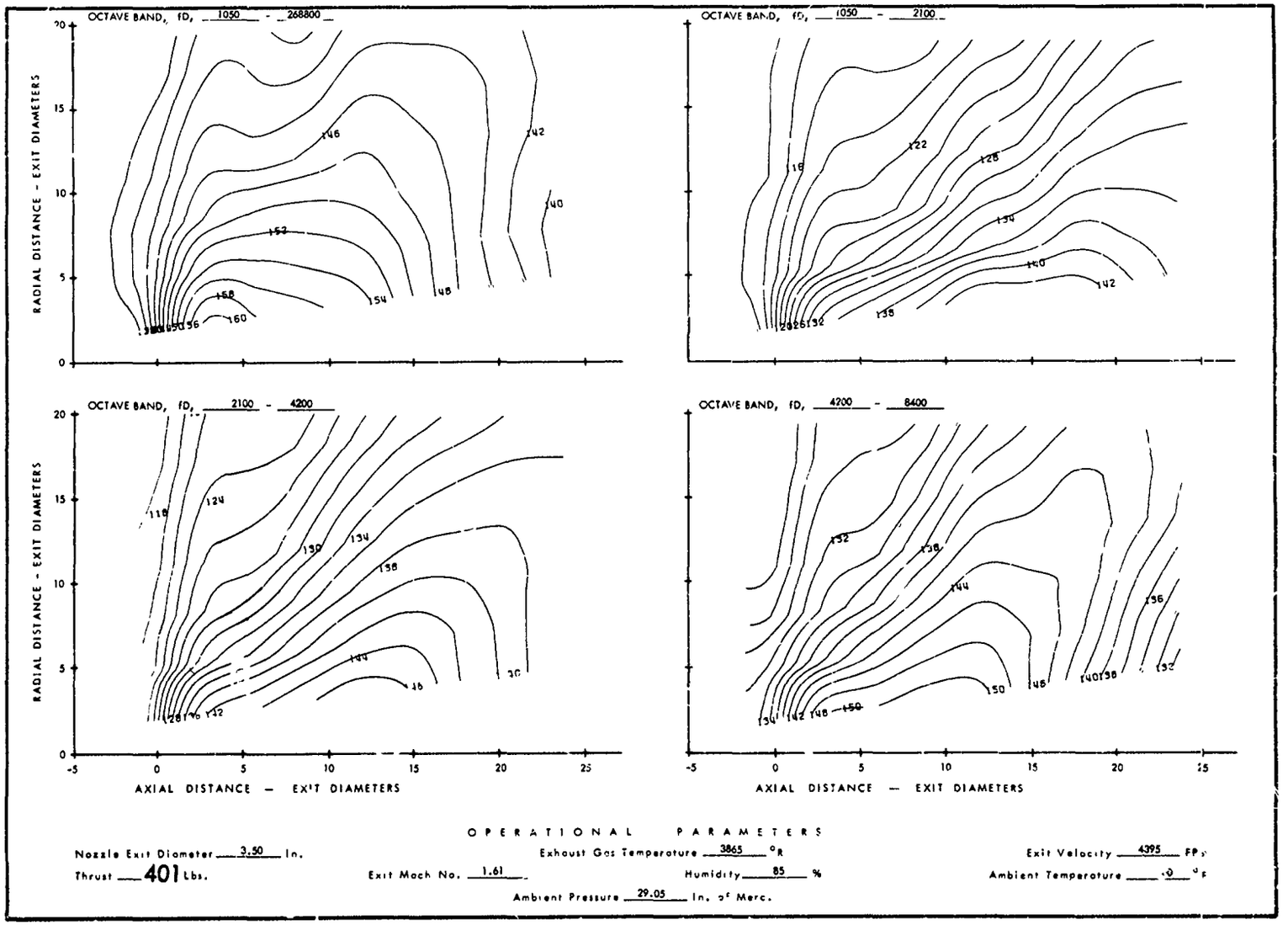

FIGURE II-21. BASIC JET SPL CONTOURS; MACH NO. = 1.59, TEMP. = 3865°R

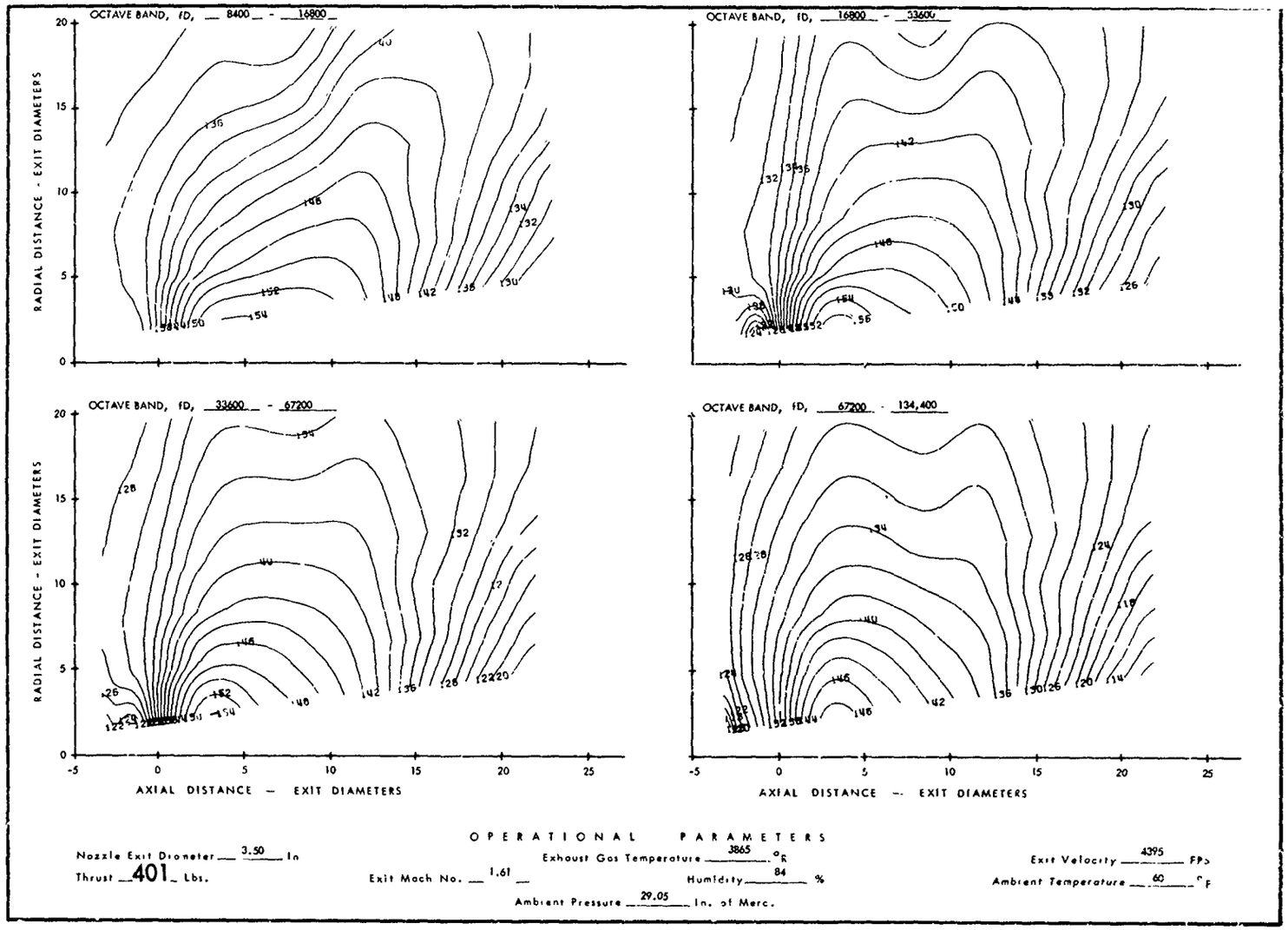

FIGURE II-21. BASIC JET SPL CONTOURS; MACH NO. = 1.59, TEMP. = 3865°R (CONTINUED)

REFERENCES

1. P. A. Franken and E. M. Kerwin, Jr., "Methods of Flight Vehicle Noise Predictions," WADC TR 58-343, November 1958.

2. P. H. Hermes and D. L. Smith, "Measurement and Analyses of the J57-P21 Noise Field," AFFDL-TR-66-147, 1967.

3. W. L. Howes and H. R. Mull, "Near Noise Field of a Jet-Engine Exhaust, I - Sound Pressures," NACA TN 3763, October 1956.

4. W. V. Morgan, L. C. Sutherland, and K. J. Young, "The Use of Acoustic Scale Models for Investigating Near Field Noise of Jet and Rocket Engines," WADD TR 61-178, April 1961.

5. H. Dahlen, "The Near Acoustic Field of Jets," Dtsch. Forsch Anst. Luftf. Ber, 1963.

6. G. J. Franz, "The Near-Sound Field of Turbulence," David Taylor Model Basin, AD-630 684, October 1959.

7. W. L. Howes, "Ground Reflection of Jet Noise," Lewis Research Center, Cleveland, Ohio, NASA TR R-35, 1959.

8. H. S. Ribner, "The Generation of Sound by Turbulent Jets," Advances in Solid Mechanics, 8, 104-178, Academic Press, New York and London, 1964.

9. A. C. Pietrasanta, "Noise Measurements Around Some Jet Aircraft" Journal of the Acoustical Society of America, 28, 434-442, 1956.

10. M. J. Lighthill, "On Sound Generated Aerodynamically, I. General Theory," Proc. Royal Society, A211, 564-587, 1952.

11. G. M. Lilley, "On the Noise from Air Jets," ARC 20, 376-N40-FM2724, 1958.

12. J. E. Ff Williams, "Some Thoughts on the Effects of Aircraft Motion and Eddy Convection on the Noise From Air Jets," University of Southampton, Dept. of Aero/Astro, USAA Rep. 155, 1960.

13. H. S. Ribner, "New Theory for Jet Noise Generation, Directionality, and Spectra," J. Acoust. Soc. Amer., 31, 245-246, 1959.

14. H. S. Ribner, "A Theory of the Sound from Jets and Other Flows in Terms of Simple Sources," Univ. of Toronto, Inst of Aerophysics, UTIA Rep. 67, AFOSR TN 60-950, 1960.

15. H. S. Ribner, "Aerodynamic Sound from Fluid Dilatations - A Theory of the Sound from Jets and Other Flows," Univ. of Toronto, Inst. of Aerophysics, UTIA Rep. 86, AFOSR TN 3430, 1962.

16. J. E. Ff Williams, "The Noise from Turbulence Convected at High Speed," Phil. Trans. Roy. Soc. Lond., Series A, 255, 469-503, 1963.

17. A. H. Shapiro, The Dynamics and Thermodynamics of Compressible Fluid Flow, Volume I, The Ronald Press Company, New York, 1953.

18. D. Middleton, "The Noise of Ejectors," ARC R&M No. 3389, 1965.

19. R. J. Cox, H. J. Parry, and J. Clough, "A Study of the Characteristics of Modern Engine Noise and the Response Characteristics of Structures," WADD TR 60-220, December 1961.

20. J. Laufer, J. E. Ff. Williams, and S. Childress, "Mechanism of Noise Generation in the Turbulent Boundary Layer," AGARDograph 90, November 1964.

21. H. H. Hubbard and A. A. Regier, "Free-Space Oscillating Pressures Near the Tips of Rotating Propellers," NACA TN No. 1870, April 1949.

22. C. Watkins and B. Durling, "A Method for the Calculation of Free-Space Sound Pressures Near a Propeller in Flight Including Considerations of Chordwise Blade Loading," NACA TN 3809, 1956.

23. H. H. Hubbard and L. W. Lassiter, "Sound From a Two Blade Propeller at Supersonic Tip Speeds," NACA TR 1079.

24. A. A. Regier and H. H. Hubbard, "Status of Research on Propeller Noise and Its Reduction," J.A.S.A., Vol. 25, No. 3.

25. M. V. Lowson, "Reduction of Compressor Noise Radiation," paper presented at the Seventy-Second Meeting of the Acoustical Society of America, Los Angeles, Calif., November 1966.

26. N. H. Kemp and W. R. Sears, "Aerodynamic Interference Between Moving Blade Rows," J.A.S.A., 20, 585-598, 1953.

27. N. H. Kemp and W. R. Sears, "The Unsteady Forces Due to Viscous Wakes in Turbomachines," J.A.S.A., 22, 478-483, 1965.

28. R. Hetherington, "Compressor Noise Generated by Fluctuating Lift Resulting from Rotor-Stator Interactions," AIAA Journal, Vol. 1, 473-474, 1963.

29. M. V. Lowson, "The Sound Field for Singularities in Motion," Proc. Roy. Soc., A286, 559-572, 1965.

30. J. M. Tyler and T. G. Sofrin, "Axial Flow Compressor Noise Studies," S.A.E. Transactions, 309-332, 1961.

31. A. H. Marsh, et al, "A Study of Turbofan-Engine Compressor-Noise-Suppression Techniques," Douglas Aircraft Co. Report DAC-33170, 1966.

32. G. M. Rentzepis, "Tip Turbine Fan Noise," TIS Report 64GL76, General Electric Co., 1964.

UNCLASSIFIED

Security Classification

DOCUMENT CONTROL DATA - R&D

(Security classification of title, body of abstract and indexing annotation must be entered when the overall report is classified)

1 ORIGINATING ACTIVITY (Corporate author)	2a REPORT SECURITY CLASSIFICATION
Lockheed-Georgia Company Marietta, Georgia 30060	UNCLASSIFIED
	2b GROUP

3. REPORT TITLE

Near Field Noise Analyses of Aircraft Propulsion Systems with Emphasis on Prediction Techniques for Jets

4. DESCRIPTIVE NOTES (Type of report and inclusive dates)

Final July 1965 to April 1967

5. AUTHOR(S) (Last name, first name, initial)

Plumblee, H. E.
Ballentine, J. R.
Passinos, B.

6. REPORT DATE	7a. TOTAL NO. OF PAGES	7b. NO. OF REFS
August 1967	210	32

8a. CONTRACT OR GRANT NO.	9a. ORIGINATOR'S REPORT NUMBER(S)
AF 33(615)-2503	AFFDL-TR-67-43
b. PROJECT NO. 1471	
c. Task 147102	9b. OTHER REPORT NO(S) (Any other numbers that may be assigned this report) ER-8983
d.	

10. AVAILABILITY/LIMITATION NOTICES

This document is subject to special export controls and each transmittal to foreign governments or foreign nationals may be made only with prior approval of the Vehicle Dynamics Division, AF Flight Dynamics Laboratory.

11. SUPPLEMENTARY NOTES	12. SPONSORING MILITARY ACTIVITY
	Air Force Flight Dynamics Laboratory WPAFB, Ohio 45433

13. ABSTRACT

Semi-empirical methods are presented for calculating sound pressure level in a jet near noise field, including temperature and Mach number effects. A digital computer program for calculating constant SPL contours for the overall and octave band frequencies is incorporated. Machine plotted contours from model jet tests for a basic jet, VTOL jet, deflected jet, and jet with ejector are featured. Results of tip-turbine fan tests are given. Cruise fan, VTOL shrouded fan, and wing mounted configurations were tested.

Distribution of this abstract is unlimited.

DD FORM 1 JAN 64 1473

UNCLASSIFIED

Security Classification

14. KEY WORDS	LINK A		LINK B		LINK C	
	ROLE	WT	ROLE	WT	ROLE	WT
jet near field noise prediction techniques model jets VTOL jet deflected jet tip-turbine fan cruise fan						

INSTRUCTIONS

1. ORIGINATING ACTIVITY: Enter the name and address of the contractor, subcontractor, grantee, Department of Defense activity or other organization *(corporate author)* issuing the report.

2a. REPORT SECURITY CLASSIFICATION: Enter the overall security classification of the report. Indicate whether "Restricted Data" is included. Marking is to be in accordance with appropriate security regulations.

2b. GROUP: Automatic downgrading is specified in DoD Directive 5200.10 and Armed Forces Industrial Manual. Enter the group number. Also, when applicable, show that optional markings have been used for Group 3 and Group 4 as authorized.

3. REPORT TITLE: Enter the complete report title in all capital letters. Titles in all cases should be unclassified. If a meaningful title cannot be selected without classification, show title classification in all capitals in parenthesis immediately following the title.

4. DESCRIPTIVE NOTES: If appropriate, enter the type of report, e.g., interim, progress, summary, annual, or final. Give the inclusive dates when a specific reporting period is covered.

5. AUTHOR(S): Enter the name(s) of author(s) as shown on or in the report. Enter last name, first name, middle initial. If military, show rank and branch of service. The name of the principal author is an absolute minimum requirement.

6. REPORT DATE: Enter the date of the report as day, month, year, or month, year. If more than one date appears on the report, use date of publication.

7a. TOTAL NUMBER OF PAGES: The total page count should follow normal pagination procedures, i.e., enter the number of pages containing information.

7b. NUMBER OF REFERENCES: Enter the total number of references cited in the report.

8a. CONTRACT OR GRANT NUMBER: If appropriate, enter the applicable number of the contract or grant under which the report was written.

8b, 8c, & 8d. PROJECT NUMBER: Enter the appropriate military department identification, such as project number, subproject number, system numbers, task number, etc.

9a. ORIGINATOR'S REPORT NUMBER(S): Enter the official report number by which the document will be identified and controlled by the originating activity. This number must be unique to this report.

9b. OTHER REPORT NUMBER(S): If the report has been assigned any other report numbers *(either by the originator or by the sponsor)*, also enter this number(s).

10. AVAILABILITY/LIMITATION NOTICES: Enter any limitations on further dissemination of the report, other than those imposed by security classification, using standard statements such as:

(1) "Qualified requesters may obtain copies of this report from DDC."

(2) "Foreign announcement and dissemination of this report by DDC is not authorized."

(3) "U. S. Government agencies may obtain copies of this report directly from DDC. Other qualified DDC users shall request through _____."

(4) "U. S. military agencies may obtain copies of this report directly from DDC. Other qualified users shall request through _____."

(5) "All distribution of this report is controlled. Qualified DDC users shall request through _____."

If the report has been furnished to the Office of Technical Services, Department of Commerce, for sale to the public, indicate this fact and enter the price, if known.

11. SUPPLEMENTARY NOTES: Use for additional explanatory notes.

12. SPONSORING MILITARY ACTIVITY: Enter the name of the departmental project office or laboratory sponsoring *(paying for)* the research and development. Include address.

13. ABSTRACT: Enter an abstract giving a brief and factual summary of the document indicative of the report, even though it may also appear elsewhere in the body of the technical report. If additional space is required, a continuation sheet shall be attached.

It is highly desirable that the abstract of classified reports be unclassified. Each paragraph of the abstract shall end with an indication of the military security classification of the information in the paragraph, represented as *(TS), (S), (C), or (U)*.

There is no limitation on the length of the abstract. However, the suggested length is from 150 to 225 words.

14. KEY WORDS: Key words are technically meaningful terms or short phrases that characterize a report and may be used as index entries for cataloging the report. Key words must be selected so that no security classification is required. Identifiers, such as equipment model designation, trade name, military project code name, geographic location, may be used as key words but will be followed by an indication of technical context. The assignment of links, rules, and weights is optional.

SUPPLEMENTARY

INFORMATION

Errata - 2 Jan 68

AD-822 414

H. Results

This subsection includes discussion of the analytical analysis and all jet noise tests.

1. Basic Engine Configuration

The tests conducted with the basic engine configuration are unique from the standpoint of parameter variations made. The data have been semi-empirically correlated to exhaust local Mach number and exhaust temperature. All previous data have been correlated to exhaust velocity and have implicitly left out a temperature effect, except for its effect on exhaust velocity.

The exhaust velocity is expressed as

$$V = cM \propto T^{1/2} M \tag{17}$$

and, therefore, exhaust velocity is proportional to the square root of temperature.

AD 822 414

Evaluation of Equation (15) at $\theta = 90^{\circ}$ and substitution of the values of the functions C_1, C_2, C_3, and $K_1 T^s M^n$ gives (units are in $(psi)^2$)

$$\bar{p}^2 = \frac{4.63 \times 10^{-8}}{r^2}\left[T^{1.54} M^{6.34} + 0.0312 \frac{T^{2.47} M^4}{r^2} - 0.0146 \frac{T^{2.65} M^{4.89}}{r^4}\right] \tag{18}$$

One very important result in the far field ($r \gg 1$) is given by

$$\bar{p}^2 = 4.63 \times 10^{-8} \frac{T^{1.54} M^{6.34}}{r^2} \tag{19}$$

If variations in the ratio of specific heat at constant pressure to specific heat at constant temperature, k, are neglected, the speed of sound in the jet is

$$c_j = 49.4 \sqrt{T} \tag{20}$$

Substitution of Equation (20) into Equation (19) gives

$$\bar{p}^2 = 2.84 \times 10^{-13} \frac{c_j^{3.08} M^{6.34}}{r^2}$$

or (21)

$$\bar{p}^2 = 2.84 \times 10^{-13} \frac{V^{6.34}}{c_j^{3.26} r^2}$$

This shows but slight disagreement with the final expression of Hermes and Smith (Reference 2) who find